Investigations of high bit rate optical transmission systems employing a channel data rate of 40 Gb/s

vorgelegt von
Diplom - Ingenieur
Anes Hodžić
aus Berlin

Von der Fakultät IV - Elektrotechnik und Informatik -
der Technischen Universität Berlin
zur Erlangung des akademischen Grades

Doktor der Ingenieurwissenschaften
- Dr.-Ing. -
genehmigte Dissertation

Promotionsausschuss:

Vorsitzender: Prof. Dr.-Ing. Thomas Sikora
Berichter: Prof. Dr.-Ing. Klaus Petermann
Berichter: Prof. Dr.-Ing. Polina Bayvel

Tag der wissenschaftlichen Aussprache: 16. Juli 2004

Berlin 2004
D 83

Abstract

The focus of this work was set on 40 Gb/s based optical transmission systems with a varying number of channels and various spectral efficiencies in order to investigate the potential of 40 Gb/s technologies for the implementation in the next generation optical transmission networks. The results of this work can be used as design guidelines enabling a better understanding of propagation limitations in high bit rate transmission systems and give useful insights needed for the capacity upgrade of existing transmission lines.
Using conventional amplitude-shift-keying (ASK) based modulation formats and by the author proposed novel modulation formats, the optimization of the system settings is performed in 40 Gb/s based single channel, wavelength division multiplex (WDM) and dense WDM (DWDM) transmission lines, in order to enable a comparison between different modulation formats in terms of the total transmission distance and the maximum achievable spectral efficiency. The signal generation and dominant transmission characteristics of various conventional - non return-to-zero (NRZ), return-to-zero (RZ), duobinary, single side band RZ (SSB-RZ), carrier suppressed RZ (CSRZ) - and novel modulation formats - alternate chirped NRZ (alC-NRZ), novel chirped RZ (nCRZ), alternate polarized (N)RZ (alP(N)RZ) - were introduced. The idea behind the development of novel modulation formats was the performance improvement of the existing transmission lines with possibly low signal generation complexity, employing conventional ASK-based receiver configuration for the signal detection.
Dividing all modulation formats in two groups - NRZ- and RZ-based - their tolerances to linear and nonlinear transmission disturbances are investigated in single channel transmission, indicating that an implementation of NRZ-based modulation formats provides a better dispersion tolerance, but suffers from strong nonlinear limitations. The use of novel NRZ-based formats enables a significant improvement of nonlinear transmission characteristics at the cost of a slightly increased transmitter complexity. RZ-based formats are characterized by an increased sensitivity to residual dispersion and a significant nonlinear tolerance. It is shown that an additional phase or polarization modulation of RZ pulses enables more compact signal spectra and a further improvement of nonlinear transmission robustness, thus enlarging the maximum transmission distance. Strong intra-channel limitations were indicated as the dominant transmission limitation especially in RZ-based formats characterized by strong interactions of consecutive pulses within the bit stream, due to the fast broadening of short optical pulses at 40 Gb/s. This effect is accompanied by self-phase modulation (SPM) - group velocity dispersion (GVD) interplay, which becomes evident in both format groups at larger channel powers.
It is shown that the dominance of intra-channel effects requires implementation of transmission fibers with moderate dispersion values. Furthermore, it was shown, that as long as intra-channel effects dominate transmission performance, the best dispersion compensation scheme is characterized by a small amount of dispersion pre-compensation, due to suppression of interactions between adjacent pulses. Thereby, right amount of dispersion pre-compensation is dependent on the modulation format in use, because of the interplay between the pulse internal chirp induced during modulation and the local dispersion in transmission line. The importance of pre-compensation increases in long-haul transmission lines employing dispersion compensation on a span-by-span basis, because of constructive superposition of intrachannel cross-phase modulation (IXPM) contributions in each span. The modulation formats employing polarization switching between consecutive pulses were identified as best solution for the performance enhancement in 40 Gb/s single channel based transmission lines.
The 40 Gb/s based WDM systems with spectral efficiency of 0.4 bit/s/Hz showed identical transmission behavior as in single channel transmission for all modulation formats, which can be explained by the dominance of single-channel effects in 40 Gb/s systems with a channel spacing of 100 GHz. This leads to the conclusion that a system upgrade from single channel to WDM at 40 Gb/s channel data rate can be made using identical transmission infrastructure. As in the single channel case, RZ-based formats indicated a significant robustness to nonlinear propagation effects, which could be further improved by the use of novel modulation

formats. Basically, RZ-based modulation formats outperform the NRZ-based ones in 40 Gb/s single channel and WDM transmissions, and transmission advantages of RZ based formats become even more evident with an increased transmission distance.
It was shown that an increase of spectral efficiency to 0.8 bit/s/Hz in 40 Gb/s based DWDM systems results in increased pulse distortions, because of the reduced tolerance to implemented narrow-band filtering and larger impact of multi-channel nonlinearities (particularly XPM). The differences between RZ- and NRZ-based modulation formats vanish in DWDM transmissions, because of the distortion of RZ pulse shape due to narrow-band filtering needed at the transmitter side. It was shown that transmission performance of DWDM systems could profit from implementation of transmission fibers with a large chromatic dispersion, due to suppression of multi-channel effects independently of the modulation format in use. Accordingly, already deployed fibers (e.g. G.652) can be further used in next generation of DWDM transmission systems. Furthermore, considering concatenation of identical spans in a DWDM transmission line, it was observed that XPM-induced impacts superpose constructively from span to span independently of the implemented dispersion compensation scheme, resulting in an transmission penalty, which is in high power regime proportional to number of concatenated spans. This behavior enables together with already know transmission rules (e.g. Pmax) an efficient estimation of the maximum transmission performance and maximum transmission distance in 40 Gb/s DWDM systems.
This work is completed by representation of some promising technologies, e.g. polarization orthogonality between the channels or phase-shift-keying (PSK) based modulation formats, which enable a further increase of spectral efficiency (beyond 0.8 bit/s/Hz) and an enhanced maximum transmission distance. The investigations of PSK-based modulation formats showed that not all recently proposed PSK-based system could compete with ASK-based formats for implementation in DWDM systems. Differential quadrature PSK (DQPSK) based modulation formats were identified as a potential candidate for the implementation in future spectrally efficient DWDM systems.

Acknowledgement

First I would like to thank my advisor Professor Klaus Petermann for his generous support, motivating discussions and great time during my dissertation. He gave me the independence to follow different research interests and found always time to answer my questions and comment my ideas.
I also want to thank Professor Polina Bayvel from the University Collage of London and Professor Thomas Sikora from the Technical University of Berlin for acting as supervisors of my work. I want to thank the Federal Ministry of Education and Research for funding my work.
I am particularly grateful to my peers and friends from the Photonics Group at Technical University of Berlin - Hadrian Louchet, Fabian Kerbstadt, Wieland Mann, Miroslawa Malach, Beate Konrad, Alessandro de Melo, Sebastian Randel, Martin Schnarrenberger and Torsten Mitze - for fruitful discussions and helpful comments. I would especially like to thank my students Johannes Fischer, Marcus Winter and Martin Herzog for their support of my work. I would like to thank to Metin Talan for his support in the final phase of my work.
I would like to express my sincere thanks to my parents Hadija and Osman, my brother Adnan and my girlfriend Sanela for their support, patience and understanding during my dissertation.

Contents

Abstract i

Acknowledgement iii

Abstract v

Acknowledgement v

1 Introduction 1
- 1.1 Scope of this work . . . 6

2 System components 9
- 2.1 Overview . . . 9
- 2.2 Optical transmitter . . . 9
  - 2.2.1 Laser diode model . . . 10
  - 2.2.2 Mach-Zehnder Modulator (MZM) . . . 11
  - 2.2.3 Electroabsorption Modulator (EAM) . . . 12
- 2.3 Optical fibers . . . 14
  - 2.3.1 Linear fiber characteristics . . . 15
  - 2.3.2 Fiber parameters . . . 22
- 2.4 Nonlinear processes . . . 25
  - 2.4.1 Kerr nonlinearities . . . 25
  - 2.4.2 Stimulated scattering processes . . . 32
- 2.5 Numerical model of optical fiber . . . 34
- 2.6 Dispersion compensation in optical transmission lines . . . 36
  - 2.6.1 In-line compensation devices . . . 36
  - 2.6.2 Dispersion compensating schemes . . . 38
- 2.7 Optical filters . . . 41
- 2.8 Optical amplifiers . . . 46
- 2.9 Optical receivers . . . 51

3 Optical modulation formats 53
- 3.1 Overview . . . 53
- 3.2 Optical signal generation . . . 53
- 3.3 NRZ-based modulation formats . . . 56
  - 3.3.1 Non-return-to-zero (NRZ) modulation . . . 56
  - 3.3.2 Duobinary modulation . . . 57
- 3.4 RZ-based modulation formats . . . 60
  - 3.4.1 Return-to-zero (RZ) modulation . . . 60
  - 3.4.2 Carrier-suppressed RZ (CSRZ) modulation . . . 61
  - 3.4.3 Single side band RZ (SSB-RZ) modulation . . . 63
  - 3.4.4 Chirped RZ (CRZ) modulation . . . 65
- 3.5 Novel modulation formats . . . 67
  - 3.5.1 Alternate Chirped NRZ (alCNRZ) modulation . . . 67
  - 3.5.2 Alternate chirped RZ (al-RZ) modulation . . . 68
  - 3.5.3 Novel chirped RZ (nCRZ) modulation . . . 69

3.5.4 Alternate polarized modulation formats . . . 70

4 Performance evaluation criteria 75
4.1 Overview . . . 75
4.2 Bit error rate (BER) . . . 75
4.3 Q-factor . . . 80
4.4 Optical signal-to-noise ratio (OSNR) . . . 82
4.5 Eye opening penalty (EOP) . . . 84
4.6 Relation between different evaluation criteria . . . 86

5 40 Gb/s single channel investigations 89
5.1 Overview . . . 89
5.2 Investigated system setups . . . 89
5.3 Dispersion tolerance in 40 Gb/s single channel transmissions . . . 90
5.4 Nonlinear tolerance in 40 Gb/s single channel transmissions . . . 93
5.5 Optimization of system settings for 40 Gb/s single channel transmission . . . 95
5.5.1 Optimum power setting for different fiber infrastructures . . . 96
5.5.2 Optimum dispersion compensating scheme . . . 102
5.5.3 40 Gb/s transmission performance with optimized system settings . . . 108
5.6 40 Gb/s single channel long-haul (> 500 km) transmissions . . . 113
5.7 Conclusion and outlook . . . 117

6 40 Gb/s WDM and DWDM investigations 119
6.1 Overview . . . 119
6.2 Investigated system setups . . . 119
6.3 Optimized optical filtering in WDM and DWDM systems . . . 120
6.3.1 NRZ-based modulation formats . . . 121
6.3.2 RZ-based modulation formats . . . 123
6.3.3 Novel modulation formats . . . 125
6.4 Optimized amplifier spacing . . . 126
6.5 Optimized power settings . . . 127
6.5.1 NRZ-based modulation formats . . . 128
6.5.2 RZ-based modulation formats . . . 129
6.5.3 Novel modulation formats . . . 130
6.6 Optimized dispersion compensating schemes . . . 132
6.6.1 NRZ-based modulation formats . . . 132
6.6.2 RZ-based modulation formats . . . 135
6.6.3 Novel modulation formats . . . 137
6.7 Optimum transmission fiber investigations . . . 140
6.7.1 NRZ-based modulation formats . . . 140
6.7.2 RZ-based modulation formats . . . 142
6.7.3 Novel modulation formats . . . 144
6.8 Transmission performance investigations . . . 146
6.8.1 NRZ-based modulation formats . . . 146
6.8.2 RZ-based modulation formats . . . 147
6.8.3 Novel modulation formats . . . 149
6.9 Investigation of 40 Gb/s based WDM and DWDM long-haul (> 500 km) transmissions . . . 151
6.10 Conclusions and outlook . . . 156

7 Enabling technologies for future transmission systems **159**
7.1 Overview 159
7.2 Narrow-band filtered ASK-based modulation formats 159
7.3 Orthogonally polarized channels 160
7.4 PSK-based modulation formats 163

8 Summary **167**

Bibliography **171**

A List of symbols **189**

B Acronyms **191**

C Sufficient amount of bits for 40 Gb/s numerical investigation **193**

D Optimized power settings for 40 Gb/s single channel transmission **195**

Publications **199**

1 Introduction

Since their first development and deployment, optical transmission networks offer improved possibilities for dealing with ever growing demands on transmission bandwidth and system capacity. In the last 20 years, the optical transmission networks have become one of the most important part in the telecommunication hierarchy, whose seamless integration with conventional network applications and services forces a further development and a broader deployment of optical networks in all telecommunication areas. Making a classification of different optical transmission networks, it can be distinguished between **Access**, **Metro** and **Core** (or back-bone) networks (Fig. 1.1). This is the most convenient network classification made regarding to the transmission distance or network diameter. Access networks as the base of the telecommunication hierarchy, are characterized by the interaction between numerous different network technologies based on different transmission media e.g. wire, wireless or fiber. These networks possess a small total capacity and inter-operational functionality between different transmission protocols (e.g. TCP/IP, ATM) and services (e.g. ISDN, DSL). The conventional wire based data transmission dominates the access area, making these networks to become a bottleneck of data transmission in the future. The implementation and deployment of optical networks in this region e.g. fiber-to-the-home (FTTH) and fiber-to-the-business (FTTB) would address the bottleneck problems, hence enabling an even broader bandwidth access than with conventional wire based technologies (e.g. DSL). But this is rather a question of deployment strategy and cost than of the achievable transmission performance. Metro area networks (MANs) accumulate the traffic from the access networks with different protocols and services, enabling its further transmission over longer distances. The MANs are based on optical transmission technologies and they are characterized by a limited transmission distance (< 200 km) and an increased network complexity. Furthermore, MANs have to deal with different communication protocols, thus requiring close interaction between the network management and transmission infrastructure, which results in the fact that the channel data rates used here are rather small (<10 Gb/s/ch, at the moment).

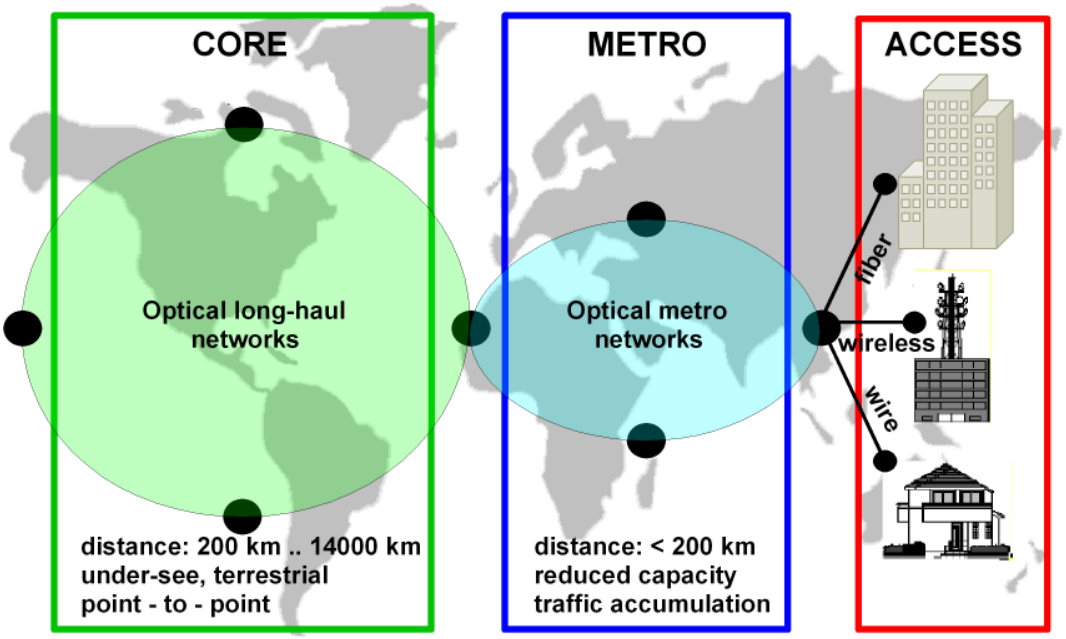

Figure 1.1: Networks classification

The core networks connect numerous MANs over distances larger than 200 km. Basically, it can be distinguished between terrestrial and under-sea core networks. The under-sea networks are characterized by point-to-point transmission, ultra long-haul transmission distances (>1000 km), and specialized component characteristics (e.g. component life times and customized fiber types). The core networks possess an increased transmission capacity based on larger channel data rates. The upgrade of core networks represents the first step for a faster world wide communication.
The deployment of future optical networks and upgrade of existing ones will be governed by the growth of the traffic in all network areas. Taking a look on the traffic growth trends up to year 2004 illustrated in Fig. 1.2, it can be observed that data based services and applications, e.g. internet or broad-band access represent the driving forces for the future capacity enlargement. The vast majority of future data traffic will be IP-based services e.g. telecommuting, video-conferencing or e-learning, requiring a better interaction between the existing transmission protocols (e.g. ISO/OSI-protocol stack) and the physical layer, realized by means of optical transmission. The expected capacity increase caused by voice based services, which up to recently were most important for the network evolution, is almost negligible (4 %) compared to other possible services (Fig. 1.2). The capacity and traffic needs of new transmission services were expected to require, according to analyst predictions in year 1998 ([1]), the upgrade of existing networks to system capacities larger than 3 Tbit/s (Fig. 1.2) after the year 2001.

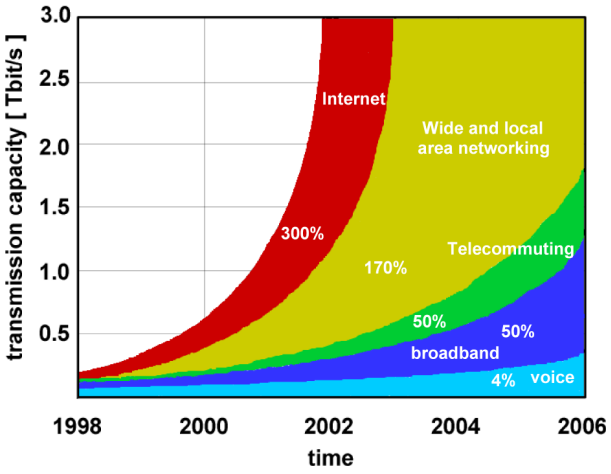

Figure 1.2: Traffic growth trends [1]

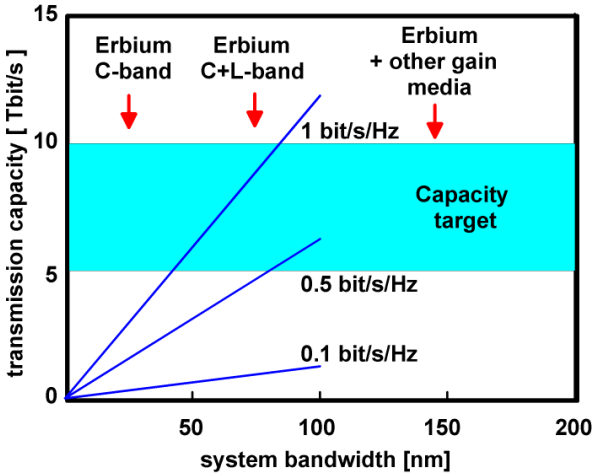

Figure 1.3: Traffic growth boundaries [2]

Being limited by the fundamental losses of optical fibers, the improvement and a further development of optical amplifier technologies, e.g. erbium doped fiber amplifiers (EDFAs) or distributed amplification, dominates the network evolution, enabling a significant extension of the usable bandwidth regions. The system bandwidth in today's optical networks is limited by the gain characteristics of employed optical amplifiers (EDFAs), which enable the use of approximately 35 nm bandwidth in the C-band wavelength region (Fig. 1.3). As a possibility for a further bandwidth increase, additional frequency bands, e.g. L- and S-band can be used, accomplishing novel amplifier and transmission technologies. The use of some novel amplification media (e.g. Raman-amplification) would even enlarge the usable system bandwidth. But this could be a rather complicated issue, because all other system components (first of all transmission fibers) have to be available for the operation in the desired bandwidth regions. The other way of capacity enlargement would be a better utilization of the existing system bandwidth. As a measure of the bandwidth utilization, the spectral efficiency expressed in bit/s/Hz is used. The spectral efficiency is defined as the relation between the channel data rate and the spacing between adjacent channels. The transmission systems implemented in the field today are characterized by a rather small spectral efficiency (<0.2 bit/s/Hz). Using existing systems with a small spectral efficiency, the implementation of e.g. new amplification bands (L-, S-band) and optical regeneration technologies would be mandatory for the realization of next generation networks with a desired transmission capacity in a region between 5-10 Tbit/s (Fig. 1.3). This could be avoided by the increase of the

system's spectral efficiency, which can enable the continued use of existing network infrastructure. Accordingly, a spectral efficiency larger than 0.4 bit/s/Hz would be needed for the targeted capacity in a bandwidth limited range using already existing system technologies.
The question arising here, is what is the best transmission technology to be implemented in future systems. The key technologies for providing a better exploitation of the existing transmission infrastructure are wavelength division multiplexing (WDM) and optical time domain division multiplexing (OTDM). In the WDM case, each channel uses a certain wavelength range of the total system bandwidth, whereas in OTDM the channels are multiplexed in the time domain using multiple time-slots. According to the less complex signal generation and an improved system upgrade capability of the WDM technology, it seems at the moment that this technology represents the best choice for the future system design. On the other hand, the OTDM or electronic TDM (ETDM) can be efficiently used for the generation of higher channel data rates (>10 Gb/s), which in a combination with WDM can be a good solution to meet the bandwidth demands in the future. The pure OTDM based systems are characterized by a large complexity of realization both in terms of component fabrication and transmission performance. For enabling system capacities larger e.g. 100 Gb/s in a pure OTDM environment, additional sophisticated components are needed, e.g. all-optical regeneration, clock recovery, all-optical demultiplexing to data rates at which electronics can be used for the signal processing. Furthermore, the transmission of ultra-short pulses in the sub-picosecond region raises additional propagation disturbances to become significant performance limitations, e.g. higher order dispersion and intra-channel nonlinear effects. Recently presented single channel OTDM experiments at channel data rates of 160 Gb/s can be seen as the first step in the implementation of higher channel data rates in future WDM transmission systems.

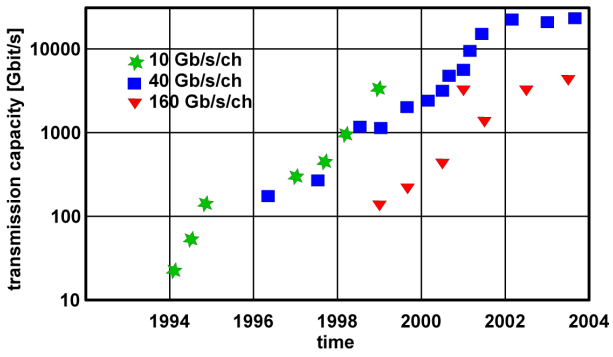

Figure 1.4: Capacity improvement experiments [3]

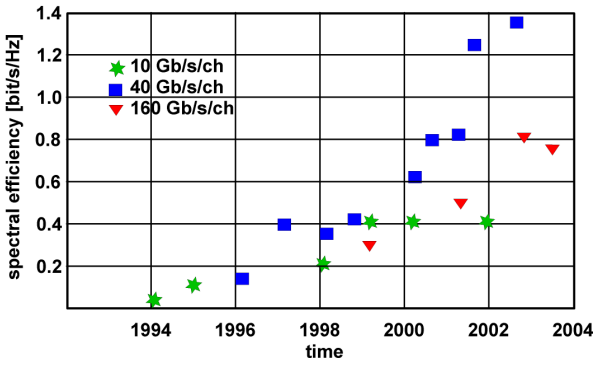

Figure 1.5: Spectral efficiency increase [3]

Another important question is, which channel data rate should be employed in future WDM systems in order to reach a maximum transmission performance and spectral efficiency. In an overview of transmission experiments with channel data rates exceeding 2.5 Gb/s (Figs. 1.4 and 1.5), two dominant trends can be observed in order to meet the bandwidth demands. First, there is a trend for increasing the overall system capacity. Summarizing the most important works with channel data rates of 10, 40 and 160 Gb/s regarding the achievable system capacity from the year 1994 up to now, it can be observed (Fig. 1.4) that for enabling of an increased system capacity, a moderate channel data rate of e.g. 40 Gb/s shows the best transmission potential. This tendency can be explained by a reduced complexity in realization and availability of required 40 Gb/s system components e.g. narrow-band filters on the one hand, and compatibility of 40 Gb/s data rates with existing transmission infrastructure on the other hand. The increased system capacity in 40 Gb/s experiments is enabled by implementation of some new sophisticated technologies, e.g. novel modulation formats, new fiber and amplifier types, which are becoming mature, because of the possibility to realize them using only electronics or some hybride (electro-optics) solutions, which seems to be impossible at increased channel data rates e.g. 160 Gb/s, due to the fact that 40 Gb/s technology represents the limit for electronics. But, considering 10 Gb/s based experiments with an increased system capacity, it can be observed that even with conventional commercially available technologies the system capacities beyond 1 Tb/s can be achieved, thus

questioning the reasons for 40 Gb/s channel data rates. Another network evolution trend, which is supported by the need for a better utilization of the existing system bandwidth, is the enhancement of the system's spectral efficiency. Figure 1.5 gives an overview of the achievable spectral efficiencies using different channel data rates. It can be observed, that the achieved maximum efficiency values in 10 Gb/s based transmissions are not larger than 0.4 bit/s/Hz, which is primary caused by the fact that narrow-band filters for ultra dense channel spacings (25 GHz or lower) are not available at the moment. This fact lets the higher channel data rates appear more convenient for achieving an increased spectral efficiency. Here again, the 40 Gb/s based systems indicate the best choice characteristics, which can be explained by the signal generation of 40 Gb/s signals (compared to 160 Gb/s) and an easier realization of performance enabling technologies at 40 Gb/s, thus recommending the 40 Gb/s channel data rate as a candidate for the realization of next generation WDM and dense WDM (DWDM) optical transmission systems. At the same time, the implementation of higher channel data rates larger than 10 Gb/s bears issues e.g. reduced tolerance to fiber dispersion, to polarization mode dispersion (PMD) and to noise disturbances in the transmission line, whose suppression requires unconventional technologies and methods for achievement of improved transmission characteristics, making the high bit rate based transmission becoming a long term issue with long implementation times.

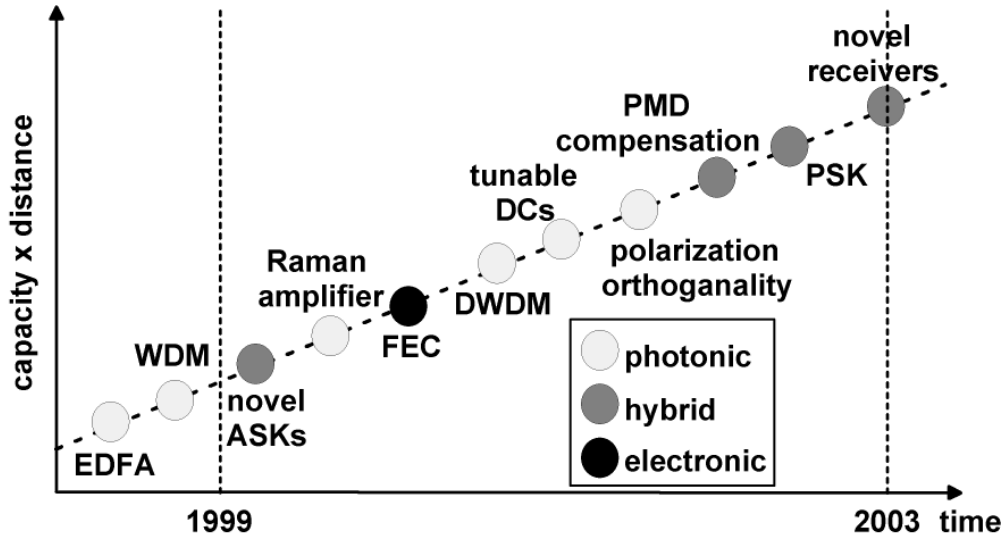

Figure 1.6: Enabling technology trends

Historically speaking, the transmission data rate of commercially deployed systems increased up to now approximately by a factor of four every five years [4]. This makes the 40 Gb/s channel data rate the next "natural" data rate to be deployed in commercial transmission systems, whose implementation should, besides improved transmission performance, enable a reduced system complexity and reduced system costs (40 % cost reduction expected). Indicating 40 Gb/s transmission as a mainstream technology in research and experimental works in the last years, it can be said that much work has to be done before its straightforward system implementation and the benefits to other channel data rates have to be figured out. The key for the maturity of 40 Gb/s transmission technology lies in enabling technologies presented in Fig. 1.6. Depending on the realization and operation domain, it can be distinguished between electronically, hybrid and pure photonics based concepts for the performance improvement. From the viewpoint of component complexity and component cost, the electronics, e.g. forward error correction (FEC) codes, and hybrid solutions, e.g. novel modulation formats, are preferable for the future system implementation, because of the large existing know-how in electronics and due to the fact that implementation of these technologies would enable an easy upgrade of existing networks to higher channel data rates. The photonics based solutions for transmission improvement, e.g. DWDMs, tunable dispersion compensation (DC), tunable PMD compensation, distributed optical amplification, enable a significant enhancement of the total transmission performance, but they are at the moment not mature for system deployment due to their fabrication complexity and the fact that some

of them have to be standardized first. Even more, the implementation of these technologies, e.g. tunable PMD and dispersion compensation, would make the system infrastructure become even more complex, so that before these technologies are employed some simple approaches for an improved robustness of 40 Gb/s transmission have to be investigated intensively.
The recent developments and research works considering 40 Gb/s based transmission systems can be divided in three groups of so called "hero" experiments regarding the maximum system capacity, maximum spectral efficiency, and maximum transmission distance oriented experiments. These experiment are called "hero" experiments because of their large realization complexity and due to the fact that rather limited conclusions can be drawn for the real system implementation in existing transmission lines. The maximum capacity oriented "hero" experiments [5], [6], [7], [8], [9] are characterized by the implementation of sophisticated transmission technologies e.g. distributed amplification or bidirectional transmission with a large number of channels over limited transmission distances (<400 km). These works are less relevant for the future system design and they are characteristic for the beginning phase of 40 Gb/s investigations (years 1999-2001), whose aim was the feasibility study of 40 Gb/s transmissions with an increased system capacity (>1 Tb/s). The following works [10], [11], [12] [13], [14], [15] were focused on enabling a spectral efficiency larger than 0.2 bit/s/Hz. By the use of some novel technologies, e.g. novel amplitude shift keying (ASK) based modulation formats and orthogonal polarization between adjacent channels, record spectral efficiencies were achieved over limited transmission distances. The extreme system capacities and extreme spectral efficiency values are important for the system realization, but due to the fact that the high bit rate systems should be implemented primarily in core networks with large transmission distances, the 40 Gb/s transmission systems should possess improved characteristics in terms of capacity-distance relation, because already existing 10 Gb/s systems enable long-haul transmission distances over several thousand kilometers. The recently presented experimental 40 Gb/s works [16], [17], [18], [19], [20] over large transmission distances (>1000 km) indicate the potential of 40 Gb/s channel data rates even in ultra-long haul transmission lines (up to 10.000 km). These experiments employ sophisticated transmission technologies, e.g. super FEC codes and phase shift keying (PSK) based modulation formats, e.g. differential PSK (DPSK), with novel receiver structures (e.g. balanced receiver).

1.1 Scope of this work

The scope of this work are transmission lines employing single and multiple channels with channel data rates of 40 Gb/s, which represents a compromise between electronics and photonics. The reason for focusing on 40 Gb/s transmission was the tendency observed from recent experiments (Fig. 1.4), which showed that 40 Gb/s based systems can enable an improved system capacity and an enhanced spectral efficiency, which seems to be necessary for future transmission systems, because the increasing bandwidth demands make the better utilization of existing system bandwidth an important target for the future design works. Better bandwidth utilization does not mean increased spectral efficiency at any cost, e.g. with a significant reduction of transmission distance or an increased complexity of transmission line. It is rather the introduction of novel transmission technologies, e.g. modulation formats, sophisticated filtering methods and dispersion compensation schemes, which are characterized by a compatibility with the existing transmission line infrastructure and by a reduced complexity enabling a straightforward system upgrade from lower channel date rates. Focusing on a simple and easy system upgrade to 40 Gb/s channel data rates, the upgrade scenario considered in this work is characterized by a component upgrade at the system edges, e.g. transmitter line card, and use of transmission line infrastructure already deployed in field. In doing so, the focus is set on the role and characteristics of the conventional and novel ASK-based modulation formats as the most important technology for the deployment of high bit rates in existing transmission lines. After presenting optical signal generation of conventional and novel modulation formats, their propagation characteristics are investigated in order to identify the advantages and drawbacks of each format and to determine the optimum operating regime (system environment), hence deriving simple design criteria for a future system upgrade. For highlighting the system upgrade aspects of 40 Gb/s transmission, the numerical investigations were performed considering single and multi-channel transmission lines with varying spectral efficiencies. The comparison between different modulation formats in different transmission regimes is made considering optimized system settings in all investigated cases, derived from extensive numerical investigations. After intensive 40 Gb/s investigations, the question of the optimum channel data rate is addressed by comparing the propagation characteristics of transmission lines with 10, 40 and 160 Gb/s channel data rates. Furthermore, promising transmission and spectral efficiency enabling techniques are presented giving an outlook of future works and transmission technology trends.

Starting with **Chapter 2**, an insight of the state-of-the-art technologies for 40 Gb/s transmission systems, e.g. optical filters, amplitude and phase modulators, optical amplifiers and dispersion compensations devices is given. According to the numerical (theoretical) nature of this work, the numerical models, which are used for the modeling and characterization of signal propagation in optical fibers are introduced. Furthermore, linear (ASE-noise) and nonlinear (Kerr-effects, stimulated processes) propagation disturbances in optical fibers are described, as well as methods for their suppression.

In **Chapter 3**, the evaluation criteria are introduced, which are applied for the performance evaluation in investigations presented in this work. The different evaluation criteria for characterization of transmission performance are defined, describing their validity for numerical and experimental investigations. By describing the advantages, drawbacks, and relations between various evaluation criteria, the complexity of performance evaluation as well as of comparison between numerical and experimental results is highlighted.

The signal generation of various ASK-based modulation formats is presented in **Chapter 4**. Using the optical signal shape as the characterization criterion, the modulation formats are divided in NRZ- and RZ-based modulation formats. Furthermore, it is distinguished between conventional modulation formats (e.g. NRZ, RZ, duobinary) and novel modulation formats recently proposed, which indicate the potential of improving spectral efficiency and transmission characteristics in 40 Gb/s based transmission lines. The expected advantages and weaknesses are indicated for each modulation format.

Due to the need for an improved understanding of transmission disturbances and system upgrade aspects in 40 Gb/s based transmission systems, the investigations were started considering 40 Gb/s single channel propagation over short- (<400 km) and long-haul (up to ≈1000 km) transmission distances. These works are presented in **Chapter 5**. Investigating various ASK modulation formats, the numerical works regarding format robustness are performed regarding e.g. dispersion tolerance and nonlinear tolerance. Taking into account the effects of different line infrastructure on the total transmission propagation, the investigation

of dispersion maps and power settings along the transmission line is made, and dominant propagation limitations are identified and explained. Considering optimized system settings, which are determined for each modulation format, the comparison between different modulation formats is accomplished, yielding the recommendations for a future 40 Gb/s single channel based system design. Additional investigations were made for a characterization of transmission performance of different modulation formats in long-haul transmission systems in order to identify the length dependent accumulation of propagation disturbances and propose the methods for transmission length enhancement.

As the next step in the evolution of 40 Gb/s transmission systems, the investigation of 40 Gb/s based WDM and DWDM transmission systems is presented in **Chapter 6**. The WDM and DWDM systems are characterized by spectral efficiencies of 0.4 and 0.8 bit/s/Hz, respectively. Since the DWDM transmission at 0.8 bit/s/Hz was an critical issue, at the time the this work was started, the improved narrow-band filtering is introduced and described as an enabling technology for the improved spectral efficiency. The transmission line settings, e.g. filter settings in multiplexers and demultiplexers, power settings, amplifier spacing, transmission fiber and dispersion compensation scheme, are optimized by numerous numerical investigations, both for WDM and DWDM systems, in order to deliver simple design and upgrade criteria for the next generation systems, and to address some of never-ending questions e.g. about the optimum fiber type. The focus is set on length and power dependence of optimum dispersion compensating scheme and importance of fiber settings for total performance both in WDM and DWDM systems. All investigations are made separately for different modulation formats, hence identifying the optimum implementation areas for each modulation method. Finally, as in the single channel case, the investigations are completed considering an enhanced total system reach ($\approx$1000 km).

Several promising enabling technologies for an increased spectral efficiency and an enhanced system reach in 40 Gb/s based WDM and DWDM transmissions are introduced in **Chapter 7**. The numerical investigations of techniques e.g. orthogonal polarization between adjacent channels and PSK modulation formats, are presented, indicating dominant characteristics of each technology and determining their importance for a future system design.

Chapter 8 contains the summary of presented works, and gives an outlook of future research activities, required for a further characterization of high speed optical transmission systems.

2 System components

2.1 Overview

The complexity of the system design in optical communications can be seen as the consequence of the large number of components with different parameters and operational characteristics. The description of the interaction between the optical signal and transmission disturbances is a multi dimensional issue, whose solution depends on the relation between different system parameters. The right approach for the optimization of system settings and derivation of design rules must take into account the interaction of effects which take place in each component. The system components needed for the realization of an optical transmission line are presented in this chapter. They are divided into three groups: optical transmitter, transmission line and optical receiver. The operation principles and state-of-the-art technologies are introduced as well as mathematical models of conventional transmission components used for numerical investigations.

2.2 Optical transmitter

The role and the realization of the optical transmitter become important with increased channel data rates in the system. While the optical transmitters at lower channel data rates are less complex and easier to realize by direct modulation of the laser diode, the realization becomes more complex with the increasing channel data rate, thus requirements on electrical and optical components of the optical transmitter raise. The conventional optical transmitter (Fig. 2.1) implores amplitude/intensity modulation (AM, IM) of the laser light better known as on-off keying (OOK), because different signal levels for marks and spaces are characterized by the presence of optical power. The amplitude modulation can be realized by direct or external modulation of the laser diode. For the realization of transmission systems with channel data rates larger than 10 Gb/s, the external modulation represents a better solution because the impact of laser internal chirp on optical signal can be reduced efficiently, but on the other hand, the complexity of optical transmitters increases. The external modulation is realized by the modulation of the laser light in an external modulator. This can be a Mach-Zehnder (MZM) or an electroabsorption (EAM) modulator. The external modulator is driven by an electrical signal with corresponding data rate. Depending on the electrical driving signal and the operation regime of the external modulator, different AM based modulation formats can be realized (see Chapter 3).

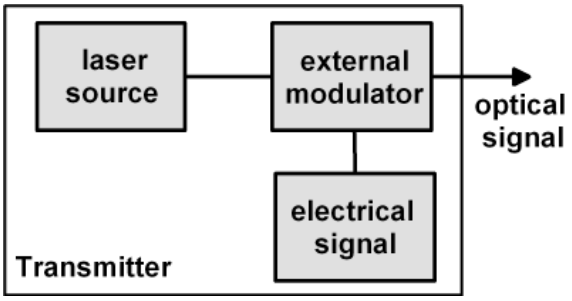

Figure 2.1: Transmitter setup with external modulation

2.2.1 Laser diode model

The direct modulation of the laser is the simplest method to generate optical pulses. In the case of the intensity modulation (IM), the injection current of the laser source is modulated with an electrical data signal resulting in a direct modulation of the output power of the laser source. Besides the pure AM modulation of the laser power, an undesirable time dependent variation of the laser frequency occurs. The resulting frequency shift $\Delta\omega_L$ can be defined as the time derivation of the laser-phase deviation ϕ_L from the zero phase $\phi_{L,0}$ [21]:

$$\Delta\omega_L(t) = \frac{d\{\phi_L(t) - \phi_{L,0}\}}{dt} = \frac{d\{\phi_L(t)\}}{dt} \tag{2.1}$$

This dynamical time response of the $\Delta\omega_L$ is called laser chirp. The laser chirp can be described by the charge carrier effects: the variation of the injection current causes a change of the charge carrier number within the active laser zone [21]. The carrier number determines the effective refractive index of the laser. The modulation of the injection current causes a modulation of the laser refractive index resulting in a phase and a frequency modulation of the laser light. Accordingly, the laser chirp is not visible in the signal shape of AM modulated output pulses, but it manifests in the broadening of the optical signal spectrum. The induced linear chirp causes the realignment of the existing spectral components. The laser chirp of a semiconductor laser can be described by the line-width enhancement factor (Henry-factor) α_L [21]. The laser chirp $\Delta\omega_L(t)$ is related to the output optical power:

$$\Delta\omega_L(t) = \frac{d\phi_L}{dt} = \frac{\alpha_L}{2}\left[\frac{d\ln P_L(t)}{dt} + \kappa_L P_L(t)\right] \tag{2.2}$$

where $P_L(t)$ represents the modulation of the optical power and κ_L is the adiabatic chirp coefficient. The first term in Eq. 2.2 is a structure-independent "transient" chirp and the second term is a structure-dependent "adiabatic" chirp. The first term has a significant meaning during the relaxation oscillations. The second term is related to the relaxation oscillation damping, since it is directly proportional to the gain compression factor. Transient chirp-dominated laser diodes exhibit significantly more overshoot and ringing in the output power and frequency deviations with a relatively small frequency difference between steady-states ones and zeros. Adiabatic chirp-dominated laser diodes exhibit attenuated oscillations and a large frequency difference between steady-states ones and zeros. The transient chirp component which is always present, will be masked by the adiabatic chirp. Typical values for transient chirp are $\kappa_L \approx 1..5\,1/\mathrm{W}$. Line-width enhancement factors are $\alpha_L < 3$ for conventional Quantum-Well-(QW)-lasers and $\alpha_L = 4..8$ for a Distributed-Feedback-(DFB)-laser diodes.

The DFB laser represents the most important and most widely used single mode laser type in the 1550 nm region. DFB lasers are realized by the implementation of a Bragg grating structure inside the cavity between the reflecting surfaces of a Fabry Perot (FP) laser [22]. The implemented grating structure causes a periodic variation of the laser mode index. The isolation of single mode originates from the Bragg condition in the grating [23].

DFB lasers are classified by the amount of chirp, which is produce when DFB is directly modulated. To separate low chirp lasers from high chirp lasers, DFB lasers are characterized by the amount of dispersion that the laser can handle before significant errors occur at the end of the fiber link. Typically, if the dispersion penalty is greater than 2 dB, then the DFB laser cannot be used for that length of fiber. The DFB laser manufacturers specify that a laser could handle a fixed amount of dispersion in ps/nm and guarantee that it could handle this dispersion with less than a 2 dB dispersion penalty. Recent advances in DFB technologies have produced lasers with less chirp allowing them to reach distances of >50 km at 10 Gb/s channel data rate [24]. Direct modulation of the laser is thus characterized by a reduced transmission distance due to a large internal laser chirp making this signal generation method less relevant for the channel data rates larger than 10 Gb/s.

External modulation can be realized with $LiNbO_3$-based Mach-Zehnder modulator (MZM) (Chapter 2.2.2) and InP-based elektroabsorption modulator (EAM) (Chapter 2.2.3). In this signal generation method, the laser source acts as a continuous wave (CW) pump. In conventional systems, the CW pumps are realized with DFB lasers. The main characteristics of the DFB lasers are high sidemode suppression ratios (SMSR)

(> 50 dB) [25] enabling stable single-mode operation, small spectral line width (0.8..10 MHz) [26], [27], and large output optical powers (10..40 mW) [28], [26]. The physical processes and parameters describing laser behavior can be efficiently modeled using laser models proposed e.g. in [21], [29], [30]. For the investigations presented in this work, a simple laser model is used [31], [32], which considers the phase noise of the laser (Eq. 2.2), but neglects the laser intensity noise. The laser output signal is given by:

$$E(t) = \sqrt{P_0}\exp(j(\omega_0 t + \phi(t))) \tag{2.3}$$

with

$$\Delta\phi = \sqrt{2\pi\Delta\nu\Delta t}\cdot x \tag{2.4}$$

where P_0 is the emitted optical power, ω_0 is the laser emission frequency, ϕ is the optical phase, $\Delta\phi$ is the phase increment in time interval Δt, and $\Delta\nu$ is the optical laser line-width. x describes the Gaussian distributed stochastic process with a variance of $\langle x^2\rangle$=1 and a mean value of $\langle x\rangle$=0 [21]. The considered $\Delta\nu$ was smaller than 10 MHz (typically 1 MHz) for all investigations presented in this work, showing a good agreement with conventional component data.

2.2.2 Mach-Zehnder Modulator (MZM)

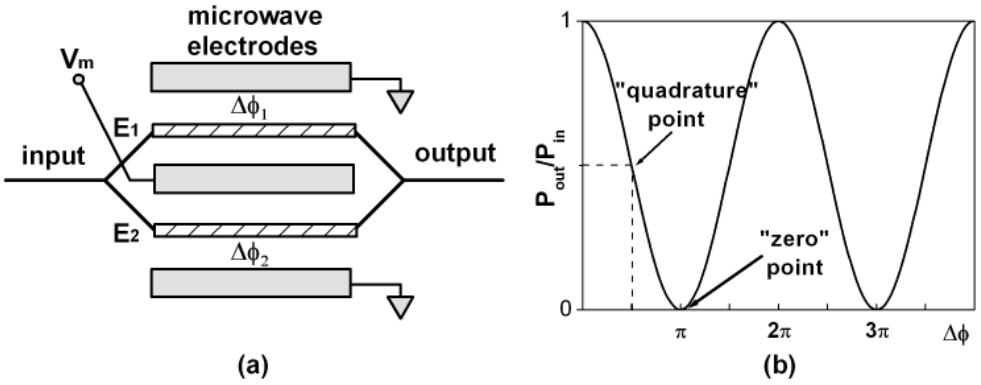

Figure 2.2: Mach-Zehnder Modulator (MZM) principles: a) structure b) transmission function

The operational principles of MZMs are based on the electro-optic effect, which is characterized by the variation of an applied electrical field causing refractive index changes in the modulator arms. The variation of the refractive index in the modulator arms induces a change of material propagation constant β, resulting in different phases in both modulator arms. The input optical signal E_0 is divided by a 3-dB coupler into two equal parts E_1, E_2, which propagate in lower and upper arm of the MZM (Fig. 2.2a):

$$E_1 = E_2 = \frac{E_0}{\sqrt{2}}\exp(j\omega t) \tag{2.5}$$

If no electrical field is applied, both signals arrive at the same time (in-phase) at the MZM output and interfere constructively. If an electrical filed is applied, signals in different arms are shifted in phase relative to each other and the MZM output signal E_{out} is given by [33]:

$$\begin{aligned} E_{out} &= \frac{1}{\sqrt{2}}\left(E_1\exp\left(j\Delta\Phi_1\right) + E_2\exp\left(j\Delta\Phi_2\right)\right) \\ &= E_0\cos\left(\frac{\Delta\Phi}{2}\right)\exp\left(j\left(\omega t - \frac{\Delta\Theta}{2}\right)\right) \end{aligned} \tag{2.6}$$

with

$$\Delta\Phi = \Delta\Phi_2 - \Delta\Phi_1 \qquad (2.7)$$
$$\Delta\Theta = \Delta\Phi_2 + \Delta\Phi_1$$

Depending on the phase difference $\Delta\Phi$ between the MZM arms, the signals can interfere constructively or destructively, resulting in an amplitude modulation of the modulator input signal. The power of the generated optical signal at the MZM output is:

$$P_{out} = P_0 \cos^2 \frac{\Delta\Phi}{2} = \frac{1}{2} P_0 \left(1 + \cos \Delta\Phi\right) \qquad (2.8)$$

The P_{out}/P_{in} relation denotes the power transfer function of MZM (Fig. 2.2b) characterized by the power dependence on the phase difference $\Delta\Phi$. Thereby, $\Delta\Phi$ describes the operating characteristic (bias-point) of the MZM. Conventional MZMs are biased at the "quadrature" ($\Delta\Phi = \frac{\pi}{2}$) point, while biasing at the "zero"-point ($\Delta\Phi = 2\pi$) enables the generation of improved modulation formats (see Chapter 3). Considering an electrical field applied at the MZM, $\Delta\Phi$ can be defined as:

$$\Delta\Phi = \frac{\pi V_m}{V_\pi} \qquad (2.9)$$

where V_m is the voltage applied to the modulator and V_π is the voltage required to obtain an internal phase difference of π. Typical V_π values in 40 Gb/s MZMs are smaller than 3 V [34]. The amplitude modulation in MZM is accompanied by a phase modulation, which results in an internal modulator chirp given by [35]:

$$\frac{d\Theta}{dt} = \frac{\alpha}{2} \cdot \frac{1}{P_{out}} \cdot \frac{dP_{out}}{dt} \qquad (2.10)$$

with α (α-parameter of the MZM) determining the amount and the sign of the frequency chirping. By a combination of α parameter and MZM transfer function, different values of internal chirp can be realized. If the α-parameter is positive, the frequency chirp is positive at the leading edge of the pulse, resulting in a frequency increase (blue-shift). The α-parameter is defined as [36]:

$$\alpha = \frac{\Delta n_1 + \Delta n_2}{\Delta n_1 - \Delta n_2} \cdot \cot\left(\frac{\pi V_m}{2V_\pi}\right) \qquad (2.11)$$

where $\Delta n_1, \Delta n_2$ represent the index changes per volt in the MZM arms. The first term in Eq. 2.11 describes the intrinsic symmetry of the modulator function and the second term describes the α dependence of the operating point (Fig. 2.2b). The first part of Eq. 2.11 is also known as chirp parameter δ:

$$\delta = \frac{\Delta n_1 + \Delta n_2}{\Delta n_1 - \Delta n_2} \qquad (2.12)$$

The internal chirp of the MZM can be used to reduce dispersion induced penalty in the transmission line [37]. Thereby, the modulator internal chirp has to possess the opposite sign to the dispersion induced chirp. Typical chirp values α for commercially available MZMs are 0, 0.7 or -0.7. The MZM based 40 Gb/s external modulators are characterized by large extinction ratios (15-25 dB) [34], low insertion losses (< 6 dB) [38], [39] and a relatively large bandwidth (> 20 GHz) [40]. The drawback of the MZM concept is usually a strong polarization dependence of the device, with the consequence that a polarization maintaining fiber (PMF) has to be used to connect the modulator to the laser source.

2.2.3 Electroabsorption Modulator (EAM)

The most important advantage of EAM modulators, compared to MZMs is the fact that EAMs are made in a similar process as semiconductor lasers and can be monolithically integrated with a laser source (e.g.

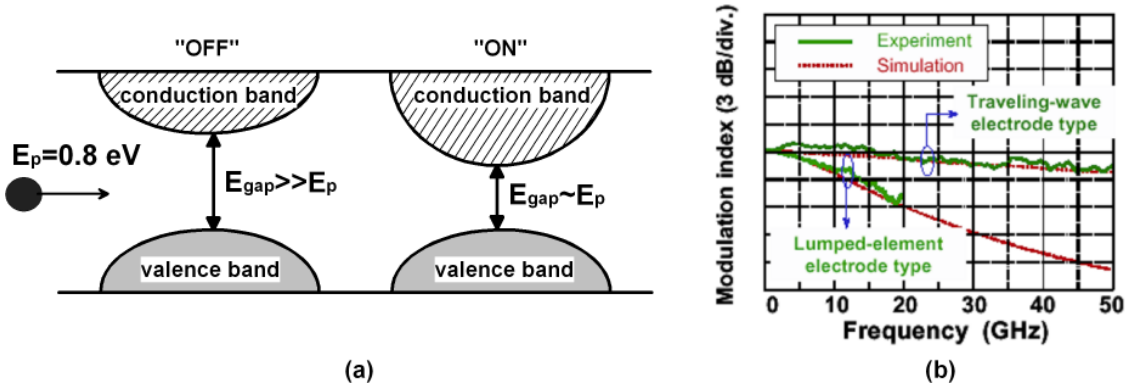

Figure 2.3: Electroabsorption modulator (EAM) principles: a) principles of operation b) modulation response differences between different MZM concepts [41]

DFB) on single chip. The EAMs are traditionally called loss modulators, because their operation is based on variation of the absorption coefficient of semiconductor based materials. The modulation characteristics of EAMs can be realized by two basic physical mechanisms: the Franz Kaldysh effect (FKE) and quantum-confined Stark effect (QCSE). The Franz Kaldysh effect refers to the variation of the absorption coefficient of a bulk semiconductor medium by applying an electrical field. If no electrical field is applied, the energy gap between the valence and conduction band is larger that the photon energy E_P (Fig. 2.3). In this case, the incoming light passes through the EAM structure. If an electric field is applied, the energy gap between the bands shrinks and an absorption of the incoming light occurs. Thus, the amplitude modulation of the laser light is realized by the variation of the electrical field over the EAM. In order to realize a FKE-based EAM, the materials (e.g. InP) are used with an energy band gap larger than a light energy. Since EAM absorption coefficients can be varied significantly by the applied electrical field, this mechanism for external modulation is quite efficient and fast. The conventional EAMs are fabricated using this technique.
The quantum-confined Stark effect (QCSE) occurs in quantum-wells, which are realized as a combination of two different materials (e.g. InGaAs and InP), whose energy bands form a quantum well [22] by the spatial overlap of the valence bands. The overlaps between the valence bands can be improved by use of multiple quantum well (MQW) structures. The incoming light in a MQW-EAM delivers the energy needed for an electron from the valence band to reach the conduction band. This electron interacts with a hole created in the valence band in form of an exciton state. The basic characteristic of the exciton state is a sharp absorption peak at the shorter wavelength. By applying an electrical field to MQW-EAMs, the exction peak is shifted to longer wavelengths and it broadens, resulting in a large absorption coefficient of the MQW-EAM structure. The variation of absorption coefficient in MQW-EAMs is 5 to 10 times larger than in FKA-based EAMs, resulting in a better extinction ratio.
The benefits of 40 Gb/s EAMs are possible integration with DFB lasers (e.g. EAM-DFBs) [42], high extinction ratios at small peak-to-peak drive voltage [43], [44], [45] and a large bandwidth >40 GHz [46], [47]. The modulator bandwidth can be further enhanced by some specific EAM structures (e.g. traveling-wave EAM (TW-EAM)) [41], which enable a bandwidth larger than 50 GHz (Fig. 2.3b) and an improved efficiency-speed relation [48]. Contrary to MZMs, which can be fabricated chirp free, the modulator chirp of EAMs caused by the variations of the propagation index due to variations of the absorption coefficient is large and induces wavelength shifts on the trailing and falling edge of the optical signal [49]. EAM chirp can be used to cancel the dispersion impact in the optical fiber [50]. The drawback of EAMs is a large device loss (> 12 dB) caused by a large attenuation coefficient of the EAM material (15-20 dB/mm).

2.3 Optical fibers

The propagation of optical fields in dielectric fibers can be described by Maxwell's equations:

$$\nabla \times \mathbf{E} = -\frac{\partial \mathbf{B}}{\partial t} \tag{2.13}$$

$$\nabla \times \mathbf{H} = \mathbf{J} + \frac{\partial \mathbf{D}}{\partial t} \tag{2.14}$$

$$\nabla \cdot \mathbf{D} = \rho_f \tag{2.15}$$

$$\nabla \cdot \mathbf{B} = 0 \tag{2.16}$$

where $\mathbf{E}$ and $\mathbf{H}$ are the electric and magnetic field vectors and $\mathbf{D}$ and $\mathbf{B}$ are the electric and magnetic flux densities. $\mathbf{J}$ represents the current density vector and ρ_f is the charge density. The flux densities $\mathbf{D}$ and $\mathbf{B}$ are caused by the propagation of $\mathbf{E}$ and $\mathbf{H}$ inside the medium:

$$\mathbf{D} = \varepsilon \mathbf{E} + \mathbf{P} \tag{2.17}$$

$$\mathbf{B} = \mu_0 \mathbf{H} + \mathbf{M} \tag{2.18}$$

where ε_0 is vacuum permittivity, μ_0 is the vacuum permeability and $\mathbf{P}$ and $\mathbf{M}$ are the induced electric and magnetic polarizations. Using the Maxwell's equations, the propagation of light in the optical fiber can be described [23] as:

$$\nabla^2 \mathbf{E} - \frac{1}{c^2}\frac{\partial^2 \mathbf{E}}{\partial t^2} = -\mu_0 \frac{\partial^2 \mathbf{P}(\mathbf{E})}{\partial t^2} \tag{2.19}$$

where $\mathbf{P}$ is the polarization of the medium, which is dependent on the electrical field and in a weak nonlinear medium it can be expressed by a Taylor polynomial:

$$\mathbf{P} \approx \varepsilon_0 \left\{ \underbrace{\chi^{(1)}\mathbf{E}}_{\mathbf{P}_L} + \underbrace{\chi^{(2)} : \mathbf{EE} + \chi^{(3)} : \mathbf{EEE}}_{\mathbf{P}_{NL}} \right\} \tag{2.20}$$

where the parameter $\chi^{(i)}$ is the susceptibility of the medium. The term $\chi^{(1)}$ is the linear susceptibility describing the linear part ($\mathbf{P}_L$) of polarization. The nonlinear part ($\mathbf{P}_{NL}$) is determined by the second and third order tensors $\chi^{(2,3)}$, which determine the nonlinear behaviour of the medium. $\chi^{(2)}$ can be neglected in optical fibers because of the inversion symmetry at the molecular level [23]. Thus, $\chi^{(3)}$ governs the nonlinearities in the fiber. The real part of $\chi^{(3)}$ is responsible for the Kerr effect (Chapter 2.4.1) and the imaginary part for the stimulated processes (Chapter 2.4.2).
Considering x-polarized light propagation in z direction, the electric field of the signal is given by [23]:

$$\mathbf{E} = \mathbf{e}_x F(x,y)\frac{1}{2}A(z,t)\exp(j\omega_0 t - j\beta(\omega)z) + c.c \tag{2.21}$$

where $F(x,y)$ is the modal distribution of the fundamental fiber mode, $A(z,t)$ is the field amplitude, ω_0 the carrier frequency and $\beta(\omega)$ is the propagating constant given by:

$$\beta(\omega) \approx \beta_0 + \beta_1(\Delta\omega) + \frac{\beta_2}{2}(\Delta\omega)^2 + \frac{\beta_3}{6}(\Delta\omega)^3 \tag{2.22}$$

From Eq. 2.19, the scalar propagation equation can be derived by applying the slowly varying envelope and rotating wave approximations yielding partial differential equation known as the nonlinear Schrödinger

equation (NLSE) [23]:

$$\begin{aligned}\frac{\partial}{\partial z}A(z,t) &= -\underbrace{\frac{\alpha}{2}A(z,t)}_{attenuation} + \underbrace{j\frac{\beta_2}{2}\frac{\partial^2}{\partial T^2}A(z,t)}_{\text{1.order GVD}} \\ &+ \underbrace{\frac{\beta_3}{6}\frac{\partial^3}{\partial T^3}A(z,t)}_{\text{2.order GVD}} - \underbrace{\frac{\gamma}{\omega_0}\frac{\partial}{\partial t}(|A(z,t)|^2A(z,t)}_{self-steepening} \\ &- \underbrace{j\gamma|A(z,t)|^2A(z,t)}_{Kerr\,effect} - \underbrace{j\gamma T_R\frac{\partial}{\partial T}|A(z,t)|^2A(z,t)}_{SRS}\end{aligned} \tag{2.23}$$

where α represents the fiber attenuation, T is measured with the frame of reference moving with the pulse at group velocity ν_g (T=t-z/ν_g), T_R refers to the slope of the Raman gain (Chapter 2.4.2), and γ is the nonlinear coefficient of the fiber (Chapter 2.3.2). The terms on the left side of Eq. 2.23 describe the fiber propagation limitations divided in two groups: the linear - attenuation and GVDs - and nonlinear - Kerr effect, self-steepening and stimulated Raman scattering (SRS)- group. In the following chapters, these effects will be further described. The self-steepening is a higher order nonlinear effect, which originates from the intensity dependence of the group velocity [23]. Since it occurs only for ultra-short optical pulses with widths smaller than 1 ps [23], this effect is not considered in investigations presented in this work.

2.3.1 Linear fiber characteristics

The linear fiber characteristics comprises fiber attenuation, chromatic dispersion (GVD) and polarization mode dispersion (PMD). These fiber characteristics dominate the behaviour of an optical transmission system in the low power transmission region and in interaction with nonlinear effect in high power region limit the maximum transmission distance of the system.

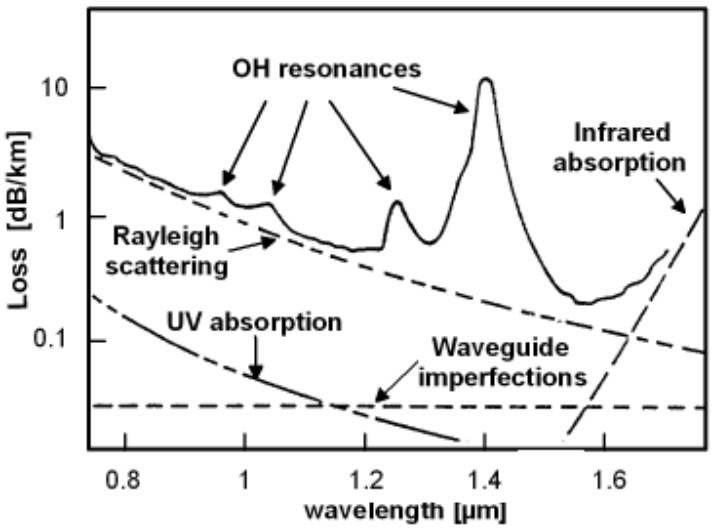

Figure 2.4: Loss spectra of silica single mode fiber [51]

Fiber attenuation

The light propagation in optical fibers is characterized by reflections on the core-cladding boundary. These reflections are caused by difference between the refractive indices of the core and the cladding. The signal propagation in an optical fiber is always accompanied by loss of the input power $P(0,t)$. The signal power after propagation through a fiber length z is given by:

$$P(z,t) = P(0,t) \cdot \exp(-\alpha z) \tag{2.24}$$

The parameter α is called fiber attenuation and represents a sum of different losses in the fiber. The conventionally used unit for α is [dB/km] (derived from Eq. 2.24):

$$\alpha\,[\mathrm{dB/km}] = -\frac{10}{z}\log_{10}\left(\frac{P(z,t)}{P(0,t)}\right) = 4.343 \cdot \alpha\ \left[\mathrm{km}^{-1}\right] \tag{2.25}$$

The attenuation exhibited by the optical fiber is dependent on the wavelength of the propagating signal. A typical loss spectrum of a silica fiber is presented in Fig. 2.4. The total loss is caused fundamentally by three different mechanisms: material absorption, Rayleigh scattering and waveguide imperfections. Considering material absorption, it can be differentiated between intrinsic and extrinsic absorption losses. The intrinsic losses are caused by the absorption of the incoming light by electron and molecular-vibrational resonances. In silica based fibers, the electron resonances occur in the ultraviolet region (λ <0.4 μm)(Fig. 2.4) whereas the molecular resonances take place in infrared region ($\lambda > 7\,\mu m$)(Fig. 2.4). The key resonances occur at wavelengths far from 1.55 nm, which is the wavelength relevant for conventional transmission systems, because of low total attenuation in this region. However due to the amorphous structure of silica fibers, the higher harmonics cause attenuation in the low wavelength region. The extrinsic absorption losses are caused by the presence of material impurities induced during the fabrication. The impurities (e.g. Fe, Cu, Co) give rise to an increased absorption in a specific wavelength region. Water vapor (OH-ion) presents the most important impurity in conventional fibers, whose increased concentration causes a significant increase of absorption. The vibrational resonances of OH-ions occur near 2.73 μm with higher harmonics at 1.39 μm, 1.24 μm and 0.95 μm (Fig. 2.4). The OH resonance at 1.39 μm can be efficiently suppressed by an improvement of the manufacturing process. Recently presented, so called *dry fibers* realized by the reduction of OH concentration have an absorption loss below 0.5 dB at 1.39 μm [51]. Rayleigh scattering represents the most dominant loss mechanism especially near 1.55 μm (Fig. 2.4). The Rayleigh scattering is caused by molecular density fluctuations in the optical fiber. The density fluctuations cause scattering of the incoming light. The scattering characteristic is similar to the Hertz dipole [52], where the scattering cross section varies with λ^4. The total loss α_R caused by Rayleigh scattering is given by [51]:

$$\alpha_R = \frac{C}{\lambda^4} \tag{2.26}$$

where C represents the Rayleigh constant varying between 0.8-1.2 $\left[\mathrm{dB \cdot km^{-1} \cdot \mu m^4}\right]$ for various lightguide compositions [53]. Large α_R values (0.12-0.15 dB/km)[23] near 1.55 μm indicate Rayleigh scattering as the most important loss source in this wavelength region. A small amount (< 0.05 dB/km) of fiber attenuation is caused by waveguide imperfections (Fig. 2.4) due to the imperfection of the core-cladding boundary. Additional losses may occur due to fiber splices and when multiple fibers are put into fiber bands [23].

Chromatic dispersion in single mode fibers

One of the most important features of the optical transmission is the signal broadening during propagation of different spectral components in an optical fiber. This phenomenon known as chromatic dispersion refers to propagation time differences in the fiber. This can be understand as a frequency dependence of the refractive mode index which causes different spectral components of the pulse to propagate at different group velocities. Accordingly, chromatic dispersion is known as group-velocity dispersion (GVD). The consequence of chromatic dispersion is the broadening of the single pulse and interference between adjacent pulses known

as inter-symbol-interference (ISI).
The group velocity v_g is given by:

$$v_g = \frac{1}{\frac{d\beta}{d\omega}} = \frac{c}{n_g} \tag{2.27}$$

with the propagation constant β given as:

$$\beta = nk_0 = n\frac{\omega}{c} \tag{2.28}$$

and the group index parameter n_g:

$$n_g = n + \omega\left(\frac{dn}{d\omega}\right) \tag{2.29}$$

The total pulse broadening ΔT after a propagation through a fiber with a length L is:

$$\Delta T = \frac{dT}{d\omega} \cdot \Delta\omega = \frac{d}{d\omega}\left(\frac{L}{v_g}\right) = L\frac{d^2\beta}{d\omega^2}\Delta\omega = L\beta_2\Delta\omega \tag{2.30}$$

with $\Delta\omega$ describing the spectral width of the pulse and β_2 defined as GVD parameter. Equation 2.30 transformed into wavelength terms according to $\omega = 2\pi c/\lambda$ becomes:

$$\Delta T = \frac{d}{d\lambda}\left(\frac{L}{v_g}\right)\Delta\omega = DL\Delta\lambda \tag{2.31}$$

where D represents the dispersion parameter in [ps/nm·km] given by:

$$D = \frac{d}{d\lambda}\left(\frac{1}{v_g}\right) = -\frac{2\pi c}{\lambda^2}\beta_2 \tag{2.32}$$

The chromatic dispersion can be understood as the sum of material and waveguide dispersion:

- **Material dispersion** occurs due to the changes of the refractive index of optical fiber with optical frequency. This effect can be understood as the interaction between the propagating optical field and the electrons and molecules of the fiber material resulting in a frequency dependent change of the refractive index. In the relevant wavelength region for optical transmission (around 1.55 μm), the refractive index of the fiber core can be approximated by the Sellmeier-series [52]:

  $$n^2(\omega) = 1 + \sum_{i=1}^{K}\frac{S_i \cdot \omega_i^2}{\omega_i^2 - \omega^2} \tag{2.33}$$

  with ω_i describing the i-th resonance frequency and S_i is the Sellmeier-parameter describing the resonator strength. A sufficient description of n can be achieved if two ultraviolet and one infrared resonances are considered (K=3). The wavelength dependent changes of n results in changes of the group mode index n_g (Fig. 2.5a). The material dispersion D_M refers to the slope of the group velocity index n_g over wavelength and according to Eq. 2.32 can be given as:

  $$D_M = \frac{1}{c}\frac{dn_g}{d\lambda} \tag{2.34}$$

  The slope of n_g equals zero at $\lambda = 1.276\,\mu$m (Fig. 2.5a). This wavelength is called zero-dispersion wavelength λ_{ZD}, and depending on the doping of core and cladding, it varies between 1.27-1.29 μm. D_M is negative for $\lambda < \lambda_{ZD}$ and positive for $\lambda > \lambda_{ZD}$ (Fig. 2.5a).

- **Waveguide dispersion** is the consequence of the frequency dependent mode propagation constant at the code-cladding interface. Considering the propagation constants of the core $\beta_1 = k_0 n_1$ and the cladding $\beta_2 = k_0 n_2$, the optical field at lower frequencies propagates in the cladding and the field

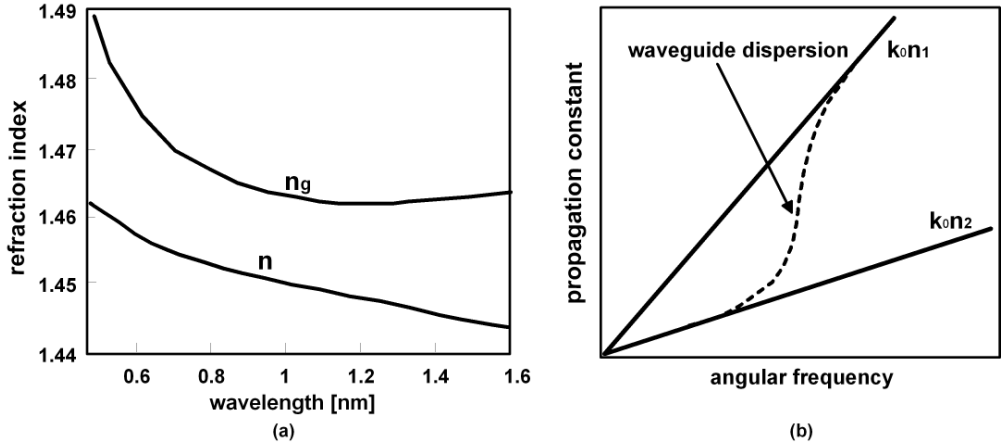

Figure 2.5: Dispersion types: a) material dispersion - refractive index n and group index n_g versus wavelength b) waveguide dispersion - propagation constant versus angular frequency

with higher frequency in the core. In the frequency region where the transition between core and cladding takes place, the frequency dependent mode propagation constant β_{mode} indicates a curvature in its distribution which represents the origin of waveguide dispersion D_W (Fig. 2.5b). Accordingly, the amount of D_W is dependent on the fiber profile which is described by the fiber parameter V [22]:

$$V = k_0 a \sqrt{n_1^2 - n_2^2} \tag{2.35}$$

where a stands for the fiber core radius. Assuming an equal wavelength dependence of refractive indices n_1 and n_2

$$\frac{dn_1}{d\omega} = \frac{dn_2}{d\omega} \tag{2.36}$$

the waveguide dispersion D_W is given by [51]:

$$D_W = -\frac{2\pi\Delta}{\lambda^2}\left[\frac{n_g^2}{n\omega}\frac{Vd^2(Vb)}{dV^2}\right] \tag{2.37}$$

with Δ representing the refractive index difference and b the normalized propagation constant:

$$b = \frac{\frac{\beta}{k_0} - n_2}{n_1 - n_2} \tag{2.38}$$

Due to the fact that D_W depends on the core radius and the index difference Δ, the waveguide dispersion D_W can be tuned to create fibers with flattened or shifted total dispersion (Fig. 2.6a).

The total fiber dispersion varies for a conventional standard single mode fiber (SSMF) in the $1.55\,\mu m$ region between 16-20 [ps/nm·km]. The λ_{ZD} of D_M and of the total fiber dispersion can be shifted in the wavelength range between 1.3-1.6 μm. By the variation of D_W, fibers with a flattened dispersion characteristic and shifted λ_{ZD} can be realized at $1.55\,\mu m$ (Fig. 2.6b). The larger shifts of λ_{ZD} enable positive GVD parameter β_2 making possible the fabrication of dispersion compensating fibers (DCF). For the realization of dispersion modified fibers, multiple cladding layers and a precise tailoring of the fiber profile is essential.
The additional propagation impairments occur due to wavelength dependence of chromatic dispersion. This effect is known as differential dispersion or dispersion slope S:

$$S = \frac{dD}{d\lambda} = \left(\frac{2\pi c}{\lambda^2}\right)^2 \beta_3 + \left(\frac{4\pi c}{\lambda^3}\right)\beta_2 \tag{2.39}$$

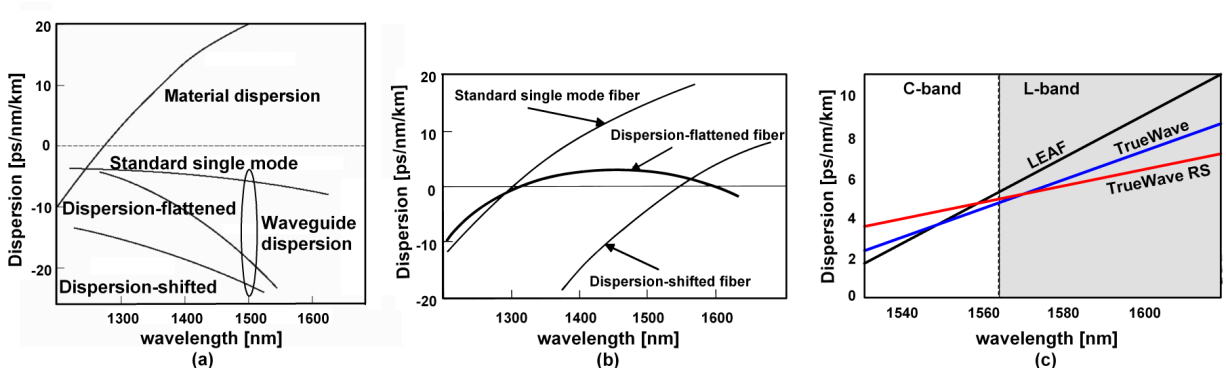

Figure 2.6: Dispersion in optical fibers: a) material and waveguide dispersion [51] b) total fiber dispersion [51] c) novel fiber types [54]

where $\beta_{2,3}$ are the derivatives of the propagation constant $\beta(\omega)$ which can be described for $\Delta\omega \ll \omega_0$ as a Taylor series around the center frequency ω_0:

$$\beta(\omega) \approx \beta_0 + \beta_1(\Delta\omega) + \frac{\beta_2}{2}(\Delta\omega)^2 + \frac{\beta_3}{6}(\Delta\omega)^3 \tag{2.40}$$

with

$$\Delta\omega = \omega - \omega_0 \tag{2.41}$$

$$\beta_m = \left(\frac{d^m\beta}{d\omega^m}\right)_{\omega=\omega_0} \tag{2.42}$$

The slope parameter S represents an important issue in transmission systems with the large system bandwidth, resulting in a large accumulated residual dispersion for wavelengths different from ω_0. Recently presented transmission fibers (Fig. 2.6c) show a reduced dispersion slope.
For the analytical estimation of the GVD impact, the following formulation is used [51]:

$$\Delta T = \beta_2 \cdot L \cdot \Delta\omega \leq \frac{T_B}{4} \text{ or } \Delta T \cdot B \leq \frac{1}{4} \tag{2.43}$$

where T_B is the pulse width (assuming non return-to-zero (NRZ) pulses) and $B{=}1/T_B$ is the signal bit rate. According to Eq. 2.43 the pulse broadening has to be less than a quarter of the original pulse width implying:

$$\beta_2 \Delta\omega B L \leq \frac{1}{4} \tag{2.44}$$

Equation 2.44 is used for the definition of the bit-rate-length product:

$$B \cdot L \ll \frac{c}{4\lambda^2 D \Delta f_{sig}} \tag{2.45}$$

where Δf_{sig} represents the signal bandwidth which, depending on the modulation of the optical signal, is defined as:

$$\Delta f_{sig} = \xi^{-1} \cdot \frac{B}{2} \tag{2.46}$$

where parameter ξ differs for different modulation formats. With Eqs. 2.45 and 2.46 the bit-rate-length product is given by:

$$B^2 \cdot L \leq \xi \frac{c}{2\lambda^2 D} \tag{2.47}$$

Fiber type single mode	D [ps/nm km]	S [ps/$(nmkm)^2$]	attenuation α [dB/km]	γ [1/W/km]	A_{eff} [μm^2]
SSMF	16..20	0.09	0.22	1.317	80
LEAF	2..6	0.06	≤ 0.25	1.46	72
TrueWave-RS	2.6..6	0.05	≤ 0.5	2.1	50
DCF	-50..-230	0.3..0.8	0.3..0.8	3..5	15..30

Table 2.1: Typical parameter of conventional fibers

With an increased channel bit rate, the total length of a dispersion limited systems becomes reduced. For a transmission system employing intensity modulation of optical pulses, the bit-rate-length product is given by [51]:

$$B^2 \cdot D \cdot L \leq 104000 \left[\frac{\text{Gbit}^2\text{ps}}{\text{nm}}\right] \tag{2.48}$$

Polarization mode dispersion (PMD)

Polarization mode dispersion (PMD) represents another dispersion type, which becomes important with the increased channel data rates [55], [56], [57]. The origin of PMD lies in the fiber core asymmetry or stress (Fig. 2.7). The degenerate nature of the orthogonally polarized modes holds only for an ideal cylindrical core with a uniform diameter over the fiber length [51]. In the real world, the realization of an ideal fiber symmetry represents a critical issue. The fiber asymmetry may be inherent in the fiber from the manufacturing process, or it may be a result of mechanical stress on the deployed fiber. The inherent asymmetries of the fiber are fairly constant over time, while the mechanical stress can vary, resulting in a dynamic aspect of PMD. The mechanical stress on the optical fiber originates from a variety of sources, e.g. day/night and seasonal heating and cooling of the optical fiber, and can be also caused by nearby sources of vibration, e.g. railway, wind.

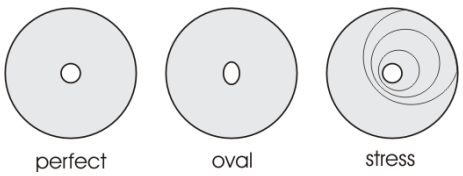

Figure 2.7: PMD causes - fiber core imperfections

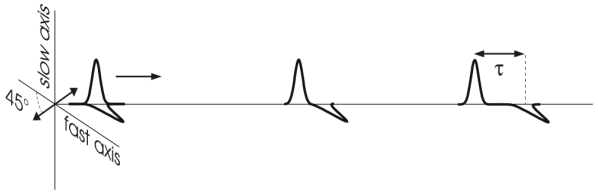

Figure 2.8: Pulse splitting due to birefringence

Considering the pulse propagation in the fiber, it can be distinguished between two orthogonal polarization axes called principle states of polarization (PSPs) (Fig. 2.8). These axes are not necessarily in the vertical and horizontal planes. In fact, their random orientation depends upon the stresses in the fiber. The light polarized along one of the axes experiences a different refractive index than light polarized along the other axis. This effect is known as birefringence. As the index of refraction is a measure of how fast light moves through the material, the linear-polarized light launched into one principal axis travels through the fiber faster than the light launched into the other axis. It also means that the relative phase of the light in the two axes changes as it propagates along the fiber. This phase difference changes the overall state of polarization (SOP) of the light leaving the fiber (Fig. 2.9). An optical pulse with the polarization aligned with one of the principal axes emerges at the fiber output in the same state of polarization without any PMD impact. For a pulse with randomly oriented polarization, one part of the pulse is transmitted along one of the principal axes, and the other part is transmitted along the other principal axis. The received pulse becomes broadened, because the two parts arrive with a delay time $\Delta\tau$, called differential group delay (DGD)(Fig. 2.8). The total pulse

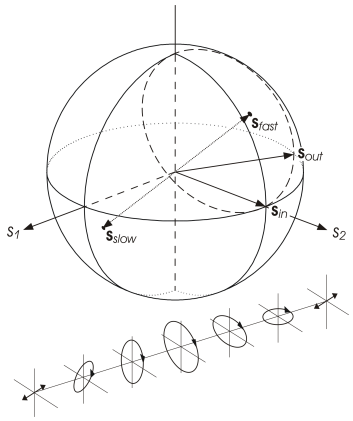

Figure 2.9: Evaluation of output signal polarization (s_{out}) along a birefringent element

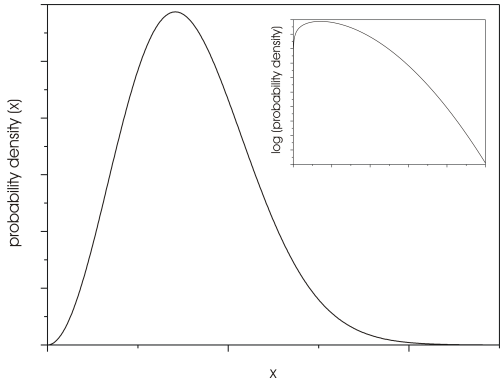

Figure 2.10: Maxwellian distribution of probability density function (PDF(x), with $x = \Delta\tau/\langle\Delta\tau\rangle$)

broadening due to PMD can be estimated from the time delay $\Delta\tau$ between the two polarization components (Fig. 2.8). In a fiber with length L, the DGD is given by [51]:

$$\Delta\tau = \left|\frac{L}{\nu_{gx}} - \frac{L}{\nu_{gy}}\right| = L\left|\beta_{1x} - \beta_{1y}\right| = L\Delta\beta_1 = L\frac{\omega\Delta n_g}{c} \tag{2.49}$$

where x and y are the two orthogonal polarized fiber modes and $\Delta\beta_1$ is group delay difference related to the fiber birefringence. The DGD between the polarization states in a non-polarization preserving fiber is a random variable, with a mean value $\langle\Delta\tau\rangle$. The time-averaged DGD between the two orthogonal SOPs in a fiber can be defined as:

$$\langle\Delta\tau\rangle = D_{PMD}\sqrt{L} \tag{2.50}$$

where D_{PMD} stands for the fiber PMD parameter, measured in $[\mathrm{ps}/\sqrt{\mathrm{km}}]$, and L is the fiber length. Typical values of D_{PMD} are in the range of 0.1 to 1 $[\mathrm{ps}/\sqrt{\mathrm{km}}]$, although in old fibers D_{PMD} larger than 1 $[\mathrm{ps}/\sqrt{\mathrm{km}}]$ can occur. Nowadays, fiber manufactures offer fibers with D_{PMD} smaller than 0.05 $[\mathrm{ps}/\sqrt{\mathrm{km}}]$ [58], [54]. For fiber lengths in excess of a few km with strong random polarization mode coupling, the DGD can be modeled as having a Maxwellian distribution [59] (Fig. 2.10) with a probability density function (PDF) defined as [60]:

$$PDF(\Delta\tau) = 32\frac{\Delta\tau^2}{\pi^2\langle\Delta\tau\rangle^3}\exp\left[\frac{-4\Delta\tau^2}{\pi\langle\Delta\tau\rangle^2}\right] \tag{2.51}$$

where $\Delta\tau$ represents the DGD and $\langle\Delta\tau\rangle$ is its mean value. At a given time instant, the system will experience a specific $\Delta\tau$. The instantaneous value of $\Delta\tau$ depends on the spatial fluctuations of the PSPs and the relative orientation of the input SOP to the PSPs. Due to a statistical nature of PMD the relation between the maximum allowable DGD in the system and mean DGD shows a probabilistic nature (Maxwell statistics). The maximum DGD for a transmission line is defined as a DGD value, which can be tolerated by the system and which causes a maximum sensitivity degradation of 1 dB. In ITU-T recommendations [61], the ratio between maximum and mean DGD values is determined for a certain outage probability (Table 2.2). The outage probability can be understood as the probability of exceeding the mean DGD $\langle\Delta\tau\rangle$. Integrating Eq. 2.37 from $\Delta\tau_1$ to ∞ gives the outage probability P($\Delta\tau \geq \Delta\tau_1$):

$$P(\Delta\tau \geq \Delta\tau_1) = \int_{\tau_1}^{\infty} PDF(\Delta\tau)d(\Delta\tau) \tag{2.52}$$

Due to the statistical behavior of PMD, the maximum admissible DGD should be no larger than one-tenth of the bit-length [61]:

$$\langle \Delta\tau \rangle \leq \frac{T_{bit}}{10} \tag{2.53}$$

Setting $T_{bit} = 1/B$ in Eq. 2.53 yields:

$$L \leq \frac{1}{100 \cdot B^2 \cdot D_{PMD}^2} \tag{2.54}$$

Figure 2.11 shows how important PMD effects in the transmission line can be. The impact of PMD becomes important with an increasing channel data rate. The maximum PMD value in a 40 Gb/s systems has to be less than 0.1 ps/$\sqrt{\text{km}}$ in order to achieve a maximum transmission distance longer than 1000 km. The same PMD value in 10 Gb/s case increases the transmission distance by a factor of 10. For the realization of 160 Gb/s transmission, the use of PMD compensators [62], [63] becomes mandatory for distances larger than 100 km.

$\Delta\tau_1/\langle\Delta\tau\rangle$	Outage probability
3.0	4.2×10^{-5}
3.5	7.7×10^{-7}
4.0	7.4×10^{-9}

Table 2.2: Outage probabilities [61]

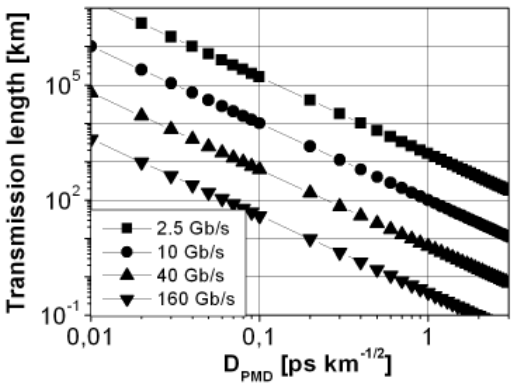

Figure 2.11: Impact of PMD on the maximum transmission distance

2.3.2 Fiber parameters

In this section, the typical parameters for characterization of the optical pulse propagation in single mode fibers are introduced. The nonlinear parameter γ, effective length L_{eff}, linear length L_D and nonlinear length L_{NL} give an insight into the dominant system limitations and represent efficient tools for determination of dominant system limitations in different pulse propagating regimes (e.g. linear, nonlinear, quasi-linear).

Nonlinear parameter

The nonlinear parameter γ describes the nonlinear changes of the propagation constant β due to the fact that the refractive index consists of a linear and a nonlinear part. It is defined as:

$$\gamma = \frac{n_2 \omega_0}{c A_{eff}} \tag{2.55}$$

where c is the speed of light in vacuum, n_2 the nonlinear refractive index, and A_{eff} is the effective core area given by:

$$A_{eff} = \frac{\int\int_{-\infty}^{\infty} |F(x,y)|^2 dxdy}{\int\int_{-\infty}^{\infty} |F(x,y)|^4 dxdy} \tag{2.56}$$

$F(x,y)$ represents the modal field distribution of the fundamental fiber mode [23]. Depending on the fiber type, A_{eff} values vary between 20-100 μm^2. Large A_{eff} values can be beneficial for the reduction of γ and limiting nonlinear impacts in the fiber. Typical γ values in conventional fibers vary in the range of 1-10 W^{-1}/km.

Effective fiber length

The effective fiber length L_{eff} describes the nonlinear impact in dependence of the fiber length and attenuation. L_{eff} describes the length of the fiber without attenuation, which causes the same nonlinear impact as a fiber with length L and with attenuation α [51]:

$$P_0 \cdot L_{eff} = \int_0^L P_0 \exp(-\alpha z) dz \tag{2.57}$$

with P_0 representing the fiber input power. After integration of Eq. 2.57, the L_{eff} is given by:

$$L_{eff} = \frac{1 - \exp(-\alpha L)}{\alpha} \tag{2.58}$$

Hence, L_{eff} depends on fiber attenuation and the spacing between optical amplifiers. For a typical system with α=0.22 dB/km and an amplifier spacing of 80 km, L_{eff} amounts approximately 19.4 km. In a multi-span system with identical span infrastructure the total effective length $L_{TOT,eff}$ is given as the sum of the effective lengths in each transmission span [31].

Linear and nonlinear length

The linear length L_D and nonlinear length L_{NL} represent helpful means for the characterization of the transmission behaviour and a determination of dominant system limitations. L_D and L_{NL} are defined as [51]:

$$L_D = \frac{T_0^2}{|\beta_2|} \tag{2.59}$$

$$L_{NL} = \frac{1}{\gamma P_0} \tag{2.60}$$

where T_0 is the initial pulse width, β_2 is the fiber propagation constant and P_0 the input optical peak power. Depending on the initial pulse width T_0 and the peak power P_0, either dispersive or nonlinear effects may dominate the pulse propagation along the fiber. By introducing L_D and L_{NL}, the pulse propagation can be categorized in four different propagation regimes, where either none of these effects are significant, one of the effects must be considered, or both linear and nonlinear effects have to be considered. L_D and L_{NL} determine the length over which the appropriate effect becomes important. It can be distinguished between following propagation regimes:

- $L << L_{NL}$ and $L << L_D$: The fiber length is much shorter than linear and nonlinear length so that neither dispersive nor nonlinear effects play a role. In this case the transmission is limited only by the fiber attenuation.
- $L << L_{NL}$ and $L \geq L_D$: The pulse evolution is governed by the fiber dispersion. The nonlinear impacts can be neglected.
- $L \geq L_{NL}$ and $L << L_D$: The pulse evolution is governed by nonlinear effects, resulting in a phase modulation and a spectral broadening of the signal spectrum.
- $L \geq L_D$ and $L \geq L_{NL}$: In this case dispersion and fiber nonlinearities act together. The transmission performance is limited by the dispersion-nonlinearity interplay.

2.4 Nonlinear processes

The nonlinear processes occurring in optical fibers are governed by the nonlinear susceptibility $\chi^{(3)}$ of the propagation media (Eq. 2.20). Basically, the nonlinear processes can be divided into in-elastic and elastic (parametric) processes (Fig. 2.12). The in-elastic processes are dependent on the imaginary part of $\chi^{(3)}$ and become evident above some specific power threshold level. The elastic processes known as Kerr nonlinearities are characterized by the dependence on the real part of $\chi^{(3)}$. The Kerr nonlinearities are self-phase modulation (SPM), cross-phase modulation (XPM), four-wave mixing (FWM) as well as inter-pulse processes such as intra-channel four-wave mixing (IFWM) and intra-channel cross-phase modulation (IXPM), which become important at increased channel bit rates. Stimulated Raman Scattering (SRS) and Stimulated Brilloin Scattering (SBS) are inelastic processes.

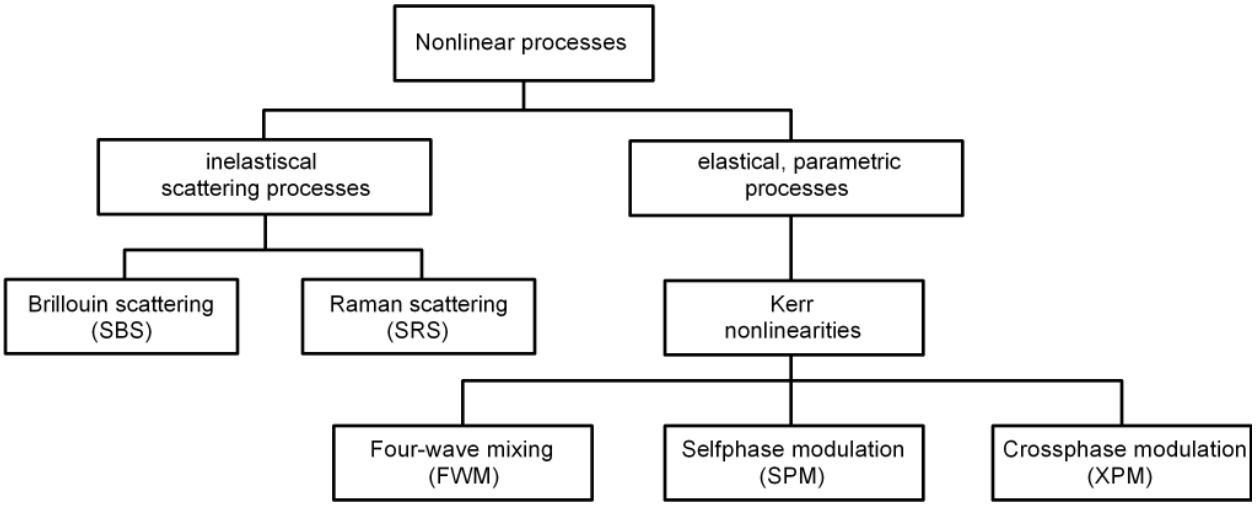

Figure 2.12: Nonlinear processes in optical transmissions

2.4.1 Kerr nonlinearities

The Kerr nonlinearities belong to the group of elastic parametric nonlinear processes in which the transmission fiber plays a passive role. The Kerr nonlinearities are characterized by the power dependent fiber refractive index $n(\omega, I)$. Depending on whether the refractive index fluctuations are caused by power in the single or neighboring channel, intra- and inter-channel nonlinearities can be differentiated. XPM and FWM are inter-channel or multi-channel nonlinearities. SPM, IFWM and IXPM are single-channel nonlinearities.

Self-phase modulation (SPM)

Self-phase modulation (SPM) is one of the nonlinear limitations caused by the Kerr-effect in optical fibers. SPM gives rise to phase modulation of the optical signal. This phase modulation results in a varying instantaneous frequency across the pulse, which can be seen as a nonlinear (SPM) chirp. Neglecting fiber attenuation and chromatic dispersion terms, the solution of the NLSE pulse propagation equation (Eq. 2.23) after a propagation over length L is given by [23]:

$$A(L,T) = A(0,T) \cdot \exp(j\phi_{SPM}(L,T)) \tag{2.61}$$

where A(0,T) is the normalized field amplitude at z=0 and the SPM-caused phase shift ϕ_{SPM} after a length L is defined as:

$$\begin{aligned} \phi_{SPM}(L,T) &= |A(0,T)|^2 \, (L_{eff}/L_{NL}) \\ &= \gamma P L_{eff} \end{aligned} \tag{2.62}$$

By the SPM-impact new spectral components are generated in the optical signal spectrum resulting in a spectral broadening. This spectral broadening can be explained as a time dependence of ϕ_{SPM} [23]. The time derivative of ϕ_{SPM} is SPM caused chirp $\Delta\omega_{SPM}$:

$$\Delta\omega_{SPM} = -\frac{\partial\phi_{SPM}}{\partial t} = -\gamma\frac{\partial P}{\partial t}L_{eff} \tag{2.63}$$

The quantity $\Delta\omega_{SPM}$ is proportional to the time derivative of the signal power P (Eq. 2.63). Correspondingly, the generation of new spectral components occur at the raising and trailing edges of the optical pulse (Fig. 2.13, Delta f equals to $\Delta\omega_{SPM}/2\pi$). The amount of generated chirp is larger for an increased steepness of the pulse edges.

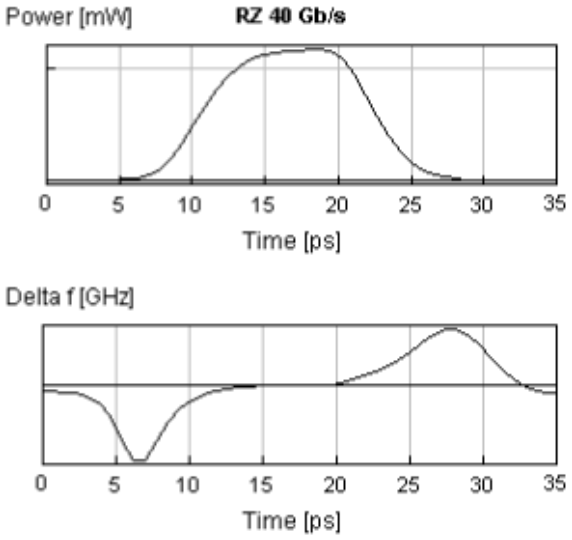

Figure 2.13: SPM induced signal changes

If SPM would occur without GVD in direct detection based transmission systems, it would not cause detectable degradations of the signal, since it causes phase modulation (PM) of the pulse. In a conventional transmission line, SPM is accompanied by GVD, which causes a PM-IM conversion, resulting in a signal amplitude distortion. The interplay between SPM and GVD depends on the local dispersion region in which pulse propagation takes place. In a "normal" dispersion regime (D<0 ps/nm·km), first-order GVD introduces a positive linear frequency chirp, which is superposed with a positive SPM chirp. In this case, the dispersion effects are stronger due to a broader optical spectrum and ISI-effects between consecutive pulses. In the "anomalous" dispersion regime (D > 0 ps/nm·km), first order GVD induces a negative frequency chirp, which can cancel the SPM induced chirp because of opposite chirp signs. The consequence is a length dependent pulse compression. The SPM-GVD interaction is exploited for a special transmission type called a soliton transmission [23]. For soliton transmission the relation between SPM and GDV has to be carefully tailored in order to enable a periodical pulse regeneration. Owing to this a careful dispersion management of the transmission line is required for a certain optical power. If further transmission impairments (e.g. amplification scheme, optical filtering, PMD) are considered, the fulfilling of soliton conditions becomes even more complicated.

Cross-phase modulation (XPM)

Contrary to SPM, where the nonlinear limitation is caused by optical power variations in a single channel, cross-phase modulation (XPM) is caused by power variations in the adjacent channels within a multi-channel system, resulting in a phase modulation. By first order GVD, XPM caused phase modulations are converted

to intensity distortions of the optical signal. If two copolarized propagating channels are considered, the NLSE (Eq. 2.23) has to be extended to two coupled equations. Neglecting the attenuation, the nonlinear interaction between two channels can be defined as [23]:

$$\frac{\partial A_1(z,t)}{\partial z} + \frac{j\beta_{21}}{2}\frac{\partial^2 A_1(z,t)}{\partial T^2} = j\gamma_1 \left(\underbrace{|A_1(z,t)|^2}_{SPM} + \underbrace{2|A_2(z,t)|^2}_{XPM} \right) A_1(z,t) \tag{2.64}$$

$$\frac{\partial A_2(z,t)}{\partial z} + d\frac{\partial A_2(z,t)}{\partial T} + \frac{j\beta_{22}}{2}\frac{\partial^2 A_2(z,t)}{\partial T^2} = j\gamma_2 \left(\underbrace{|A_2(z,t)|^2}_{SPM} + \underbrace{2|A_1(z,t)|^2}_{XPM} \right) A_2(z,t) \tag{2.65}$$

where T is a normalized time moving at velocity ν_g and d represents the difference between inverse group velocities in both channels known as "walk-off" length:

$$T = t - \frac{z}{\nu_{g1}} \tag{2.66}$$

$$d = \frac{1}{\nu_{g1}} - \frac{1}{\nu_{g2}} = D\Delta\lambda = -\frac{2\pi c}{\lambda^2}\beta_2\Delta\lambda \tag{2.67}$$

with ν_{g1}, ν_{g2} describing the group velocities of two adjacent channels and $\Delta\lambda$ representing the channel spacing. As can be seen from equations Eq. 2.64 and Eq. 2.65, XPM-caused phase shift ϕ_{XPM} is twice as large as the ϕ_{SPM} (Eq. 2.62):

$$\phi_{XPM} = 2\gamma_1 P_2 \Delta z \tag{2.68}$$

where $P_2 = |A_2(z,t)|^2$ represents the power in the interfering channel. The XPM effect is always accompanied by the SPM effect. For a separation of XPM from SPM, an efficient method is the "pump-probe" method, in which an intensity modulated channel (pump) with a large channel power distorts a CW-probe channel [64].

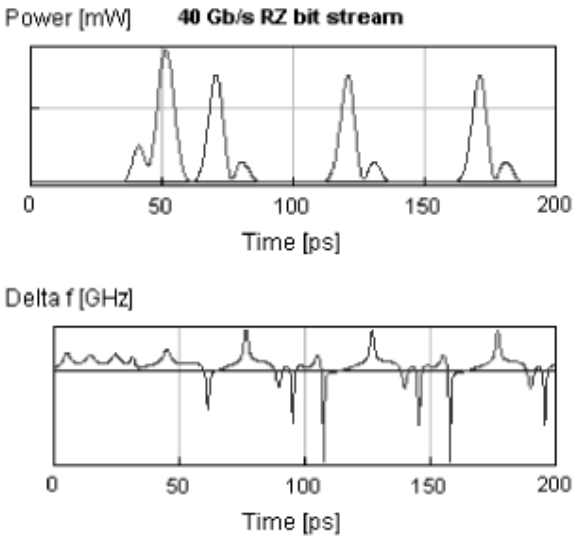

Figure 2.14: XPM induced changes in a bit stream

XPM introduces an asymmetrical broadening of the signal (Fig. 2.14) due to different amounts of chirp at the raising and the falling pulse edge. The effectiveness of XPM is determined by the channel power, the polarization relation, e.g. copolarized or orthogonally polarized, between the channels, the "walk-off"-length

(Eq. 2.67) and the nonlinear coefficient γ and dispersion of the transmission fiber. Due to its nonlinear nature, the XPM effect vanishes at smaller channel powers, but a reduced channel power results in a reduced maximum transmission distance because of ASE-noise impact in the transmission line. Considering the polarization relation between the channels, the worst case occurs for copolarized channels and the best case for orthogonal polarization between the channels suppressing the XPM impact by a factor of one third [64]. The "walk-off" length determines the propagation length needed for a total separation of two interacting pulses in adjacent channels due to a group-velocity mismatch between the channels. It is proportional to a channel separation $\Delta\lambda$ and a fiber dispersion D. Accordingly, for an efficient suppression of XPM, a large local fiber dispersion is desirable. Furthermore, XPM-induced signal distortions in dispersion shifted fibers (DSF) are larger than in standard single-mode fibers (SSMF) due to a smaller core area which determines the value of γ. On the other hand, the PM-IM conversion is lower in DSFs due to a lower fiber dispersion. The visible distortion of the signal caused by XPM are timing jitter, resulting in different arrival times of the optical pulses due to a frequency chirping, and amplitude jitter inducing a vertical signal level fluctuations. Besides its impact on the transmission quality, the XPM effect can be useful for generation of ultra-short pulses in pulse compressor devices [64].

Four wave mixing (FWM)

Four-wave mixing (FWM) is a parametric process in which three different frequencies interact and by frequency mixing generate nine new spectral components [65]. A new spectral component will be generated at:

$$f_{ijk} = f_i + f_j - f_k \tag{2.69}$$

FWM causes two types of distortions: spectral inter-modulation and spectral broadening. The spectral inter-modulation is characterized by the power (energy) exchange between discrete spectral components (e.g. channels), whereas spectral broadening takes place between spectral lines in the signal spectrum, and it is in fact the spectral inter-modulation among continuum of lines of the single channel spectrum. According to this description, SPM and XPM represent the special cases of FWM. If three different frequencies ω_i, ω_j and ω_k are considered, SPM occurs for $i = j = k$ and XPM for $j \neq k = l$ or $i = j \neq k$. In all other cases, spectral inter-modulation between all three frequencies takes place. Due to the parametric nature of FWM effect, the total energy in the optical domain is conserved. The energy conservation can be described as:

$$\mathbf{E}(\omega_i) + \mathbf{E}(\omega_j) = \mathbf{E}(\omega_k) + \mathbf{E}(\omega_{ijk}) \tag{2.70}$$

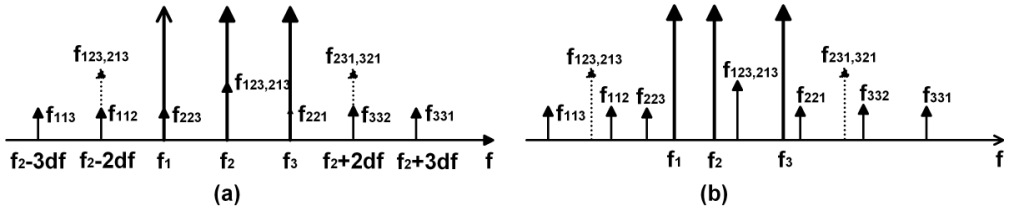

Figure 2.15: FWM induced distortions in WDM systems: a) equal channel spacing b) unequal channel spacing

The positive side of the FWM effect is that it can be used for numerous applications like wavelength conversion, phase conjugation, super-quantum generation or a parametric amplification [23]. On the other hand, the FWM may represent a dominant transmission limitation especially in spectral efficient WDM systems. The impact of FWM on the system performance depends on the wavelength at which new spectral components are generated [66]. In a transmission system with an equal channel spacing, which represents the state of the art, new spectral components overlap with a signal (Fig. 2.15a), reducing the quality of transmission. If unequal channel spacing is implemented, the overlap can be partly avoided (Fig. 2.15b) justifying this approach as a possible method for FWM suppression [67].

The power P_{ijk} of the generated spectral component is defined as [66]:

$$P_{ijk} = \left(\frac{1024\pi^6}{n^4\lambda^2c^2}\right)(\mathbf{D}\chi_{1111})^2\left(\frac{P_iP_jP_k}{A_{eff}^2}\right) \times \left|\frac{\exp(i\Delta\beta-\alpha)L-1}{i\Delta\beta-\alpha}\right|^2 \tag{2.71}$$

where L is the fiber length, n is the refractive index, λ is the wavelength, c is the velocity of light in free space and $\mathbf{D}$ describes the degeneracy factor, which amounts to 1, 3 or 6 depending whether three, two or none of the frequencies ω_i, ω_j and ω_k are equal. χ_{1111} is the third-order nonlinear susceptibility, A_{eff} is the effective area for the guided HE_{11} mode. The value of P_{ijk} is dependent on the relation between the propagation constants of interacting channels. The difference $\Delta\beta$ between wavelength dependent propagation constants in different channels (spectral components) governs the phase matching and the efficiency of FWM. $\Delta\beta$ is defined as:

$$\Delta\beta = \beta_{ijk} + \beta_k - \beta_j - \beta_i \tag{2.72}$$

$\Delta\beta$ consists of a linear ($\Delta\beta_D$) and a nonlinear ($\Delta\beta_{NL}$) part. The nonlinear part has been neglected in recent investigations, since $\Delta\beta_D$ is dominant in relevant propagation regimes. The consideration of $\Delta\beta_{NL}$ is required for a dense channel spacing ($\Delta\lambda < 50\,\mathrm{GHz}$) and a large channel power ($P > 10\,\mathrm{mW}$) in transmission fibers with a low local dispersion. The linear part of $\Delta\beta$ is given by [3]:

$$\Delta\beta_D = \left(2\pi\frac{\lambda_k^2}{c}\right)\Delta f_{ik}\Delta f_{jk}\left[D + \left(\frac{\lambda_k^2}{2c}\right)(\Delta f_{ik} + \Delta f_{jk}) \times \left\{\underbrace{\frac{\partial D(\lambda_k)}{\partial\lambda}}_{S}\right\}\right] \tag{2.73}$$

with Δf_{ij}, Δf_{ik} describing the channel spacing. The $\Delta\beta_{NL}$ can be defined (under consideration of neglected "walk-off" between the channels) as [3]:

$$\Delta\beta_{NL} = -\gamma(P_i + P_j - P_k)\{\frac{1-\exp(-\alpha L_{eff})}{\alpha L_{eff}}\} \tag{2.74}$$

As a measure of the FWM-effect the FWM-efficiency η is used [66]:

$$\begin{aligned}\eta &= \frac{P_{ijk}(L,\Delta\beta)}{P_{ijk}(L,\Delta\beta=0)} \\ &= \frac{\alpha^2}{(\alpha^2+\Delta\beta^2)}\left[1 + \frac{4\exp(-\alpha L)\sin^2(\Delta\beta L)}{(1-\exp(-\alpha L))^2}\right]\end{aligned} \tag{2.75}$$

η is proportional to the group velocity difference and the spacing between the channels. The larger the phase mismatch $\Delta\beta$, the smaller is the FWM-efficiency. The phase mismatch increases with a larger fiber dispersion (Eq. 2.73). The relation between η, fiber dispersion and channel spacing (equal channel spacing, Δf_{ij}=Δf_{ik}) is illustrated in Fig. 2.16. It is obvious that SSMF fibers perform better than NZDSF fibers in respect to FWM, because FWM impact is strongly dependent on fiber local dispersion and the dispersion management used in the system infrastructure. Using η, Eq. 2.75 can be rewritten as:

$$P_{ijk} = \eta\left(\frac{1024\pi^6}{n^4\lambda^2c^2}\right)(D\chi_{1111})^2\left(\frac{L_{eff}}{A_{eff}}\right)^2 \times P_iP_jP_k\exp(-\alpha L) \tag{2.76}$$

Furthermore, FWM indicates a dependence on the polarization relation between adjacent channels. The worst case occurs if all interacting channel are equally polarized. By using orthogonal polarization between adjacent channels, P_{ijk} vanishes or it can be suppressed by a factor of four [68]. The experimental and theoretical results showed that P_{ijk} depends on the number of channels and becomes constant if the number of channels exceeds certain value (e.g. number of channels > 24 [68]).

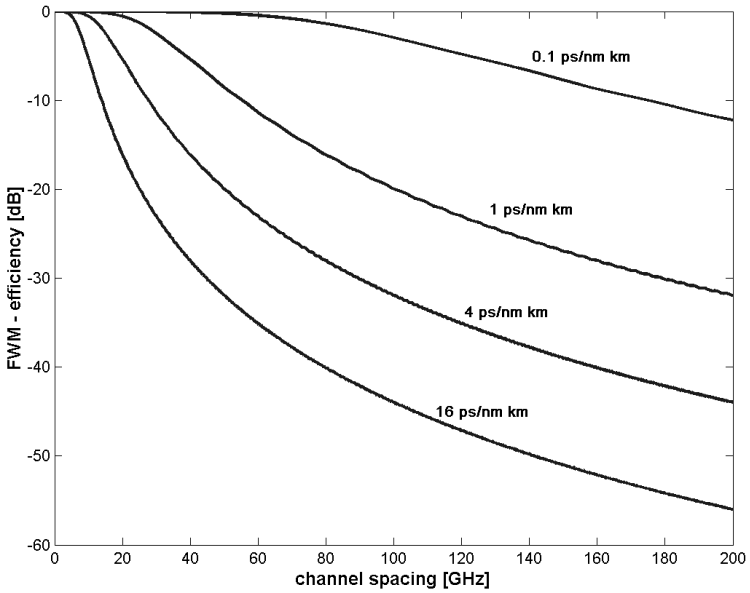

Figure 2.16: FWM efficiency vs. channel spacing (FWM-efficiency from Eq. 2.75, channel spacing=Δf_{ij}=Δf_{ik} from Eq. 2.73, L=100 km, α=0.22 dB/km)

Intra-channel effects

The intra-channel or inter-pulse effects take place between the pulses in a single channel. The intra-channel effects become significant at a higher channel data rate (>10 Gb/s). This can be explained by the fact that dispersion-caused pulse broadening is more significant at higher channel data rates causing a nonlinear interaction between adjacent and distant pulses. Fundamentally, there are two types of intra-channel effects: intra-channel XPM (IXPM) and intra-channel FWM (IFWM) [69]. Considering three propagating pulses B_1, B_2 and B_3, the interactions between them can be described by [70]:

$$\frac{\partial B_1}{\partial z} - \frac{\beta_2}{2}\frac{\partial^2 B_1}{\partial t^2} + \gamma\left[\left(\underbrace{|B_1|^2}_{SPM} + \underbrace{2|B_2|^2 + 2|B_3|^2}_{IXPM}\right)B_1 + \underbrace{B_2^2 B_3^*}_{IFWM}\right] = 0 \tag{2.77}$$

$$\frac{\partial B_2}{\partial z} - \frac{\beta_2}{2}\frac{\partial^2 B_2}{\partial t^2} + \gamma\left[\left(\underbrace{|B_2|^2}_{SPM} + \underbrace{2|B_1|^2 + 2|B_3|^2}_{IXPM}\right)B_2 + \underbrace{2B_1 B_2^* B_3}_{IFWM}\right] = 0 \tag{2.78}$$

$$\frac{\partial B_3}{\partial z} - \frac{\beta_2}{2}\frac{\partial^2 B_3}{\partial t^2} + \gamma\left[\left(\underbrace{|B_3|^2}_{SPM} + \underbrace{2|B_1|^2 + 2|B_2|^2}_{IXPM}\right)B_3 + \underbrace{B_2^2 B_1^*}_{IFWM}\right] = 0 \tag{2.79}$$

where the first term describes the standard SPM effect, the second term stands for the IXPM effect and describes the interaction between the neighboring pulses and the last term describes the IFWM yielding the interaction between distant pulses. Depending on the type of the intra-channel limitation, different signal distortions occur.

IXPM affects the pulse phase through a phase modulation between the overlapping pulses. The produced phase shifts are time dependent resulting in a frequency chirp of the interacting pulses. The frequency chirp causes a shift of the central pulse frequency, which is transformed by the fiber dispersion into timing- and

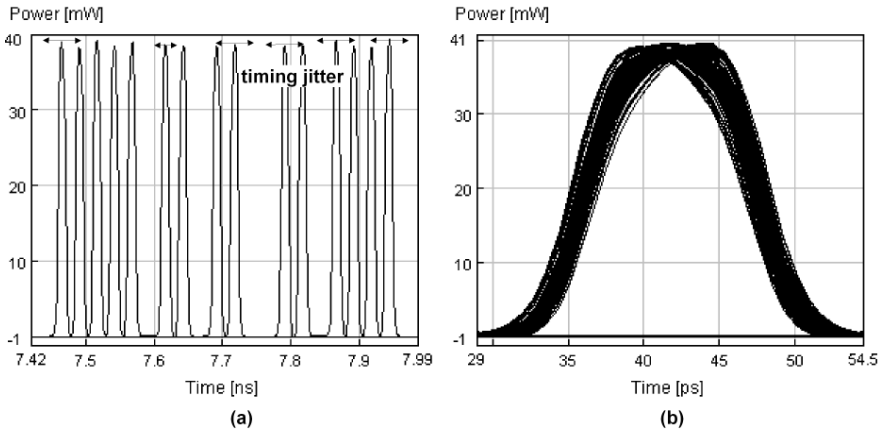

Figure 2.17: IXPM induced signal distortion: a) timing jitter b) IXPM distorted eye

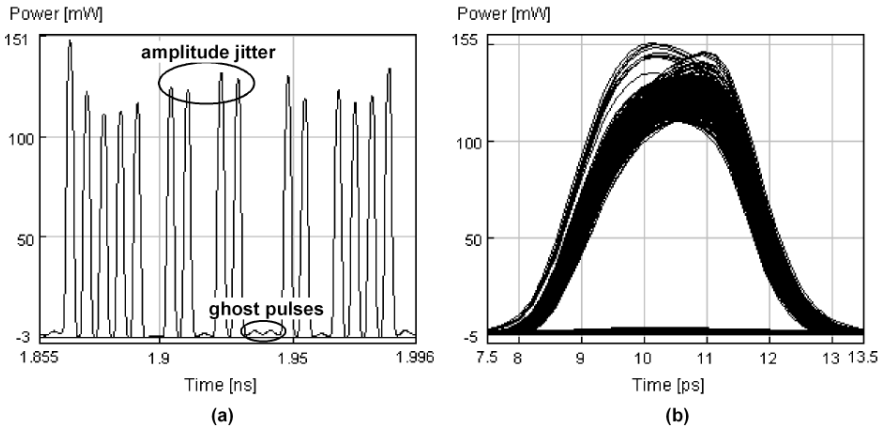

Figure 2.18: IFWM induced signal distortions: a) amplitude jitter and ghost pulses b) IFWM distorted eye

amplitude jitter (Fig. 2.17). IXPM can be seen as the consequence of the pulse overlapping and it is maximal for a partly overlap between adjacent pulses. Hence, IXPM is directly dependent on the time separation (bit slot) between the adjacent pulses and the fiber dispersion in the transmission line. Although the pulse energy remains constant, the IXPM caused fluctuations of the pulse width and the pulse amplitude result in an additional amount of the amplitude-jitter (Fig. 2.17). In high bit rate (>10 Gb/s) transmission systems with low dispersion fibers [71] and a periodical span-by-span dispersion compensation, IXPM represents the dominant transmission limitation [72]. This can be explained by the fact that the pulse width is periodically recovered after each span, limiting the intra-channel interactions on the neighboring pulses.
IFWM process can be seen as a special case of the FWM effect between the spectral components in the single channel. Thereby, considering anomalous dispersion regime (D>0 ps/nm·km) the blue spectral components propagate faster than the red ones, according to the wavelength dependence of propagation constant β. A fiber dispersion causes a pulse broadening due to the fact that blue components of the optical spectrum propagate faster than the red ones. In the case of IFWM, the blue component of a pulse interacts with the red one of the adjacent pulse causing an energy transfer in the time slot between them. If in this time slot is a space, ghost pulses (Fig. 2.18) will be generated. If this time slot is occupied by a mark, an amplitude-jitter occurs (Fig. 2.18). The IFWM can be understood as the successive process of IXPM, since it reaches maximum for

a nearly complete overlap of the pulses due to a large broadening of the pulse width. On the other hand, the larger the time separation (bit period) between the pulses, the smaller is the energy transfer [70]. The worst case degradation due to IFWM occurs if the pulses are equally spaced (constant phase) since the nonlinear interaction between optical pulses is resonant. Hence, an efficient IFWM suppression can be realized by alternate phase modulation between adjacent pulses. IFWM represents a dominant performance limitation in systems with a short bit slot (e.g. 160 Gb/s systems) [73] and a sequential dispersion compensation scheme in which the dispersion compensation is done partly at the transmitter and partly at the receiver side [72]. Several approaches exist for suppression of intra-channel effects in high bit rate WDM systems. Since the IXPM and IFWM effects show a strong dependence on the dispersion compensation scheme, the optimization of dispersion compensation e.g. by the use of a certain amount of a pre-compensation [74], is crucial for their efficient suppression. By pre-chirping of optical pulses at the transmitter side (e.g. by phase modulation), different spacings between pulses and a reduction of the nonlinear resonance can be accomplished [70].

2.4.2 Stimulated scattering processes

Contrary to the elastic nature of the Kerr effect, the second group of nonlinear processes have an in-elastic scattering nature. In stimulated scattering processes the optical fiber plays an active role in the interactions between two spectral components or two optical channels. Optical fiber enables an energy and momentum conservation by providing phonons with a correct energy and momentum. It can be distinguished between Stimulated Raman Scattering (SRS) and Stimulated Brillouin Scattering (SBS).
The SRS process is characterized by the interaction of the signal wave and the molecular oscillations in a nonlinear medium. Therein, one part of the optical power is absorbed by the medium and the other part is shifted with a frequency shift of $\Delta\omega_s = \omega_p - \omega_v$ (Fig. 2.19a). Typically, a shifted power maximum occurs at ω_s for a frequency shift of 13 THz. SRS can be understood as scattering of a photon on the moleculs to a lower frequency photon, while photons cause transition to a higher energy vibrational state. The SRS effect induces an intensity gain at the shifted frequency which can be used for the optical amplification in Raman-amplifiers [75], [76], [77], [78], [79], enabling optical amplification over a wide bandwidth region.

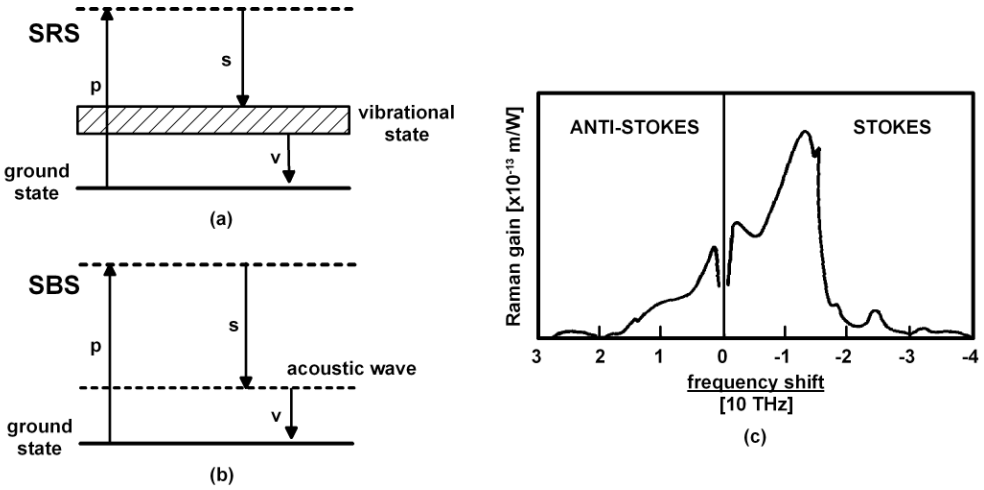

Figure 2.19: Principles of Stimulated Scattering: a) SRS process b) SBS process c) SRS gain spectrum in silica based medium

In the case of SBS, the signal wave is reflected at acoustic waves in the nonlinear medium (Fig. 2.19b). By overlapping of reflected waves along the medium, a SBS-wave will be generated reaching its maximal value if the phase-matching condition (Doppler-effect) between reflected waves is fulfilled. The SBS induced frequency shift amounts to $\sim$ 10 GHz. In both processes, the power transfer occurs from the channel with a smaller wavelength to a channel with a larger wavelength. The channel with the larger wavelength is called Stokes-channel. An energy loss occurs in the nonlinear medium, since the energy is necessary for the generation of

phonons. The inverse process is called anti-Stokes channel generation describing the consumption of phonons in the nonlinear medium. For a transmission system design, the generation of the Stokes-channel is the more relevant phenomenon. The difference between SRS and SBS lies in the nature of the phonons. Due to the acoustic nature of phonons in the case of SBS, the generated Stokes waves propagate in backward direction. On the other hand in the case of SRS, optical phonons are involved, making SRS isotropic and the Stokes wave can propagate in backward and forward direction. The intensity at the shifted frequency is defined as:

$$\frac{\partial I_S}{\partial z} = g_R I_P I_S \tag{2.80}$$

where I_S is the Stokes-channel intensity, I_P stands for a pump intensity and g_R describes a Raman-gain factor. The above equation can also be used for the description of SBS, where instead of Raman-gain the Brillouin-gain g_B parameter is used. The Raman-gain spectrum in a silica based medium is presented in Fig. 2.19b. It can be seen that a gain maximum (typically, $g_R = 6 \times 10^{-13}$ m/W) occurs at a frequency shift of 13 THz. Raman-gain possesses a broad spectrum of 30 THz. Accordingly, the SRS-effect becomes important transmission limitation in systems with a large number of channels and a large system bandwidth. The Brillouin-gain parameter is three orders of magnitude larger than the Raman-gain and its maximum is approximately $g_B = 5 \times 10^{-11} m/W$. In contrast to SRS, the SBS induced frequency-shift is rather small ($\sim$11 GHz) and its gain-spectrum is narrow (<100 MHz).
Both stimulated scattering effects show a threshold-like behavior, because the frequency shift and energy transfer occur only after certain power level P_{th} is reached. The SRS-threshold power is given by [80]:

$$P_{th,SRS} \approx \frac{16\alpha A_{eff}}{g_R \cdot L_{eff}} \tag{2.81}$$

The threshold power in the case of SBS is defined as [80]:

$$P_{th,SBS} \approx \frac{21 b A_{eff}}{g_B L_{eff}} \left(1 + \frac{\Delta f_{source}}{\Delta f_B}\right) \tag{2.82}$$

where b lies between 1 and 2, depending on the relative polarization of the pump and Stokes wave, Δf_{source} is the spectral width of the signal source and Δf_B the spectral width of the Brillouin-gain spectrum. The SBS threshold power increases significantly for an increased spectral width of the signal source $\Delta\lambda_{source}$, which depends on the modulation scheme and type of laser devices (e.g. DFB-laser, CW-pump, external modulator) used for the signal generation. For example, in phase modulation schemes the SBS-penalty can be efficiently reduced due to the fact that the amount of the power in the optical carrier is reduced. A typical value for the SBS-threshold varies between 5..10 mW [23]. The SRS and SBS transmission limitations are caused by the energy transfer between the short and long wavelengths resulting in channel-to-channel crosstalk and spectral distortions. The performance impact of the SBS effect occurs in single channel transmission due to the smaller gain-spectrum and it is less relevant for the design of high bit rate systems (>10 Gb/s). The SRS-caused performance degradation occurs in WDM systems limiting the optical signal to noise ratio (OSNR) of the system due to a significant power depletion at shorter wavelength channels. The degradation caused by SRS is measured by the degradation or power loss at the shortest wavelength channel. The SRS-induced fractional power loss P_{loss} at the shortest wavelength channel, assuming scrambled polarization in the channels and linear Raman-gain, is defined as [81]:

$$P_{loss} = \sum_{i=1}^{N-1} \frac{\lambda_i}{\lambda_0} P_i g_i \frac{L_{eff}}{2A_{eff}} \tag{2.83}$$

where P_i is injected power in the i-th channel, λ_i is the wavelength of the i-th channel, λ_0 is the wavelength of the shortest wavelength channel, N is the number of channels and g_i is the Raman gain coefficient coupling the ith and the zeroth channels. The impact of SRS depends on the total system bandwidth $\Delta\lambda_{tot} = (N-1)\cdot\Delta\lambda$, with $\Delta\lambda$ describing the channel spacing. Considering a WDM system with an equal channel spacing and Raman-gain ($g_i = 6 \times 10^{-13}$ m/W), using Eq. 2.83, P_{loss} depending on $\Delta\lambda$ amounts to:

- $\Delta\lambda_{tot} < 15\,\mathrm{THz} \rightarrow P_{loss} = 3.3 \times 10^{-13} P \Delta\lambda N(N-1)[m/W]$
- $\Delta\lambda_{tot} > 15\,\mathrm{THz} \rightarrow P_{loss} = 7.4 \times 10^{-13} P/\Delta\lambda[m/W]$

The bandwidth of the Raman-gain spectrum in both cases is assumed to 15 THz since a significant SRS-effect occurs only in a certain spectral region (Fig. 2.19b). If all channels are within the Raman-gain spectrum ($\Delta\lambda_{tot} < 15\,\mathrm{THz}$), an increased SRS impact occurs since the energy of the shortest wavelength channel is transferred to all other channels. In the second case ($\Delta\lambda_{tot} > 15\,\mathrm{THz}$), the total system bandwidth is broader than the Raman-gain spectrum and the SRS interaction takes place only between the channels within the Raman-gain spectrum. The resulting P_{loss} is used for a derivation of the SRS induced system penalty:

$$SRS_{penalty}[dB] = -10\log(1 - P_{loss}) \tag{2.84}$$

The maximum input power per channel needed for $SRS_{penalty}$ <0.5 dB can be derived from Eq. 2.84. The SRS-penalty (Eq. 2.84) can be alleviated by a reduction of the channel number, by a dense channel spacing, or a lower power per channel ($P_{ch} < P_{th,SRS}$), which indirectly results in a reduced amplifier spacing. The trade-off between these parameters governs the SRS-induced system limitations. For the investigations presented in this work, the SRS-effect was considered in investigated transmission lines, but due to a fact that the considered systems consist typically of a small number of channels, the SRS induced penalty was rather small.

2.5 Numerical model of optical fiber

The nonlinear Schrödinger equation (NLSE) (Eq. 2.23) is a nonlinear partial differential equation, an analytical solution for which is possible only for some specific cases. Several numerical models were proposed for the investigation of nonlinear effects in optical fibers [82], [83]. The most frequently used numerical model is the split-step Fourier method (SSFM) [84], [85], which belongs to the group of pseudo-spectral models characterized by a small computing time for a sufficient accuracy. The principle of SSFM is based on the separate consideration of nonlinear and linear propagation effects in a single fiber segment Δz. Using the SSFM approach, Eq. 2.23 can be rewritten as [23]:

$$\frac{\partial A}{\partial z} = (\hat{D} + \hat{N})A \tag{2.85}$$

where $\hat{D}$ is the differential operator describing the dispersion and attenuation effects:

$$\hat{D} = -j\frac{\beta_2}{2}\frac{\partial^2}{\partial T^2} + \frac{\beta_3}{6}\frac{\partial^3}{\partial T^3} - \frac{\alpha}{2} \tag{2.86}$$

and operator $\hat{N}$ represents nonlinear impacts in the fiber:

$$\hat{N} = j\gamma\left(|A|^2 + \frac{j}{\omega_0}\frac{\partial}{\partial T}\left(|A|^2 A\right) - T_R\frac{\partial |A|^2}{\partial T}\right) \tag{2.87}$$

It is assumed that, if the fiber length Δz is sufficiently small, the dispersive and nonlinear effects act independently in succession over Δz. The pulse propagation from z to $z+\Delta z$ is carried out in two steps. In first step, the dispersion and attenuation of the fiber are neglected and the fiber nonlinearities govern the propagation behavior of the optical signal. As the nature of $\hat{N}$ is imaginary, the optical phase of $A(z,t)$ will be affected with a nonlinear, time dependent, dynamic chirp as a consequence. In the second step, the fiber nonlinearities are neglected ($\hat{N} = 0$) and dispersion and attenuation affect signal propagation. After propagation over a length Δz, the optical signal is given as:

$$A(z + \Delta z, T) \approx \exp(\Delta z\hat{D}) \cdot \exp(\Delta z\hat{N}) \cdot A(z, T) \tag{2.88}$$

While the nonlinear impact of $\hat{N}$ on the optical signal can be calculated by a multiplication of the signal amplitude $A(z,t)$ with a parameter $\exp(z,\hat{N})$ in time domain, the calculation of the linear part $\hat{D}$ has to

be done in frequency domain. The transformation between the time and frequency domain is realized by discrete fast-Fourier-transformation (FFT), which increases calculation time. The approximation in Eq. 2.88 is valid for $\Delta z \rightarrow 0$. In all other cases, a certain inaccuracy occurs, depending on the chosen step width Δz. The conventional SSFM is accurate to the second order of the step width Δz [23]. The SSFM accuracy can be increased by using a more sophisticated step width resolution known as symmetrical SSFM, where the nonlinearities are included in the middle of each step according to:

$$A(z+\Delta z,T) \approx \exp\left(\frac{\Delta z}{2}\hat{D}\right) \cdot \exp\left(\int_{z}^{z+\Delta z} \hat{N}(z`)dz`\right) \cdot \exp\left(\frac{\Delta z}{2}\hat{D}\right) \cdot A(z,T) \tag{2.89}$$

For a symmetrical SSFM, an increased accuracy ($\sim \Delta z^3$) is achievable [23]. The accuracy of conventional SSFM can be increased for a reduced step width, but this would cause an increased simulation time. The trade-off between accuracy and time efficiency can be found by monitoring of the propagation conditions. For example, by monitoring of the nonlinear chirp Φ_{NL} generated by $\hat{N}$:

$$\Delta\phi_{NL} = \gamma \cdot P_{max} \cdot \Delta z \tag{2.90}$$

even small changes of the pulse envelope $A(t,z)$ can be detected. Due to the power dependence of $\Delta\phi_{NL}$, the step size Δz has to be reduced for an increased optical power P_{max} per channel. For the numerical investigation of single channel transmission, a maximum chirp value of $\Delta\phi_{NL}$=1..3 mrad provides accurate numerical results. This $\Delta\phi_{NL}$ value implies step widths of Δz=50 m..1 km. For the single channel investigation in this work, the $\Delta\phi_{NL}$ is set to 1 mrad using a step Δz of 1 km. For the multi channel investigations, Δz is reduced in order to avoid the overestimation of nonlinear effects (e.g. XPM, FWM) and generation of spurious sideband instability (SI) [86]. The proper step width has to be recognized considering system parameters such as channel spacing, power per channel or number of channels [87], [88], which are responsible for $\Delta\phi_{NL}$ generation. For the numerical multi-channel investigation in this work, a maximum phase change $\Delta\phi_{NL}$ of 3 mrad is considered implying a step width of Δz of 25 m.

2.6 Dispersion compensation in optical transmission lines

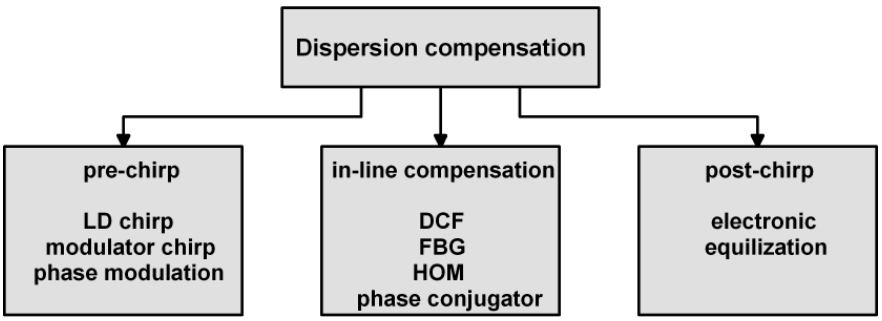

Figure 2.20: Dispersion compensation methods

The chromatic dispersion in single-mode transmission fibers represents one of the most important performance limitations in today's transmission systems, resulting in a reduced maximum transmission distance and a poor quality of transmitted signals. The impact of chromatic dispersion becomes even larger with a system upgrade to higher channel bit rates (>10 Gb/s). Another dispersion limitation is the dispersion slope which represents an issue in WDM systems with a large number of channels, resulting in different accumulated dispersion values per channel.
Depending on the place and realization where the dispersion compensation is made in a system, it can be distinguished between three compensating methods: a) pre-chirp techniques at the transmitter side b) dispersion compensation in the transmission line (in-line compensation) and c) dispersion compensation at the receiver side (Fig. 2.20). The idea behind the pre-chirping at the transmitter side is the implementation of chirp with the opposite sign to the fiber chirp in order to counter the GVD effects in the fiber. The pre-chirp can be realized by several methods, e.g. exploiting the internal chirp of the laser source [89], [90] or of an external modulator [37], [91] and by the implementation of complex transmitter structures using additional components such as phase modulators [57] or electrical pre-coding [92], [93]. The main implementation area of this technique are cost effective, optical short-reach systems (e.g. MANs) with smaller channel bit rates, but in combination with other dispersion compensation techniques (e.g. in-line compensation) it can enable a performance improvement even in high-bit rate transmission systems over long distances [94].
In-line dispersion compensation represents the key enabling technology for the realization of long-haul transmission systems. The dispersion compensation is realized in the optical domain without electro-optical conversion of the signal, enabling better compensation of the signal because the optical phase is maintained. Typically, the dispersion compensation is employed in the transmission line on a span-by-span basis. The in-line dispersion compensation can be realized by various optical components, e.g. dispersion compensating fiber (DCF), fiber Bragg grating (FBG), higher order mode (HOM) compensators and phase conjugator. The principles of operation and basic characteristics of different in-line compensations are presented in the following section.
The post-chirp techniques at the receiver side are characterized by the compensation of the chromatic dispersion in electrical domain. Through the use of sophisticated decision algorithms, e.g. maximum likelihood detection [95], [96], [97], the accumulated residual dispersion in the detected optical pulse can be efficiently compensated. This compensation method is cost effective, and in combination with in-line compensation, enables an enhanced transmission performance.

2.6.1 In-line compensation devices

Implementation of in-line compensation devices in the transmission line affects the transmission performance of the system because of the interaction of dispersion map with transmission disturbances (e.g. ASE-noise, nonlinearities). The following dispersion compensating devices are used for the realization of in-line dispersion compensation:

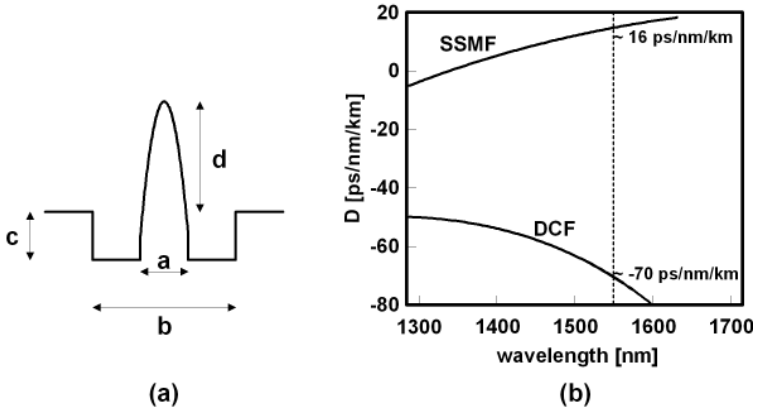

Figure 2.21: DCF characteristics: a) DCF fiber profile b) dispersion spectra of SSMF and DCF [98]

- **Dispersion Compensating Fiber (DCF)**: the DCF represents the most widely used in-line dispersion compensation technique in today's transmission systems. The DCFs are characterized by a large negative dispersion and a small core diameter. The large negative dispersion values can be achieved by variation of the fiber profile by doping the fiber cladding (e.g. by fluorine) [99], introducing an increase in the refractive index difference between the core and cladding. A significant increase of negative fiber dispersion can be achieved using sophisticated refractive index profiles like matched-cladding type [100], a W-shape type enabling the realization of a negative dispersion slope or a segmented core type [101] enabling an enlargement of the effective core area by the implementation of rings around the depressed cladding type. An example of a DCF refractive index profile is illustrated in Fig. 2.21a (W-shape DCF) with **a** describing the core diameter, **b** the depressed core diameter and **c** and **d** the refractive index differences of depressed and center core, respectively. Through changes of the ratio between the depressed and center core, the negative dispersion can be enlarged. The demands on DCFs are a large negative dispersion (-70..-300 ps/nm), low insertion losses, low polarization dependent (PDL) losses, a low polarization mode dispersion (< 0.05 ps/$\sqrt{\text{km}}$), a large effective area (A_{eff}) and a negative dispersion slope (Fig. 2.21b). The DCF loss is characterized by the figure of merit (FOM), given as a relation between the DCF dispersion D_{DCF} and the attenuation α:

$$FOM = \frac{|D_{DCF}|}{\alpha} \left[\frac{\text{ps}}{\text{nm}} \cdot \text{dB}\right] \tag{2.91}$$

  The FOM in typical DCFs is larger than 150 (ps/nm)·dB. DCFs with large negative dispersion are characterized by a small effective area ($A_{eff} < 20\ \mu m^2$), which results in a reduced nonlinear tolerance of the DCF device. An A_{eff} enlargement could be partly achieved by the implementation of specific refractive index profiles (e.g. segmented core) [102]. The realization of slope compensation with DCF is a critical issue, because conventional DCFs have positive β_3 as do the conventional transmission fibers. In order to achieve the slope compensation, the variation of wave guide dispersion of DCFs is needed e.g. by double cladding structure [103], [104]. The DCFs can be used for simultaneous compensation of several channels, but due to imperfections in slope compensation, a small amount of residual dispersion remains especially in outer channels.

- **Fiber Bragg Grating (FBG)**: FBGs modules are fabricated by implementing refractive index changes in the fiber core. The regions with different refractive indices are called gratings. Depending on the distance between the gratings known as grating period, which can be realized as constant or varying (chirped) [105], the shorter wavelengths will be reflected before the longer ones. The consequence is a pulse compression and a dispersion compensation [106]. The traditional chirped FBG are limited to narrow-band dispersion compensation on a single channel base [107]. In recently presented complex FBGs or XBGs structures [108], the specific index profiles are fabricated in order to reflect

a larger number of channels. The complex refractive index profile is a combination of various single channel profiles. In the past, the dispersion compensation functionality of FBGs was limited by the short device lengths due to the fabrication process, e.g. limited size of phase mask used for the writing of gratings [109], but recently presented long FBGs [110], [111] can compensate much larger amounts of accumulated dispersion over the entire C-band. FBGs represent a promising technology for the realization of dynamic dispersion compensation in tunable dispersion compensators [112]. The FBGs tunability can be achieved by slight stretching or by the implementation of a thermal gradient across the grating. The advantages of FBGs are large nonlinear tolerance and lower device loss. The main FBG drawback is an increased device complexity because of the implementation of optical circulators and large ripples in insertion losses (IL) and group delay (GD).

- **Higher Order Mode (HOM) devices**: this compensation technique is based on the propagation of the dispersed pulse in a higher order mode (HOM) fiber with few modes. HOM-based devices are realized using two discrete mode convertors (MCs) for converting the LP_{01} mode to some higher order mode (e.g. LP_{11} or LP_{02}) [113], [114]. The most important advantages of HOMs are the large negative dispersion resulting in a reduced device length and losses, and a large effective area (>60 μm^2) [115] resulting in a better nonlinear tolerance of this device. Furthermore, HOMs can efficiently compensate dispersion slope making this technology a potential candidate for dispersion compensation in high capacity WDM systems. Another advantage of HOMs is its multi-channel functionality. The drawbacks of the HOM concept are large losses induced by MCs (>1 dB per MC) and the inter-modal interference in HOM fiber, which results in an increased addition of noise to the optical signal and large multi path interference (MPI) values, thus limiting the system performance [116], [117]. Recently presented HOM devices show reduced losses and reduced MPI (<-42 dB) values [118], [119].
- **Phase conjugator**: this concept is known as mid-span spectral inversion (MSSI). The principle of MSSI is the spectral inversion of the optical signal spectrum in the middle of the transmission span by applying an active component (e.g. semiconductor laser) [120] or highly nonlinear fiber (e.g. nonlinear phase-conjugating mirror) [121], [122], [123]. The short wavelengths of the signal are interchanged with the longer wavelengths making use of a nonlinearity based phase conjugation. This concept enables a full compensation of dispersion and dispersion slope, but it is less practical for the implementation in the transmission systems because of its complexity.

device type	component realization	dispersion slope matching	nonlinear tolerance	dispersion compensation	device loss
DCF	simple	partial	medium	continuous	medium
FBG	complex	partial	high	channalized	medium
HOM	medium	full	continuous	continuous	large
phase conjugator	complex	full	medium	continuous	small

Table 2.3: Devices for in-line dispersion compensation

For the system investigations presented in this work, conventional DCF based compensation devices were considered because of the fact that they represent the state-of-the-art technology in today's optical communication systems.

2.6.2 Dispersion compensating schemes

Depending on the placement and the combination of in-line compensation devices in the transmission line, several different dispersion compensation schemes can be realized (Fig. 2.22). Common for all dispersion compensation schemes enabling the full dispersion compensation is that the compensation of the accumulated dispersion in the transmission fiber has to be performed according to the following rule:

$$D_{SMF} \cdot L_{SMF} + D_{DCF} \cdot L_{DCF} = 0 \tag{2.92}$$

where D_{SMF}, D_{DCF} are the chromatic dispersion values of transmission and compensating fibers, respectively, and L_{SMF}, L_{DCF} the lengths of these fibers. This rule can be fulfilled by placing DCFs in different positions within a transmission line. Typically, a transmission line consist of several cascaded spans. Depending on the realization of the span infrastructure, it can be distinguished between three basic dispersion compensation schemes: pre-, hybrid- and post-compensation (Fig. 2.22). In pre- and post-compensation the DCFs are placed before or after the SMF fiber. In hybrid-compensation 50 % of the SMF dispersion is compensated before the SMF and the other 50 % is compensated afterwards. The system behavior can be quite different for the different schemes because of the influence of dispersion compensation on the linear and nonlinear effects. This influence varies for different channel data rates making a system upgrade becoming a critical issue.

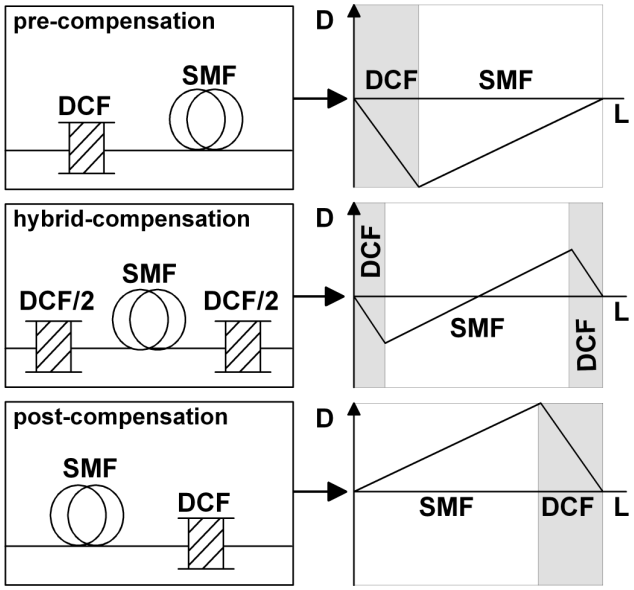

Figure 2.22: Principles of dispersion compensation

Figure 2.23 illustrates the accumulation of chromatic dispersion in more complex dispersion compensation schemes realized by the concatenation of single spans. The full dispersion post-compensation scheme provides full compensation and signal shape regeneration after each span. This scheme is interesting for the practical implementation because the optical signal form is maintained after each span and the signal can be easily accessed or detected. The nonlinear characteristics of this scheme are rather poor, because the walk-off between adjacent channels in the system vanishes after each span resulting in an increased impact and accumulation of inter-channel nonlinearties (e.g. XPM), depending on the local dispersion of the transmission fiber. The nonlinear tolerance of this scheme can be improved by implementation of the pre-chirp at the transmitter side [124], [94], [125]. A similar effect can be achieved by under-compensation of chromatic dispersion along the transmission line. Depending on the amount of under-compensation, the accumulated residual dispersion varies (Fig. 2.23) from span to span. The drawback of this approach is the necessity of an additional or a tunable dispersion compensation at the end or within the transmission line, if some channel has to be dropped or switched. This can be critical in systems with higher channel bit rates (>10 Gb/s) because of a reduced dispersion tolerance. A more exotic, but recently proposed [126], [127] compensation scheme, are known as compact dispersion compensation (Fig. 2.23), where dispersion compensation of the total accumulated system dispersion is realized directly after the transmitter and before the receiver. The advantage of this approach is that the impact of nonlinearities in the transmission line can be significantly suppressed, because the pulses are fully dispersed during propagation [125]. This scheme is less relevant for the practical implementation, because the optical channels cannot be accessed within the transmission line. As stated above, the compensation of only β_2 (chromatic dispersion) alone is insufficient for the compensation

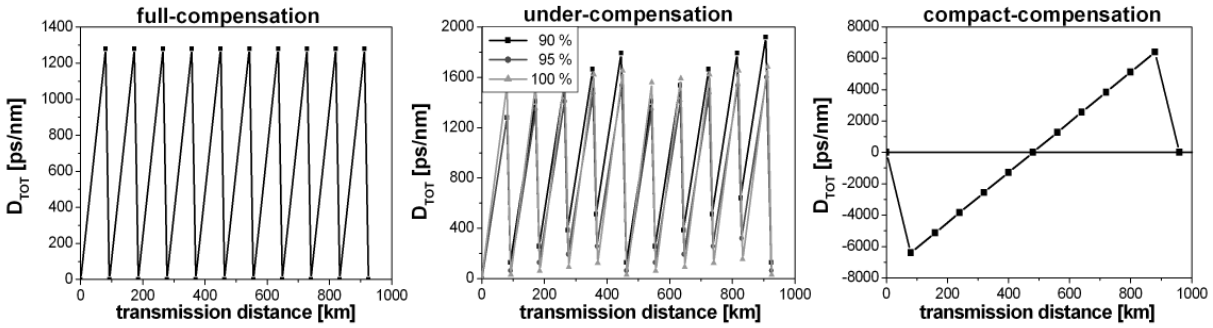

Figure 2.23: Dispersion compensation schemes in multi-span systems

of accumulated dispersion in high speed transmission systems, because of the existence of dispersion slope, which results in a wavelength dependent residual dispersion. Theoretically, the complete slope compensation could be realized if the DCF slope (S_{DCF}) can be tailored to:

$$S_{SMF} \cdot L_{SMF} + S_{DCF} \cdot L_{DCF} = 0 \tag{2.93}$$

Practically speaking, negative DCF slope can be realized (Chapter 2.6.1), but it cannot ideally match the SMF slope.

2.7 Optical filters

Optical filters used in multiplexers (MUXs) and demultiplexers (DMUXs) in a WDM system represent the key components for enabling dense WDM transmission systems. The MUX and DMUX filters become more important with an increased spectral efficiency (>0.4 bit/s/Hz) since a precise narrow-band filtering both at the transmitter and receiver side is necessary. Due to dense channel spacing, the filter bandwidth and shape have to be carefully chosen. Depending on the technology used for the realization of MUX and DMUX filters, different behaviors and filter characteristics can be realized. It is the trade-off between filter shape, crosstalk between adjacent channels, chromatic dispersion, temperature stability and filter losses (e.g. PDL), which has to be considered in order to determine the best choice filter. The basic technologies used for the fabrication of MUXs and DMUXs in WDM systems with 50 and 100 GHz channel spacing are arrayed wave gratings (AWG), fiber Bragg gratings (FBG), dielectric thin film resonant cavity filters (TFF) and Mach-Zehnder interferometers (MZI).

Thin film filter (TFF)

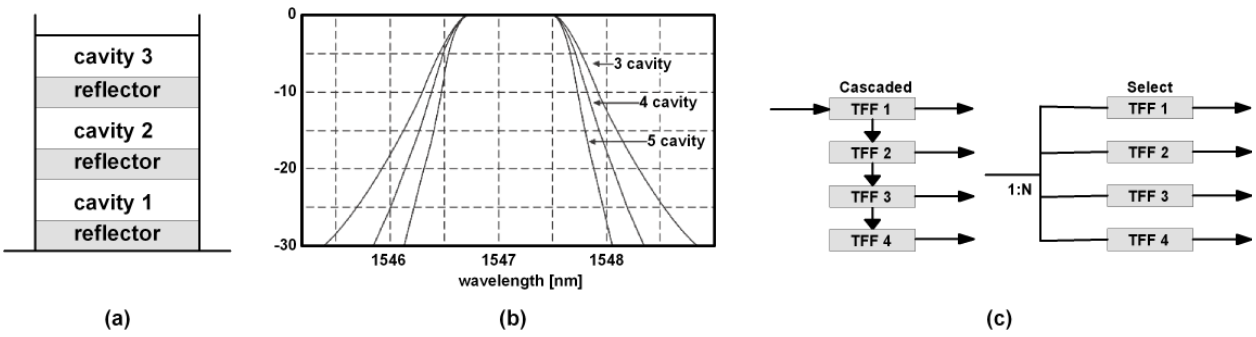

Figure 2.24: Principles of TFF filters: a) multi layer structure b) filter response c) TFF based DMUX realization

Thin film resonant cavity filters (TFF) are today's major deployed commercial filter type in optical transmission systems characterized by low device costs and high reliability. TFFs represent a special case of Fabry-Perot or etalon filters with multiple cavities, where the mirrors around the cavity are realized by using reflective dielectric thin film layers (Fig. 2.24a). Similar to external cavity lasers, the wavelengths passing through the reflective mirrors in TFFs are determined by the length of the cavity. All the wavelengths transmitted through the thin film layers are superimposed. Multiple cavities are necessary in order to create a filter shape with a flat top pass-band and sharp edges (Fig. 2.24b). For N channels functionality of MUX and DMUX, N TFF filter devices have to be combined. It can be distinguished between cascade- and select-architectures. In a DMUX realized as a cascade of TFFs (Fig. 2.24c left), a certain wavelength is passed through each TFF, while all other wavelengths are reflected into the following cascade. The drawback of this concept is the varying filter loss at different wavelengths. In select-structure architecture (Fig. 2.24c right), all incoming wavelengths are broadcasted by a 1:N splitter to N filters . The filter loss is identical for different wavelengths, but larger than in cascaded structure and increases with the number of channels. The TFF-based MUXs and DMUXs are characterized by a small temperature drift coefficient (no active temperature control needed) and a flat-top filter response favorable for the use in DWDM systems. According to a large filtering loss for large number of channels, this technology is suitable for 50 GHz MUX and DMUX realizations with a low number of channels (N < 16).

Mach-Zehnder interferometer (MZI)

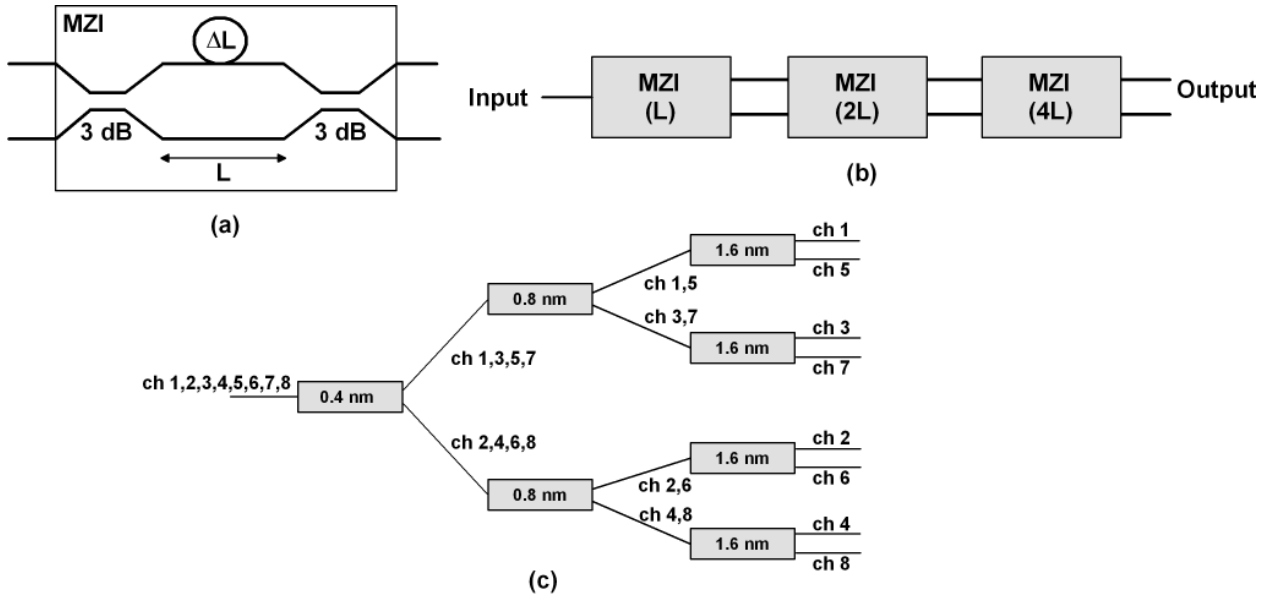

Figure 2.25: Principles of MZI based filters: a) MZI structure b) realization of narrow band filters c) MZI based DMUX architecture

Mach-Zehnder interferometer based filters (MZIs) are interferometric devices in which the filtering is realized by the length variations in the MZI arms. A MZI-based filter consists of two 2x2 3-dB couplers at the input and output and MZI arms between them. The path difference between the MZI arms equals ΔL (Fig. 2.25a). The input signal is divided equally into both arms by the first 3-dB coupler. The signal in the upper arm is shifted by $\pi/2$ by the coupler compared to the signal in the lower arm. Additionally, a signal phase delay βL occurs in upper arm. After the second 3-dB coupler, signal from the upper arm experiences $\pi/2$ phase shift by the second coupler. The total phase difference between the signals in MZI arms at the upper and lower MZI output are given by:

$$\phi_{tot,upper} = \pi/2 + \beta(L + \Delta L) + \pi/2 \tag{2.94}$$

$$\phi_{tot,lower} = \pi/2 + \beta L - \pi/2 \tag{2.95}$$

If $\beta L = k\pi$, the wavelengths for which $\beta \Delta L$ is odd appear on the upper output and the wavelengths for which $\beta \Delta L$ are passed to the lower output. Thus, the path difference ΔL becomes the dominant parameter for the characterization of the MZI transfer function. The MZI filter response is given by [128]:

$$I(f) = I_0 \cos^2\left(f \frac{n_e \Delta L \pi}{c}\right) \tag{2.96}$$

where f is the optical frequency and n_e is the effective refractive index of the delay line. The 3-dB bandwidth of the filter is given by:

$$\Delta f = \frac{c}{2 n_g \Delta L} \tag{2.97}$$

with

$$n_g = n_e(f_0) + f_0 \frac{dn_e}{df} \tag{2.98}$$

representing the group refractive index evaluated at central frequency f_0. The filter characteristics are dependent on the coupling ratio of the 3-dB couplers, which is not ideally 50:50 and it has to be precisely

controlled owing to its wavelength dependence. The frequency response function shape of MZI filters is $\cos^2$. A narrow pass-band and steep filter edges can be realized by cascading of several MZIs (Fig. 2.25b). MZIs can be used to realize MUX as well as DMUX filter devices. A MZI-based 1:N DMUX consists of N-1 MZI cascaded devices (Fig. 2.25c). A 0.4 nm DMUX device is made of three stages with 0.4, 0.8 and 1.6 nm filters. The simple upgrade to a denser channel spacing can be achieved by adding an additional MZI structure at the input of the existing DMUX device [129]. The drawbacks of the MZI concept are the insufficient channel separation, making additional filtering necessary, and the need for an active temperature stabilization, reducing the reliability and increasing component costs.

Arrayed Waveguide Grating (AWG)

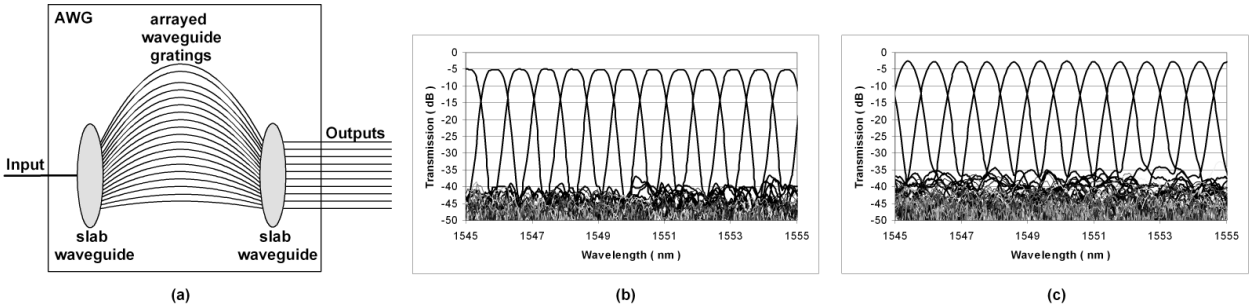

Figure 2.26: Principles of AWG filters: a) AWG structure (DMUX) b) flat-top AWG c) gaussian AWG

The arrayed waveguide grating (AWG) concept for the realization of optical filters is basically a generalization of the MZI concept. The AWG is made of two slab waveguides at the input and output and arrayed waveguide gratings between them (Fig. 2.26a). The slab wave guides can be understood as optical lenses and the arrayed waveguide gratings as a prism. At the AWG input, the incoming light is coupled into the arrayed waveguides. The coupled copies of the input signal have different phases due to the different propagation distances in the slab waveguides. The length of the arrayed waveguides is set such that the path difference between adjacent waveguides is proportional to an integer multiple of the center wavelength. The length difference between adjacent waveguides ΔL is constant. If this condition is fulfilled, the fields of different wave guides arrive with equal phase at the second slab waveguide. Due to the length differences between the arrayed waveguides, different wavelengths experience different phase changes. Accordingly, the second slab waveguide reproduces and couples wavelengths into the different output waveguides (Fig. 2.26a). The relative phases of the signal propagating from AWG input i to output j through k arrayed waveguide gratings is given by [109]:

$$\phi_{ijk} = \frac{2\pi}{\lambda}\left(n_1 d_{ik}^{in} + n_2 k\Delta L + n_1 d_{kj}^{out}\right) \tag{2.99}$$

where k=1..m, $d_{ik} = d_i + k\delta_i, d_{kj} = d_j + k\delta_j$ are the propagation distance differences in input and output slab waveguide and $n_{1,2}$ are the refractive indexes in slab and arrayed waveguides. Thus, if:

$$n_1\delta_i^{in} + n_2\Delta L + n_1\delta_j^{out} = p\lambda \tag{2.100}$$

the input wavelengths will be added in phase at the output j, if p is an integer. Thereby, periodic pass frequencies occur at each output waveguide. The spacing between two adjacent pass-bands is called free spectral range (FSR) of the AWG. The FSR is proportional to the number of channels and their channel spacing. Additional interference filters may be needed to suppress unwanted passbands. AWGs enable the fabrication of MUXs and DMUXs as well as router devices. An AWG based router is a NxN AWG realized as a combination of MUX and DMUX with a static wavelength cross-connect functionality. Depending on the realization of the slab waveguides and arrayed gratings, the AWG- based MUX and DMUX devices may have a flat-top or gaussian filter characteristic. The flat-top AWGs (Fig. 2.26b), characterized by a flat passband and steep edges, are desirable for the implementation in DWDM systems. AWG filters deployed

in the field today possess a gaussian shape (Fig. 2.26c) and present a good solution for WDM systems with a reduced spectral efficiency. AWG-based MUXs and DMUXs can be realized as silica on silicon devices, InP, polymer or SOI devices allowing an integration with additional components (e.g. semiconductor optical amplifiers). Chromatic dispersion in AWG components is low and it possesses a linear phase characteristic. The AWG technology meets the technological and commercial requirements of 50 GHz MUX and DMUX devices, especially for a large number of channels (> 16), since insertion losses and component costs can be reduced compared to other filter devices. The drawbacks of this technology are related to phase errors arising from manufacturing imperfections and temperature variation as well as large PDL losses.

Fiber Bragg grating (FBG)

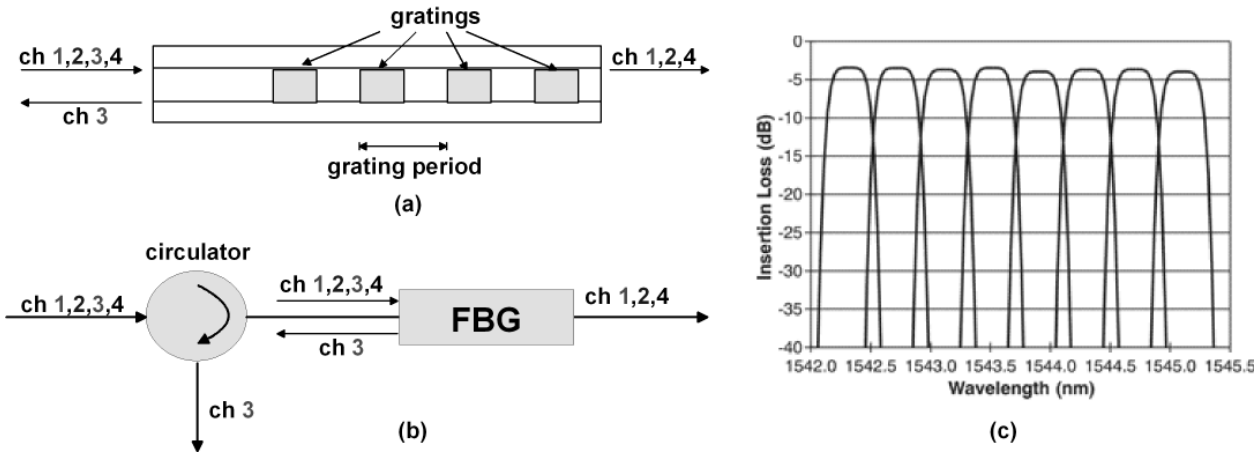

Figure 2.27: Principles of FBG filters: a) FBG structure b) FBG DMUX architecture c) DMUX spectrum

Fiber Bragg grating (FBG) structures are characterized by a periodic perturbation of the refractive index over structure length. The grating patters are written in the fiber, exploiting photo-sensitivity of germanium doped silica fibers. Exposing a fiber to ultra violet (UV) light causes refractive index changes in the fiber core. The change of the refractive index needed to obtain gratings is quite small ($\approx 10^{-4}$). The distance between two adjacent gratings is called grating period Λ, determining which wavelength will be reflected by the grating according to:

$$\lambda_{Bragg} = 2n_{eff}\Lambda \tag{2.101}$$

where n_{eff} represents the effective refractive index. The reflected wavelength is called Bragg wavelength. Due to the fact that the reflection of the grating is not ideal, a small amount of power leaks through the grating, resulting in optical losses. Depending on the grating period, it can be distinguished between short- and long-period gratings. FBGs in MUX and DMUX devices are short-period gratings. Long-period gratings are used in erbium doped amplifiers (EDFAs) for tailoring the amplifier spectrum (Chapter 2.8). FBG-based MUX (Add-Drop filters) and DMUX (Fig. 2.27b) devices possess a flat-top passband shape (Fig. 2.27c). Further advantages of FBGs are lower losses compared to other filter devices, a high wavelength accuracy and high adjacent channel separation. Temperature stabilization in FBGs is passive, because FBGs can be integrated in combination with a material with a negative temperature expansion coefficient.

The drawbacks of FBGs are a large chromatic dispersion and dispersion ripples due to grating inaccuracies as well as the need for additional components (e.g. circulators, couplers) for the separation of channels, resulting in large costs due to a hybrid design. Chromatic dispersion of a FBG-based filter is proportional to the difference of delay times at different wavelengths. In most filters type, the variations of the time delay are larger at the edges of the filter passband and they are less critical as long as the channel spectral width is

[1] depends on the component design

parameter	dielectric filters	FBG	AWG	MZI
filter shape	flat top	flat top	flat top	sinusoidal
channel isolation [dB]	28	30	30	30
group delay variation [ps]	< 1	10	< 1	< 2
complexity	N devices	N devices	1 device	N-1 devices
insertion loss [dB]	5.5	0.3/FBG	5	5
bandwidth @ -0.5 dB [nm]	> 0.13	0.16[1]	0.16	> 0.1
PDL [dB]	0.3	< 0.1	0.3	< 0.3

Table 2.4: Characteristics of commercially available optical 1x8 DMUX filters with 50 GHz grid

much smaller than the passband width of the filter [130], but in FBG-based filters large delay time variations occur in the passband, resulting in an increased chromatic dispersion and dispersion ripple. FBGs can be used for implementation in MUX and DMUX devices at 50 GHz channel spacing with a smaller number of channels ($N < 8$), because of the increased complexity regarding fabrication and packaging.
In conclusion, all filter types described above can be used for fabrication of MUX and DMUX filters in DWDM systems with 100 and 50 GHz channel spacing. The realization of 50 GHz devices is a more critical issue. Comparing different filters for DMUX fabrication (Table 2.4) concerning filter shape, channel isolation, group delay variation, complexity of realization, integration losses, PDL and insertion loss, thin film filter TFFs would be the best choice technology for a reduced number of channels ($N < 16$) and AWGs for a larger number of channels. These two technologies are advantageous primarily due to the flat-top filter form and low group delay variations.

2.8 Optical amplifiers

Optical amplifiers represent one of the crucial components in an optical transmission system. Despite of the minimum attenuation at 1.55 μm (theoretically, 0.16 dB/km), fiber losses significantly limit the transmission performance with increased transmission distance (>20 km). Optical amplification can be realized using different amplifier concepts and mechanisms e.g. semiconductor optical amplifiers (SOA), rare-earth doped fiber amplifiers (e.g. erbium, holmium, thelium, samarium) or more recently Raman amplifiers. All these amplifier types are based upon different physical mechanisms resulting in different device characteristics and implementation areas. The rare-earth doped fiber amplifiers provide optical amplification in the wavelength region from 0.5-3.5 μm. The most important representative of these amplifier type are erbium doped fiber amplifiers (EDFAs), which is today's widely used amplifier type in optical transmission systems due to the fact that it provides an efficient optical amplification in the 1.55 μm region.

Erbium doped fiber amplifier (EDFA)

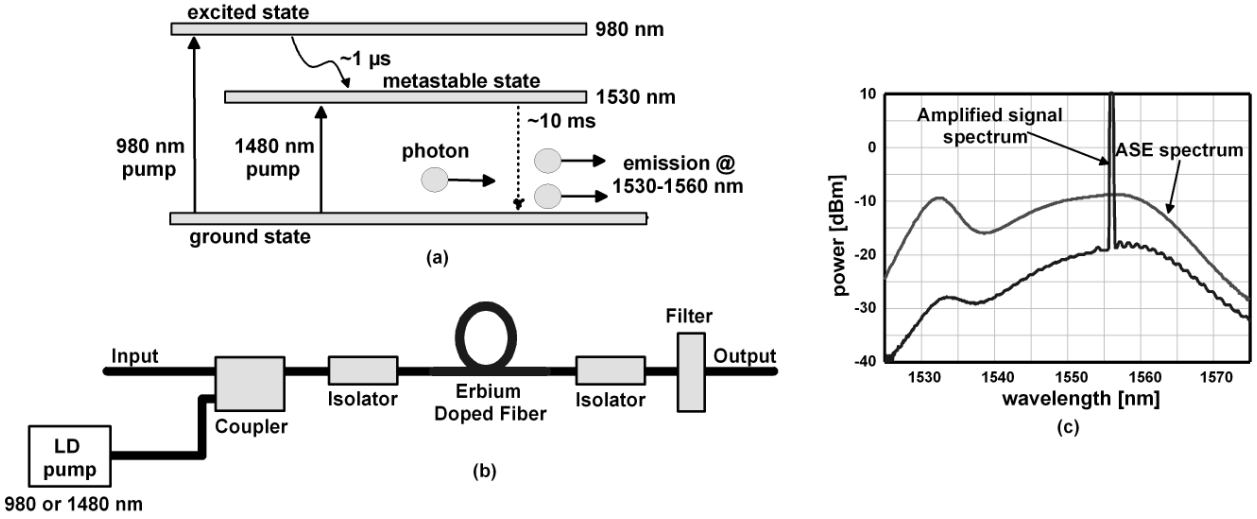

Figure 2.28: EDFA priciples: a) stimulated emission b) EDFA realization c) EDFA spectrum

The principle of the operation of an EDFA is presented in Fig. 2.28. The silica core of the fiber used in EDFA is doped with Er^+ ions. The amorphous structure of silica broadens the discrete Er^+ energy levels into energy bands. The energy bands at 980 and 1530 nm are favorable for the realization of optical amplification due to the commercial availability of semiconductor lasers at 980 and 1480 nm. By pumping of the Er^+-doped fibers, electrons from the ground state are transformed to the excited state, but after a short time ($\approx 1\,\mu s$) the excited electrons deplete to a metastable state (Fig. 2.28a). Due to a large time constant of metastable state ($\approx$10 ms), electron concentration results in an occupancy inversion relating to a ground state. The electrons falling back from the metastable to the ground state emit light in the 1.55 μm wavelength range (Fig. 2.28a). The optical pumping is realized with a pump power of 10-100 mW. The pump and optical signal can propagate in the same or in opposite directions. There is no difference between these two pumping schemes if the signal power is small, because in this case EDFA is not saturated [51]. The conventional EDFAs (Fig. 2.28b) are made of a semiconductor pump laser, a coupler which multiplexes signal and pump wave, an Er^+ doped fiber, two isolators and an optical filter at the output. More recent EDFAs consist of several amplifier stages (2-3) in order to enable a lower noise figure and a larger amplifier gain. The pumps at 980 nm are more commonly used because they can provide an optical power >100 mW, enabling the use of shorter Er^+-fibers within the EDFAs. The Er^+-fiber length typically amounts to 10-25 m in conventional so-called lumped or in-line EDFAs. Optical gains of 20-45 dB can be realized with output powers of 20-50 mW. The amplification process (stimulated emission) in an EDFA is accompanied by the amplified spontaneous

emission (ASE) noise. The ASE-noise is not polarized nor coherent. It can be approximated by the noise figure F_{EDFA} defined for high amplifier gains as [51]:

$$F_{EDFA}[\text{dB}] \approx \log(2n_{sp}) \tag{2.102}$$

where n_{sp} is the spontaneous emission factor which depends on the electron populations in the ground (N_1) and excited state (N_2):

$$n_{sp} = \frac{N_2}{N_2 - N_1} \tag{2.103}$$

The theoretical minimum for the noise figure F_{EDFA} amounts to 3 dB. 980 nm pump based EDFAs can achieve a F_{EDFA} of 3.2 dB [3], whereas F_{EDFA} in 1480 nm based EDFA is larger than 4 dB due to the difficult realization of a complete population inversion ($N_1 = 0$). In order to reduce the impact of ASE-noise which propagates in the backward direction and depletes the pump power, isolators are used at the input and at the output of the Er^+-fiber (Fig. 2.28b).
One of the most important EDFA features is its gain spectrum. The typical EDFAs provide an optical amplification in a 35-40 nm broad wavelength region. The shape of the gain spectrum depends on several parameters such as the structure and the purity of silica fiber, the erbium ion concentration, amplifier length as well as the pump power. The differences in the gain spectrum can be observed depending on the signal power applied at the EDFA input (Fig. 2.28c). An input optical signal causes a slight EDFA saturation and a generation of the gain peak near 1.55 μm. If multiple EDFAs are implemented in a transmission line, the total usable gain spectrum bandwidth shrinks. This effect is known as gain-peaking and it is analogous to spectral forming in a cascades of electrical filters. The gain-peaking can be an issue in ultra long-haul and submarine systems. Another characteristic of the EDFA spectrum is its spectral nonuniformity resulting in wavelength dependent amplifier gain. The gain nonuniformity impacts the performance in systems with a large number of channels and cascaded EDFAs. A better utilization of the EDFA gain spectrum can be achieved by flattening the gain spectrum by introducing wavelength selective losses by the use of an optical filter (e.g. TFF, MZI, FBG). This technique is called static gain flattening. The gain flattening filter introduces additional losses and is placed before or after the Er^+-fiber (Fig. 2.28b). The placement before the Er^+-fiber results in larger ASE-noise generation and after the Er^+-fiber in a smaller output power. Due to the fact that the gain characteristic of an EDFA depends on the number of channels, which can vary along the transmission line, a dynamic flattening of the EDFA gain has to be performed as well. It can be realized by the implementation of an additional laser source, which operates outside the used amplifier bandwidth. This concept is known as the gain-clamping [51]. EDFAs present the state-of-the-art technology in conventional optical transmission systems and they can be used as in-line amplifiers (placed every 30-80 km, good noise figure), power boosters (amplifiers at the transmitter side) or pre-amplifiers (low noise amplifiers in front of the receiver) independently of the channel bit rate in the system.

ASE-noise accumulation in multi span systems

For the characterization of the ASE-noise impact on the transmission performance, the investigation has to begin with a definition of the noise figure F of transmission line, which can be calculated as concatenation of noise figures of single transmission components (e.g. EDFA, fibers, couplers, switches). Starting with an EDFA, its noise figure is defined as a relation between the optical signal to noise ratio (SNR) at the input and output of the amplifier:

$$F_{EDFA} = \frac{OSNR_{in}}{OSNR_{out}} \tag{2.104}$$

The OSNR values are defined by signal S and noise N powers at input and output, respectively.

$$F_{EDFA} = \frac{S_{in}}{S_{out}} \cdot \frac{N_{out}}{N_{in}} \tag{2.105}$$

$$= \frac{1}{G_{EDFA}} \cdot \left[1 + \frac{(G_{EDFA} - 1) \cdot n_{sp} \cdot h\nu}{N_{in}}\right] \tag{2.106}$$

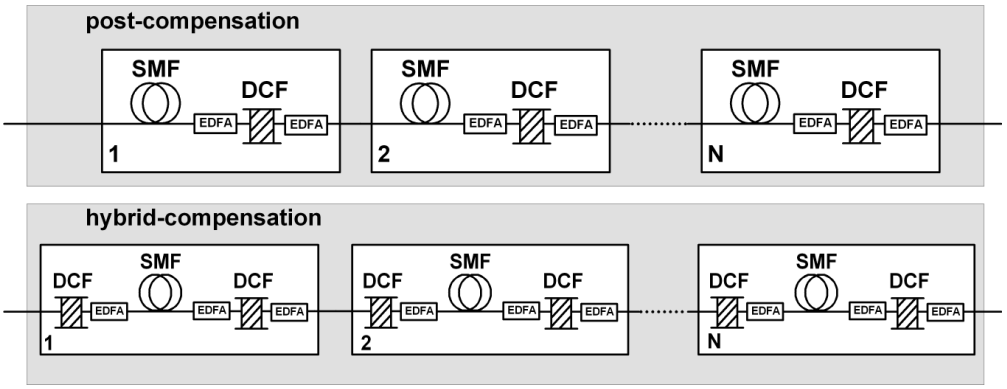

Figure 2.29: Span infrastructures in multi-span systems

with

$$S_{out} = G_{EDFA} \cdot S_{in} \tag{2.107}$$

and

$$N_{out} = N_{in} + (G_{EDFA} - 1) \cdot n_{sp} \cdot h\nu \tag{2.108}$$

where n_{sp} denotes the inversion factor of the EDFA, and N_{in} corresponds to the zero point energy W_0 of the quantum mechanic oscillator or vacuum fluctuations defined as [52]:

$$W_0 = \frac{1}{2} \cdot h\nu = N_{in} \tag{2.109}$$

According to the above equation, F_{EDFA} is thus given as:

$$F_{EDFA} = \frac{1}{G_{EDFA}} \cdot [1 + (G_{EDFA} - 1) \cdot 2 \cdot n_{sp}] \tag{2.110}$$

For extremely large values of the optical gain ($G_{EDFA} \gg 1$), the noise figure can be reduced to $F_{EDFA,G\gg1} = 2 \cdot n_{sp}$, thus reaching its minimum value.
The ASE impact is dependent on the infrastructure of the single span. The span noise figure F_{SPAN} represents a combination of noise figures of EDFAs and optical fibers used in the span. The noise figure of the optical fiber F_{fib} is given by:

$$F_{fib,i} = \frac{1}{G_{fib,i}} \tag{2.111}$$

Depending on the dispersion compensation scheme, a single span can consist of several fibers with different noise characteristics $F_{fib,i}$. In a dispersion post-compensation scheme, the F_{SPAN} (Fig. 2.29) is defined as:

$$\begin{aligned} F_{SPAN} \quad = \quad & F_{fib,1} + \frac{F_{EDFA,1} - 1}{G_{fib,1}} + \frac{F_{fib,2} - 1}{G_{fib,1} \cdot G_{EDFA,1}} + \\ & + \frac{F_{EDFA,2} - 1}{G_{fib,1} \cdot G_{EDFA,1} \cdot G_{fib,2}} \end{aligned} \tag{2.112}$$

where $G_{EDFA,1}$ represents the amplifier gain after SMF and $G_{EDFA,2}$ after DCF fiber. Substituting equations Eqs. 2.110 and 2.111 into Eq. 2.112 yields:

$$F_{SPAN} = 1 + 2 \cdot n_{sp} \left[G_{fib,2} \cdot G_{EDFA,2} \cdot (G_{EDFA,1} - 1) + (G_{EDFA,2} - 1) \right] \tag{2.113}$$

Thus, F_{SPAN} depends on the length and the attenuation of the fibers as well as on the gain and inversion factor of EDFAs. The total gain per span G_{SPAN} is defined as the product of all component gains and it is set to 1 in order to compensate all span losses:

$$G_{SPAN} = G_{fib,1} \cdot G_{EDFA,1} \cdot G_{fib,2} \cdot G_{EDFA,2} = 1 \tag{2.114}$$

In a multi span transmission line with N spans, the total noise figure F_{tot} of the system is calculated as:

$$\begin{aligned} F_{tot} &= 1 + \sum_{i=1}^{N} [F_i - 1] \\ &= 1 + 2 \cdot n_{sp} \cdot N \cdot [G_{fib,2} \cdot G_{EDFA,2} \cdot (G_{EDFA,1} - 1) + (G_{EDFA,2} - 1)] \end{aligned} \tag{2.115}$$

Thereby, the n_{sp} of the EDFA dominates F_{tot} (Fig. 2.31). The gain and noise figure of EDFAs used in each span depend on the relation between the desirable input powers in SMF (P_{SMF}) and DCF (P_{DCF}). P_{DCF} has to be small due to increased nonlinear effects according to the smaller core area in DCFs. If the difference between P_{SMF} and P_{DCF} is large, the EDFA after the DCF operates in a high gain region and the impact of the ASE-noise increases (Fig. 2.30).

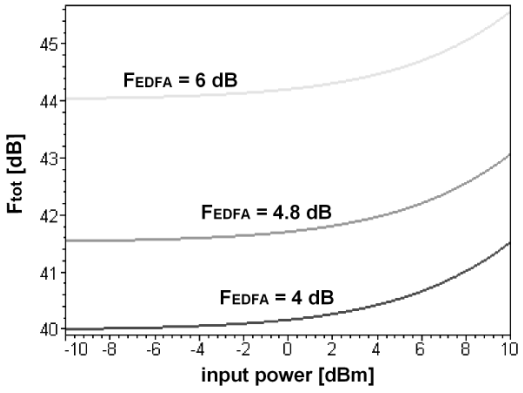

Figure 2.30: Total noise figure F_{tot} after 10 spans versus input power (P_{DCF}=0 dBm)

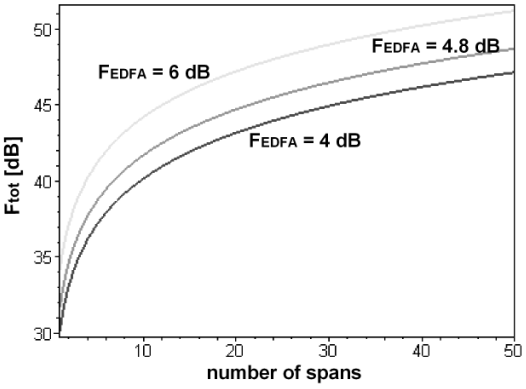

Figure 2.31: Total noise figure F_{tot} distance (P_{SMF}=0 dBm, P_{DCF}=0 dBm)

Impact of the span configuration on the noise figure of the span

Depending on the chosen dispersion compensation scheme in the system, the span configuration may be changed, resulting in different accumulation of ASE-noise. For example, if a hybrid dispersion compensation per span (Fig. 2.29) is considered with a constant P_{DCF}, three EDFAs are necessary in order to compensate the fiber losses and enable constant input power in SMF and DCF. The transmission performance of the system profits from the increased number of EDFAs in the systems, because the impact of ASE-noise is reduced. In this case, the noise figure of the span $F_{SPAN,hybrid}$ is given as:

$$\begin{aligned} F_{SPAN,hybrid} &= F_{fib,1} + \frac{F_{EDFA,1} - 1}{G_{fib,1}} + \frac{F_{fib,2} - 1}{G_{fib,1} \cdot G_{EDFA,1}} + \\ &+ \frac{F_{EDFA,2} - 1}{G_{fib,1} \cdot G_{EDFA,1} \cdot G_{fib,2}} + \frac{F_{fib,3} - 1}{G_{fib,1} \cdot G_{EDFA,1} \cdot G_{fib,2} \cdot G_{EDFA,2}} + \\ &+ \frac{G_{EDFA,3} - 1}{G_{fib,1} \cdot G_{EDFA,1} \cdot G_{fib,2} \cdot G_{EDFA,2} \cdot G_{fib,3}} \end{aligned} \tag{2.116}$$

and the noise figure after N spans is, according to the definition in Eq. 2.112:

$$\begin{aligned} F_{tot,hybrid} &= 1 + 2 \cdot n_{sp} \cdot N \cdot [G_{fib,2} \cdot G_{EDFA,2} \cdot G_{fib,3} \cdot G_{EDFA,3}(G_{EDFA,1} - 1) \\ &+ G_{fib,3} \cdot G_{EDFA,3}(G_{EDFA,2} - 1) + (G_{EDFA,3} - 1)] \end{aligned} \tag{2.117}$$

If all EDFAs in a such system are identical (equal n_{sp}) and if P_{DCF} and P_{SMF} are maintained, the differences between F_{tot} in various span infrastructures, which are realized by as a combination of a dispersion pre- and post-compensation per span, are rather small (Fig. 2.32) and becomes even smaller with a reduced DCF length.

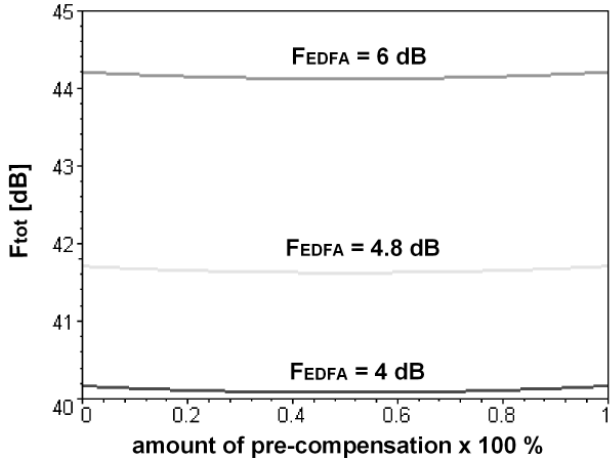

Figure 2.32: Total noise figure F_{tot} for different span infrastructure (span configurations from Fig. 2.29, full dispersion compensation per span, 10 spans, L_{SMF}=100 km, α_{SMF}=0.22 dB/km, α_{DCF}=0.5 dB/km, P_{SMF}=0 dBm, P_{DCF}=0 dBm)

Numerical model of the optical amplifier (EDFA)

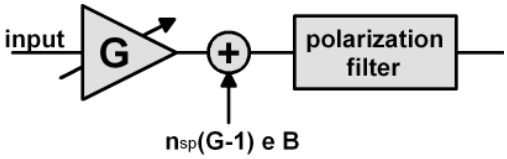

Figure 2.33: Numerical model of EDFA

Several recently proposed numerical models of EDFAs [3], [131] enable an efficient modeling of EDFA features (e.g. gain, noise figure). The principle of the simplified EDFA numerical model used in this work is illustrated in Fig. 2.33. The EDFA is characterized by its gain G and inversion factor n_{sp}. The input signal is amplified with a gain G. The amplified signal is superposed with a gain-dependent ASE-noise spectral density with a Gaussian distribution:

$$N_{out} - N_{in} = \rho_{ASE}(G) = n_{sp} \cdot (G-1) \cdot h\nu \tag{2.118}$$

ASE-noise is modeled by a Gaussian distributions and superposed in both signal polarization components [32]. The total simulated ASE-noise noise power P_{ASE} is given by:

$$P_{ASE} = \rho_{ASE}(G) \cdot B_{tot} \tag{2.119}$$

where B_{tot} represent the total system bandwidth. The noise figure F_{EDFA} in the considered numerical model is given as [3]:

$$F_{EDFA} = 10 \log \left[2n_{sp} \cdot \frac{G-1}{G} + \frac{1}{G} \right] \tag{2.120}$$

The role of the polarization filter at the EDFA output (Fig. 2.33) is to suppress a specified signal polarizations in order to enable a reduced simulation time. The simplified EDFA model considered in this work is characterized by a flat wavelength independent gain spectrum.

2.9 Optical receivers

The role of the optical receiver is the detection of the transmitted signal by the opto-electrical transformation of the received signal in a photo diode (e.g. pin, APD). Furthermore, additional electrical equalization is performed together with an electrical signal amplification enabling further signal-processing (e.g. clock-recovery) and performance evaluation (e.g. quality measurements). Depending on the pulse generation technique employed in the transmission line, it can be distinguished between the direct detection and coherent detection. Direct detection is used in amplitude modulated (AM) systems, and according to its simple realization and robustness, direct detection based receivers are used in all operating and commercially available transmission systems.

Direct detection receiver

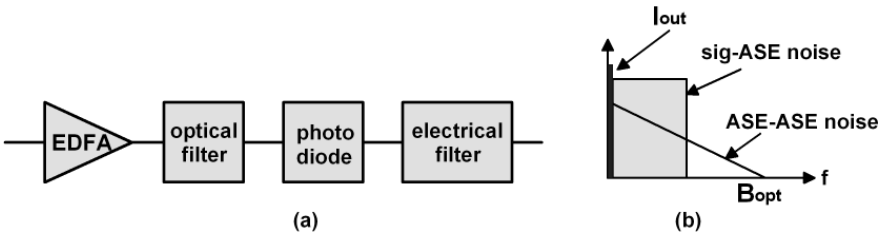

Figure 2.34: Receiver principles: a) direct detection receiver with an EDFA based pre-amplifier b) beat-noise contributions

The direct detection based receiver illustrated in Fig. 2.34a is used for all investigations presented in this work. It consists of an optical pre-amplifier followed by an optical filter, a semiconductor photodetector (e.g. pin-diode) and an electrical filter. The optical filter with a bandwidth B_{opt} reduces ASE-noise impact on the optical signal. In WDM-based systems the additional role of the optical filter is the channel isolation (demultiplexing). The role of the electrical filter is the equalization of the detected signal, and a Bessel-Thomson filter of 3-5 order with a 3-dB bandwidth of 0.7 × bit rate [GHz] (e.g. 28 GHz for 40 Gb/s data rate) is typically used. The incoming light P_{in} at the photo-diode generates a photo current I_{ph}:

$$I_{ph} = R \cdot P_{in} \tag{2.121}$$

R is the responsitivity of the photo-diode given by:

$$R = \frac{e\eta}{h\nu} \approx \frac{\eta\lambda}{1.24\mu m} \left[\frac{A}{W}\right] \tag{2.122}$$

where e is the electron charge, η is the quantum efficiency representing the relation between the electron generation rate and photon incidence rate and $h\nu$ is photon energy ($h = 2.34 \cdot 10^{-34}$ - Planck's quantum efficiency). Typical R values in 40 Gb/s photo-diodes amount to 0.6-1 A/W. Recently presented photo diode modules [132], [133], [134], [135] enable the realization of high-speed detectors for 40 Gb/s based transmission systems. These photo diodes are characterized by a large bandwidth (>50 GHz) and a low operating voltage (e.g. -1.5 V) [136]. The detected electrical signal is filtered by an electrical filter with bandwidth B_{el}. Through direct-detection additional noise terms are added to the electrical signal resulting in a variation - beating - of the signal level. The resulting noise terms are called beat noise. It can be distinguished between different beat noise contributions:

- signal-ASE beat noise $i^2_{sig-ASE}$
- ASE-ASE beat noise $i^2_{ASE-ASE}$
- ASE-shot noise $i^2_{ASE-shot}$

- signal-shot noise $i^2_{sig-shot}$

The beat noise terms are given by [137]:

$$i^2_{ASE-ASE} = 4R^2\rho^2_{ASE}B_{opt}B_{el} = (\eta GFe)^2 \cdot B_{opt}B_{el} \quad (2.123)$$

$$i^2_{ASE-shot} = 4Re\rho_{ASE}B_{opt}B_{el} = 2e^2\eta GFB_{opt}B_{el} \quad (2.124)$$

$$i^2_{sig-ASE} = 2R^2GP_S\rho_{ASE}2B_{el} = 2(e\eta G)^2P_sFB_{el}/h\nu \quad (2.125)$$

$$i^2_{sig-shot} = 2ReGP_SB_{el} = 2e^2\eta GP_sb/h\nu \quad (2.126)$$

where ρ_{ASE} is the optical (ASE) noise density defined as the relation between noise power (P_{ASE}) and optical bandwidth B_{opt}, B is the single-sided receiver noise bandwidth and P_S is the signal power into the pre-amplifier with gain G and noise figure F. Additionally, thermal noise (i^2_{therm}) occurs at the photo diode:

$$i^2_{therm} = 4k_BT \cdot \frac{B}{R_{ph}} \quad (2.127)$$

where k_B is the Bolzmann constant, T is the temperature and R_{ph} the resistor of the photo diode. The ASE-ASE beat noise $i^2_{ASE-ASE}$ spectrum is calculated as the auto-correlation of the ASE optical spectrum. Taking the frequency response of the electrical filter into account, the $i^2_{ASE-ASE}$ noise is calculated as [137]:

$$i^2_{ASE-ASE} = \int_0^\infty i^2_{ASE-ASE}(f)|H(f)|^2df \quad (2.128)$$

where $i^2_{ASE-ASE}$ is the ASE-ASE single-sided beat noise spectrum and H(f) is the complex amplitude response of the electrical filter. Figure 2.34b shows the single-sided noise spectral densities used for the calculation of $i^2_{sig-ASE}$ and $i^2_{ASE-ASE}$ by the integration from 0 to B_{el} [137]. $i^2_{sig-ASE}$ has a rectangular spectrum proportional to the electrical filter bandwidth B_{el}. $i^2_{ASE-ASE}$ has a triangular spectrum (Fig. 2.34b).
The most dominant noise limitation is caused by the sig-ASE noise term, which is dependent on the signal power and ASE-noise of the pre-amplifier. The impact of ASE-ASE noise is governed by the optical filter after the pre-amplifier and it can be efficiently suppressed by tailoring the optical filter bandwidth at the receiver side. Signal-shot, ASE-shot and thermal noise terms can be neglected in practically relevant system investigation since they are much smaller than ASE-noise [23], [138].

3 Optical modulation formats

3.1 Overview

In this chapter, the methods for the optical signal generation are introduced. The focus is set on modulation formats employing the amplitude modulation of the optical carrier, because of their importance in today's optical transmission systems. The generation and transmission characteristics of conventional and novel modulation formats are presented.

3.2 Optical signal generation

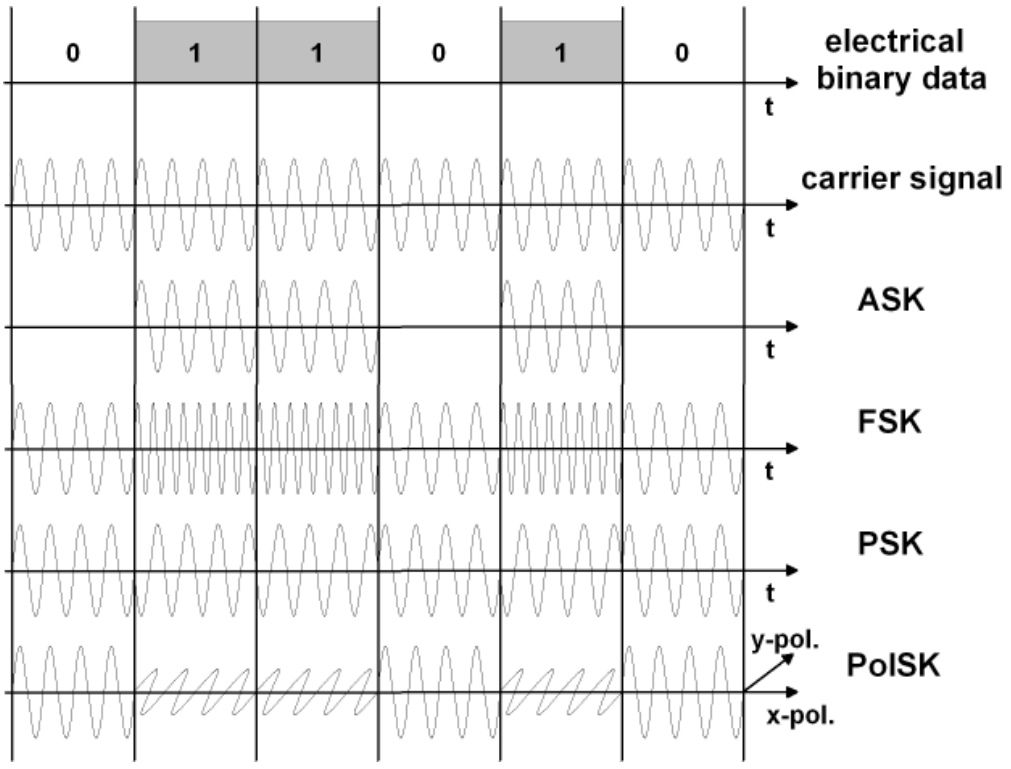

Figure 3.1: Principles of optical signal modulation

The signal generation in terms of optical transmission systems can be understood as the modulation of a laser source with an electrical binary signal. According to this, we are speaking of the optical signal modulation and modulation formats. The modulated complex electric field is given by:

$$\overrightarrow{E}_L(t) = A_{0,L}(t) \cdot \overrightarrow{e}_L(t) \cdot cos\left\{\omega_L t + \varphi_L(t)\right\} \tag{3.1}$$

where $A_{0,L}(t)$ is the amplitude of the optical field, ω_L is the optical angular frequency of the light source, φ_L is the optical phase and $\overrightarrow{e}_L$ represents the polarization vector known as Jones-vector of the signal. These four parameter are four degrees of freedom employed for the optical signal generation. Each of these

parameters can be modulated by an electrical binary baseband signal $q(t)$:

$$q(t) = \sum_{i=-\infty}^{\infty} q_i \cdot g(t - iT_b) \tag{3.2}$$

with the information coefficients $q_i \in [0, 1]$ and the baseband pulse shape $g(t)$ delayed by multiples of the bit period T_b. Basically, depending on which signal parameter is modulated, it can be distinguished between: amplitude shift keying (ASK), frequency shift keying (FSK), phase shift keying (PSK) and polarization shift keying (PolSK).

Amplitude-Shift-Keying (ASK) known as "On-Off"-keying (OOK) is the technique of modulating the intensity of the carrier signal. In the simplest form, a source is switched between **on** and **off** states (Fig. 3.1). The signal representation is therefore:

$$A_{0,L}(t) = \begin{cases} A_0 = 0 & \text{, if } q(kT_b) = 0 \\ A_1 = \sqrt{\frac{2E_b}{T_b}} & \text{, if } q(kT_b) = 1 \end{cases} \tag{3.3}$$

The ASK modulation is characterized by the relation between the signal levels in **on** (marks) and **off** (spaces) states called extinction ratio (ER):

$$ER = \frac{A_1^2}{A_0^2} \tag{3.4}$$

The ER value is dependent on the approach used for the signal generation: direct or external modulation of the laser source. In case of external modulation, the ER is limited by the extinction ratio of the external modulator. Typical ER values vary between 8-12 dB depending on the signal bit rate in use. The ASK-based modulation formats are characterized by simple signal generation and detection, with the consequence that all currently deployed optical transmission systems employ ASK-based modulation formats. The scope of this work are transmission systems with various ASK-based formats, which will be presented in detail in following sections. Due to the use of different modulation methods for generation of these formats, they posses different signal shapes (e.g. return-to-zero or non return-to-zero) and spectral characteristics, resulting in different transmission behaviors.

Frequency Shift Keying (FSK) is realized by switching the laser light frequency between two frequency values for marks and spaces (Fig. 3.1). Thereby, the optical signal envelope remains unchanged and the complexity of signal generation and detection increases compared to ASK modulation. The complex amplitude of the FSK signal is given by Eq. 3.1 with [31]:

$$\frac{d\phi_L}{dt} = \begin{cases} +2\pi\Delta f_{FSK} & \text{, if } q(kT_b) = 0 \\ -2\pi\Delta f_{FSK} & \text{, if } a(kT_b) = 1 \end{cases} \tag{3.5}$$

where $2 \cdot \Delta f_{FSK}$ is the frequency shift between marks and spaces. FSK modulation is characterized by the modulation index m_{FSK}, which describes the relation between the Δf_{FSK} and the signal bit rate B:

$$m_{FSK} = \frac{2\Delta f_{FSK}}{B} \tag{3.6}$$

By the variation of m_{FSK}, different FSK-based modulation format can be realized (e.g. $m_{FSK} = 0.5$ - Minimum Shift Keying (MSK)). The differences between FSK formats are reflected in the optical signal spectra [31], whereby a smaller m_{FSK} enables more compact optical spectra. The FSK-based formats are not used in already deployed transmission systems because of complex signal detection. More recently, FSK-based modulation known as Dispersion Supported Transmission (DST) [89] format was intensively investigated for the implementation in MAN networks [90]. The idea behind DST is that a FSK modulated signal (e.g. MSK) interacts with the dispersion in the transmission line, causing a FM-IM transformation of the optical signal

resulting in an ASK-modulated signal at the receiver side, so that a conventional direct detection receiver can be used [139]. The main drawback of this new technique is that the transmitter and receiver parameters (e.g. m_{FSK} and receiver filter settings) have to precisely match the characteristics of the transmission line, requiring a detailed characterization of the dispersion in the transmission line.

Phase Shift Keying (PSK) uses the phase of the signal to encode information. Optical PSK signals posses a narrow spectrum and a constant signal envelope (Fig. 3.1), which enables improved nonlinear tolerance, but on the other hand the PSK signals are sensitive to a phase modulation induced by multi-channel effects, which can result in decoding errors at the receiver side. At the same time, PSK-based modulation enables an improved receiver sensitivity (up to 6 dB) [140] compared to ASK-formats. Especially interesting method of PSK modulation is differential PSK (DPSK). In DPSK signals, the information is encoded in the phase change between two successive bits. The signal in DPSK representation is given by:

$$\varphi_{signal}(kT_b) - \varphi_{signal}[(k-1)T_b] = \begin{cases} 0 & \text{, if } q(kT_b) = 0 \\ \pi & \text{, if } q(kT_b) = 1 \end{cases} \tag{3.7}$$

Basically, PSK signals only allow coherent detection, which require a local oscillator at the receiver to compare the phase of transmitted with the phase of the local signal, making the feasibility of this modulation more difficult. Also, a phase-locked-loop (PLL) is required to synchronize the local oscillator to the received signal. Pure PSK modulation is rather inapplicable for the system implementation, but some special binary and multilevel variants of PSK like DPSK [141] or differential quaternary PSK (DQPSK) [142] allow the use of direct detection methods. DQPSK enables a further improvement of the code efficiency using 4 different phases [140], where the signal symbol rate is half of that in DPSK case. The DQPSK bit stream must be differentially encoded using a digital pre-coder. The signal detection in DPSK formats can be made using MZI interferometer based configurations [142], [143], which enable a reduced detection complexity compared to coherent detection. In spite of increased realization complexity of PSK modulation, recently presented DPSK and DQPSK investigations in 40 Gb/s based WDM systems [144], [145], [146] identified these formats as good alternatives to ASK-based modulation formats in future high speed WDM systems.

Polarization Shift Keying (PolSK) is the most exotic modulation format among all already presented. The optical PolSK signals are generated by switching the signal polarization between two orthogonal states of polarization. The PolSK is characterized by a constant signal envelope enabling an improved nonlinear tolerance [147], an improved sensitivity (3 dB) [148] compared to ASK-based modulation, and enables a better utilization of the system bandwidth by the use of orthogonal polarization as an additional degree of freedom. PolSK is a good alternative for the realization of multilevel modulation formats [149]. The drawbacks of PolSK are an increased complexity of signal generation and detection, as well as, the sensitivity to polarization disturbances (e.g. PMD, PDL) in the transmission line, whose impact increases with an increased channel data rate. Despite the fact that, PolSK may not be interesting for the implementation in commercial transmission systems, because of its complexity and sensitivity, it can be used as additional modulation stage for the improvement of nonlinear tolerance of ASK-based modulation formats.

3.3 NRZ-based modulation formats

A basic classification of the various ASK-based modulation formats can be made according to the shape of the optical pulses. All modulation formats can be divided into three groups: NRZ-based, RZ-based and novel modulation formats. In this chapter, the NRZ modulation formats are introduced. Non-return-to zero (NRZ) and duobinary modulation belong to this group.

3.3.1 Non-return-to-zero (NRZ) modulation

The Non-return-to-zero (NRZ) is the major applied modulation format in today's optical transmission systems. The technique for generation of NRZ pulses is well known from classical telecommunication theory. The information source emits a bit sequence of binary symbols at a bit rate of R=$1/T_B$, where T_B is a time interval of each bit known as the bit slot. The electronic sequences of bits can be described as:

$$x(t) = \sum_{n=-\infty}^{\infty} q_i \cdot f(t - nT_b) \tag{3.8}$$

where b_n are information symbols represented by a binary sequence of 0's and 1's. The function $f(t)$ describes the pulse shape, an almost square pulse of duration T_0, which is proportional to the employed bit rate. The pulse duration of the NRZ pulses is equal to the length of the time slot ($T_0 = T_b$). During one time slot NRZ pulse retains the same amplitude and between successive 1's no change of the signal amplitude occurs. The electronic sequence, which drives the external modulator, is generated in a NRZ coder. The rise-time of the electrical signal is tailored by the use of an electrical filter and amounts typically to 25 % of the pulse width. The rise-time describes the edge steepness of NRZ pulses and depends on the filter type used for electrical pulse forming. The complex envelope of resulting optical NRZ signal can be defined as:

$$E_{NRZ}(t) = \sum_{n} a_n \cdot h(t - nT_b) \tag{3.9}$$

where T_b is the bit length and $h(t)$ is the elementary pulse shape created in the MZM by the convolution of pulse shape and filter transfer function. a_n represents the coefficient of encoded sequence with a value of 1 or 0 for marks and spaces, respectively. The optical signal generation of NRZ pulses is illustrated in Fig. 3.2.

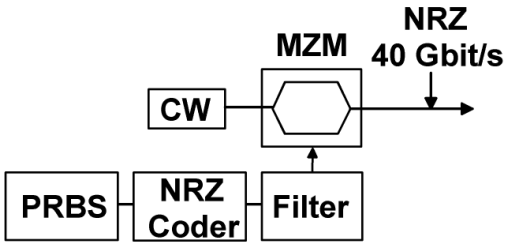

Figure 3.2: Generation of 40 Gb/s NRZ signals

The light of the continuous wave (CW) pump is externally modulated in a $LiNbO_3$ MZM. The MZM is driven at the quadrature-point of the modulator power transfer function (Chapter 2.2.2) with an electrical NRZ signal. The generation of NRZ pulses can also be realized with an electro-absorption modulator (EAM). The disadvantages of an EAM are relatively small extinction ratio (about 10 dB) and an internal modulator chirp [43]. On the other hand, the bias voltage for the EAM is smaller and an EAM can be integrated on the same chip with a laser [42], resulting in a reduction of production costs. The signal waveform and spectrum of a 40 Gb/s optical NRZ signal are shown in Fig. 3.3. A criterion for the pulse width of an optical signal is the duty cycle (duty ratio). The duty cycle is defined as the relation of the full pulse width at the half maximum (FHWM) to the bit slot. In the case of NRZ, the duty cycle equals to 1 (Fig. 3.3b), indicating the extremely steep signal edges of NRZ pulses. The chirp observed in Fig. 3.3b is caused actually by the CW-pump chirp,

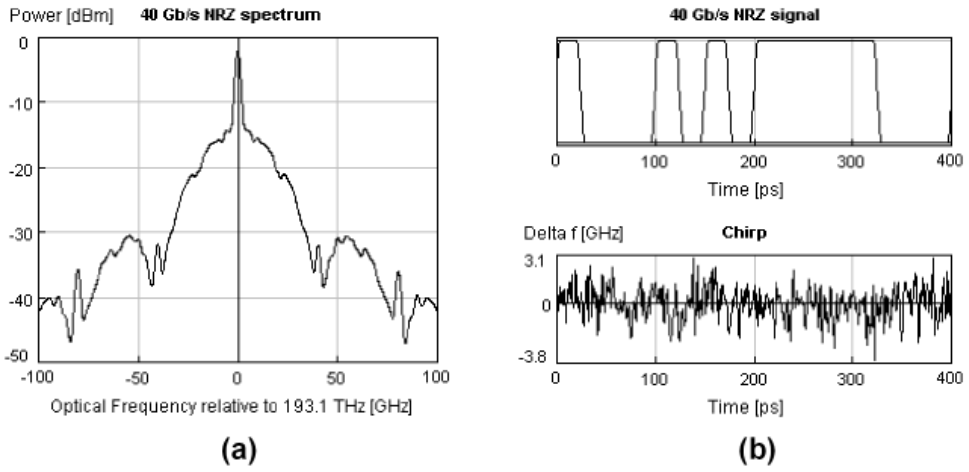

Figure 3.3: 40 Gb/s NRZ signal: a) optical spectrum b) signal shape and chirp

which is proportional to the laser line-width. The edge steepness affects the nonlinear characteristics of NRZ-based optical transmission, increasing the impact of SPM effect, which is directly proportional to the steepness of the signal edges (Chapter 2). The steeper the edges the stronger is the generation of new spectral components due to the SPM effect, resulting in a spectral broadening of the signal spectrum. The additional interplay between SPM and group velocity dispersion (GVD) transforms SPM-induced phase modulation to intensity modulation (PM-IM transformation) giving rise to significant system limitations [150], [151] in NRZ-based transmission systems.
NRZ pulses possess a narrow optical spectrum due to the lower on-off transitions in NRZ bit streams. The spectral width at -30 dBm power level of a 40 Gb/s NRZ optical spectrum amounts to 60 GHz (Fig. 3.3a). The NRZ spectrum is concentrated around the carrier frequency. The compact bandwidth of generated optical pulses represents an important modulation characteristic, which governs the impacts of different propagation effect e.g. GVD and inter-symbol interference (ISI). A reduction of the spectral width improves the dispersion tolerance of the modulation format, but on the other hand it affects the ISI effects between the pulses. This becomes evident for isolated spaces between sequences of the marks where the energy of neighboring marks becomes transformed in the time slot of the isolated space resulting in ISI effects and a reduced transmission quality. The narrow spectrum of NRZ pulses yields a better realization of a dense channel spacing in DWDM systems, enabling a better utilization of the system bandwidth and makes NRZ pulses more robust to the impacts of chromatic dispersion, resulting in a higher dispersion tolerance. A large dispersion tolerance can be important in 40 Gb/s WDM systems with large number of channels, because of a permanent presence of the residual dispersion, whose amount depends on the total system bandwidth and the employed transmission fiber types.

3.3.2 Duobinary modulation

Duobinary modulation can be described as a combination of a conventional ASK-based modulation and phase shift keying (PSK). Depending on the realization, optical duobinary transmission can be understood as a multilevel transmission with phase encoded bits and a reduced spectral width. Duobinary transmission technology was introduced for the first time by A. Lender [151] in the 1960s as a mean of transmitting binary data over an electrical cable with high-frequency cutoff characteristics. Recently, duobinary modulation [152], [153], [92] has been applied to high-speed optical transmission systems with a channel data rate of 10 Gb/s in order to improve their dispersion tolerance. Figure 3.4 illustrates the coding process of duobinary signal generation. The signals are generated by adding bits delayed by one bit period to the current bit. The complex envelope of the optical duobinary signal is defined using Eq. 3.9 considering a coefficient a_n of 1, 0 and -1. In optical duobinary signals, the three-levels are mapped into three optical states "1", "0" and "-1"

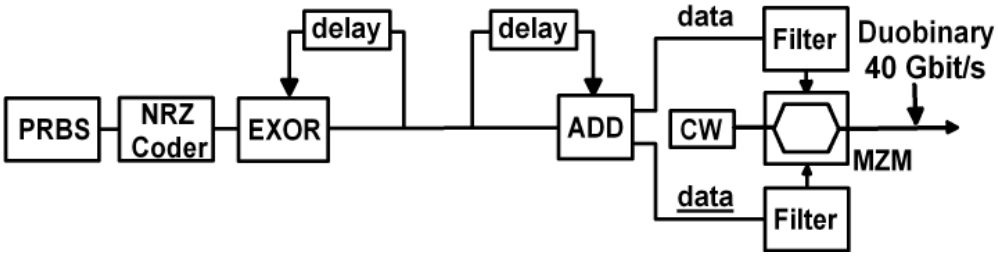

Figure 3.4: Generation of 40 Gb/s duobinary signals

by modulating both the amplitude and the phase of the signal. The "1" and "-1" levels have the same optical intensity, but opposite phase. The distance between the levels is almost equal to that of the binary signal. In addition, the optical duobinary signals can be demodulated into a binary signal with a conventional direct detection type optical receiver. This is an important advantage in terms of reduced complexity for the future system implementation.
For duobinary generation, electrical NRZ signals are pre-coded in an encoder (EX-OR circuit) (Fig. 3.4). The pre-coded binary signals are converted to 3-level duobinary signals by band-limiting electrical filters. This can be explained by the fact that a narrow-band filtering of a two-level electrical signal produces an additional signal level. At the same time, the band limiting of electrical pulses provides a reduction of the duobinary spectrum compared to a conventional NRZ spectrum. The realized spectral reduction depends on the filter type used. A sharp cutoff filter is preferable for duobinary signal generation [92]. The optimum filter type would be an ideal rectangular filter, but since the practical realization of this filter type is rather complex, a duobinary filter [92] (e.g. cosine filter) - 5^{th} order Bessel or Bessel-Thomson low-pass filter (LPF) - can be used, as well. The cutoff frequency of the LPF equals a quarter of the bit rate. The LPF acts as an analog converter, which simultaneously converts signals from binary to duobinary and trims high frequency components in the duobinary signal spectrum. The three signals levels are mapped into optical "1", "0" and "-1" levels by a push-pull type $LiNbO_3$ chirp-free MZM, which is driven by the duobinary signal and its inverted version (Fig. 3.4). At the receiver side the modulated signals are detected with a conventional binary direct detection receiver. The photo diode at the receiver side converts the optical duobinary signal back to an electrical binary signal. The detected signal has to be inverted for the detection of the original binary signal making a logic inverter necessary for the data recovery.
Figure 3.5 illustrates an optical spectrum and a signal waveform of a 40 Gb/s duobinary signal. Due to the narrow-band duobinary filtering in the electrical domain, the spectral width of the signal (Fig. 3.5a) is reduced twice compared to a conventional NRZ signal. The signal waveform shows a typical NRZ shape and the transmitted pulses are encoded in phase (Fig. 3.5b).
The reduction of the spectral width of the optical duobinary signal is the reason for its better dispersion tolerance compared to NRZ signals and enables an improved spectral efficiency in WDM systems. A further advantage of duobinary modulation is the suppression of SBS-effect, since in the optical duobinary spectrum the carrier is effectively suppressed [92]. In quasi-linear operating regime (power per channel P_{IN} <2 dBm/ch) duobinary modulation, compared to NRZ modulation, shows an enhanced dispersion tolerance by a factor of two [154]. In the nonlinear regime (P_{IN} >8 dBm/ch) both formats possess similar transmission characteristics due to a strong impact of SPM-induced spectral broadening. In recent works [155], [156], [157] spectral efficiencies larger than 0.4 bit/s/Hz were reported for duobinary based WDM systems with co-polarized adjacent channels. Therein, a proper optical filtering was essential for the realization of enhanced spectral efficiency. The spectral efficiency can be even further increased up to 1 bit/s/Hz by the use of polarization interleaved multiplexing technique between adjacent channels [155].
The main disadvantage of duobinary signals, similar to NRZ signals, is a relatively strong impact of fiber nonlinearities, which represents the main limiting factor for the maximum transmission length and the achievable transmission quality. Several methods were recently proposed to enhance the duobinary nonlinear tolerance. The implementation of pre-chirp at the transmitter side, which can be realized by a modulator internal chirp [158], by a fiber piece, or by a reduced electrical filter bandwidth [159], [160], reduces the dispersion toler-

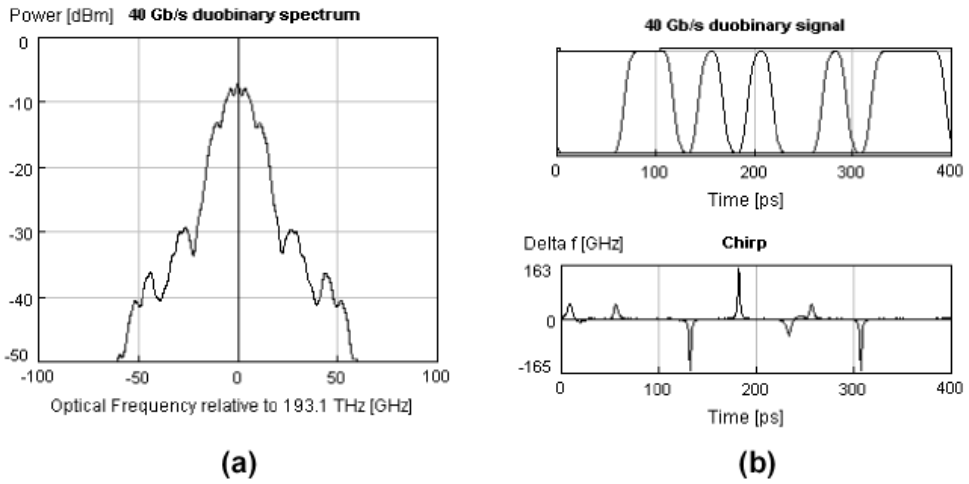

Figure 3.5: 40 Gb/s duobinary signal: a) optical spectrum b) signal shape and chirp

ance, but on the other hand improves transmission robustness of duobinary based WDM systems. Another possibility would be a combination of duobinary modulation with nonlinearly robust modulation formats (e.g. RZ, CSRZ), which enables a better nonlinear characteristics (e.g. duobinary carrier suppressed RZ (DCS-RZ) [161], duobinary RZ (DRZ) [162]), where the generated pulses possess a duobinary spectral characteristics and RZ pulse shape. These new duobinary based modulation methods enable the realization of WDM systems with a dense channel spacing according to a narrower optical spectrum and with an improved transmission performance due to the use of RZ-based signal forms. Several experimental works [157], [156] presented methods for implementation of duobinary technology in 40 Gb/s WDM systems. Due to its large dispersion tolerance, the duobinary modulation is suitable for optical metro area networks (MANs) [163], in which the component costs and a signal generation realized in electrical domain play an important role.

3.4 RZ-based modulation formats

The signal generation of RZ-based modulation formats is presented in this chapter. The RZ-based modulation formats considered here are return-to-zero (RZ), carrier-suppressed RZ (CSRZ), single side-band RZ (SSB-RZ) and chirped RZ (CRZ) modulation. The collective characteristics of these formats are a duty ratio smaller than 1 and a broad signal spectrum.

3.4.1 Return-to-zero (RZ) modulation

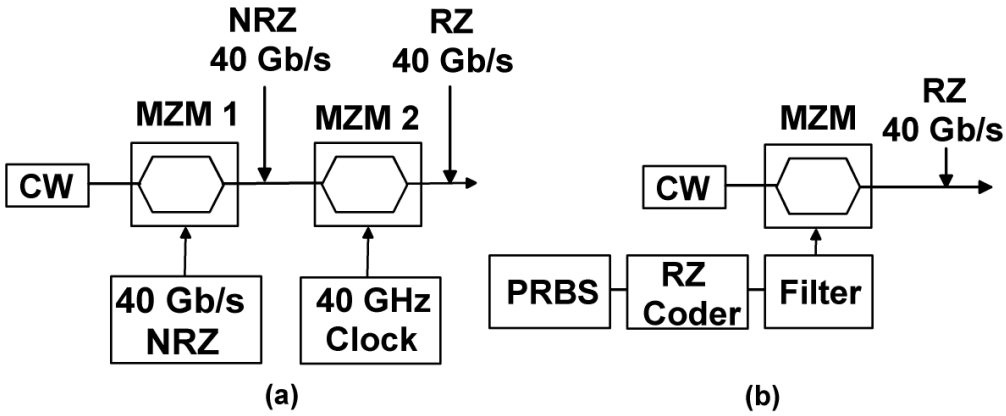

Figure 3.6: Generation of 40 Gb/s RZ signal: a) practical generation setup b) ideal generation setup

The RZ pulses occupy just a part of the bit slot, resulting in a duty cycle value smaller than 1. Various methods can be used for the RZ generation. Starting with an electrical or optical time division multiplexing (ETMD/OTDM) of several lower data rate channels, over an actively mode-locked laser in addition to a NRZ data modulator [164] and a generation with two modulation stages [165], up to the generation with a phase modulator and delay line interferometer [166], the complexity and costs of RZ signal generation are varying. Figure 3.6 illustrates two different methods for generating optical RZ pulses. The widely used method for RZ generation employs two modulator stages (Fig. 3.6a). In the first modulator stage, optical NRZ pulses are generated in a $LiNbO_3$ MZM, which is driven by an electrically filtered NRZ signal at 40 GHz. In a second MZM, a signal shape transformation from NRZ to RZ takes place. The second MZM (Fig. 3.6a) is driven by a 40 GHz sine-clock signal at the "quadrature"-point of the modulator power transfer function. Although widely used and practically more relevant, this method is difficult to realize because of the synchronization issues between two modulator stages, and the pulse shaping being limited by transmission characteristics of the second MZM, resulting in a reduced extinction ratio (ER) of the generated RZ pulses. Figure 3.6b illustrates an ideal approach for the RZ signal generation. With this approach, the RZ shaping is done by an electrical RZ coder and an additional electrical filter. This modulation method shows a reduced complexity and lower costs due to the use of a single MZM, but the problem in this case is the difficult realization of the electrical coder at 40 GHz, because the 40 GHz technology represents the upper limit of electrical signal generation. Therefore, RZ coders are not yet commercially available. In order to reduce the complexity of generation, RZ pulses can be generated by a combination of a phase modulator and a delay line interferometer [167], [168]. This technique requires no synchronization of the two electrical drive signals and enables a larger sensitivity ($>$ 2 dB), but the delay in the interferometer has to be precisely made. The limited modulator bandwidth can become a problem in the RZ case due to its broader optical spectrum. For a RZ detection, the conventional NRZ detector can be used.
Figure 3.7 illustrates the waveform and the optical spectrum of a 40 Gb/s RZ signal. As can be seen, the RZ signal amplitude between adjacent 1s returns to zero. For the same average power of a RZ pulse and a NRZ pulse, the peak-power of RZ pulse is twice as large and its pulse width is half as wide as in NRZ case. The main characteristic of RZ modulated signals is a relatively broad optical spectrum. The spectral

width between the two first side-bands amounts to 80 GHz (Fig. 3.7a). The large spectral width results in a reduced dispersion tolerance and a reduced spectral efficiency of RZ-based WDM systems. The RZ pulse shape enables an increased robustness to fiber nonlinear effects [169], [150] and to the effects of polarization mode dispersion (PMD) [170]. The small amount of chirp observed in RZ pulses (Fig. 3.7b) is actually the internal chirp of the CW-pump with a spectral line width of 10 MHz. This implies that higher optical powers per channel can be tolerated in a RZ-based WDM system, resulting in an improved maximum transmission length. The RZ system implementation improves the system receiver sensitivity up to 3 dB [171], [167]. A possible method for a further improvement of RZ transmission characteristics in a WDM system with a spectral efficiency of up to 0.4 bit/s/Hz is the use of so-called "tedon" [172], [173], [174] pulses. Tedon stands for a RZ pulse with a reduced duty cycle (τ <0.3) and a short pulse width (several ps). Its main feature is an increased robustness to fiber nonlinearities caused by the fact that short pulses disperse faster that the wider ones, enabling a fast reduction of the pulse peak power. Up to date, 40 Gb/s tedons were realized using OTDM-techniques [172]. The reduced pulse width in the tedon-case implies a broader signal spectrum making this technique less interesting for the implementation in DWDM systems with an increased spectral efficiency (>0.4 bit/s/Hz).

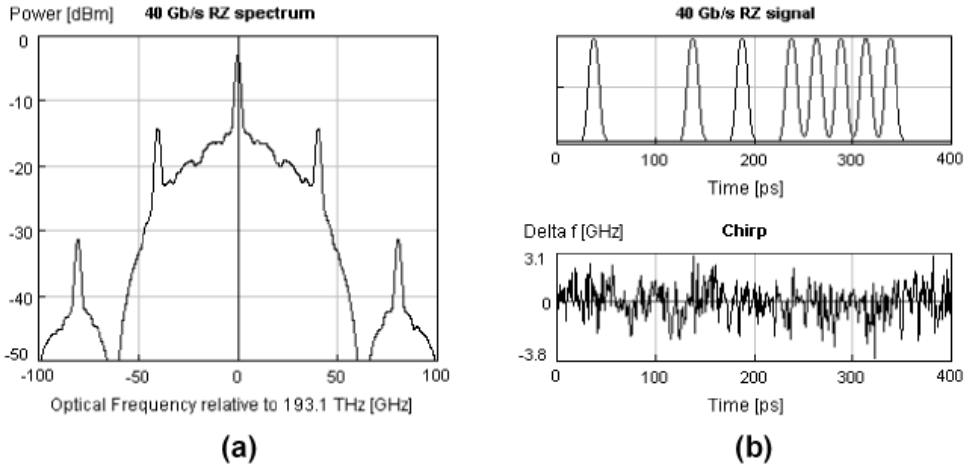

Figure 3.7: 40 Gb/s RZ signal: a) optical spectrum b) signal shape and chirp

In order to enable a dense channel spacing in RZ-based DWDM transmission systems, narrow-band filtering both at the transmitter and receiver side would be necessary [175], [176]. The RZ modulation would be a better candidate than NRZ for long-haul 40 Gb/s WDM transmissions, because of its better nonlinear robustness. Considering the PMD limitations presented in Chapter 2.3.1, the approximated maximum transmission length in 40 Gb/s RZ based systems is limited to about 1600 km by the PMD impact of first and higher order.

3.4.2 Carrier-suppressed RZ (CSRZ) modulation

Carrier-suppressed RZ (CSRZ) modulation is one of the recently proposed modulation formats for high bitrate transmission systems, which has been intensively investigated in numerical and experimental works [177], [178], [179], [180]. The main target of this modulation format is a reduction of the nonlinear impacts in a transmission line and an improvement of the spectral efficiency in high bit rate WDM systems. Additionally, it can be expected that the dispersion tolerance of the transmission can be improved as well by CSRZ modulation , due to its reduced spectral width compared to conventional RZ modulation. Recent publications [12], [18], [181] verified partly these expectations.

The generation of CSRZ pulses is presented in Fig. 3.8. The first MZM modulator (MZM 1) (Fig. 3.8) generates a 40 Gb/s NRZ optical signal by external modulation of the CW-pump light. MZM 1 is driven

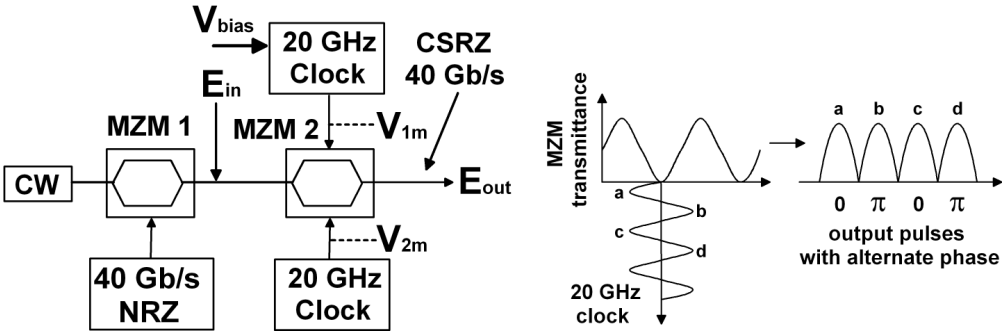

Figure 3.8: Generation of 40 Gb/s CSRZ signal

with a 40 GHz electrical NRZ signal at the "quadrature"-point of the modulator power function. The CSRZ signal forming is realized in the second MZM (MZM 2), which is biased at the "zero"-point. CSRZ signal generation can be mathematically described as:

$$E_{OUT} = jE_{IN} \sin\left[\frac{(\phi_1 - \phi_2)}{2}\right] \exp\left[j\frac{(\phi_1 + \phi_2)}{2}\right] \tag{3.10}$$

where E_{IN} and E_{OUT} describe the optical input and output fields of the second MZM. E_{IN} represents the optical field of a 40 Gb/s NRZ signal, which is generated in MZM 1. ϕ_1 and ϕ_2 are the optical phases of the two modulator arms and ϕ_1 is biased with a voltage V_{bias}. ϕ_1 and ϕ_2 and are defined as:

$$\phi_1 = \frac{\pi}{2}\frac{V_{1m}}{V_\pi}\sin(\omega t + \Psi) + \frac{\pi}{2}\frac{V_{bias}}{V_\pi} \tag{3.11}$$

$$\phi_2 = \frac{\pi}{2}\frac{V_{2m}}{V_\pi}\sin(\omega t) \tag{3.12}$$

where V_{1m} and V_{2m} are the amplitudes of a sine-clock signal, and Ψ stands for a phase difference between the two sine-clock signals. V_π is the voltage required for a π-phase shift. The second MZM used for CSRZ generation is biased at V_{bias}=0 and $V_{1m} = V_{2m} = V_\pi$. Ψ equals π. The frequency of the sine-clock amounts to f_0=20 GHz (equivalent to the half bit rate). The mathematical representation of the generated CSRZ signal can be given as:

$$\begin{aligned}
E_{CSRZ} &= jE_{IN}\exp(-j\beta L)\sin\left[\frac{(\phi_1 - \phi_2)}{2}\right]\exp\left[j\frac{(\phi_1 + \phi_2)}{2}\right] \\
&= jE_{IN}\exp(-j\beta L)\sin\left[\frac{\pi}{2}(\sin(\omega_0 t + \pi) - \sin(\omega_0 t))\right] \\
&\quad \cdot\exp\left[j\frac{1}{2}\left(\frac{\pi}{2}(\sin(\omega_0 t + \pi) + \sin(\omega_0 t))\right)\right] \\
&= jE_{IN}\exp(-j\beta L)\sin\left[\frac{\pi}{4}(-2\sin(\omega_0 t))\right] \\
&= -jE_{IN}\exp(-j\beta L)\sin\left[\frac{\pi}{2}\sin(\omega_0 t)\right]
\end{aligned} \tag{3.13}$$

with

$$\phi_1(CSRZ) = \frac{\pi}{2}\sin(\omega_0 t + \pi) = -\frac{\pi}{2}\sin(\omega_0 t) \tag{3.14}$$

$$\phi_2(CSRZ) = \frac{\pi}{2}\sin(\omega_0 t) \tag{3.15}$$

The optical CSRZ spectrum and signal shape are illustrated in Fig. 3.9. The carrier component of the CSRZ signal spectrum (Fig. 3.9a) is suppressed due to the external modulation at "zero"-point in the second MZM.

The spectral width between the two first spectral side-bands amounts to 40 GHz. Compared to the RZ case (Fig. 3.6a) a spectral reduction with a factor of 2 occurs. The CSRZ pulses possess a RZ signal shape with an optical phase difference of π between adjacent bits (Fig. 3.9b). This inter-pulse phase condition can be beneficial for an increased nonlinear tolerance [178].

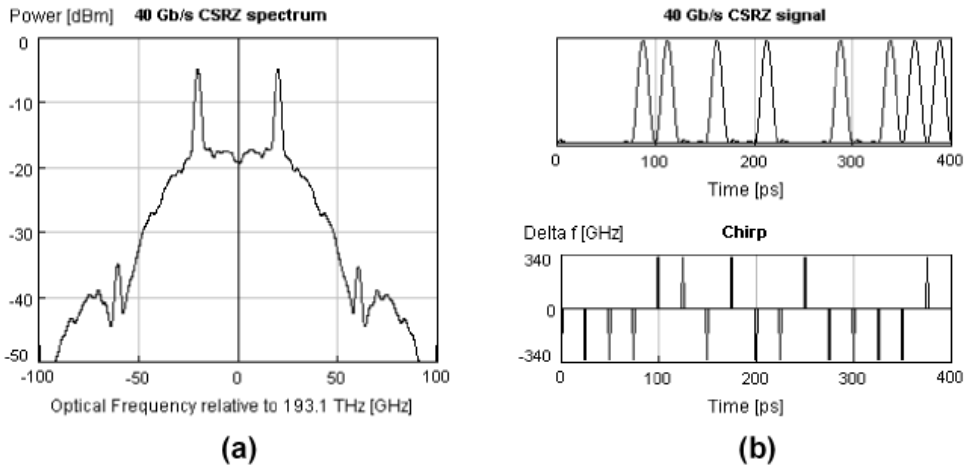

Figure 3.9: 40 Gb/s CSRZ signal: a) optical spectrum b) signal shape and chirp

Due to the reduced spectral width, CSRZ modulation shows an increased dispersion tolerance [165] and it is more robust to nonlinear impairments [177] than conventional NRZ and RZ formats. The nonlinear tolerance of CSRZ modulation can be enhanced by the implementation of pre-chirp at the transmitter side [182]. Therein, the amount of pre-chirp has to be carefully optimized in order to avoid an increase of the linear crosstalk and waveform distortions. Due to an RZ pulse shape, the CSRZ modulation offers a better receiver sensitivity than conventional NRZ modulation [178]. By the implementation of sophisticated filtering methods (e.g. asymmetrical filtering) [181], the robustness of CSRZ modulation to narrow-band filtering can be improved, which can be beneficial for DWDM systems [183]. By the use of an optimized narrow-band filtering [18] or a polarization multiplexing [12] in 40 Gb/s CSRZ based DWDM transmission systems, a spectral efficiency beyond 0.4 bit/s/Hz can be realized.

3.4.3 Single side band RZ (SSB-RZ) modulation

Single side-band (SSB) modulation is a modulation method well known from classical telecommunication theory. It can be realized by an additional modulation or filtering stage in combination with NRZ generation. The basic idea behind SSB modulation is the suppression or isolation of one side-band in conventional RZ spectrum because of its redundancy for direct detection [184]. Therein, the RZ signal shape is maintained. There are several different techniques for generation of optical SSB-RZ signals [185], [186], [187]. The simplest approach known as vestigial side-band (VSB) modulation [9], [188] uses an optical filter to suppress one of the side-bands. The side-band suppression can be done at the transmitter [185], [189] or at the receiver side [9], [190]. The bandwidth and the order of the optical filter must be carefully chosen in order to achieve the optimum operating range for a desired channel bit rate. A more complex method for the SSB-RZ generation [184] is presented in Fig. 3.10. There are some similarities to signal generation of CSRZ pulses (Fig. 3.8). Compared to CSRZ generation, the differences lie in the realization and operation of the second modulator stage and in parameter settings of the driving electrical signals. Equation 3.10 can be used for a mathematical description of the SSB-RZ pulses. For a generation of SSB-RZ signals, both amplitudes of the sine-clock signals are equal and amount to $V_{1m} = V_{2m} = \sqrt{0.5}V_\pi$. The phase difference Ψ is set to $\pi/2$. The second MZM is biased at the "quadrature"-point. The final mathematical description of the optical SSB-RZ

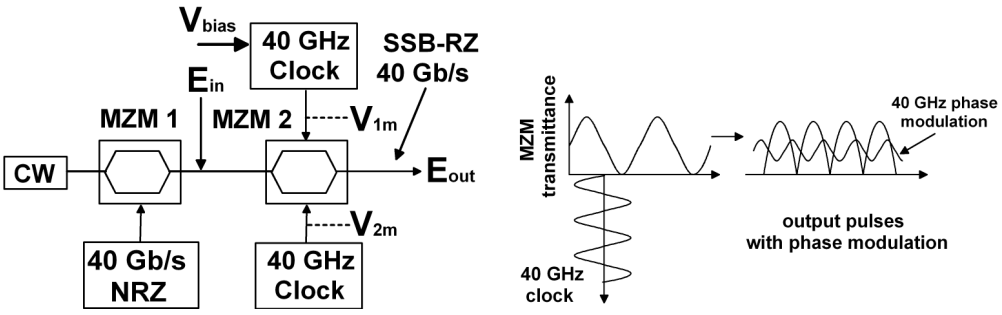

Figure 3.10: Generation of 40 Gb/s SSB-RZ signal

signal is:

$$
\begin{aligned}
E_{SSB-RZ} &= jE_{IN}\exp(-j\beta L)\sin\left[\frac{(\phi_1-\phi_2)}{2}\right]\exp\left[j\frac{(\phi_1+\phi_2)}{2}\right] \\
&= jE_{IN}\exp(-j\beta L)\sin\left[\frac{\pi}{4}\left(\frac{1}{\sqrt{2}}\sin(\omega_1 t+\frac{\pi}{2})+1-\frac{1}{\sqrt{2}}\sin(\omega_1 t)\right)\right] \\
&\quad \cdot\exp\left[j\frac{\pi}{4}\right]\exp\left[j\frac{\pi}{4}\left(\frac{1}{\sqrt{2}}\sin(\omega_1 t+\frac{\pi}{2})+\frac{1}{\sqrt{2}}\sin(\omega_1 t)\right)\right] \\
&= jE_{IN}\exp\left[j\frac{\pi}{4}\right]\exp(-j\beta L)\sin\left[\frac{\pi}{4}\left(\frac{1}{2}\left[\sin(\omega_1 t+\frac{\pi}{4})+\sin(\omega_1 t+\frac{3\pi}{4})\right]+1\right.\right. \\
&\quad \left.\left.-\frac{1}{2}\left[\sin(\omega_1 t-\frac{\pi}{4})+\sin(\omega_1 t+\frac{\pi}{4})\right]\right)\right] \\
&\quad \cdot\exp\left[j\frac{\pi}{4}\left(\frac{1}{2}\left[\sin(\omega_1 t+\frac{\pi}{4})+\sin(\omega_1 t+\frac{3\pi}{4})\right]+\right.\right. \\
&\quad \left.\left.+\frac{1}{2}\left[\sin(\omega_1 t-\frac{\pi}{4})+\sin(\omega_1 t+\frac{\pi}{4})\right]\right)\right] \\
&= jE_{IN}\exp\left[j\frac{\pi}{4}\right]\exp(-j\beta L)\sin\left[\frac{\pi}{4}\left(1-\left[\sin(\omega_1 t-\frac{\pi}{4})\right]\right)\right] \\
&= -jE_{IN}\exp\left[j\frac{\pi}{4}\right]\exp(-j\beta L)\sin\left[\frac{\pi}{4}\sin(\omega_1 t-\frac{\pi}{4})-\frac{\pi}{4}\right] \\
&\quad \cdot\exp\left[j\frac{\pi}{4}\sin(\omega_1 t+\frac{\pi}{4})\right] \qquad (3.16)
\end{aligned}
$$

with

$$\phi_1\,(SSB-RZ)=\frac{\pi}{2}\frac{1}{\sqrt{2}}\sin(\omega_1 t+\frac{\pi}{2})+\frac{\pi}{2} \qquad (3.17)$$

$$\phi_2\,(SSB-RZ)=\frac{\pi}{2}\frac{1}{\sqrt{2}}\sin(\omega_1 t) \qquad (3.18)$$

where f_0 is the angular frequency of the second MZM (f_0=40 GHz). The optical spectrum of a SSB-RZ signal is presented in Fig. 3.11a. Through the modulation in the second MZM, the left side band of the RZ spectrum is suppressed. The amount of side-band suppression is 30 dB. Due to the suppression of one side band, an improved transmission characteristic compared to RZ signals can be expected [165]. The reduced spectral width of SSB-RZ pulses enables an increased dispersion tolerance and improved nonlinear characteristics. Even after transmission lengths of several hundred kilometers, no reconstruction of the suppressed side band occurs [189]. On the other hand, it could be expected that 40 Gb/s SSB-RZ based WDM systems with a higher spectral efficiency can be realized, because of the robustness of the SSB-RZ signals to narrow-band filtering. SSB/VSB-RZ based 40 Gb/s WDM systems reach a spectral efficiency up to 1.28 bit/s/Hz when employing polarization multiplexing [11] or an unequal channel spacing between adjacent channels [13].

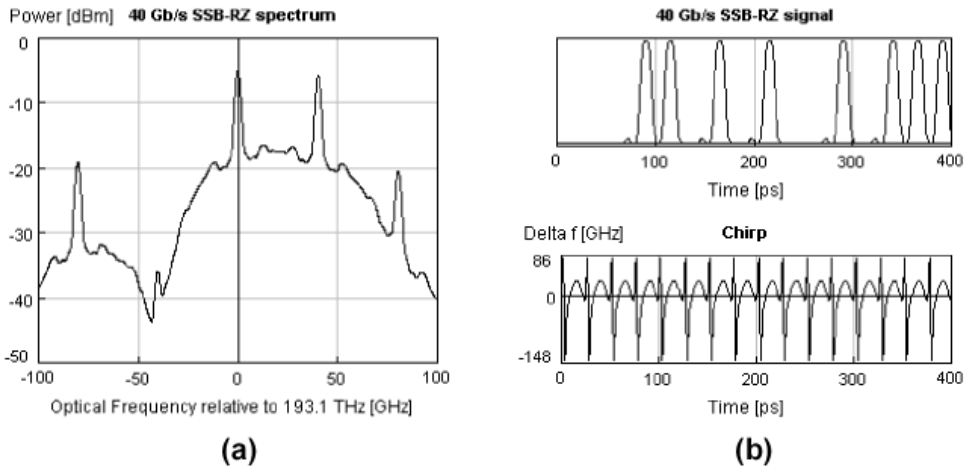

Figure 3.11: 40 Gb/s SSB-RZ signal: a) optical spectrum b) signal shape and chirp

3.4.4 Chirped RZ (CRZ) modulation

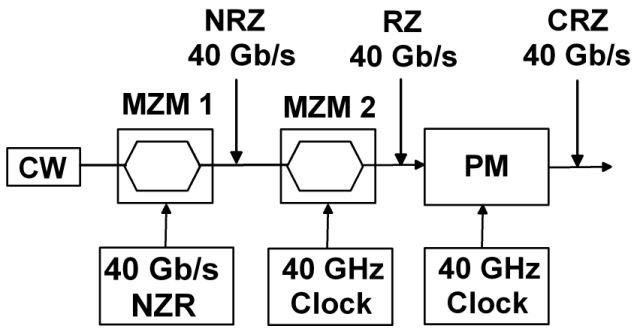

Figure 3.12: Generation of 40 Gb/s CRZ signal

Chirped RZ (CRZ) modulation is a special case of RZ modulation realized by the implementation of the pre-chirp on the conventional RZ pulses at the transmitter side. To date, CRZ modulation is basically used in long-haul under-sea transmission systems at channel data rates up to 10 Gb/s [191], [192], [193]. The pre-chirping of RZ pulses can be realized in various manners [194], [94], [195], [196]. The conventional CRZ generation is realized by a phase modulation in an additional modulation stage. The signal generation of CRZ pulses is presented in Fig. 3.12. In a CRZ transmitter, a CW laser is modulated with a conventional data stream in order to generate a NRZ signal. The CRZ signal is formed by re-modulating the NRZ signal's amplitude and phase with a sinusoidal electrical drive into an amplitude MZM and PM (Fig. 3.12). The complex amplitude of CRZ pulses is given by [197]:

$$E_{CRZ} = \sqrt{P_{RZ}} \cos\left(a \cdot \pi \cdot \sin\left(\pi f t\right)\right) \exp\left(i \cdot b \cdot \cos\left(2\pi f t\right)\right) \tag{3.19}$$

where P_{RZ} is the RZ pulse power, f is the clock frequency, and a and b are the modulation indices used for MZM 2 and PM modulation (Fig. 3.12) The phase modulation index of PM impacts the spectral forming of the CRZ signal and the spectral changes are governed by the PM drive signal. For example, higher clock frequencies would cause larger spectral broadening. In CRZ pulses a sine-clock is used with the frequency equal to the signal bit rate (e.g. 40 GHz).

The optical spectrum and signal waveform of a 40 Gb/s CRZ signal are shown in Fig. 3.13. It can be seen that the signal shape (Fig. 3.13b) remains unchanged compared to the RZ case, but changes occur in the optical

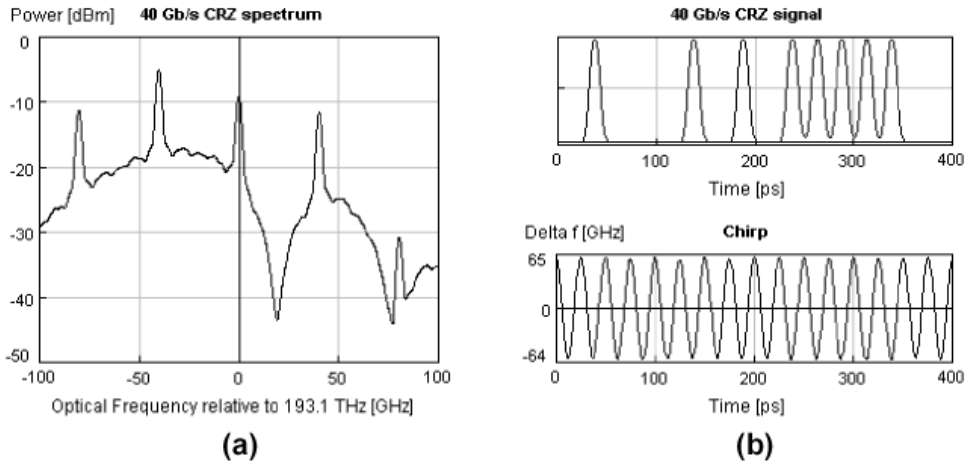

Figure 3.13: 40 Gb/s CRZ signal: a) optical spectrum b) signal shape and chirp

spectrum of the CRZ signal caused by the phase modulation with a 40 GHz clock signal and relatively high phase modulation index (typically, b=1.5 rad) [192]. Recent experimental studies [198], [195] showed that an system implementation of the CRZ modulation format can reduce the waveform distortions associated with conventional transmission formats. CRZ pulses enable an improvement of transmission characteristics due to the enhanced nonlinear tolerance. The drawback of CRZ is relatively wide optical spectrum reducing the system spectral efficiency and dispersion tolerance. Due to its good transmission characteristics CRZ modulation can be of interest for 40 Gb/s WDM systems with a spectral efficiency smaller than 0.4 bit/s/Hz.

3.5 Novel modulation formats

As a result of intensive research activities in the field of 40 Gb/s based WDM transmission systems several novel modulation formats have been proposed by author [199], [200], [201], [202]. The research aim was the proposal of novel modulation formats, which can be used in already deployed networks to improve maximum transmission distance and to better utilize the available system bandwidth. All novel formats target at ASK-based systems with conventional direct detection receivers. The possible implementation areas are 40 Gb/s based WDM and DWDM transmission systems over short- and long-haul distances. The optical signal generation and transmission characteristics of proposed novel modulation formats are presented in this chapter.

3.5.1 Alternate Chirped NRZ (alCNRZ) modulation

The pre-chirping of optical pulses at the transmitter side enables an improvement of transmission performance of the system. Therein, the pre-chirp can be realized using passive (e.g. fiber piece, optical filter) or active (e.g. MZM, phase modulator) components. The implementation of the pre-chirp causes a broadening of the signal spectrum, thus reducing the tolerance to residual dispersion and to narrow-band filtering. Accordingly, the amount of the pre-chirp and the method of its implementation have to be carefully chosen in order to meet desirable system requirements.
Modulation formats with a reduced nonlinear tolerance (e.g. NRZ-based formats) could primarily profit from the implementation of a pre-chirp. The main reason against pre-chirping of NRZ pulses until recently was the induced spectral broadening resulting in a stronger impact of group velocity dispersion (GVD). This effect can be partly avoided by implementing a carefully chosen amount of phase modulation on NRZ pulses. This is realized in alternate chirped NRZ (alCNRZ) pulses. alCNRZ modulation could be a good candidate for a performance improvement in deployed optical transmission systems because of its simple generation. The improved nonlinear tolerance would provide an enhancement of the maximum transmission length. Therefore, the main target of alCNRZ modulation is to enable a high speed optical transmission over long-haul (>400 km) distances.

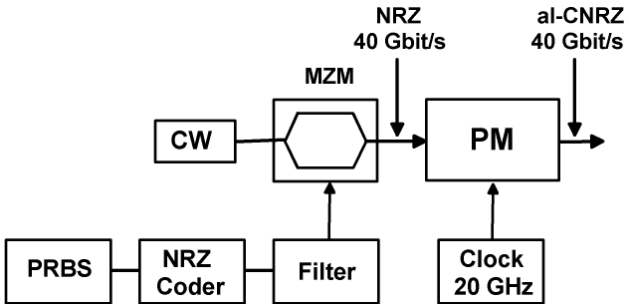

Figure 3.14: Generation of 40 Gb/s alCNRZ signal

The alCNRZ generator is presented in Fig. 3.14. Starting from a conventional generation of NRZ signals, alCNRZ pulses are generated by a phase modulation of NRZ pulses in an additional phase modulator (PM) [199], which is driven by a clock signal at half the bit rate. The neighboring pulses are alternate chirped. Contrary to some recent works [124], the half bit rate clock is used in order to avoid an excessive spectral broadening, which could impact the system's spectral efficiency. The complex amplitude of the generated alCNRZ signal is derived as:

$$E_{alCNRZ} = \sqrt{P_{NRZ}} \cdot \exp\left(i \cdot m \cdot (0.5 + 0.5 \cdot \cos(2\pi f t))\right) \tag{3.20}$$

P_{NRZ} is the peak power of the NRZ signal at the output of the MZM and m is the phase modulation index in radians. The signal shape and the optical spectra for different phase modulation indices in an alCNRZ

signal are presented in Fig. 3.15. Because of phase modulation, new spectral components arise (Fig. 3.15), hence broadening the signal spectrum depending on the implemented amount of phase modulation. At the same time, the modulation index according to Eq. 3.20 governs the phase shifts between adjacent bits (Fig. 3.15 bottom line). By the implementation of an optimum amount (m=2.25 rad) of the alternate phase shift, alCNRZ modulation can enable an even better transmission performance than a conventional RZ modulation in 40 Gb/s based WDM systems, which was showed by author in [199].

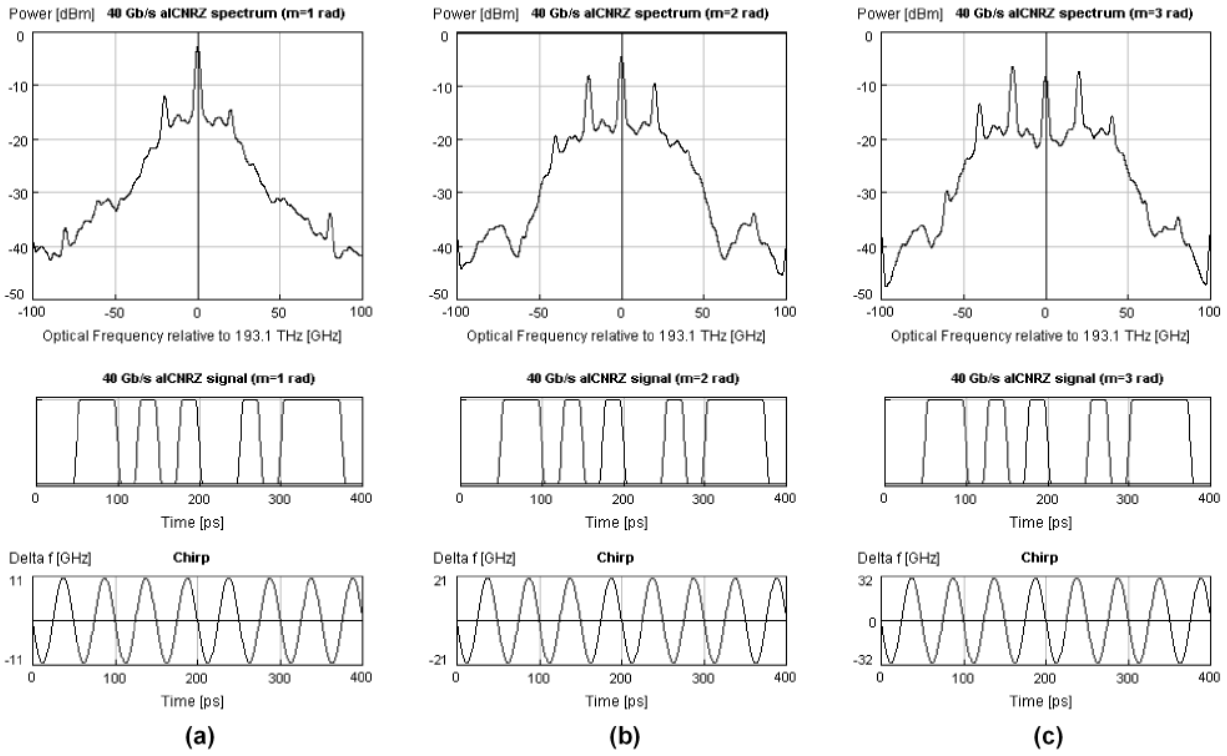

Figure 3.15: 40 Gb/s alCNRZ optical spectrum and signal shape for different values of modulation index: a) m=1 rad b) m=2 rad c) m=3 rad

3.5.2 Alternate chirped RZ (al-RZ) modulation

The alternate-chirped RZ (al-RZ) modulation format was proposed for the first time at OFC 2001 [203]. Its spectral form show similarities to a CSRZ spectrum (Fig. 3.9a) with a small amount of additional pre-chirp. The generation of the al-RZ pulses is illustrated in Fig. 3.16. Using a phase modulator (PM), the output of a CW-pump is modulated by a 20 GHz clock signal with a oscillation voltage of V_π. The narrow-band filter extracts the carrier and the first side-bands. A flat-top interleaver with 3 dB bandwidth of 0.35 nm is used as the narrow-band filter [203]. The intensity modulator (IM) is used for encoding 40 Gb/s data. The clock based modulation used in this case does not require any bias-voltage control between modulation stages and is driven by a single clock at half the bit rate.
The optical spectrum and a signal waveform of 40 Gb/s al-RZ are shown in Fig. 3.17. The al-RZ spectrum consists of three dominant components: carrier and two side-bands at 20 GHz left and right (Fig. 3.17b). The spectral width is similar to CSRZ and the signal shape shows no difference compared to conventional RZ pulses. This combination of the phase modulator and the narrow band filter provides not only the generation of 40 Gb/s al-RZ pulses, but also the realization of a sinusoidal chirp, causing the alternate chirp inversion between neighboring bit slots (Fig. 3.17b), which can be useful for the suppression of the interferences between neighboring pulses [204]. Due to a strong concentration of the optical spectrum around the carrier

and a narrow spectrum, al-RZ could be a potential candidate for 40 Gb/s based DWDM systems.

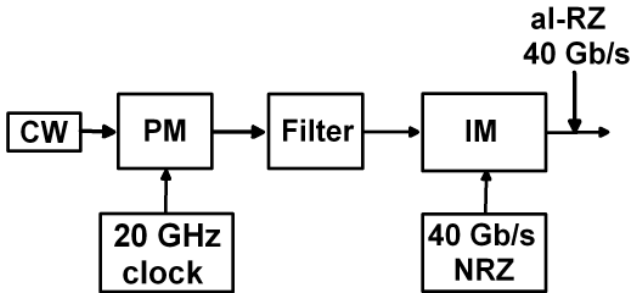

Figure 3.16: Generation of a 40 Gb/s al-RZ signal

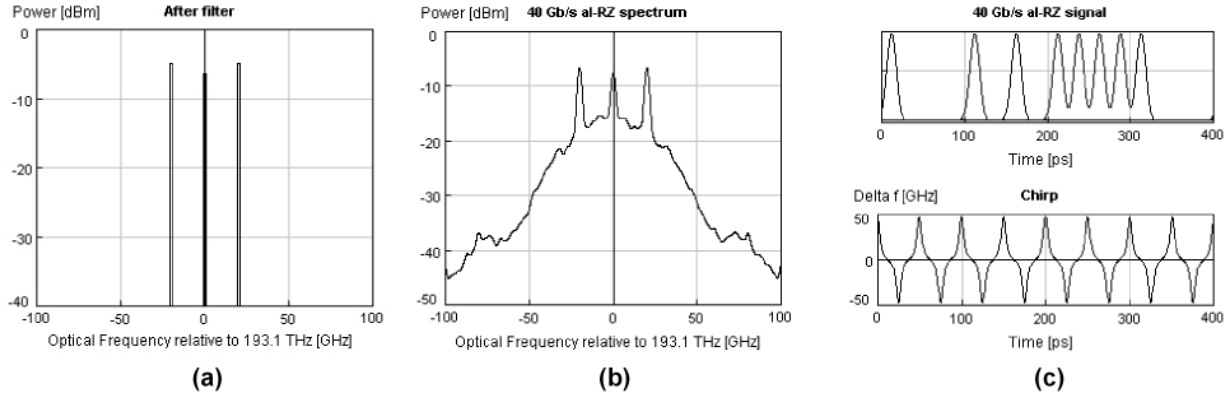

Figure 3.17: 40 Gb/s al-RZ signal: a) optical spectrum after filter (Fig. 3.16) b) final optical spectrum c) signal shape and chirp

Comparison with CSRZ and RZ [203] in 40 Gb/s single channel and WDM (channel spacing 100 GHz) transmissions showed that the al-RZ modulation is superior in terms of nonlinear tolerance, and offers the possibility of drastically extending the power margin. Last but not least, all components for 40 Gb/s al-RZ generation are commercially available and the same setup with different parameter setting can be used for generation of different modulation formats (e.g. NRZ, RZ, CSRZ).

3.5.3 Novel chirped RZ (nCRZ) modulation

The novel chirped RZ (nCRZ) [200] modulation is a method for the generation of alternate chirped RZ pulses. Using a phase modulator at the transmitter side, it is possible to achieve a spectral forming (e.g. narrower signal spectrum) of RZ pulses enabling a higher spectral efficiency and an increased nonlinear tolerance. The generation of nCRZ pulses is presented in Fig. 3.18.

The light of the CW-pump is externally modulated in a $LiNbO_3$ MZM with a RZ encoded electrical signal. 40 Gb/s RZ optical pulses are additionally phase-modulated in a phase modulator (PM)(Fig. 3.18), which is driven by a sine-clock signal at half the bit-rate. This leads to a compact spectral form and a better concentration of the signal spectrum around the carrier wavelength. The complex amplitude of the generated nCRZ pulses is given by:

$$E_{nCRZ} = \sqrt{P_{RZ}} \cdot \exp\left(i \cdot m \cdot \sin\left(2\pi f t\right)\right) \tag{3.21}$$

where P_{RZ} stands for the peak power of the RZ signal on the input of the PM and m is the phase modulation index in radians. The signal spectrum is similar to that of al-RZ, but significant differences are: the chirping

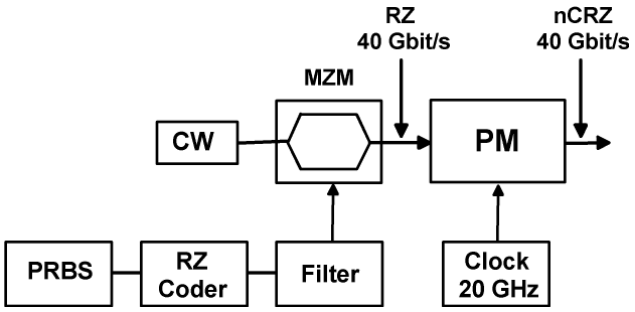

Figure 3.18: Generation of 40 Gb/s nCRZ signal

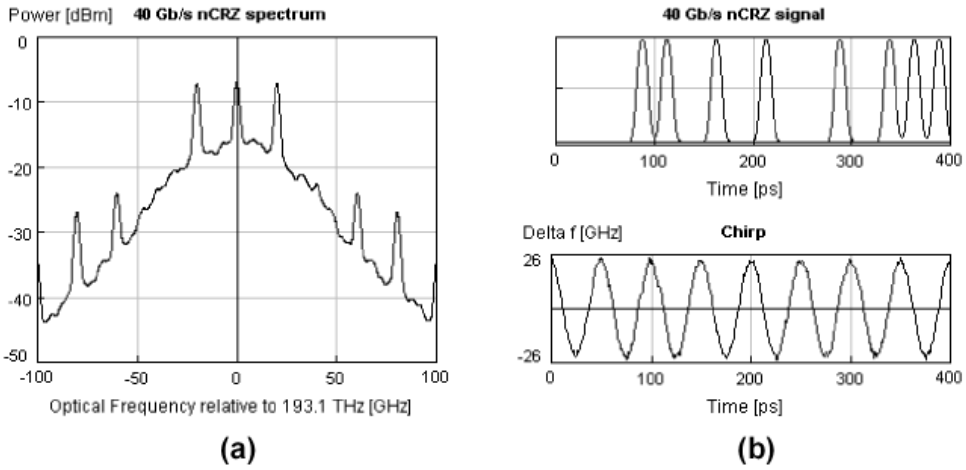

Figure 3.19: 40 Gb/s nCRZ signal: a) optical spectrum b) signal shape and chirp

of the RZ signal is realized by a phase modulation and the higher harmonics are suppressed by choosing an optimal value of phase modulation index (m=1.15 rad), which enables a signal spectrum with only two side bands and a carrier component, causing less spectral broadening of the signal. In nCRZ, no additional optical filtering has to be done at the transmitter side.
Figure 3.19 shows the optical nCRZ spectrum and the pulse shape of a 40 Gb/s nCRZ signal. The spectral width of a nCRZ pulse measured between the two side bands equals 40 GHz. Accordingly, the nCRZ spectrum is narrower by a factor of 2 than the spectrum of a conventional RZ signal and the carrier peak possesses an equal amplitude as the peaks of both side bands. Because of this, nCRZ modulation possesses an increased dispersion tolerance compared to conventional RZ modulation [200]. The spectrum of nCRZ-modulated pulses shows similarities to the spectrum of al-RZ pulses. These two formats have similar transmission characteristics in terms of dispersion and a nonlinear tolerance. The difference becomes visible first at a smaller channel spacing, where nCRZ shows better performance. The results [200] confirmed that the nCRZ signal form reduces SPM-GVD impairment in SSMF-based transmission systems, compared to conventional RZ signals. It was shown that a 40 Gb/s nCRZ based WDM system over SSMF could be realized with a spectral efficiency of 0.8 bit/s/Hz [200].

3.5.4 Alternate polarized modulation formats

The alternate polarized or polarization-switched modulation formats belong to the group of novel modulation formats targeting the suppression of nonlinear system degradations and an enhancement of the maximum transmission length in high bit rate transmission systems. By the specific polarization relation between the

adjacent bits, a strong reduction of nonlinear effects (SPM, IXPM, IFWM, XPM) can be achieved. The polarization switching between adjacent bits disables power interactions between them, resulting in a lower pulse interaction and a larger nonlinear tolerance. At the same time, the orthogonal polarization between bits is maintained over long transmission distances independently of PMD impacts in the transmission line [205]. The signal detection of alternate polarized modulations is done with a conventional NRZ detector. Polarization switching between orthogonal bits can be implemented as additional modulation stage in combination with various ASK-based modulation formats (e.g. RZ, CSRZ).

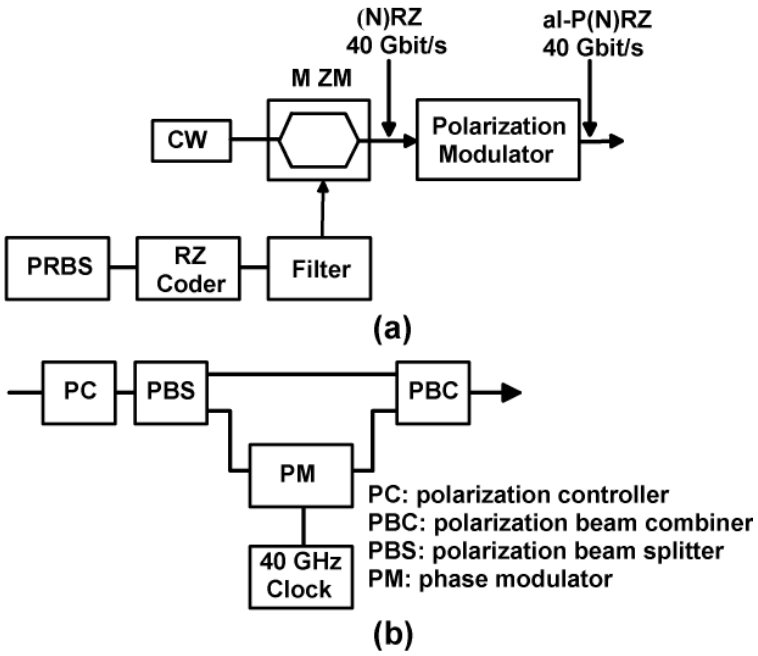

Figure 3.20: Generation of 40 Gb/s alP(N)RZ signals: a) signal generation setup b) polarization modulator setup

The signal generation of alP(N)RZ signals is presented in Fig. 3.20. The polarization switching between adjacent RZ/NRZ pulses is realized by the polarization modulation of pulses in an additional polarization modulator (PolM). The schematic diagram of a PolM is depicted in Fig. 3.20b. The polarization state of the optical signal is adjusted to a linear polarization (angle of 45^0) at the PolM input by a polarization controller (PC). By a polarization beam splitter (PBS), a (N)RZ signal is separated into x- and y-polarization components. The modulation of y-polarization component in realized in the phase modulator (PM). As drive signal of the phase modulator a rectangular electrical clock or an electrical bit pattern with alternating bits (1010101..) can be used (Fig. 3.20b). The two polarization components are joined with a polarization beam combiner (PBC). If the PM drive signal is a mark ("1") the phase of the y-polarization component will be shifted by 180^0 causing a polarization switching of 90^0 in the total signal polarization. This results in a pulse polarization angle of -45^0 after the PBC. For a space ("0") drive signal at the input of PM, no phase modulation occurs and the total pulse polarization at the PolM output remains unchanged (45^0).

Figures 3.21 and 3.22 illustrate optical spectra and signal shapes of 40 Gb/s alP(N)RZ pulses. al-P(N)RZ pulses possess a (N)RZ like pulse shape. The alternately polarized optical spectra (Fig. 3.22b) are broader than conventional RZ or NRZ spectra. This can be explained by the fact that the spectrum of an alternate polarized format is a superposition of two polarization components with different optical spectra. The spectrum of x-polarization is conventional (N)RZ spectrum (Fig. 3.22b), whereas the spectrum of the y-component (Fig. 3.22b) is a CSRZ spectrum (see Eq. 3.13) due to the employed phase modulation. This explains the side bands at 20 GHz left and right of the carrier if the PM is driven with a 20 GHz clock

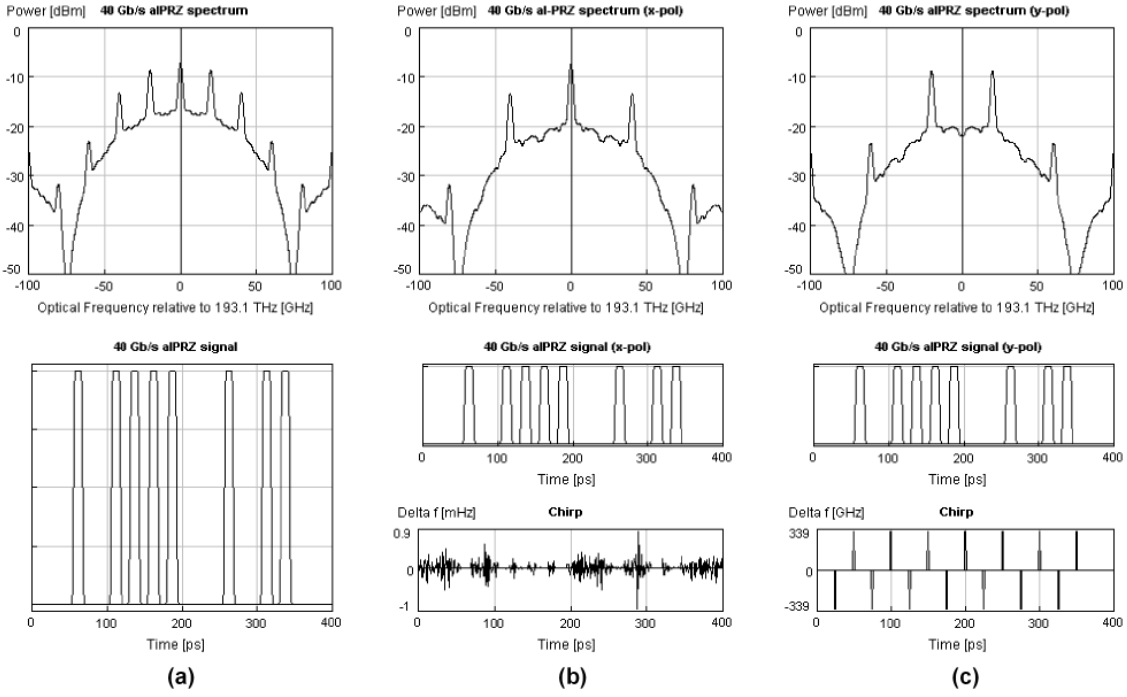

Figure 3.21: 40 Gb/s alPRZ signal: a) alPRZ signal shape b) x-polarization c) y-polarization

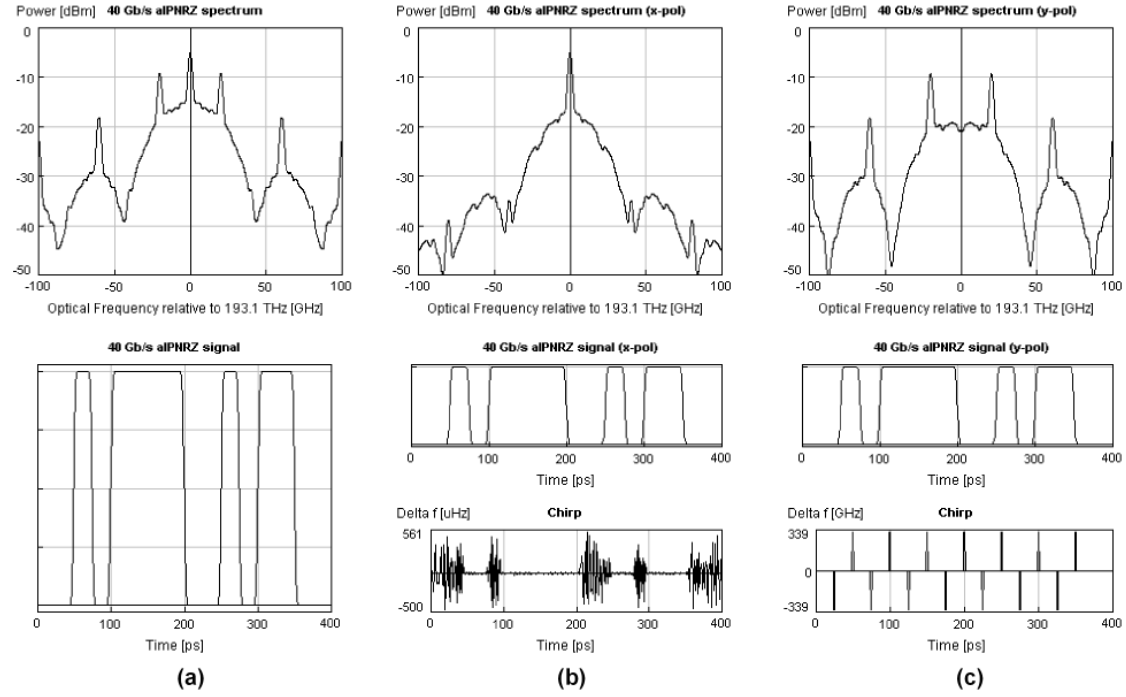

Figure 3.22: 40 Gb/s alPNRZ signal: a) alPNRZ signal shape b) x-polarization c) y-polarization

(Fig. 3.21). From soliton [10], [206] and OTDM [207] based transmission systems, it is already known that alternate polarization between adjacent pulses can significantly improve transmission quality, because of the reduction of intra- and inter-channel nonlinear effects. The recent investigations in 40 Gb/s WDM systems

confirmed that alP(N)RZ modulation can suppress the SPM-GVD and XPM effects as well as the intra-channel effects [208], [74] enabling significant improvement compared to conventional RZ and NRZ formats. 40 Gb/s based alPRZ WDM system with a spectral efficiency of 0.8 bit/s/Hz are numerically demonstrated with large channel powers (≈8 dBm/ch) [201].

4 Performance evaluation criteria

4.1 Overview

The right choice of the performance evaluation criteria for the characterization of optical transmission lines represents one of the key issues for an effective design of future high speed systems. The evaluation criteria should provide a precise determination and separation of dominant system limitations, making them crucial for the suppression of propagation disturbances and a performance improvement. On the other hand, they provide a comparison of experimental and numerical investigation, which is useful for the verification of applied numerical models. In this chapter, evaluation criteria known from recent experimental and numerical works are introduced and described. The presented criteria are used for system investigations and optimizations in the following chapters of this thesis.

4.2 Bit error rate (BER)

The bit error rate (BER) evaluation is a straightforward and relatively simple method for performance estimation based on the counting of errors in received bit streams. When the number of errors is known, the BER can be determined as:

$$\mathrm{BER} = \frac{\text{Number of errors}}{\text{Number of transmitted bits}} \tag{4.1}$$

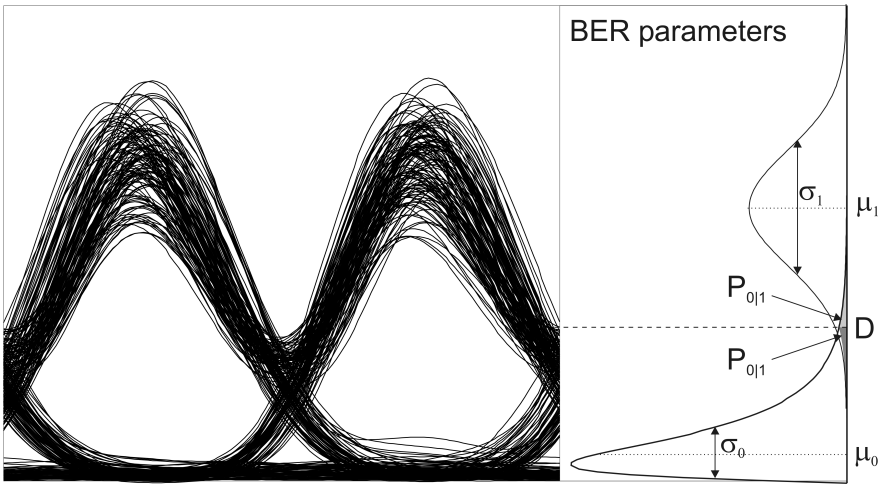

Figure 4.1: Bit Error Rate (BER) estimation

The error counting in the practical system can be a long process especially for realistically low BER values ($< 10^{-12}$). The implementation of BER calculation is rather complicated and time consuming in numerical simulation due to limited computing resources. The method for a numerical calculation of realistic BERs is known as Monte Carlo method [209], [210], used in the classical telecommunication theory as a method for probability characterization of rare events. The duration of Monte Carlo simulations is determined by the accuracy and variance of calculated BERs. For a BER variance of 50 % at 10^{-9} and an error probability of 5 %, $23{\times}10^9$ bits have to be simulated [211], which is quite unrealistic with today's computer resources. To cope with the problem of time consuming simulations, some specific assumptions considering error statistics in

marks and spaces have to be met in order to calculate the BER with a reduced number of bits. Accordingly, the BER can be understood as the occurrence probability of errors (P_E), which depends on the error probabilities for marks $P(1)$ and spaces $P(0)$:

$$\mathrm{BER} = P_E = P(1)P(0|1) + P(0)P(1|0) \tag{4.2}$$

where $P(0|1)$ and $P(1|0)$ are the conditional probabilities for detecting 0 if 1 is sent and vice versa. The assumption of equal occurrence probabilities for 1s and 0s ($P(1)$=$P(0)$=0.5) yields:

$$\mathrm{BER} = \frac{1}{2}\left[P(0|1) + P(1|0)\right] \tag{4.3}$$

Thus, the BER value is entirely determined by the conditional probabilities $P(0|1)$ and $P(1|0)$. Considering an ideal decision circuit, the decision between 0 and 1 is made by comparing the input signal x and a threshold level (I_D) at the sample instant. If $x > I_D$, a "1" is detected and a "0" otherwise. The conditional probabilities $P(0|1)$ and $P(1|0)$ are given by:

$$P(0|1) = \int_{-\infty}^{I_D} PDF_1(x)dx \tag{4.4}$$

$$P(1|0) = \int_{I_D}^{\infty} PDF_0(x)dx \tag{4.5}$$

where $PDF_{1,0}$ are the probability density functions of 1s and 0s. The approximation of correct PDFs is crucial for the numerical determination of the BER because their overlap determines the probability of errors (Fig. 4.2). But, at the same time, the PDFs are dependent on the system configuration in use and are not known exactly, so that their correct approximation is made numerically or by fitting of some known functions to the histogram distributions of the receiver output signals (Fig. 4.2a) [32].

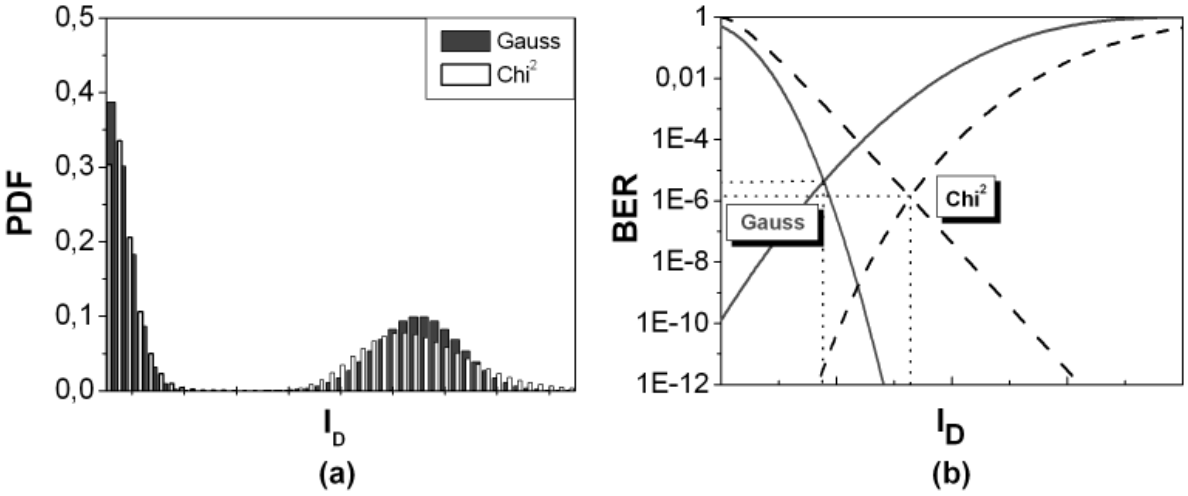

Figure 4.2: PDF approximations: a) comparison between Gaussian and χ^2 PDF approximations b) BER versus decision level for Gaussian and χ^2 PDFs

For the PDF approximations, Gaussian and chi-squared (χ^2) distributions are normally assumed. The Gaus-

sian and χ^2 PDFs P_i(X) corresponding to symbol i are given by [3]:

$$P_{i,Gauss}(X) = \frac{1}{\sigma_i\sqrt{2\pi}} \exp\left(-\frac{(X-\langle I_i\rangle)^2}{2\sigma_i^2}\right) \tag{4.6}$$

$$P_{0,\chi^2}(X) = \frac{1}{N}\left(\frac{X}{N}\right)^{Mm-1} \frac{1}{(Mm-1)!} \exp\left(-\frac{X}{N}\right) \tag{4.7}$$

$$P_{1,\chi^2}(X) = \frac{1}{N}\left(\frac{X}{MS}\right)^{(Mm-1)/2} \exp\left(-\frac{MS+X}{N}\right) I_{Mm-1}\left(2\frac{\sqrt{MSX}}{N}\right) \tag{4.8}$$

where X is a dimensionless photocurrent, N is the (single polarization) mean ASE photon number, S is the mean amplified signal photon number, M=1 or 2 is the number of ASE polarizations and $m = B_o/2B_e$ (optical to electrical bandwidth ratio) is the number of degrees of freedom.
Owing to the fact that the exact PDFs are not symmetrical around their maximum value (Fig. 4.2a), the χ^2 distribution provides a better approximation of the error probability [212], [213]. The conditional probabilities in this case are calculated numerically, but recently presented works indicate that a complex analytical estimation of χ^2 PDF is possible using special mathematical techniques, e.g. saddle point or steepest descent method [212]. The Gaussian distribution enables a simple analytical BER approximation, characterized by overestimation of the BER by approximately one order of magnitude (Fig. 4.2b) and lower decision thresholds (I_D) compared to χ^2 distribution (Fig. 4.2b) [214], [3]. The deviation of the Gaussian approximation from the exact distribution can be explained by the fact that the signal-to-noise beating remains Gaussian and the noise-to-noise beating has a χ^2-distribution [215]. The accuracy of the Gaussian approximation can be improved by using specific mathematical methods, e.g. Wilson-Hilferty transformation [213].
The numerical BER calculations in conventional simulation tools made assuming Gaussian noise approximations enable a fast performance estimation and give a first insight of transmission characteristics, but for a better comparison with experimental results the PDFs have to be described more precisely. Assuming a Gaussian distribution, the conditional probabilities $P(0|1)$ and $P(1|0)$ are given by:

$$P(0|1) = \frac{1}{\sigma_1\sqrt{2\pi}} \int_{-\infty}^{I_D} \exp(-\frac{(I-I_1)^2}{2\sigma_1^2})dI = \frac{1}{2} erfc\left(\frac{I_1-I_D}{\sigma_1\sqrt{2}}\right) \tag{4.9}$$

$$P(1|0) = \frac{0}{\sigma_1\sqrt{2\pi}} \int_{I_D}^{\infty} \exp(-\frac{(I-I_0)^2}{2\sigma_0^2})dI = \frac{1}{2} erfc\left(\frac{I_D-I_0}{\sigma_0\sqrt{2}}\right) \tag{4.10}$$

where $\sigma_{1,0}$ are the corresponding standard deviations for 1s and 0s (Fig. 4.1), and $erfc$ stands for the complementary error function, defined as:

$$erfc(x) = \frac{2}{\sqrt{\pi}} \int_x^{\infty} \exp(-y^2)dy \tag{4.11}$$

Substituting equations Eqs. 4.3 and 4.9 in Eq. 4.2, the BER is defined as:

$$\text{BER} = \frac{1}{4}\left[erfc\left(\frac{I_1-I_D}{\sigma_1\sqrt{2}}\right) + erfc\left(\frac{I_D-I_0}{\sigma_0\sqrt{2}}\right)\right] \tag{4.12}$$

In order to minimize the BER, it is necessary to optimize the value of I_D. The optimum BER occurs if I_D is chosen as:

$$\frac{(I_D-I_0)^2}{2\sigma_0^2} = \frac{(I_1-I_D)^2}{2\sigma_1} + \ln\left(\frac{\sigma_1}{\sigma_0}\right) \tag{4.13}$$

The last term in this equation depends on the extinction ratio (Chapter 2) between 1s and 0s and it can be neglected in most practical cases. I_D can than be obtained as:

$$I_D = \frac{\sigma_0 I_1 + \sigma_1 I_0}{\sigma_0 + \sigma_1} \tag{4.14}$$

Assuming that $\sigma_1 = \sigma_0$ yields $I_D = (I_1 + I_0)/2$, corresponding to setting the decision threshold in the middle of the signal eye. This is the case in most p-i-n receivers whose noise is dominated by thermal noise and is independent of the average current [3].
The numerical determination of the BER with a reduced number of bits can be realized by a Q-factor extrapolation [216] method assuming Gaussian PDF distribution. If the decision threshold is far away from its optimum value, the total BER can be divided into two BERs - one for 0s and one for 1s (Fig. 4.2b). The intersection point of both BER curves indicates the optimum threshold I_D and the minimum BER depends only on the Q-factor as:

$$\mathrm{BER} = \frac{1}{2} erfc\left(\frac{\mathrm{Q}}{\sqrt{2}}\right) \approx \frac{\exp(-\mathrm{Q}^2/2)}{\mathrm{Q}\sqrt{2\pi}} \tag{4.15}$$

with

$$\mathrm{Q} \equiv (I_D - I_0)/\sigma_0 = (I_1 - I_D)/\sigma_1 \tag{4.16}$$

The Q-factor extrapolation method enables a good BER estimation, but according to the inaccuracy of Gaussian distribution the predicted BER values are typically larger then the minimum expected BER [3] and determined I_D may deviate significantly from the real optimum.

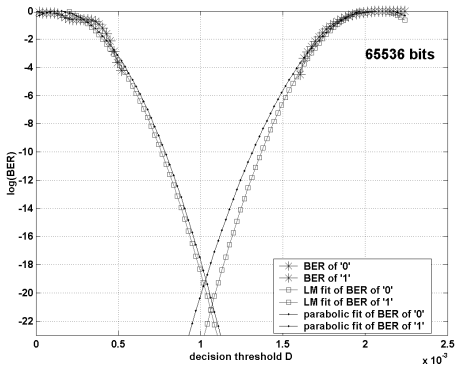

Figure 4.3: Direct BER extrapolation with parabolic and Lavenberg-Marquardt (LM) algorithms

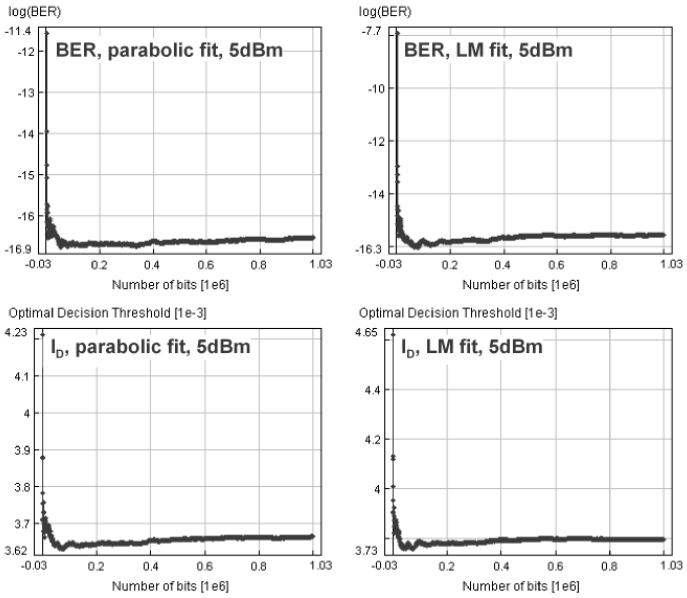

Figure 4.4: BER and I_D calculation versus number of calculated bits with parabolic and LM fit in single channel transmission (40 Gb/s, 4x80 km SSMF, with ASE-noise)

Recently presented approaches for alternative BER estimation like parabolic data fitting [3] and a sophisticated nonlinear data-fitting algorithm - Lavenberg-Marquardt (LM) [217] enable a direct BER estimation with improved accuracy using a reduced number of bits. Figure 4.3) illustrates the performance evaluation (threshold extrapolation) for a 40 Gb/s transmission of 4x80 km under consideration of ASE-noise in the

transmission fibers and considering 65536 bits for numerical investigation. For a reduced impact of transmission distortions (e.g. due to ASE-noise, nonlinear effects) both data fitting algorithms show similar results. With an increased scattering error, the LM method shows better BERs and I_Ds because in case of heavily distorted transmissions the BER curves have to be approximated taking into account all data points and noise fluctuations. For both approximating algorithms, strong BER and I_D fluctuations (derived as in Fig. 4.3, for each amount of bits) can be observed for an insufficient amount of simulated bits (Fig. 4.4). On the other hand, beyond a certain amount of bits the BERs and I_D converge, thus indicating that for an exact simulation a reduced amount of bits can be used, whereby the starting points of BER and I_D convergence depend on the propagation disturbances in the transmission line.

Receiver sensitivity penalty

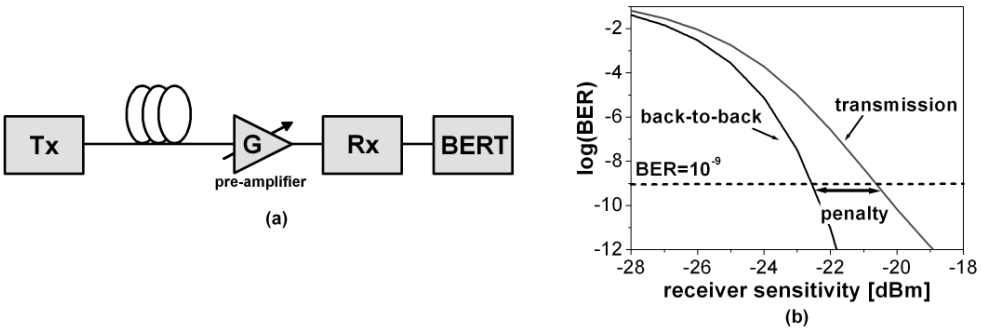

Figure 4.5: Receiver sensitivity penalty determination: a) experimental setup b) penalty definition

The receiver sensitivity penalty (RSP) estimation is a widely used BER quantification criterion both in numerical and experimental works. The setup for RSP determination is illustrated in Fig. 4.5a. The RSP is derived from BER-measurements of the system in back-to-back and transmission case. Therein, the measured BER depends on the receivers sensitivity and receiver input power. By the variation of receiver input power employing different pre-amplifier gains, a BER scan versus receiver sensitivity can be realized (Fig. 4.5b). For the calculation of the RSP, the receiver input power in back-to-back ($P_{Rx,BTB}$) and transmission case ($P_{Rx,trans}$) needed for a BER value of 10^{-9} are considered. The RSP is defined as:

$$\mathrm{RSP\,[dB]} = P_{Rx,trans}@(BER = 10^{-9}) - P_{Rx,BTB}@(BER = 10^{-9}) \tag{4.17}$$

The RSP differs depending on the dominant system limitation in the transmission line. RSP quality limit equals typically 10-12 dB [218], [141]. RSP provides a conservative performance evaluation, because of the relatively small BER values considered for the estimation. RSP is mainly used for the characterization of the penalty accumulation over transmission distance [218] and represents a good evaluation method for the comparison of numerical and experimental works [141]. It is less effective for the visualization of single transmission limitations, but in combination with additional estimation methods, e.g. EOP, Q-factor, it provides a powerful system design tool.

4.3 Q-factor

The Q-factor criterion for the performance evaluation of optical transmission systems frequently used in combination with BER measurements enables an efficient representation of relevant noise statistics [219]. Q-factor is defined by:

$$\mathrm{Q} = \frac{|\mu_1 - \mu_0|}{\sigma_1 + \sigma_0} \tag{4.18}$$

where μ_1, μ_0 and σ_1, σ_0 are the mean and standard deviations of marks and zeros, respectively. On the other hand, the Q-factor can be defined as a function of the optimum decision threshold (I_D) by:

$$\mathrm{Q} = \frac{I_D - \mu_0}{\sigma_0} = \frac{\mu_1 - I_D}{\sigma_1} \tag{4.19}$$

with

$$I_D = \frac{\sigma_0\mu_1 + \sigma_1\mu_0}{\sigma_0 + \sigma_1} \tag{4.20}$$

The relation between Q-factor and BER for ASK based modulation formats presented in Eq. 4.15 is derived under the assumption that the probabilities of marks and spaces possess a Gaussian statistic with an optimum decision threshold I_D (Eq. 4.20) and an optimum sampling point at the receiver side.

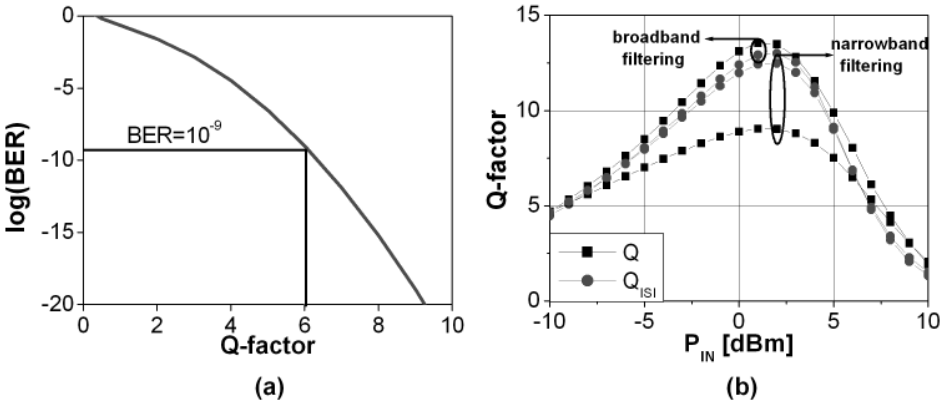

Figure 4.6: Q-factor measurements: a) relation between BER and Q-factor b) Q and $\mathrm{Q_{ISI}}$ dependence on narrow-band filtering (40 Gb/s single channel transmission over 4x80 km with broadband (160 GHz) and narrow-band (60 GHz) filtering before transmission line)

According to Eq. 4.15, a Q-factor of 6 corresponds to a BER=10^{-9} (Fig. 4.6). For a correct Q-factor calculation, the minimum number of simulated bits has to be determined through multiple calculations of Q with increasing lengths of bit sequences. Above a certain number of simulated bits, the Q-factor converges, hence this number of bits can be used for system simulations. The sufficient amount of bits has to be determined for each investigated system configuration before numerical simulations are made.
The Q-factor definition presented in Eq. 4.19 possesses a limited validity and it becomes incorrect [220] or too pessimistic if excessive pattern effects are present in a bit stream. The assumption that the detected signal consists of only two Gaussian distributions is no longer valid. For example, the narrow band filtering in a DWDM system causes strong ISI-effects between adjacent bits and the standard deviations in marks and zeros become overestimated resulting in a poor value of the Q-factor (Fig. 4.6). Hence, in ISI-limited systems, the BER has to be calculated considering pattering effects in a bit stream. The pattering on each bit is dependent on adjacent bits. Fundamentally, each bit stream can be realized as a combination of eight different bit patterns (e.g. 010, 111, 110 etc.), which represent eight separated noise distributions. Dividing the received bit sequence in patters (triplets of bits), the error probability of each bit pattern can be calculated

as [220]:

$$P(pattern) = erfc\left(\frac{I_D - \mu_p}{\sigma_p}\right) \tag{4.21}$$

where μ_p and σ_p represent the mean and the standard deviation of the pattern p. The $\mathrm{BER_{ISI}}$ can be defined as a sum of different pattern contributions scaled with the occurrence of a single pattern:

$$\mathrm{BER_{ISI}}(I_D) = \sum_{p=1}^{8} \frac{n_p}{n'} BER_p(I_D) \tag{4.22}$$

where n_p describes the occurrence frequency of pattern p and n' is the total number of triples. The difference between conventional Q (Eq. 4.19) and Q_{ISI} derived from $\mathrm{BER_{ISI}}$ becomes visible only if ISI effects dominate (e.g. narrow-band filtering Fig. 4.6b). The drawback of the Q_{ISI} method is a necessity of a large number of simulated bits (factor of 4 compared to conventional Q) [220] in order to enable a larger occurrence frequency of single patterns used for the $\mathrm{BER_{ISI}}$ calculation.
Besides the use of Q-factor as evaluation criterion, it can be used for performance monitoring and for validation of connection attributes in optical networks. For these purposes different measurement methods, e.g. tail-extrapolation, level separation, have been recently proposed [221], [222].

Dynamic range (DR)

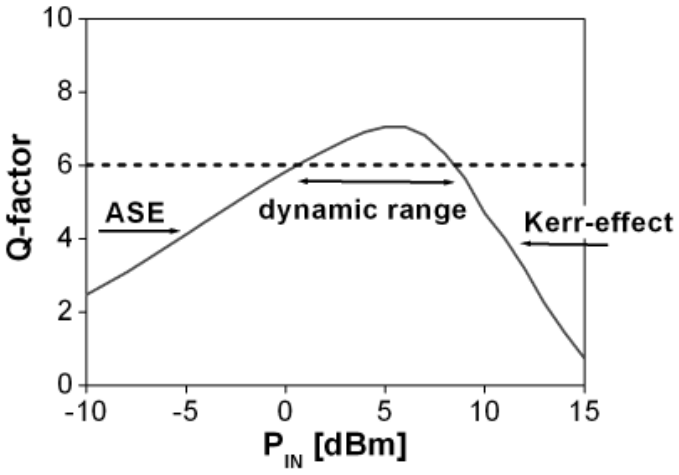

Figure 4.7: Dynamic range (DR) definition

The dynamic range (DR) is an useful criterion for the estimation of the maximum transmission distance of the system using Q-factor calculation. The DR describes the power tolerance at Q=6:

$$\mathrm{DR\,[dB]} = P_{max}@(Q=6) - P_{min}@(Q=6) \tag{4.23}$$

The DR value depends on linear (e.g. ASE) and nonlinear (e.g. Kerr-effect) effects. Both, linear and nonlinear impairments affect the maximum length of the transmission line [223], [224]. An increase of the number of transmission spans by a factor of two causes a reduction of the DR of up to 6 dB, whereby approximately 3 dB occurs at the left side of the DR due to ASE-noise impact [223] and 3 dB on the high-power side due to the nonlinear effects [224]. Using DR-based performance quantification, conclusions about the system performance in long haul transmissions can be drawn out of numerical works considering smaller transmission distances [200], hence enabling a time and resource efficient system design.

4.4 Optical signal-to-noise ratio (OSNR)

The Optical Signal-to-Noise Ratio (OSNR) represents a widely used evaluation criterion for the characterization of system performance in already deployed transmission lines. The OSNR can be understood as a measure of the ratio of the signal (P_S) to noise (P_N) power in an optical channel:

$$\mathrm{OSNR} = \frac{P_S}{P_N} \tag{4.24}$$

The optical noise around the optical signal (Fig. 4.8) reduces the receiver's ability to correctly detect the signal because of the interferences between the signal and optical noise. This effect can be suppressed by the implementation of an optical filter (ASE-filter) before the optical receiver. The optical bandwidth of the ASE-filter is large enough that optical signal can pass undisturbed, but it is much smaller than the ASE-noise bandwidth.

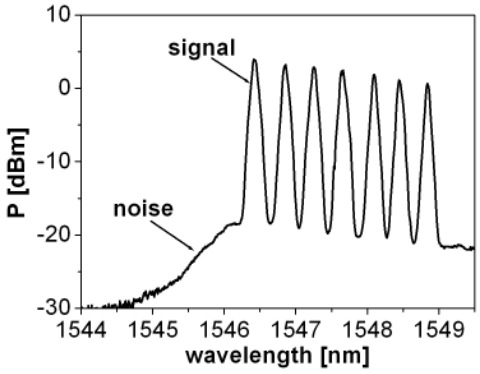

Figure 4.8: Optical signal to noise ratio

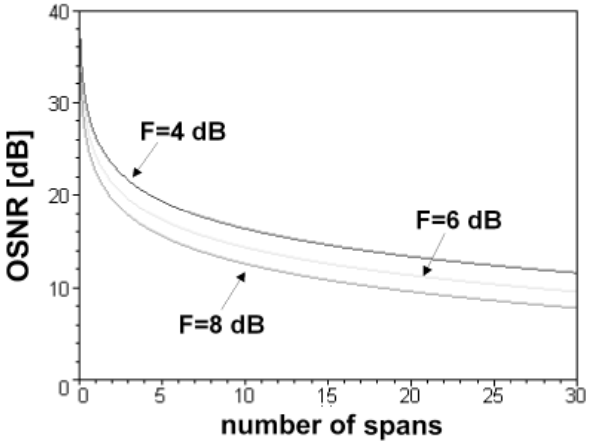

Figure 4.9: OSNR versus distance for different EDFA noise figures according to Eq. 4.25 (P_{in}=0 dBm, $\mathrm{L_{SPAN}}$=80 km, $\alpha = 0.22$ dB/km, B_r=0.1 nm)

Depending on the amplifier infrastructure used in a transmission system, the OSNR value is proportional to the number of optical amplifiers as well as to the gain flatness of a single amplifier. Especially gain-flattness can be a critical issue in WDM systems, because of the gain non-uniformity in multi-span transmissions. If several optical channels propagate through a cascade of optical amplifiers, the gain non-uniformity in a single amplifier results in different gains at different wavelengths and channels (Fig. 4.8). The resulting OSNR varies from channel to channel and is limited by the OSNR value of the worst case channel. This effect can be avoided by the use of "flat-gain" amplifiers (Chapter 2.8). If ideal flat-gain amplifiers are used, the OSNR value can be calculated as:

$$\mathrm{OSNR}[dB] = P_{in}[dBm] - \alpha \cdot L[dB] - F[dB] - 10\log(N)[dB] - 10\log(h\nu B_r)[dBm] \tag{4.25}$$

where P_{in} is the signal power at the receiver side, L is the length of the transmission line, F is the noise figure of the single EDFA, N stands for a number of amplifiers and B_r describes the resolution bandwidth used for OSNR measurement (typically 0.1 nm). According to the equation above, the dominant limiting parameters for OSNR calculation are the total length (number of amplifiers) and the noise figure F, because these two parameters determine the ASE-noise accumulation over the distance. Lower noise figure values of a single optical amplifier will result in better OSNR values of the system (Fig. 4.9). Assuming non-flat gain amplifiers in transmission line, the OSNR value is limited by the variation of the gain regarding to the wavelength [3].

Generally speaking, the OSNR measurement can be realized by measuring the signal power as the difference between the total power of the signal peak and the amount of the background noise. The background noise is measured by determining the noise contributions on either side of the signal peak. However, the separation and measurement of the signal and noise power is difficult to realize in practice, because the noise power in an optical channel is included in the signal power. The noise power determination in a WDM system can be made by interpolating the noise power between the adjacent channels [225]. The polarization extinction [226] is another method for the signal from noise separation. It is based on the fact that the ASE-noise is unpolarized and the data signal remains polarized during the propagation. Hence, by using a polarization filter the data signal can be suppressed, enabling a measurement of the unpolarized noise power.

4.5 Eye opening penalty (EOP)

The evaluation and quality criteria (e.g. BER, Q-factor, OSNR) presented in the previous section are used in experimental works and practice. Using these criteria, it would be difficult to identify origins of different system impairments, which is required for an improvement of the system performance. The promising method for the separation between different transmission effects in numerical works would be the precise analysis of the detected signals eye diagrams. An eye diagram is created by the superposition of detected/received bits (Fig. 4.10). If an optical signal propagates ideally through a transmission line without any disturbance, a widely opened eye diagram is observed at the receiver side (Fig. 4.10a).

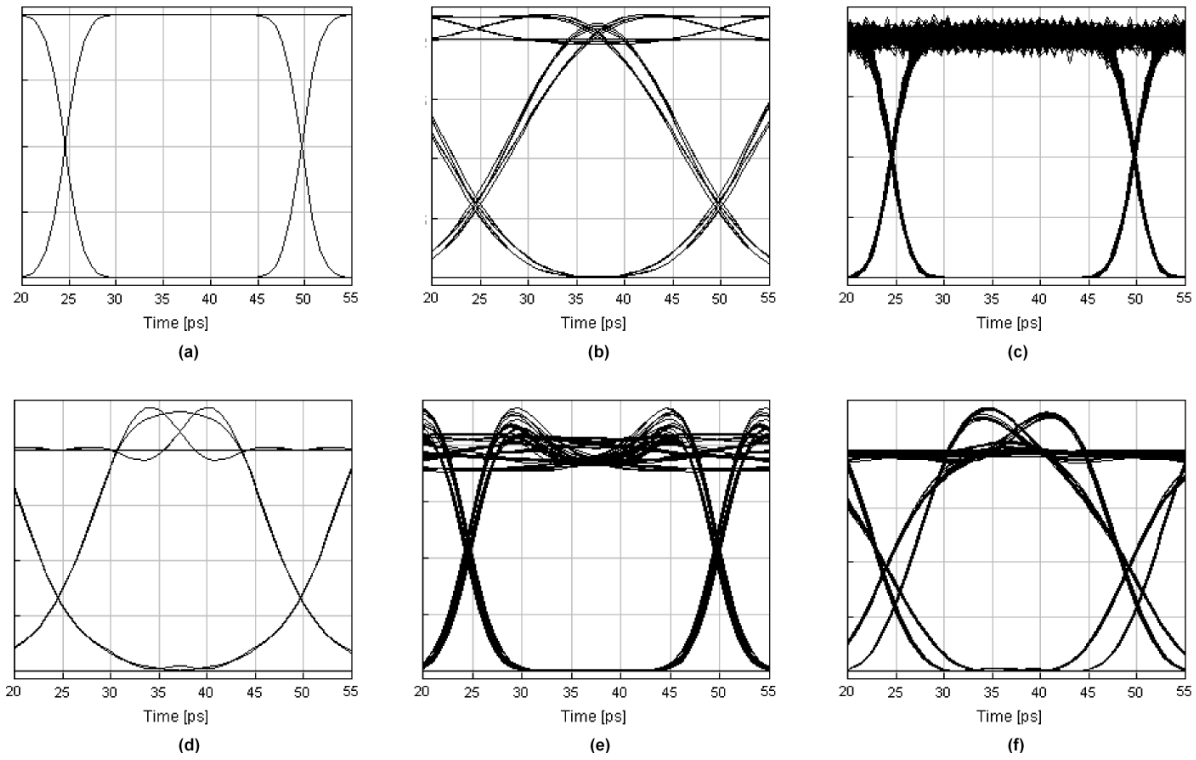

Figure 4.10: Eye distortions caused by different impacts in an optical transmission line: a) back-to-back b) narrow-band filtering c) ASE-noise limitations d) GVD-limitation e) single channel nonlinearities f) multi-channel nonlinearities

The eye diagram is a powerful tool for the characterization of the transmission limitations, because different limitations cause characteristic distortions of the signal eye. The extreme narrow-band filtering of the optical signal causes, for example, a broadening of the single pulses and results in ISI-effects between the adjacent bits (Fig. 4.10b). The ASE-noise induces, depending on the signal extinction ratio, stronger signal level fluctuations in marks (Fig. 4.10c) than in spaces. The accumulation of chromatic dispersion during the transmission causes a pulse broadening resulting in variations of the signal levels, and as a consequence the overlapping occurs between adjacent pulses (Fig. 4.10d). The interaction between linear (e.g. GVD) and nonlinear effects (e.g. SPM) is reflected in the symmetrical fluctuations of the signal power at the rising and trailing edges of the signal (Fig. 4.10e). Because of the nonlinear interaction between adjacent channels (e.g. XPM) in presence of GVD, the asymmetrical power fluctuations accompanied with the timing and amplitude jitter occur at pulse edges (Fig. 4.10f). Hence, the interpretation of the eye diagrams enables a selective characterization and selective suppression of different transmission limitations.
The impact of a propagation distortion causing a reduction of the ideal (back-to-back) eye opening can be

quantified by a transmission penalty or Eye Opening Penalty (EOP). Many different definitions of EOP are known and used today for performance estimation. In following some of them are introduced:

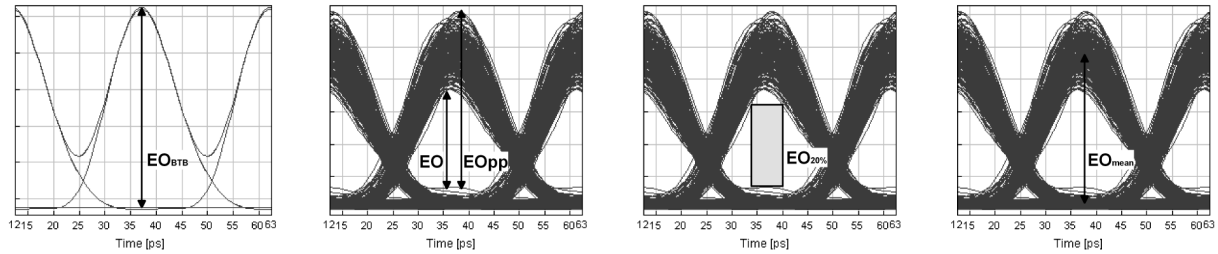

Figure 4.11: Eye opening parameters

- **EOP**: the widely used conventional EOP definition as:

$$\mathrm{EOP}\,[\mathrm{dB}] = 10\log\left(\frac{EO_{BTB}}{EO}\right) \tag{4.26}$$

  where the eye opening (EO) is defined as a difference between the minimum 1 and maximum 0 level in the middle of the eye ($EO = \min(1) - \max(0)$) (Fig. 4.11). Herein, the EO_{BTB} stands for the back-to-back eye opening calculated without a transmission line. This EOP definition represents the worst case evaluation characterized by a significant sensitivity to single bit distortions. It can be used for the characterization of the system performance in single channel transmission without ASE-noise. The quality limit of EOP evaluation equals 1 dB and corresponds to a 80 % opened eye.

- **Mean EOP** ($\mathrm{EOP_{mean}}$): the mean EOP is a further EOP definition derived from conventional EOP:

$$\mathrm{EOP_{mean}}\,[\mathrm{dB}] = 10\log\left(\frac{EO_{mean}}{EO}\right) \tag{4.27}$$

  where EO_{mean} is the difference between mean values of 1s and 0s. In EOP_{mean}, the EO is determined in the middle of the eye and the penalty calculation is made without consideration of EO_{BTB}.

- **Peak-to-peak EOP** ($\mathrm{EOP_{pp}}$): calculates EOP without consideration of EO_{BTB} as a relation of the peak-to-peak signal voltage and the inner eye opening EO:

$$\mathrm{EOP_{pp}}\,[\mathrm{dB}] = 10\log\left(\frac{EO_{pp}}{EO}\right) \tag{4.28}$$

  This method cannot be used for the characterization of the systems with large nonlinear effects, because power fluctuation results in large EOP_{pp} values even if the detected signal eye is widely open.

- **Gaussian EOP** ($\mathrm{EOP_{Gauss}}$): the calculation of the $\mathrm{EOP_{Gauss}}$ is made under assumption of Gaussian statistic of the system distortions. EOP_{Gauss} is given by:

$$\mathrm{EOP_{Gauss}}\,[\mathrm{dB}] = 10\log\left(\frac{EO}{EO_{Gauss}}\right) \tag{4.29}$$

  where EO_{gauss} is defined as:

$$EO_{Gauss} = \mu_1 - \mu_0 - 3\sigma_1 - 3\sigma_0 \tag{4.30}$$

  with μ_1, μ_0 and σ_1, σ_0 describing the mean values and standard deviations of 1s and 0s. According to Gaussian statistic assumption, by the subtraction of three times the standard deviation from the mean value approximately 99% of possible cases (signal levels) are included within this definition. $\mathrm{EOP_{Gauss}}$ enables a transformation of EOP to Q-factor and can be a good evaluation criteria for comparison of numerical and experimental results [32].

- **Eye Mask EOP** ($\mathrm{EOP_{EM}}$): this is a novel EOP definition [227], where the penalty calculation is made without consideration of the back-to-back eye. The $\mathrm{EOP_{EM}}$ is determined using an eye mask (EM) (rectangle) placed in the middle of the eye (Fig. 4.11). The EM width equals 20% of the signal time slot. The $\mathrm{EOP_{EM}}$ is defined as:

$$\mathrm{EOP_{EM}\,[dB]} = 10\log\left(\frac{EO_{mean}}{EO_{20\%}}\right) \tag{4.31}$$

where $EO_{20\%}$ represents the height of the eye mask. The determination of the EO in 20 % region of the eye is more practically relevant than the EO determination precisely in the middle of the eye, because of decision threshold instability of conventional receivers. $\mathrm{EOP_{EM}}$ enables a good performance evaluation in WDM systems with a quality limit of 3 dB in NRZ case corresponding to a 50% closed eye [227].

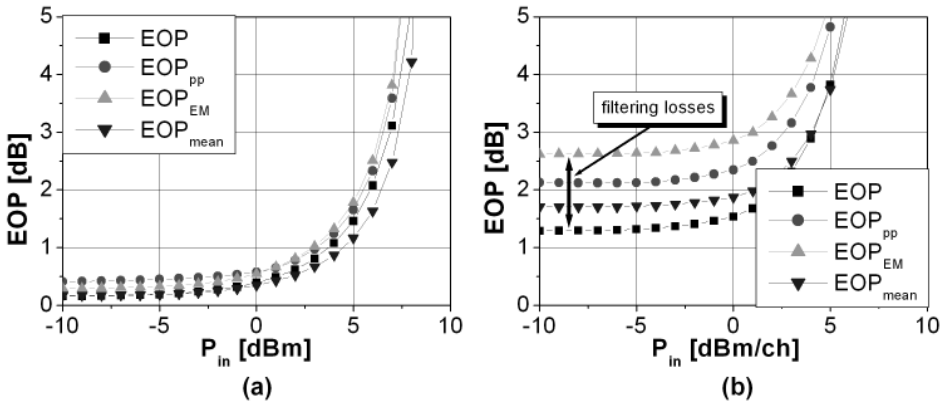

Figure 4.12: Comparison of different EOP methods for the characterization of the transmission performance (4x80 km, SSMF, dispersion post-compensation, without ASE-noise, MUX/DMUX=42.5 GHz) : a) 40 Gb/s single channel transmission b) 4x40 Gb/s WDM transmission (50 GHz channel spacing)

Generally speaking, the EOP criteria can be used for the characterization of single channel and WDM based transmission line without ASE-noise. While in the single channel case, all different EOP criteria show similar values (Fig. 4.12a) indicating similar quality limits. The relationship between different EOP definitions changes in WDM case (Fig. 4.12b). Due to the fact that an ideal signal eye (directly after transmitter) is used for EO_{BTB} calculation presented in Fig. 4.12b, the calculated EOPs indicated larger values (>1 dB, Fig. 4.12b) in low power region although no ASE-noise is considered in this investigation. These large EOP values are caused by narrow-band filtering implemented at the transmitter and the receiver side. This can be explained by the fact that the EOPs, which consider back-to-back signal eye with filtering losses, give the expression that the system performance is better than it really is, because in case of the narrow-band filtering at the transmitter and receiver side even back-to-back eye is distorted, so that badly transmitted eye is compared to a bad back-to-back eye.
The EOP based investigations should be handled with care and can be used just for a characterization of isolated transmission disturbances, e.g. dispersion tolerance, SPM. In this thesis, the conventional EOP is used for single channel investigation without ASE-noise, because EOP can not be efficiently used in systems with ASE-noise due to stochastic ASE nature, which is simulated using a random number generator [32].

4.6 Relation between different evaluation criteria

The derivation of the relationship between different evaluation criteria represents an important issue, because of the different definitions and assumptions used for their calculation. The right conclusions can be drawn

only in some specific cases and specific system infrastructure. For example, due to the fact that the decision between the erroneous and correct bit is dependent on the electrical signal-to-noise (SNR) in the decision circuit and the position of the decision threshold (I_D), it could be concluded that the BER is related to the electrical/optical SNR and the right decision threshold. On the other hand, with EOPs and BER or Q-factor evaluation the transmission characteristics can be identified, but any comparison between these estimation methods is questionable.

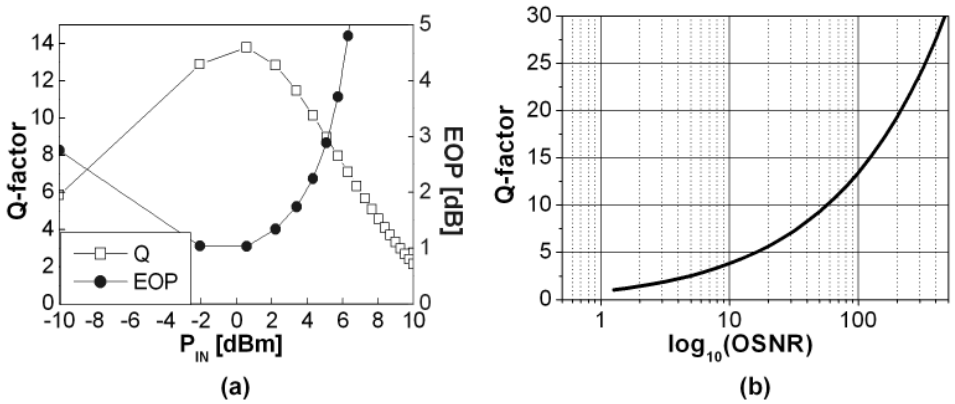

Figure 4.13: Relation between different evaluation criteria: a) Q-factor versus EOP at different powers b) Q-factor versus OSNR (according to Eq. 4.32)

The investigations performed during this work showed that the EOP and Q-factor estimation show optimum (maximal/minimal) values in identical parameter (e.g. power, dispersion) regions (Fig. 4.13), but the conclusions of total transmission distance and maximum system capacity can not be derived using only EOP criteria. Conceptually, the Q-factor defined figure of merit is similar to OSNR evaluation, because it represents a relation between signal and noise statistics, but in difference to OSNR, Q-factor can be used for BER estimation and considers signal dependent noise fluctuations [228]. The relation between Q-factor and OSNR can be approximated by [3]:

$$Q \approx \frac{2\sqrt{2 \cdot T \cdot B_{opt}}\,\mathrm{OSNR}}{1+\sqrt{1+4 \cdot \mathrm{OSNR}}} \tag{4.32}$$

where T is the bit period and B_{opt} is the bandwidth of the optical filter. Using the Q-factor definition, the relation between the OSNR and BER can be established according to Eq. 4.32 as:

$$\mathrm{OSNR}\,(\mathrm{BER} = 10^{-9}) = 22.24 \approx +13.5\,\mathrm{dB} \tag{4.33}$$

For high values of OSNR, the Q-factor can be reduced to $Q \approx \sqrt{2\mathrm{OSNR}}$.
In order to enable the investigation in different transmission regimes by numerical simulations, various estimation criteria (e.g. Q-factor, conventional EOP Eq. 4.26, dynamic range) are used in this work.

5 40 Gb/s single channel investigations

5.1 Overview

The realization and the field implementation of 40 Gb/s single channel transmission systems will be the first step to a deployment of 40 Gb/s based WDM and spectrally efficient DWDM transmission systems. A 40 Gb/s single channel transmission can in combination with OTDM-techniques efficiently replace today's 2.5 and 10 Gb/s WDM systems. Accordingly, the optimization of component characteristics and system settings in 40 Gb/s single channel transmissions is required. In order to deliver sufficient rules for a future system design, it would be necessary to consider not just characteristics of single transmission components (e.g. fibers, amplifiers, modulators), but also the interaction of different components and their interplay with different transmission limitations.
In this chapter, optimization of transmission settings and design rules for the implementation of 40 Gb/s single channel systems are presented over short- and long-haul transmission. The system setting optimization is provided for different ASK-based signal modulation techniques considering effects of different system characteristics, e.g. fiber infrastructure, dispersion compensation schemes, input powers in transmission and dispersion compensating fibers. With optimized system settings, the total performance of 40 Gb/s based transmission lines with different modulation formats is analyzed.

5.2 Investigated system setups

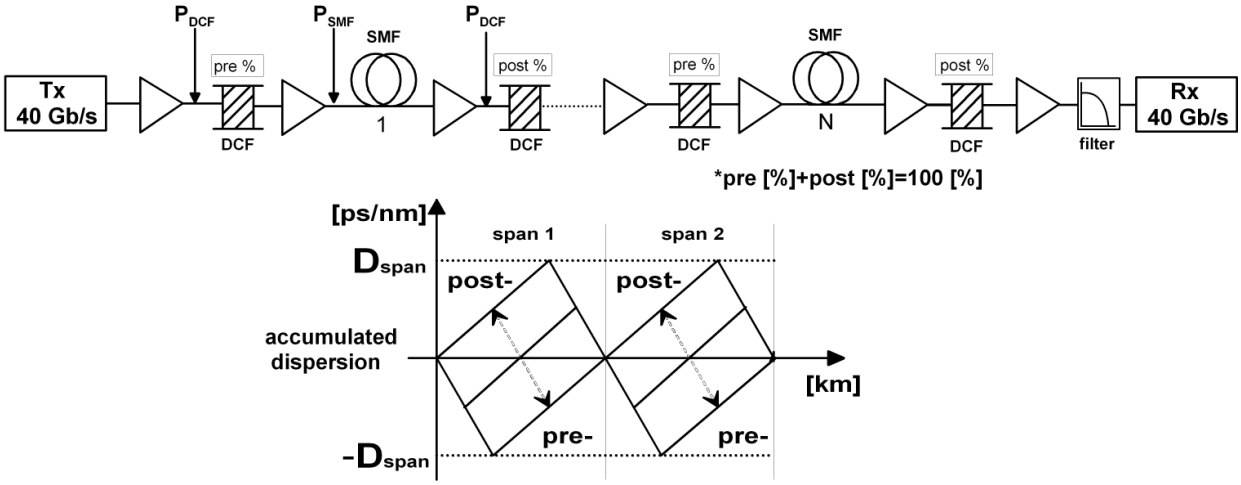

Figure 5.1: Transmission setup used for the investigations of optimum dispersion schemes and optimum power settings

The exemplary transmission line setup used for the investigations of optimum system settings for 40 Gb/s single channel propagation is illustrated in Fig. 5.1. Transmission at 1550 nm was investigated. For different modulation formats, transmitter setups presented in Chapter 3 are used. The same optical direct detection NRZ receiver with an electrical Bessel-Thomson filter of 3rd order and a bandwidth of 28 GHz is used for all modulation formats. The transmission line is made of 80 km long spans according to the fact that this span length is favorable by network providers (e.g. Deutsche Telekom), because it enables a compromise between system costs and performance. This span length represents a good compromise between linear (e.g. ASE-

noise) and nonlinear limitations [229]. Different transmission lengths are realized as cascades of identical spans. Each span consists of a single-mode fiber (SMF) and dispersion compensating fibers (DCF). The optical amplification is done by use of EDFAs with a noise figure of 4 dB, and all investigations presented here are made considering ASE-noise in the transmission line. The role of EDFAs, besides signal amplification, is the ensurance of certain constant power levels in SMFs and DCFs. An optical Bessel 3rd-order filter with a 3-dB bandwidth of 160 GHz is placed after the last EDFA in order to suppress ASE-noise impacts before signal detection. The linear Q_{ISI}-factor is used as the evaluation criteria with a quality limit at Q=6 for all investigations presented in this chapter. Furthermore for dispersion tolerance investigation conventional EOP (section 4.5 with a quality limit of EOP=1 dB. The bit word length of 2^9 is used, which represents a sufficient length for 40 Gb/s investigations (Appendix C).
In order to focus on the limiting effects, which take place in a transmission line, the assumption is made that no pre- and post-compensation is implemented before and after the transmission line (e.g. at the transmitter or at the receiver side), hence all accumulated dispersion is fully compensated by DCFs on a span-by-span basis. This is a rather conservative approach which, depending on the system infrastructure, can be seen as a worst case compensation scenario. It can be expected that the system performance in 40 Gb/s single channel transmissions can be improved by applying some amount of pre-compensation at the transmitter side, but this effect is disregarded in this investigation, because of the assumption that active/tunable dispersion compensation will be required at the transmitter or the receiver side in future 40 Gb/s systems due to a reduced dispersion tolerance and a permanent residual dispersion as a consequence of e.g. path-to-path dispersion variations or temperature changes. In order to get a better insight into the importance of span infrastructure, transmission spans are realized as a combination of pre- and post-inline dispersion compensation enabling a full dispersion compensation (Fig. 5.1a). By the combination of different amounts of pre- and post-compensation different dispersion compensation schemes are achieved (Fig. 5.1b). For giving practically relevant design rules and recommendations, the fiber parameters used for the optimization are taken from data sheets of commercially available and already buried fibers [54], [58]. These fiber parameters are presented in Table 5.1. Besides conventional SSMF (G.625) fibers, two NZDSF fibers with varying parameters are considered in order to analyze dependence of system performance on fiber parameters. For the investigations presented in this work the PMD in transmission and DCF fibers was not considered. All considered transmission fibers are compensated using the identical DCF parameters (Table 5.1) with a variable length depending on the amount of accumulated dispersion.

	Fiber parameters						
fiber type	α [dB/km]	β_2 [ps^2/km]	β_3 [ps^3/km]	D [ps/nm · km]	S [ps/nm^2 · km]	γ [1/Wkm]	A_{eff} [μm^2]
SSMF	0.22	-20.41	0.164	16	0.08	1.32	80
NZDSF1	0.21	-10.2	0.082	8	0.04	1.68	62.7
NZDSF2	0.25	-5.36	0.043	4.2	0.021	2.05	51.3
DCF	0.5	114.79	-0.925	-90	-0.45	3.51	30

Table 5.1: Fiber parameters

5.3 Dispersion tolerance in 40 Gb/s single channel transmissions

The first step for the transmission characterization of 40 Gb/s single channel transmissions are analysis and determination of the transmission tolerance to residual dispersion known as dispersion tolerance in the transmission line. The smaller pulse widths and broader signal spectra characterizing 40 Gb/s transmission, result in an increased pulse broadening during propagation caused by the GVD effect and an interaction between linear and nonlinear effects (e.g. GVD-SPM) in optical fibers making a precise dispersion compensation necessary. Compared to 10 Gb/s systems, which are characterized by a large dispersion tolerance ($\sim \pm$400ps/nm), 40 Gb/s systems show a strong reduction of achievable dispersion tolerance values. A possible method to

improve the dispersion tolerance could be the implementation of spectrally efficient modulation formats with a narrow and compact signal spectrum. Figure 5.2 illustrates the results of dispersion tolerance investigations for different ASK-based modulation formats, which can be basically divided in two groups: NRZ- and RZ-based formats. The dispersion tolerance calculations are made using different signal input powers in order to analyze the interplay between dispersion tolerance and fiber nonlinearities. The accumulated residual dispersion is distributed over four transmission spans with 80 km span length realized over SSMFs, whose dispersion is compensated in a post-compensation scheme (Fig. 5.1). As evaluation criterion, a conventional EOP definition is used with a 1 dB EOP as a quality limit corresponding to a 80 % eye-opening.
As a consequence of a narrower signal spectrum, NRZ-based formats show at lower input powers (e.g. 0 dBm) large dispersion tolerances in a range between 100 (alCNRZ)..175 ps/nm (duobinary), compared to RZ-based formats with tolerances of 45 (nCRZ)..60 ps/nm(CSRZ) (Fig. 5.2a). The tolarance curves are symmetrical around a residual dispersion of 0 ps/nm, indicating a full dispersion compensation as the optimum for 40 Gb/s single channel transmission in the low power region. It can be expected that the dispersion tolerance values will be changed in systems with narrow-band filtering at the transmitter side (e.g. future DWDM systems), which would cause disappearing of tolerance differences between NRZ- and RZ-based modulation formats.
An increase of the signal power causes a reduction of dispersion tolerance both for RZ- and NRZ-based modulation formats. The differences in dispersion tolerence between these two groups of formats vanish for an input power of 6 dBm (Fig. 5.2), according to increased nonlinear impacts. The dispersion tolerance changes at increased powers are less critical in RZ-based formats than in NRZ-based, indicating a better nonlinear tolerance of RZ-based modulation formats, which can be explained by a better robustness to Kerr nonlinearities due to the reduced pulse width and lower steepness of pulse edges, resulting in a reduction of the generated signal phase modulation. The advantages of novel modulation formats can be observed in a reduced nonlinear impact in a high power regime, but they are not able to outperform excellent dispersion tolerance of NRZ-based formats in a low power regime. The NRZ and RZ formats with orthogonal polarizations in adjacent bits (alPNRZ, alPRZ) show dispersion tolerance values almost independent of the signal power in a power range of up to 9 dBm (Fig. 5.3), whereby for all other NRZ- and RZ-based modulation formats the dispersion tolerance vanishes for signal powers larger 6 dBm. This can be explained by orthogonal polarization between adjacent bits and spectral shapes of alternate polarized signals.

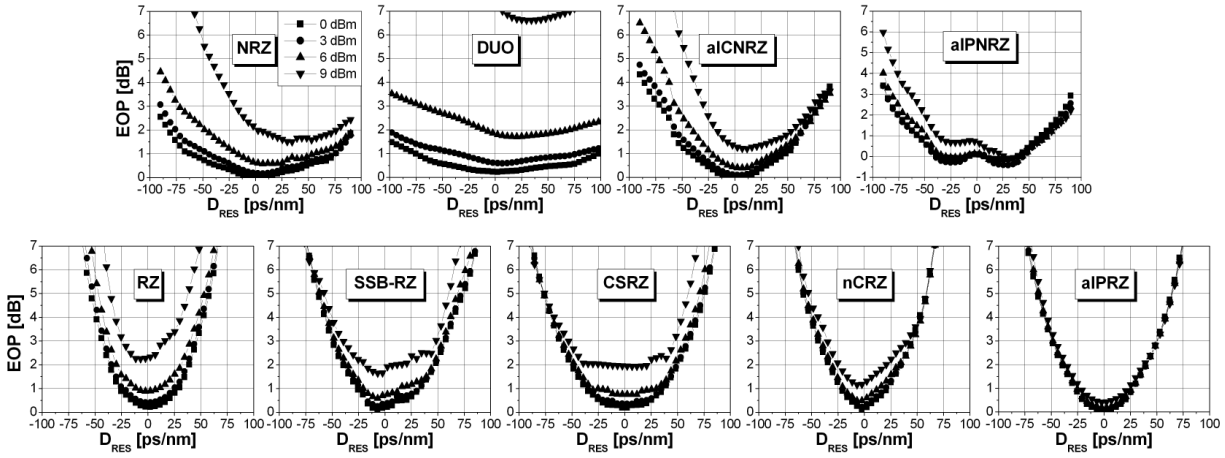

Figure 5.2: Dispersion tolerance in 40 Gb/s single channel transmission over 4x80 km SSMF with span-by-span dispersion post-compensation (P_{DCF}=-4 dBm, without ASE-noise)

Another important fact of this investigation is that for modulation formats with a reduced nonlinear tolerance (e.g. NRZ, duobinary) the full dispersion compensation does not present the optimum for an increased input power. Hence, a dispersion under-compensation in the transmission line would be preferable for improved transmission performance if NRZ and duobinary modulation are implemented employing high signal power.

This can be explained by the fact that a dispersion under-compensation per span causes a reduction the GVD-SPM interplay in the effective length L_{eff} on the beginning of each span. It could be expected that this effect will be even more evident in systems employing transmission fibers with a reduced dispersion value and fiber core areas (e.g. NZDSF), because of their worse nonlinear characteristics compared to SSMFs.

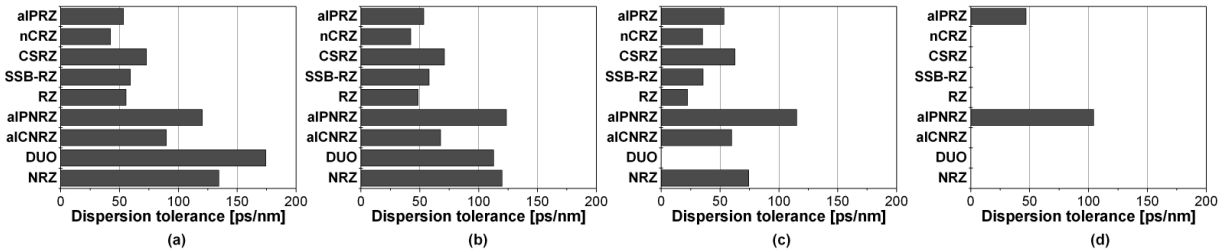

Figure 5.3: Total dispersion tolerance in 40 Gb/s single channel transmission over 4x80 km SSMF at 1 dB EOP (derived from Fig. 5.2): a) P_{IN}= 0 dBm b) P_{IN}= 3 dBm c) P_{IN}= 6 dBm d) P_{IN}= 9 dBm

5.4 Nonlinear tolerance in 40 Gb/s single channel transmissions

After the dispersion tolerance analysis gave first insights into linear and nonlinear characteristics and indicated differences between different modulation formats in 40 Gb/s single channel transmission, further investigations are performed, in order to determine and analyze their nonlinear tolerances. The importance of the nonlinear tolerance lies in the fact, that for long transmission distances a large signal power is needed, because of ASE-noise induced limitations in the transmission line. Large signal powers cause enhanced nonlinear impairments e.g. SPM and intra-channel effects (IXPM, IFWM). In interaction with GVD, the nonlinear impacts introduce in ASK-based transmission lines a penalty resulting in a reduced system reach. The nonlinear tolerance depends basically on the characteristics of the optical signal (e.g. modulation format) and on the deployed system infrastructure (e.g. dispersion compensating scheme) in the transmission line. In order to deliver design rules for 40 Gb/s single channel transmissions, nonlinear tolarances of different modulation formats are calculated considering different dispersion compensation schemes - pre-, hybrid- and post-compensation - on a span-by-span basis with a full compensation of the accumulated dispersion in each span. The characterization of nonlinear tolerance is made using the "P_{max}"-rule [224]. According to this rule, the maximum input power P_{max} for each modulation format depends on the total length (number of spans) of the transmission line and is given as:

$$P_{max}\,[\mathrm{mW}] = N \cdot P_{IN}\,[\mathrm{mW}] \tag{5.1}$$

where N is the number of spans and P_{IN} is the input signal power, for which the quality limit of 1 dB conventional EOP is reached. The modulation formats with larger P_{max} values possess a better nonlinear behavior, because they can tolerate a larger signal powers compared to other formats, considering a constant transmission length. The P_{max}-rule can be especially used for a characterization of the GVD-SPM impact. Because of the interaction between nonlinear and linear effects during signal propagation, it can be expected that the achievable P_{max}-value for different modulation formats will be dependent on the dispersion compensation scheme (fiber infrastructure) applied in the transmission line. Figure 5.4 illustrates the nonlinear tolerance

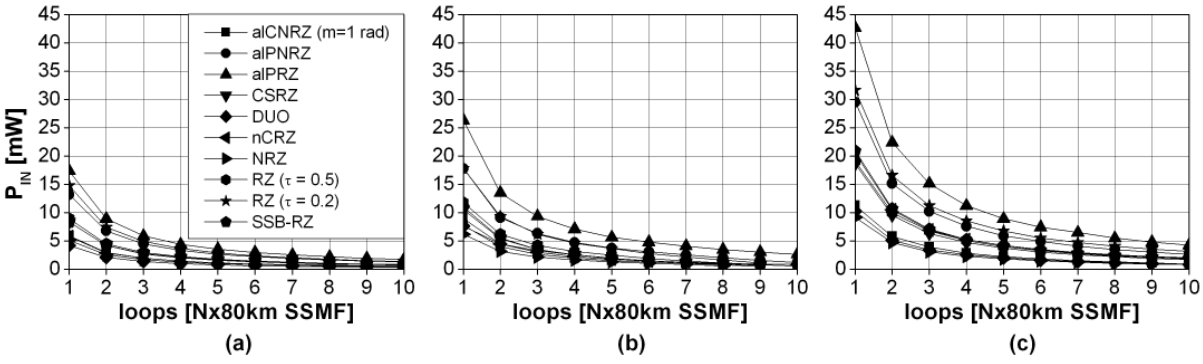

Figure 5.4: Nonlinear tolerance in 40 Gb/s single channel transmission over 4x80 km SSMF (P_{DCF}=-4 dBm, without ASE-noise): a) pre-compensation b) hybrid compensation c) post compensation

of various modulation formats as dependence of P_{max}-value on the transmission distance in a SSMF-based transmission line (Fig. 5.1). In order to concentrate on the impact of transmission effects, ASE-noise was not considered in the transmission line. It is evident that RZ-based modulation formats show better nonlinear tolerance compared to NRZ modulation formats. This can be explained by the fact that, because of a reduced pulse width (smaller than a time slot) in RZ-based formats, pulses disperse faster, thus reducing the peak power and the impact of single channel nonlinear effects (e.g. SPM). Furthermore, the steeper pulse edges in NRZ-based transmissions cause stronger SPM generation (Eq. 2.63). But on the other hand, a fast broadening of RZ-shaped pulses enhances pulse-to-pulse or intra-channel interactions (e.g. IXPM), which in periodically compensated transmission links become significantly evident after 300 km [72]. The consequence

of the IXPM impact is that P_{max} values of RZ-based formats slightly deviate from P_{max}-rule (Fig. 5.4) after certain transmission distance (4..6 spans). This observed behavior is in a good agreement with experimental works [230].
The NRZ-based formats are strongly affected by SPM, so that variations from the P_{max}-rule are smaller and occur later (after 7..9 spans). Considering different dispersion compensation schemes, deviations between nonlinear tolerances can be observed (Fig. 5.4). The post-compensation scheme represents the best-case scheme among all considered schemes. The origin for this behaviour is located in the first 18..20 km (L_{eff}) of each span, where nonlinear impacts are maximal. It can be expected that when undisturbed optical pulses are fed in transmission fibers, a large local dispersion at the beginning of each span is beneficial for the suppression of nonlinear impacts. This topic is elaborated more detailed in Chapter 5.5.2.

modulation format	P_{max} [mW]		
	pre-compensation	hybrid-compensation	post-compensation
NRZ	5.13	6.16	9.12
DUO	4.17	7.58	10.23
alCNRZ	5.89	7.76	11.22
alPNRZ	**13.18**	**17.78**	**29.51**
RZ ($\tau = 0.5$)	8.91	11.75	19.05
RZ ($\tau = 0.2$)	14.79	17.78	31.62
SSBRZ	8.32	10.96	20.89
CSRZ	8.32	10.47	18.62
nCRZ	5.75	8.91	20.41
alPRZ	**17.38**	**26.30**	**42.66**

Table 5.2: P_{max} values for different ASK-based modulation formats and dispersion compensating schemes (40 Gb/s, without ASE-noise, system setups from Fig. 5.1)

The calculated nonlinear tolerance (P_{max}) values (Table 5.2) can be applied for qualification and characterization of different modulation formats. Comparing conventional NRZ- and RZ-based formats, it can be observed that RZ shaped pulses can enable an enhancement of the signal power in terms of P_{max}-rule of 3-10 dB (Table 5.2), which is dependent on the implemented dispersion compensation schemes. Considering NRZ-based formats, NRZ and duobinary modulation show slight differences of P_{max}-values, indicating similar nonlinear tolerance in investigated transmission cases. On the other side, the SSB-RZ and CSRZ modulations can enable a performance improvement compared to conventional RZ modulation in a pure dispersion post-compensation scheme according to their good nonlinear tolerance, but this behavior get lost in other investigated schemes. Hence, the CSRZ and SSB-RZ performances could not be seen as globally better than RZ, which show a good agreement with experimental works [182], [231].
As a method for nonlinear improvement in conventional RZ formats so called "tedons" [173], [172] pulses could be used with a reduced FWHM-width (duty cycle), because these pulses disperse faster. Using an RZ pulse with a duty cycle of τ=0.2, the P_{max} value can be significantly increased in comparison to τ=0.5 RZ pulses (Table 5.2) and CSRZ and SSB-RZ cases. But, this solution would be limited to a single channel and WDM transmissions with a reduced spectral efficiency (<0.4 bit/s/Hz), because of a broader optical signal spectrum as a consequence of the pulse narrowing.
A comparison to conventional formats indicates that novel modulation formats enable a significant improvement of the nonlinear tolerance, but not in all investigated cases. Typically, in a pure post-compensation scheme, novel formats significantly outperform the conventional ones. The alternately polarized modulation formats (alPNRZ, alPRZ) show significantly better nonlinear characteristics than all others investigated NRZ and RZ formats enabling 2..3 times larger P_{max} values independent of the implemented dispersion compensation scheme. The explanation for this behavior can be found in the suppression of SPM and the inter-pulse interferences by the orthogonal polarization in adjacent bits.

5.5 Optimization of system settings for 40 Gb/s single channel transmission

The performance of optical transmission lines can be seen as a trade-off between different component and system parameters. Accordingly, for a system optimization considering various modulation formats, a multi dimensional parameter space has to be investigated in order to determine the optimum system settings. This optimization is dependent on at least three parameters: transmission fiber, fiber input powers and dispersion compensation schemes. These parameters can be further divided into subparameters e.g. the right fiber choice depending on fiber effective area, fiber dispersion, attenuation and polarization characteristics. For the optimum dispersion compensation, a combination of pre-compensation at the transmitter side, in-line compensation in the transmission line and post- or residual compensation at the receiver side, have to be investigated. Hence, for a correct optimization of system settings, all important system parameters have to be varied in a certain range, in order to find the right parameter combination and optimum operating regime. Since this procedure would require enormous time and computing resources, the practically oriented system optimization has to be made with certain assumptions considering the state-of-the-art technologies and feasibility of investigated system components.

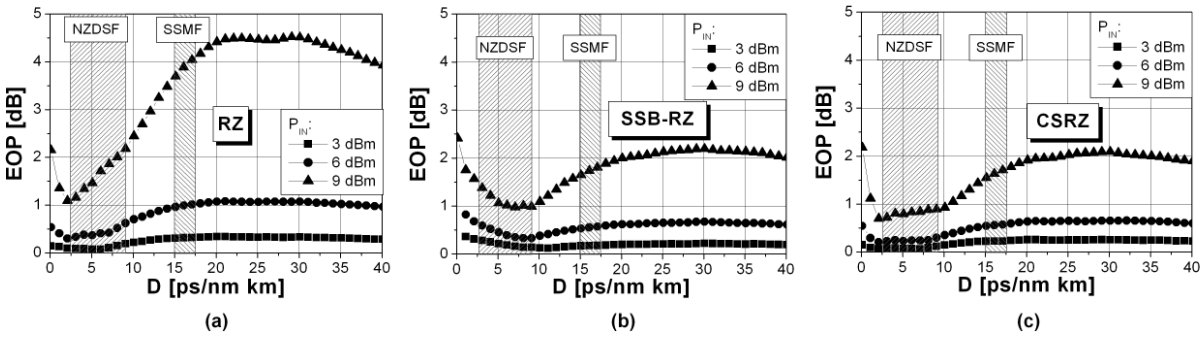

Figure 5.5: Optimum fiber dispersion for 40 Gb/s single channel transmission over 4x80 km (post-compensation, A_{eff}=80 μm^2, duty cycle τ=0.5, without ASE-noise, P_{DCF}=-4 dBm)

The first investigation step represents the choice of optimum fiber parameters, whose importance is indicated in recently presented works [73], [232]. Deployed in different dispersion compensation schemes, different power regimes and considering a varying number of channels, various transmission fibers can represent the optimum solution. This can be explained by the fact that depending on the transmission infrastructure, a system performance can be limited by different propagation effects. If, for example, a single channel 40 Gb/s transmission line over 4x80 km with a span-by-span dispersion post-compensation (Fig. 5.1) is considered with various modulation formats and various input powers, different transmission behavior can be observed for different settings of fiber dispersion 0..40 ps/nm·km (Fig. 5.5). In a low power regime (e.g. P_{IN}=3 dBm), all modulation formats indicate similar behaviour due to the linear nature of transmission disturbances. With an increasing input power, the differences between the optimum fiber dispersion settings appear. Modulation formats like SSB-RZ and CSRZ perform better than conventional RZ (Fig. 5.5), according to their better nonlinear robustness in the investigated dispersion compensation scheme. Focusing on the optimum fiber settings, it is visible that 40 Gb/s single channel transmission would profit primarily by a reduced fiber dispersion independently of the modulation format in use. This can be explained by reduced interactions between adjacent pulses in low dispersion fibers resulting in an efficient suppression of intra-channel effects (e.g. IXPM, IFWM). According to this investigation, non-zero dispersion shifted fibers (NZDSF) perform better in this system infrastructure than SSMFs. But, if a different dispersion compensation scheme is implemented (e.g. pure pre-compensation), these conclusions may not be valid any more. The right choice of dispersion compensation represents a further issue for system optimization.

5.5.1 Optimum power setting for different fiber infrastructures

Optimization of input powers in transmission and DCF fibers provides additional insights in nonlinear characteristics of different modulation formats. The investigation of the optimum fiber power regions enables a better characterization of transmission behavior, enabling e.g. an increase of amplifier spacing or reduction of fiber nonlinearities. Considering various combinations of the pre- and post compensation in a single span, optimum power settings for transmission and dispersion compensating fibers are determined for various ASK-based modulation formats. The transmission investigation is performed over four spans. For all dispersion compensation schemes the power settings in the transmission (P_{SMF}) and dispersion compensating fibers (P_{DCF}) are varied in a range of -5..5 dBm and -10..5 dBm, respectively. The investigated modulation formats are divided in two groups: NRZ- and RZ-based. In order to enable a better overview over these results, the four different dispersion compensation cases with their optimum power ranges for each fiber type (e.g. SSMF, NZDSF1 and NZDSF2) are presented: pre-compensation, optimum compensation, hybrid-compensation and post-compensation. The optimum dispersion compensation scheme denotes the scheme which enables the best performance in terms of largest Q-values (Q_{ISI} evaluation) and widest power regions for transmission and DCF input power.

NRZ-based modulation formats

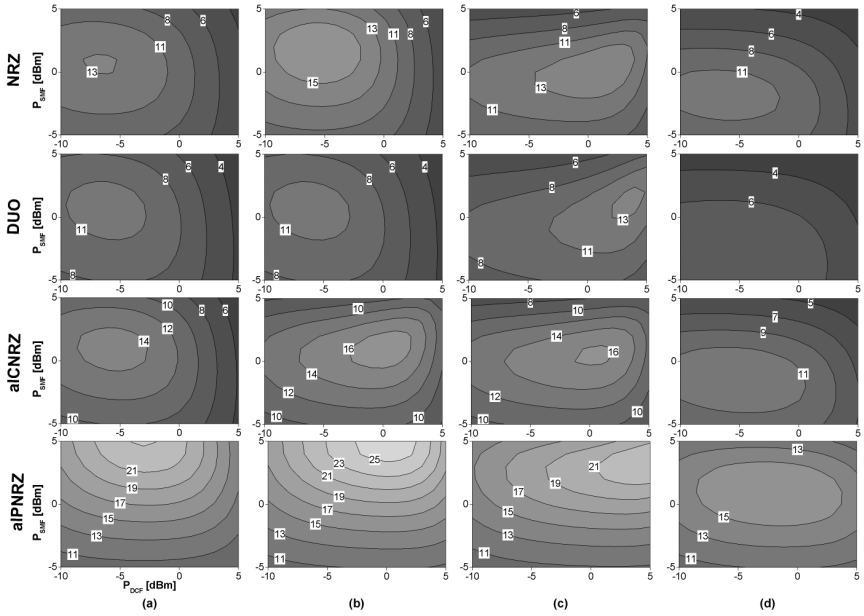

Figure 5.6: Optimum P_{SMF} and P_{DCF} powers in 40 Gb/s NRZ-based single channel transmission over 4x80 km SSMF (linear Q_{ISI} evaluation, with ASE-noise): a) post-compensation b) optimum-compensation (see Table 5.4) c) hybrid-compensation d) pre-compensation

The results of optimum power investigation for NRZ-based modulation formats are presented in Figs. 5.6, 5.7 and 5.8 for different transmission fiber types. The optimum amounts of pre-compensation for different modulation formats and different fibers are presented in Table 5.4. Considering the optimum power range and maximum performance for 40 Gb/s transmission over SSMF, conventional NRZ modulation shows better transmission characteristics than duobinary modulation, independently of the employed dispersion compensation scheme. Because of an increased nonlinear impact in DCF, due to a reduced core area and hence larger nonlinear coefficient γ, a large DCF input power is an important system limitation. By the implementation of alCNRZ modulation with a small modulation index (1 rad), it is possible to improve the nonlinear tolerance

of NRZ modulation and to relax the P_{DCF} limitations (Fig. 5.6). If a real transmission system is considered, the P_{DCF} would be rather small, because an additional amplifier at the SMF output should be avoided due to additional costs. In this case, the nonlinear problems in DCFs would vanish, but according to a low P_{DCF} the ASE-impact would become important. Optimum P_{DCF} is thus dependent on the P_{SMF} and ASE-noise generation in the optical amplifier placed before DCF. A compromise between these issues would be the use of an additional amplifier at the SMF output with a small gain and at reduced costs.
Further enlargement of power regions and an improvement of nonlinear tolerance can be achieved by imple-

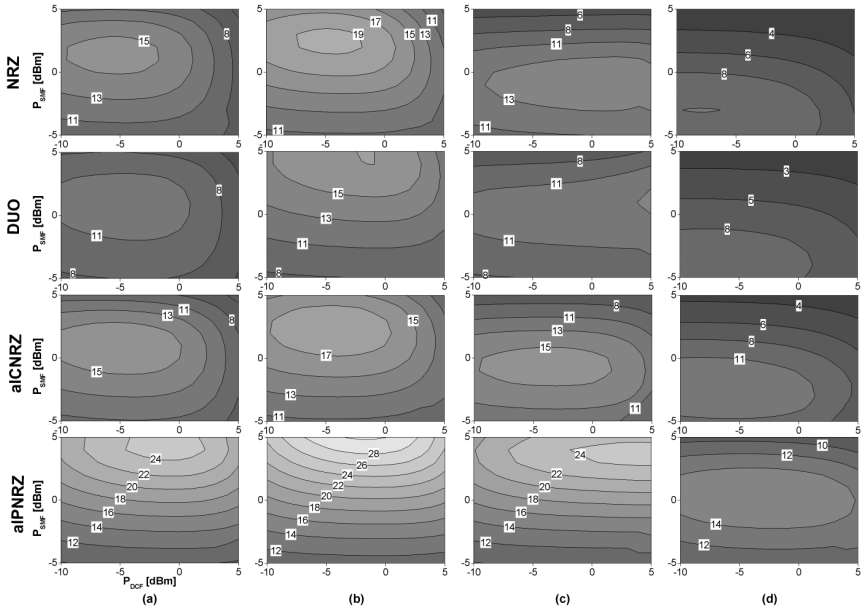

Figure 5.7: Optimum P_{SMF} and P_{DCF} powers in 40 Gb/s NRZ-based single channel transmission over 4x80 km NZDSF1 (linear Q_{ISI} evaluation, with ASE-noise): a) post-compensation b) optimum-compensation (see Table 5.4) c) hybrid-compensation d) pre-compensation

mentation of polarization switching between adjacent bits in a NRZ bit stream (e.g. alPNRZ). Using alPNRZ, DCF input powers up to 5 dBm represent no significant limitation to system performance. Considering the optimum power settings for SMF and DCF fibers, it can be concluded that for NRZ and duobinary modulation optimum power settings for the investigated transmission distance amount to P_{SSMF} ≈0 dBm and P_{DCF} <-5 dBm, whereas for alCNRZ and alPNRZ power setting are P_{SSMF} >0 dBm and P_{DCF} ≈0 dBm. In

fiber type	total transmission length [km]	OSNR [dB][1]
SSMF	376.88 km	23.27
NZDSF1	348.44 km	27.62
NZDSF2	334.93 km	26.11

Table 5.3: Total length and OSNR-value differences between transmission line infrastructures (4 spans) with span-by-span dispersion post-compensation (P_{DCF}=- 4 dBm)

comparison to SSMF, NZDSF1 fiber possesses half the chromatic dispersion and a smaller core area (A_{eff}). The consequences of the reduced dispersion value are different total transmission lengths in systems with different fibers, because the DCFs with equal dispersion settings are used for the dispersion compensation in SSMF and NZDSF1 lines (Table 5.3). Furthermore, taking into account different fiber attenuation values

[1] 0.1 nm bandwidth resolution

different OSNR values occur in transmission lines with various fiber infrastructure (Table 5.3). Further more, a slight changes of OSNR occur if different dispersion compensations schemes are employed in line (see Fig. 2.32 in Chapter 2.8). Accordingly, a fair comparison of different fiber types cannot be performed.
The results of NZDSF1 investigation (Fig. 5.7) identify that the transmission performance would from a reduced fiber dispersion, independently of the fiber core area and the modulation format in use. This can be explained by the fact, that a reduced dispersion causes a reduced GVD-SPM interplay and suppresses the interferences between consecutive pulses due to intra-channel effects, thus enlarging optimum power regions for all modulation formats. Therein, duobinary modulation represents the worst case for all dispersion compensating schemes and novel modulation formats in NZDSF1 based transmission enable a significant improvement of maximum powers in terms of extremely large Q-values. Further reduction of chromatic dispersion settings in transmission fibers (e.g. NZDSF2 case) results in an improvement of linear and nonlinear features of the transmission line (Fig. 5.8). Despite of a reduction of core area in NZDSF2 fibers, all investigated dispersion compensation cases show an enlargement of power regions and an improvement of total performance. The differences between modulation formats remain as in previous cases and the limitations of P_{DCF} are more relaxed due to the reduced DCF lengths.

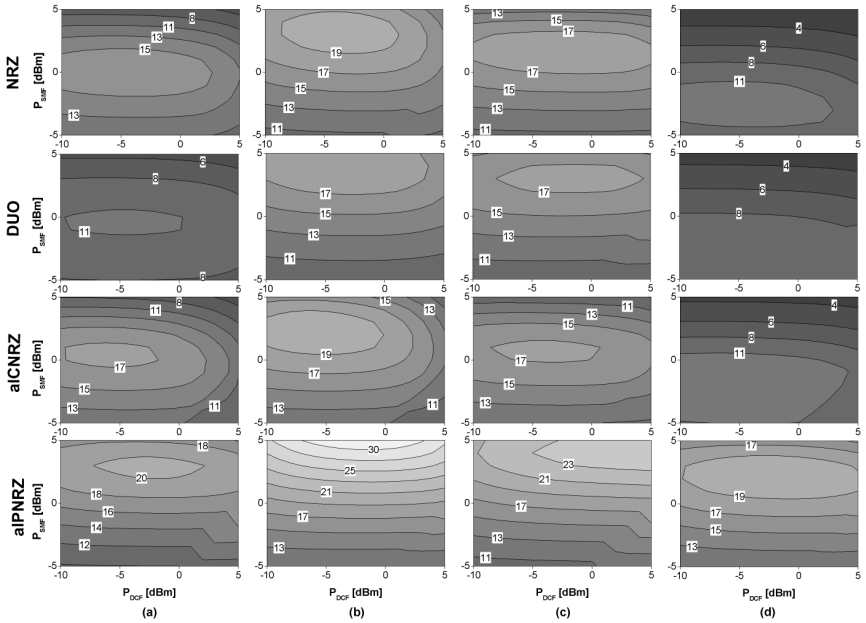

Figure 5.8: Optimum P_{SMF} and P_{DCF} powers in 40 Gb/s NRZ-based single channel transmission over 4x80 km NZDSF2 (linear Q_{ISI} evaluation, with ASE-noise): a) post-compensation b) optimum-compensation (see Table 5.4) c) hybrid-compensation d) pre-compensation

RZ-based modulation formats

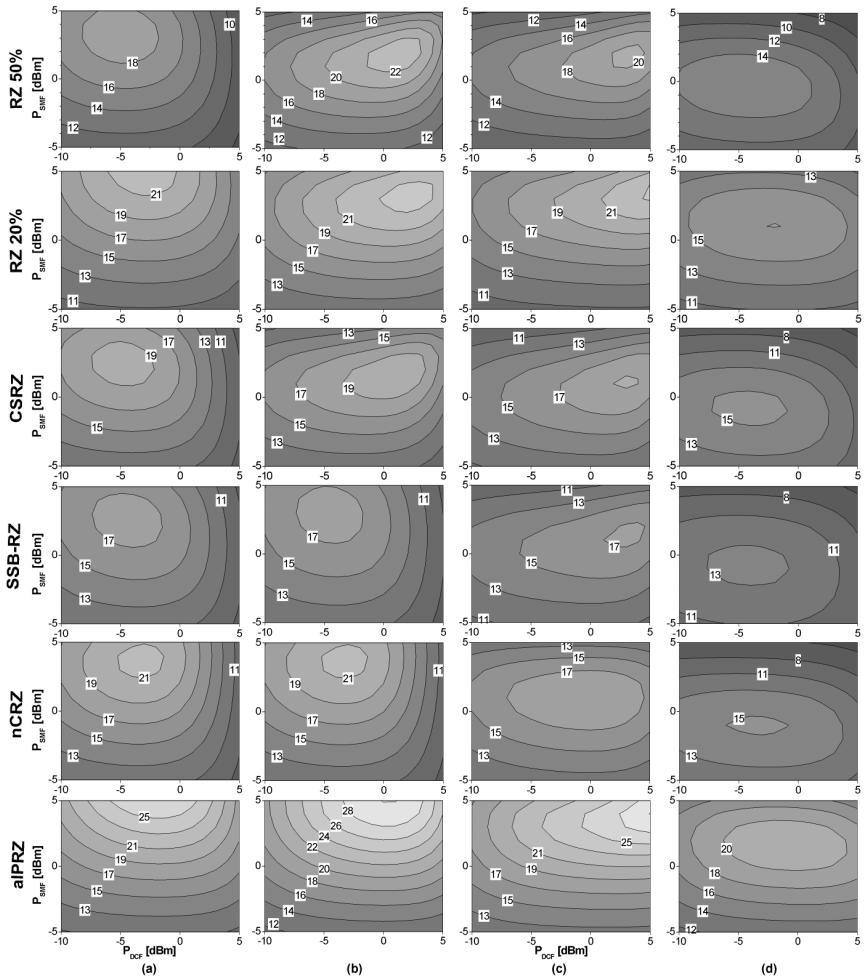

Figure 5.9: Optimum P_{SMF} and P_{DCF} powers in 40 Gb/s RZ-based single channel transmission over 4x80 km SSMF (linear Q_{ISI} evaluation, with ASE-noise): a) post-compensation b) optimum-compensation (see Table 5.4) c) hybrid-compensation d) pre-compensation

The optimum power investigations for RZ-based modulation formats showed (Fig. 5.9, 5.10 and 5.11) that these modulation formats enable an enlargement of the optimum power regions for P_{SMF} and P_{DCF}, compared to NRZ-based formats, independently of the dispersion compensation scheme and transmission fiber type in use, justifying their good nonlinear tolerance. For different modulation formats, pure pre-compensation shows worse transmission characteristic than pure post-compensation, according to an increased GVD-SPM interplay and strong pulse disturbances due to the dispersion pre-compensation which cannot be compensated in the following DCF. Even more, large pre-compensation enhances interactions between consecutive optical pulses causing strong intra-channel effects. Concentrating on achievable Q values and diameter of optimum power regions for different modulation formats, it can be observed that in the investigated P_{SMF} power range (-5..5 dBm) conventional RZ modulation shows similar transmission features as CSRZ and SSB-RZ in terms of optimum power values. This behavior can be explained by a relatively short transmission distance and rather low input powers. The significant differences among these three modulation formats would become visible for input powers above 5 dBm [64], [165].

Contrary to results of NRZ investigations, the RZ-based modulation formats indicated large P_{DCF} power

ranges. The power tolerance of RZ modulation for different dispersion compensation schemes can even be further improved by the implementation of reduced duty cycles in optical pulses (Fig. 5.9), which enables a reduction of single-channel nonlinear limitations, e.g. SPM-GVD interplay. This improvement occurs due to the reduction of pulse width at a reduced duty cycle, a consequence of which is a reduced linear length L_D. According to the categorization rules presented in Chapter 2, a reduced L_D characterizes a pulse evolution governed more strongly by fiber dispersion than by nonlinear impacts.
Using the reduced duty cycle approach, the transmission performance can be enhanced even in a pure pre-compensation scheme (Fig. 5.9). The optimum value of the duty cycle has to be carefully chosen and its practical realization is limited by the method of signal generation, e.g. in a RZ generation with two modulator stages only certain duty cycles can be realized - 33 %, 50 % and 66 % - depending on the biasing point of the second modulator stage. Newly proposed RZ based formats like nCRZ and alPRZ provide an improvement of power tolerance, which is primarily dependent on the implemented dispersion compensation scheme, and recommends these formats as a good alternative to conventional RZ-based formats in 40 Gb/s single channel transmissions where power budget and lower system complexity are desirable. The achievable improvement is significant in case of alPRZ modulation, because of an efficient suppression of nonlinear interactions between consecutive pulses due to polarization orthogonality between them.

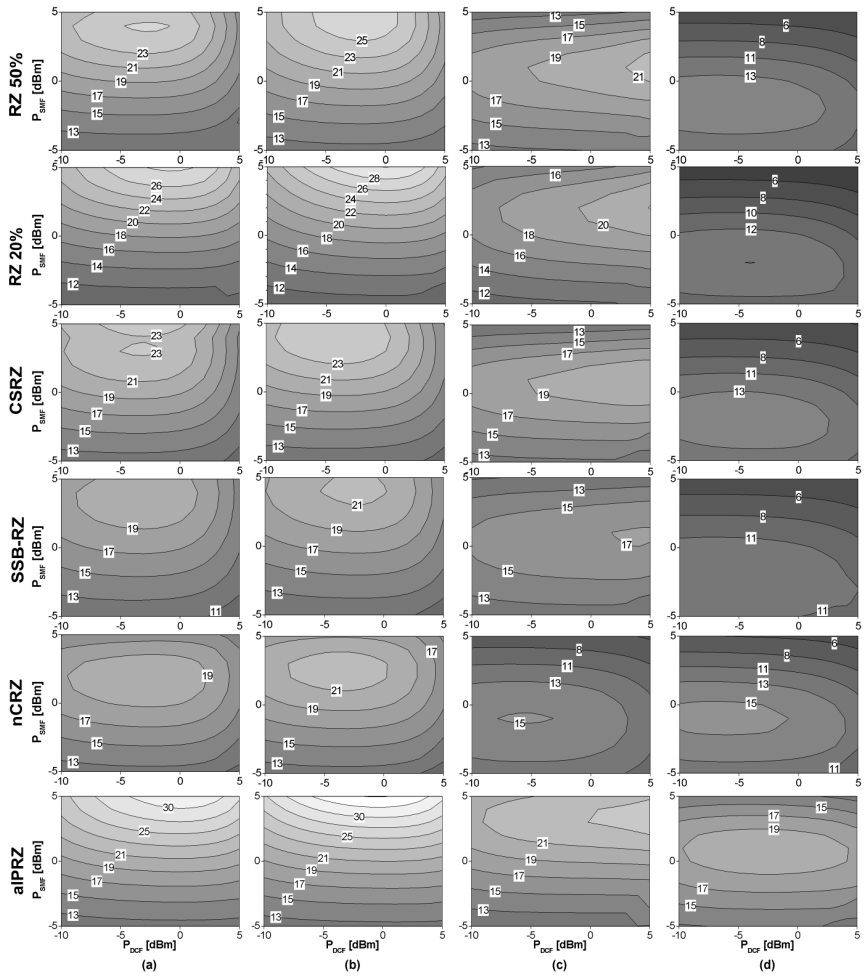

Figure 5.10: Optimum P_{SMF} and P_{DCF} powers in 40 Gb/s RZ-based single channel transmission over 4x80 km NZDSF1 (linear Q_{ISI} evaluation, with ASE-noise): a) post-compensation b) optimum-compensation (see Table 5.4) c) hybrid-compensation d) pre-compensation

Considering optimum power settings for NZDFSs (Fig. 5.10 and 5.11), it can be observed that all presented results identify that transmission performance would profit from fibers with a reduced chromatic dispersion even if their nonlinear characteristics are slightly worse compared to conventional SSMFs. This effect can be explained by the nature of the dominant propagation limitations in a 40 Gb/s single channel transmission over different fibers. SPM, IXMP and IFWM as dominant single channel propagation effects can be divided into two groups due to their dependence on the fiber dispersion. Intra-channel effects - IXPM and IFWM - belong to the group, which profits by a reduced fiber dispersion, because a reduced dispersion suppresses the interaction between the consecutive pulses. The second group contains SPM and its interplay with the GVD. The dispersion dependence of the second group is not straightforward, because the reduced chromatic dispersion causes less pulse broadening, thus enhancing SPM-induced phase modulation, but due to a reduced local dispersion the PM-IM conversion is less effective, making the total nonlinear impact less important in an ASK based system over e.g. NZDSF fibers. The nonlinear fiber characteristics govern the amount of induced phase modulation, but their final impact is dependent on the fiber local dispersion.
Accordingly, summarizing all dispersion characteristics of both groups of limitations, it can be justified that a reduced fiber dispersion would improve performance in 40 Gb/s single channel transmissions. These results are in a good agreement with recently presented works [73], [232]. It can be expected that larger fiber dispersion would enable benefits for the single channel transmission only for extremely large optical powers (>10 dBm) [229], which are less relevant from the system design point of view.

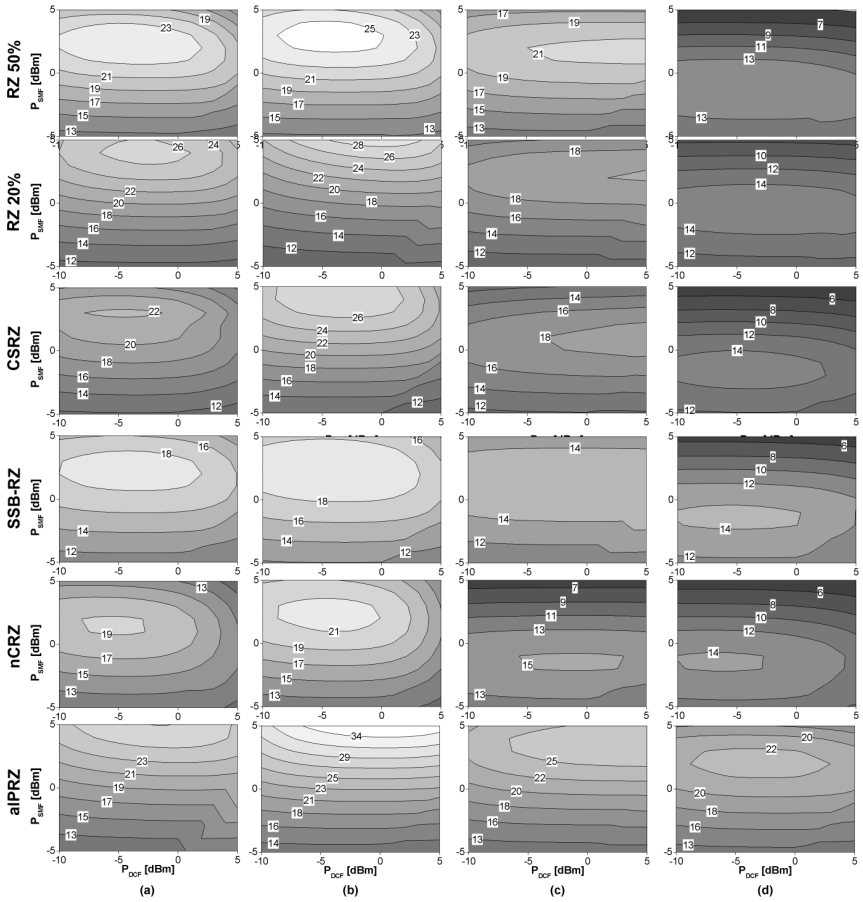

Figure 5.11: Optimum P_{SMF} and P_{DCF} powers in 40 Gb/s RZ-based single channel transmission over 4x80 km NZDSF2 (linear Q_{ISI} evaluation, with ASE-noise): a) post-compensation b) optimum-compensation (see Table 5.4) c) hybrid-compensation d) pre-compensation

5.5.2 Optimum dispersion compensating scheme

The determination of the optimum dispersion compensation scheme enables suppression of nonlinear limitations resulting in a possible transmission reach increase. The numerical analysis of the optimum dispersion compensating scheme is done in part together with the investigations of optimum fiber power settings presented in the previous section. For each combination of pre- and post-compensation in a single transmission span, the optimum power settings for transmission and DCF fibers were identified considering various ASK-based modulation formats and different fiber infrastructures. In this section, a more detailed characterization of pulse propagation is performed considering different aspects of propagation (e.g. dispersions scheme, fiber type) for NRZ- and RZ-based modulation formats.

NRZ-based modulation formats

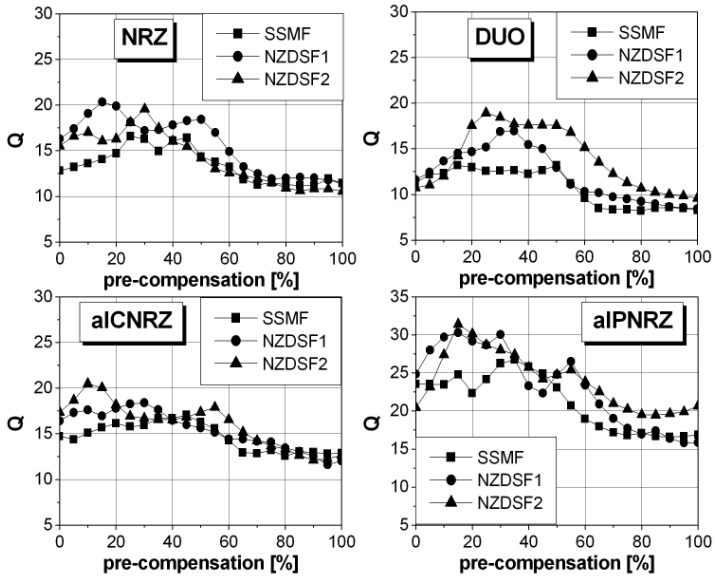

Figure 5.12: 40 Gb/s transmission over 4x80 km transmission line with optimized P_{SMF} and P_{DCF} for each amount of pre-compensation (linear Q_{ISI} evaluation, P_{SMF} and P_{DCF} settings presented in Appendix D)

Figure 5.12 illustrates the dependence of the Q-factor on dispersion compensating scheme and transmission fibers. Due to a relatively small transmission distance (4x80 km) and moderate power settings, the received signal eyes were widely open for all modulation cases, hence explaining large evaluated Q values. It is evident that a pure (100 %) dispersion pre-compensation performs worse than pure post-compensation and that an optimum dispersion compensation scheme should be employed as a combination of a certain amount of pre-compensation. This behavior is independent of the transmission fiber and modulation format in use. At the same time, novel modulation formats (e.g. alPNRZ) enable a better transmission performance, which is reflected in larger Q values.
The elaboration of these effects is done beginning with a comparison of pure pre- and post-compensation, focusing on major single channel nonlinear limitations (e.g. SPM-GVD, IXPM, IFWM). As already observed, the intra-channel or inter-pulse effects represent a relevant limitation in propagation with fast dispersing optical pulses, whose result is a strong interaction between the neighboring and distant pulses. The typical propagation regime in which intra-channel effects (e.g. IXPM) are dominant is so-called "pseudo-linear" [64] propagation regime, which is characterized by pulse widths smaller than 10 ps and a fiber chromatic dispersion larger than 2 ps/nm·km. Due to the small pulse widths in the pseudo-linear propagation regime,

it can be expected that modulation formats with a duty cycle smaller than 100% (e.g. all RZ-based formats) will suffer more from intra-channel effects. On the other hand, SPM, which can be understood as intra-pulse or single pulse limitation, and its interplay with GVD will represent a dominant transmission limitation in NRZ-based transmission lines. But, this does not mean that intra-channel effects can be neglected.
Considering only the SPM impact in the pre- or post-compensated dispersion map, it can be expected that post-compensated optical pulses disperse slower than pre-compensated ones, hence resulting in a larger SPM impact, whereas the pre-compensated pulses disperse faster, because of the induced pulse compression. But, if the GVD effects in DCF fibers are taken into account, a large amount of dispersion pre-compensation in DCF induces strong pattern dependent dispersive waveform distortions in pre-compensated pulses, which are launched in a transmission fiber after the amplification at the DCF output (see system setup in Fig. 5.1). The interactions of pre-compensation caused pulse distortions with fiber nonlinearities (e.g. SPM) in the effective length L_{eff} on the beginning of each span result in strong peak power fluctuations.
On the other hand, in the post-compensation case, optical pulses are launched undisturbed in the nonlinear region of the transmission fiber, and resulting propagation distortions can be better compensated in the following DCF [229]. The consequence of these effects is a poorer performance of pure pre-compensation in comparison to pure post-compensation. At the same time, a certain amount of pre-compensation, which can be differently implemented e.g. pre-chirp or like in this case by in-line pre-compensation, would improve the transmission performance due to the reduction of SPM. This behavior can be justified considering 40 Gb/s NRZ optical eyes for a post-, optimum and pre-compensation presented in Fig. 5.13.

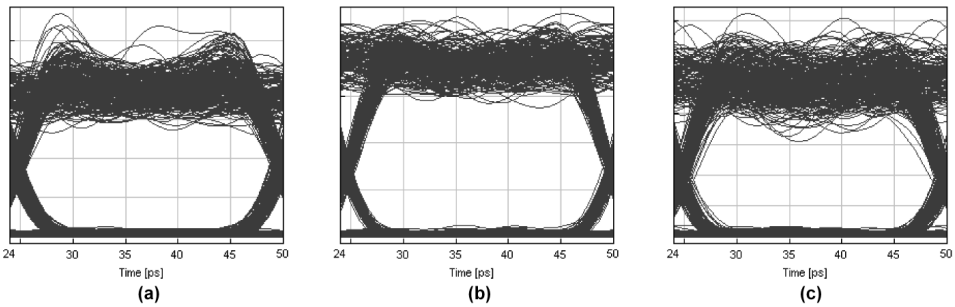

Figure 5.13: Dispersion scheme dependent NRZ eye distortions in 40 Gb/s transmission over 4x80 km SSMF with optimized P_{SMF} and P_{DCF} powers (power settings presented in Appendix D): a) post-compensation b) optimum compensation c) pre-compensation

The post-compensated signal eye shows a severe SPM-impact characterized by strong peak power fluctuations at the signal edges (Fig. 5.13a). The SPM impact can be effectively suppressed by certain amount of pre-compensation (≈20 %)(Fig. 5.13b) at the expense of signal peak power fluctuation over marks, thus showing a good agreement with recently presented investigations [232], [94], [233]. The peak power fluctuations become even larger when pure dispersion pre-compensation is implemented (Fig. 5.13c). Now looking back to Fig. 5.12, it can be observed that the optimum amount of pre-compensation varies for different modulations formats. If the signal generation for different NRZ-based formats is considered, it is obvious that the different modulation techniques induce different amount of pre-chirp during signal generation (e.g. alCNRZ). This transmitter internal chirp is responsible for shifting the optimum amount of pre-compensation for different formats and transmission fibers.
Considering the propagation effects over different fibers, it can be seen that for pure pre- or post-compensation all fibers show similar relations if optimized power settings are considered, where in all cases post-compensation represents a better solution. It can be expected that with an enhanced transmission distance the differences between dispersion schemes become even more evident according to a length dependent accumulation of nonlinear disturbances. With respect to the amount of pre-compensation, the differences occur due to varying amounts of resulting pre-chirp for different transmission fibers, which govern the significance of generated peak power fluctuations. For example, 10 % pre-compensation in NZDSF based line results in a lower effec-

tive signal pre-chirp than 10 % in SSMF case. Additionally, above a specific amount of pre-compensation (e.g. > 50%) the differences between different fibers vanish (Fig. 5.12) because of large amount of dispersion pre-compensation causing pattern dependent distortions of optical pulses, indicating that a deployment of new transmission fibers in transmission lines will enable some performance benefit only in specific system infrastructures.
Considering the propagation characteristics of different modulation formats, it can be concluded that novel modulation formats enable a performance improvement, which is dependent on the fiber infrastructure and amount of pre-compensation, and is especially significant if alPNRZ modulation is used (Fig. 5.12d). We showed experimentally in system with a reduced channel data rate (e.g. 10 Gb/s) [202] that polarization switched alPNRZ modulation enables an efficient SPM suppression and that the polarization orthogonality between adjacent pulses in a alPNRZ pulse stream is maintained even after long transmission distances (1500 km). With alCNRZ modulation, a slight performance improvement can be achieved compared to conventional NRZ transmission, but the amount of implemented phase modulation has to be carefully chosen in order to meet the characteristics of the transmission line, because of large spectral broadening induced by large phase modulation. A relatively small amount of phase modulation (1 rad) was considered for alCNRZ generation in the presented investigation, because a large phase modulation would reduce dispersion tolerance and may represent an issue for a realization of WDM and DWDM systems.

RZ-based modulation formats

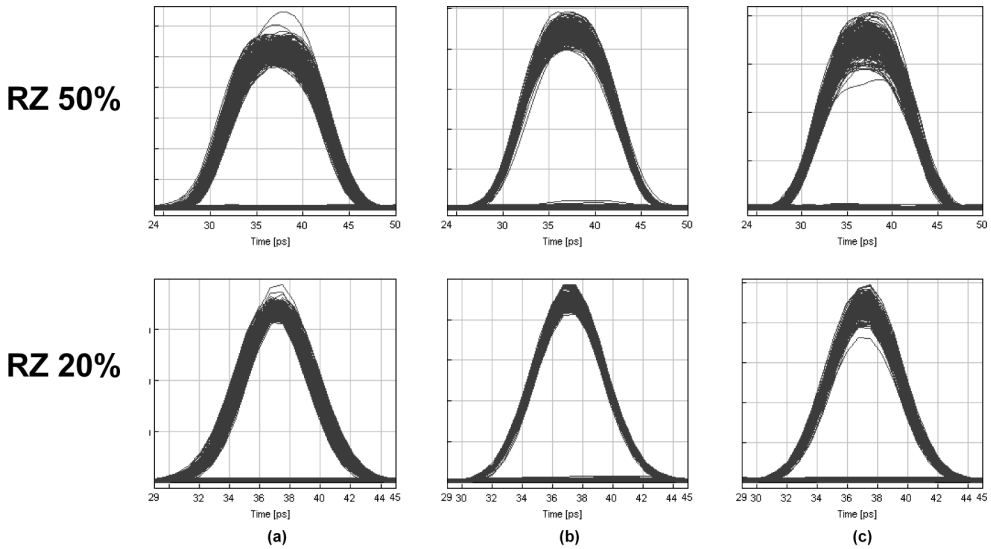

Figure 5.14: Dispersion scheme dependent eye distortions in 40 Gb/s transmission over 4x80 km SSMF with optimized P_{SMF} and P_{DCF} (power settings presented in Appendix D): a) post-compensation b) optimum compensation c) pre-compensation

Contrary to NRZ-based modulation formats where the SPM-GVD interplay represents the dominant propagation limitation, its impact is to some extent reduced in RZ-modulated transmission and it is masked by intra-channel effects. Contrary to SPM-GVD effect, which is characterized by a single pulse distortion, the intra-channel effects depend on the interactions between the fast dispersing pulses. Furthermore, intra-channel effects are pattern dependent [69], [125]. As already stated, IXPM occurs between neighboring pulses resulting in a slight amplitude jitter and strong timing jitter, whereas IFWM causes amplitude fluctuations in marks and ghost-pulse generation in spaces, and it is characterized by interaction of large number of consecutive pulses. The efficiency of intra-channel effects is governed by the local fiber dispersion and pulse power. Accordingly, the dependence of intra-channel effects on local dispersion changes in the transmission

line is crucial for the determination of the optimum dispersion compensation scheme. Before starting with the dispersion compensation analysis, it should be kept in mind that in a span-by-span dispersion compensation scheme, which were considered for the presented investigations, the regeneration (dispersion compensation) of pulse shape is performed after each span by DCFs, resulting in a reduced impact of IFWM [72].
For describing the interaction between the dispersion map and propagation effects, the conventional RZ-based transmission line is investigated with post-, optimum- and pre-compensation of accumulated dispersion. Figure 5.14 illustrates received optical eyes in different dispersion maps for two different duty cycles (τ=0.5, 0.2) considering moderate pulse power (P_{IN}=3 dBm). Starting with a transmission line without pre-compensation, strong interaction between neighboring pulses occur, thus giving rise to a timing jitter and slight amplitude jitter accompanied by a low SPM impact (Fig. 5.14a). The SPM impact would increase with an increased signal power [64]. Thereby, the SPM impact can be suppressed by the reduction of pulse width, but on the other hand the smaller pulse width gives rise to the pulse amplitude jitter (Fig. 5.14a bottom line). Implementation of some amount of pre-compensation (5-10 %) in the transmission line enables a pulse compression and reduces pulse overlaps in the nonlinear propagation regime, hence reducing the timing jitter disturbances, but certain amplitude fluctuations in the middle of the pulse remain (Fig. 5.14b). A further increase of pre-compensation accelerates pulse broadening on the beginning of each span with strong amplitude fluctuations as a consequence of nonlinear interaction between fast dispersing distant pulses (Fig. 5.14c). Accordingly, a certain amount of pre-compensation can be beneficial for the transmission performance, but a large amount of dispersion pre-compensation penalizes the performance. Typically, the amplitude fluctuations become even enhanced for a reduced pulse width (Fig. 5.14c bottom line), because the number of interacting pulses increases and intra-channel effects are not limited only on neighboring pulses. This indicates that the use of a reduced pulse width would make sense in a post-compensation scheme and in highly nonlinear regime (P_{SMF} >7 dBm) [229], because of the SPM dominance in these cases.

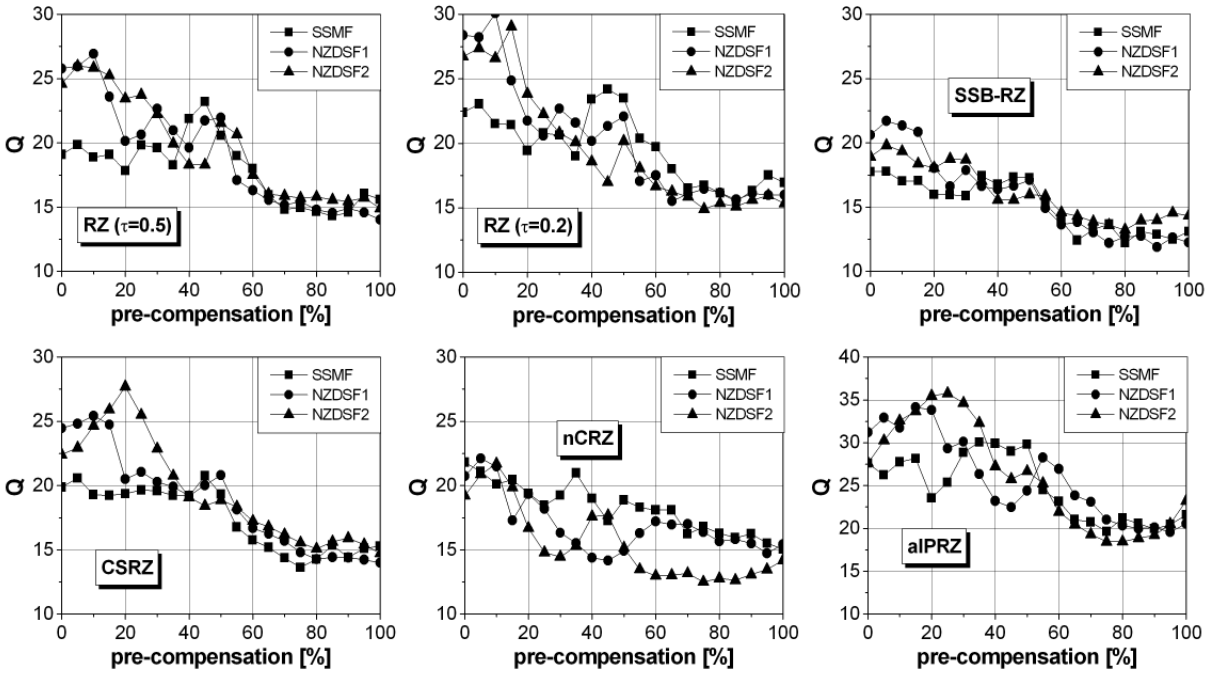

Figure 5.15: 40 Gb/s transmission over 4x80 km transmission line with optimized P_{SMF} and P_{DCF} for each amount of pre-compensation (linear Q_{ISI} evaluation, P_{SMF} and P_{DCF} settings presented in Appendix D)

Figure 5.15 illustrates the impact of the dispersion map on the transmission performance for RZ-based mod-

ulation formats and different fiber types. Considering conventional RZ formats - RZ, SSB-RZ and CSRZ - fiber dependent performance variations can be observed, where the optimum dispersion map is characterized by a certain amount of dispersion pre-compensation.
In SSMF-based transmission, all three formats show similar behaviour in a pure post-compensation and pre-compensation scheme. Here, post-compensation performs better than pre-compensation. Generally speaking, RZ and CSRZ outperform SSB-RZ in most of the investigated cases. As expected, the optimum amount of pre-compensation varies from format to format, because of different modulation features. An improvement of transmission performance can be achieved by use of NZDSF fibers, which need a smaller amount of pre-compensation compared to the SSMF case for an improved transmission performance. This can be explained by the fact that smaller local dispersion induces less pulse overlap in the nonlinear regime, resulting in a smaller needed amount of pre-compensation. A direct comparison between different fibers is rather complex, because transmission lines with different fibers have different OSNR characteristics according to different total system length and the optimized power settings differ from fiber to fiber (Table 5.5), showing that optimum power settings become reduced in NZDSF fibers according to their worse nonlinear characteristics compared to SSMF and a shorter total transmission length (Table 5.3). Nevertheless, for all fibers a large amount of dispersion pre-compensation significantly impacts total transmission performance (Fig. 5.15), inducing an overlap between distant pulses and thus giving rise to increased amplitude jitter because of an enhanced IFWM impact. Comparing transmission performances of conventional RZ formats with conventional and novel NRZ-based formats (Fig. 5.12), it can be observed that novel NRZ formats show even better transmission characteristics than conventional RZ formats, indicating novel NRZs as a potential candidates for the 40 Gb/s single channel transmissions due to their less complex signal generation compared to RZs. Considering the optimum amount of pre-compensation in NRZ- and RZ-based modulation formats, it can be observed that this amount is larger in NRZ formats than in RZs, because of strong SPM-caused limitations which profit from a larger pre-compensation [94] than intra-channel effects.

modulation format	amount of pre-compensation [%]		
	SSMF	NZDSF1	NZDSF2
NRZ	30	30	15
DUO	45	35	25
alCNRZ	45	30	10
alPNRZ	35	15	15
RZ	45	10	5
SSB-RZ	5	5	5
CSRZ	5	10	20
nCRZ	0	5	10
alPRZ	35	20	25

Table 5.4: Optimum dispersion compensation scheme in different transmission line infrastructures (40 Gb/s, 4x80 km transmission line, with ASE-noise)

The reduction of the pulse width in the RZ case enables a performance enhancement especially in case of low fiber dispersions and small amounts of pre-compensation (Fig. 5.15). Further improvement of RZ-based transmission could be enabled by implementation of phase modulation (nCRZ) and polarization switching (alPRZ) on RZ pulses. nCRZ provides a limited performance enhancement in specific dispersion maps (e.g. post-compensation) and specific fiber types (e.g. SSMF). It indicates poorer performance in NZDSF fibers according to large amount of phase modulation implemented on RZ signal in nCRZ transmitter (modulation index 1.12 rad), but a smaller amount of phase modulation could be beneficial for the suppression of intra-channel effects [234], [204], [235]. alPRZ shows the best transmission performance among all investigated modulation formats due to the suppression of nonlinear interactions between adjacent optical pulses by orthogonal polarization between them. The advantages of this modulation method lie in an efficient suppression of IXPM-caused timing jitter in RZ-based 40 Gb/s single channel transmissions [208], which was observed to be the dominant limitation.

Considering the optimum amount of pre-compensation in different fiber infrastructures (Table 5.5), it can be observed that it is reduced for all investigated modulation formats when the fiber local dispersion decreases. This behavior will be elaborated in the following sections. Analyzing the optimum amounts of pre-compensation for different RZ-based formats presented in Table 5.4 no clear trends can be observed comparing to NRZ-cases. This can be explained by intra-channel effects domination in RZ cases, whose suppression is dependent on the signal internal chirp implemented during signal generation and a dependence of intra-channel effects on the fiber local dispersion. According to different generation methods used for RZ-based formats, varying internal chirps are implemented.

5.5.3 40 Gb/s transmission performance with optimized system settings

After the optimum power settings (e.g. P_{DCF}) and optimum dispersion compensation scheme (e.g. amount of dispersion pre-compensation) are determined for various modulation formats, the obtained insights from previous investigations are used for the design of a 40 Gb/s single channel transmission line considering different fiber infrastructures. The total transmission distance equals 4x80 km and the input power into the transmission fiber was varied in a range of -10..10 dBm. For the comparison of transmission performances with different modulation formats, the optimum amount of pre-compensation and the optimum DCF input power are used (presented in Table 5.5). The P_{SMF} power is varied between -10..10 dBm. This way of investigating different modulations enables a fair comparison between them and gives a global overview of their transmission behavior.

	Fiber type					
modulation format	SSMF		NZDSF1		NZDSF2	
	P_{DCF} [dBm]	pre-comp. [%]	P_{DCF} [dBm]	pre-comp. [%]	P_{DCF} [dBm]	pre-comp. [%]
NRZ	-5	30	-5	30	-3	15
DUO	-4	45	-2	35	-3	15
alCNRZ	0	45	-4	30	-5	10
alPNRZ	0	35	-2	15	-2	15
RZ (50%)	1	45	-2	10	-4	5
RZ (20%)	2	45	0	10	0	15
SSB-RZ	-4	5	-2	5	-4	5
CSRZ	1	5	-4	10	-3	20
nCRZ	-3	0	-3	5	-4	10
alPRZ	1	35	-1	20	1	25

Table 5.5: Optimum dispersion compensation scheme and DCF power settings for 40 Gb/s single channel transmission over 4x80 km using various transmission fibers

NRZ-based modulation formats

Figure 5.16 illustrates transmission performances of all NRZ-based modulation formats over three different fiber infrastructures. The differences between the modulation formats are reflected in a different optimum power, maximum achievable transmission quality (Q-factor) and the dynamic range. It can be observed that the transmission performance varies for different transmission fibers. Up to an input power of 0 dBm, all modulation formats show almost identical characteristics. In this power region, the linear disturbances (ASE-noise and fiber dispersion) limit the system performance, whereas the nonlinear effects can be neglected. The nonlinear impairments become noticeable for an input power larger than 0 dBm. At the point where the linear and nonlinear impacts balance each other, the optimum power region characterized by maximum Q values occurs. Depending on the tolerance of the modulation format to nonlinear impacts, the optimum power value are shifted towards higher or lower powers for different modulation formats. If a position of the optimum power value is used as a comparison criteria between different modulation formats, it can be observed that in SSMF-based transmission NRZ, duobinary and alCNRZ show similar characteristics (just slight improvement in NRZ case), whereas alPNRZ enables a optimum power shift larger than 5 dB (Fig. 5.16) compared to other NRZ-based formats. But, the differences between nonlinear characteristics can be seen by looking at the optimum DCF power settings as well. Novel NRZ modulation formats tolerate increased P_{DCF} values in a SSMF-based transmission line (Table 5.5).
If the comparison between the modulation formats is made using the achievable dynamic range defined as a power tolerance for a Q-factor of 6, it can be seen that the duobinary modulation represents the worst case for SSMF-based transmission, thus implying the smallest maximum transmission distance among all NRZs.

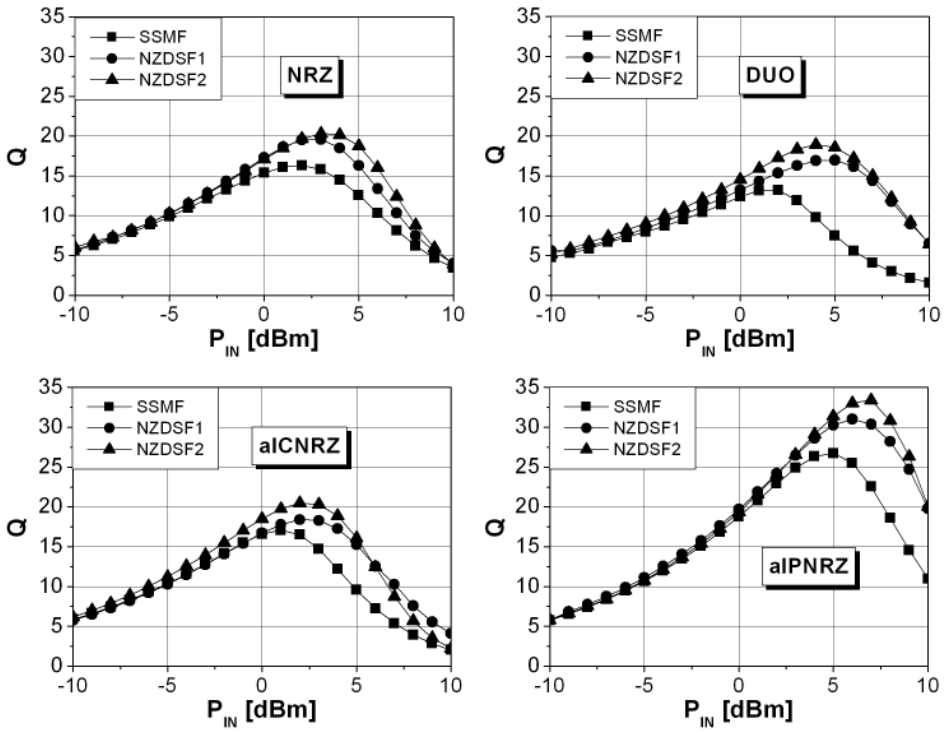

Figure 5.16: NRZ based formats 40 Gb/s transmission performance over 4x80 km with various fibers, optimized P_{DCF} power and optimized dispersion compensation scheme from Table 5.5 (linear Q_{ISI} evaluation, with ASE-noise)

The use of alPNRZ significantly improves the total performance in SSMF based transmission due to its good nonlinear tolerance already observed in previous investigations.
The implementation of NZDSF fiber in the transmission line results in two important performance changes: the dynamic ranges become wider and the optimum input power is enhanced for all modulation methods. This can be explained by the reduction of total DCF length in the transmission line for NZDSF1 and NZDSF2 (factor 2 and 4, respectively), resulting in a shorter total transmission length (compared to the SSMF case), enabling according to OSNR definition (Eq. 4.25) better transmission characteristics. The necessary amounts of pre-compensation are lowered for different modulation formats and the GVD-SPM impact is suppressed. The NRZ, duobinary and alCNRZ show again similar transmission behavior, whereas alPNRZ enables again a significant improvement of performance in NZDFS fibers.

RZ-based modulation formats

The results of investigations considering the total performance of the RZ-based modulation formats in single channel transmission over 4x80 km with different transmission fiber types are presented in Fig. 5.17. Compared to NRZ-based modulation formats, slight differences and performance improvements can be observed, but it can be expected that with an increased transmission distance the advantages of RZ modulation would become apparent. Up to an input power of 1 dBm, all RZ modulation formats show similar transmission characteristics. The optimum DCF input power values are larger than in the NRZ-based cases, hence confirming a better nonlinear tolerance of RZ-based 40 Gb/s transmission. The optimum dispersion pre-compensation values are smaller than in NRZ-based transmission, which can be explained by the strong intra-channel effects in RZ-cases.

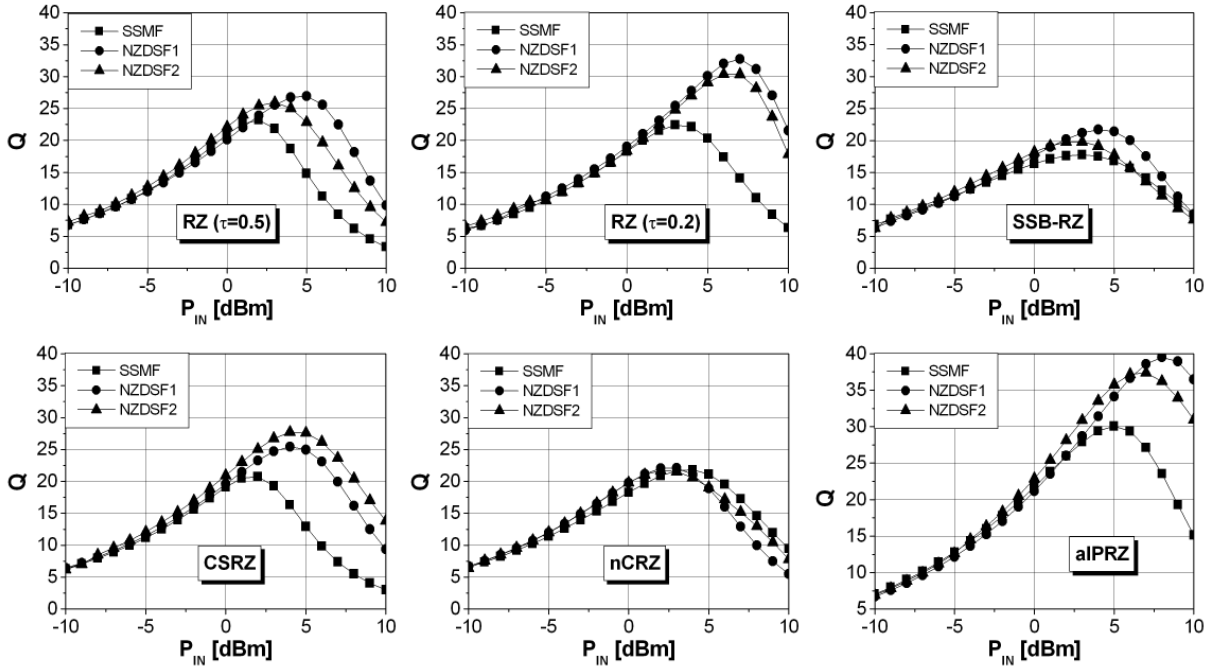

Figure 5.17: RZ based formats 40 Gb/s transmission performance over 4x80 km with various fibers, optimized P_{DCF} power and optimized dispersion compensation scheme from Table 5.5 (linear Q_{ISI} evaluation, with ASE-noise)

If a comparison is made between different RZ-based modulation formats, it can be observed that conventional RZ formats show worse transmission characteristics taking into account the optimum input power and width of dynamic ranges compared to other RZ modulation formats. Even if it can be expected that CSRZ shows better performance than conventional RZ modulation due to its good tolerance to intra-channel effects (especially IXPM) effects, the differences between these two formats are quite small. The origin for this behavior can be found in the fact that this comparison is made considering optimum system setting for both formats over relatively short distance. Contrary to SSB-RZ modulation, both RZ and CSRZ show larger P_{DCF} values (1 dBm). The width reduction of RZ pulses (Fig. 5.17) causes a shift of the optimum power point towards larger powers and broadens the dynamic range, due to a better nonlinear tolerance. The implementation of nCRZ and alPRZ modulation in the transmission line results in an improvement of system performance, independently on the fiber infrastructure. Furthermore, the optimum power values are enhanced (Fig. 5.17). Taking a look at the NZDSF-based transmission characteristics, an improvement can be observed regarding the optimum power settings and the dynamic range, which can be explained by the fact that transmission lines with strong intra-channel effects benefit from a low dispersive fibers.

The interesting point of this investigation is the very good behavior of RZ modulation employing ultra short pulse widths (Fig. 5.17b). In order to take a look at this behavior, RZ transmission characteristics are investigated considering optical pulses with different duty cycles. For simplicity, a pure dispersion post-compensation was considered over 4, 6, 8 and 16 transmission spans (span length 80 km) consisting of SSMF fiber. At the receiver side, an identical optical filter (Bessel filter 2nd order, B_{3dB}=160 GHz) is used for all investigated duty cycles. Its role was the separation of ASE-noise from signal. Three different power values - 0, 5 and 10 dBm - were considered, in order to indicate the region in which a reduced pulse width enables performance improvements.

The investigation results are presented in Fig. 5.18. Pulse propagation in low power regime (Fig. 5.18a) indicates that pulse width reduction does not cause any performance improvement, because of the strong impact

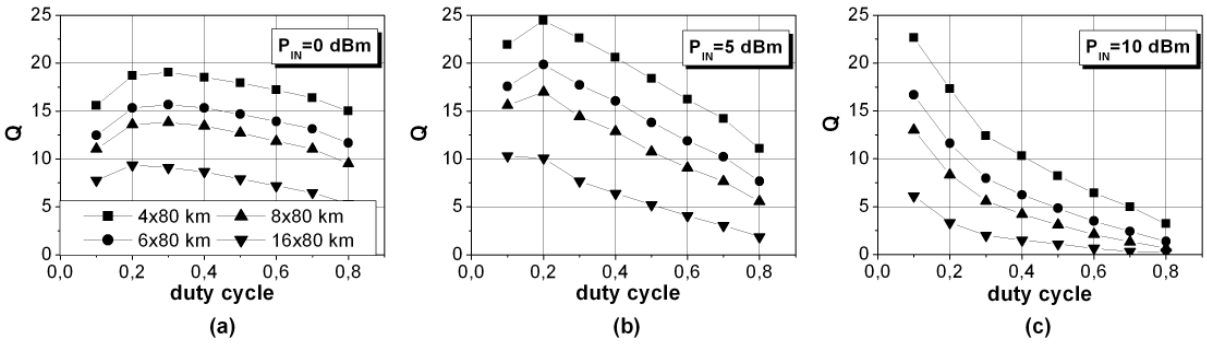

Figure 5.18: Impact of duty cycle reduction on the transmission performance for different input power (Q_{ISI} evaluation, with ASE-noise, 80 km SSMF based spans, full dispersion post-compensation scheme, P_{DCF}=-4 dBm)

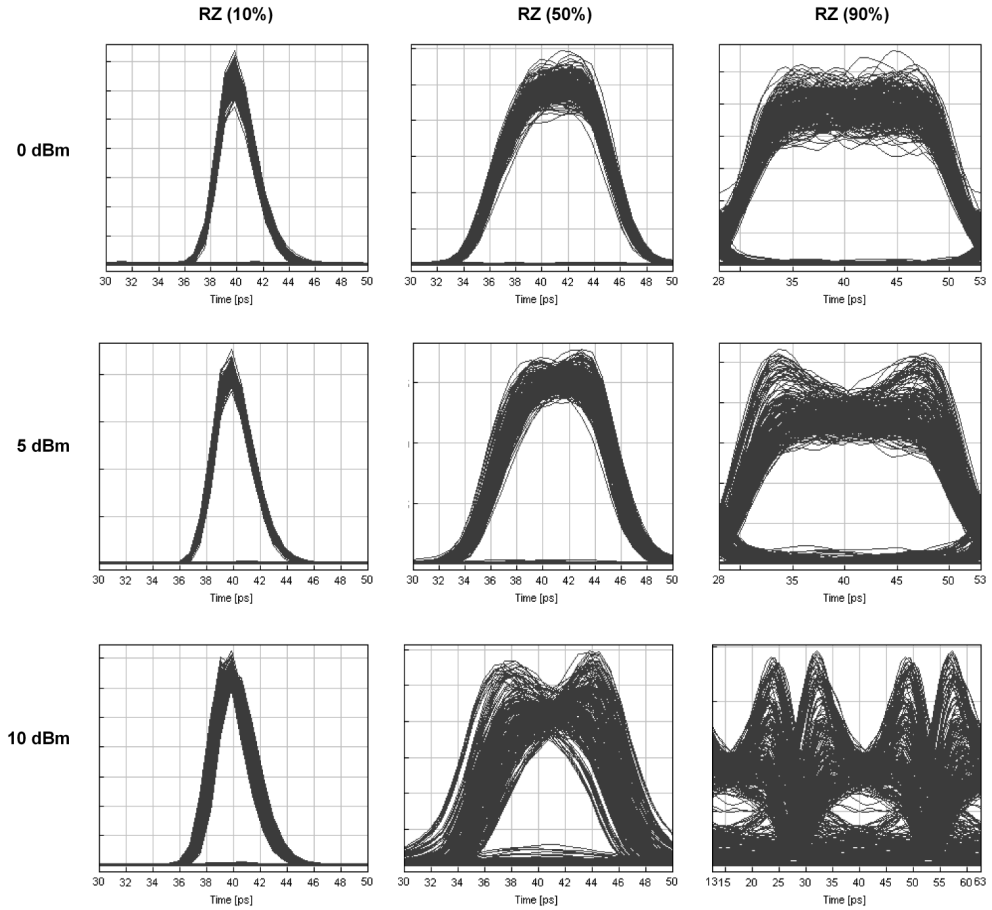

Figure 5.19: Detected signals with different duty cycle values (after 4x80 km SSMF, full dispersion post-compensation, with ASE-noise, P_{DCF}=-4 dBm)

of ASE-noise in this regime and negligible nonlinear impacts. This transmission behavior is maintained independently of the investigated total transmission length. Increasing signal power to 5 dBm (Fig. 5.18), the transmission behavior for different pulse widths is modified due to the fact that nonlinear limitations prevail and they are duty cycle dependent (Fig. 5.19). While on the one hand, pulses with a reduced width suffer from intra-channel nonlinearities (IXPM), broader pulses ($\tau > 0.5$) exhibit strong SPM-GVD impact (Fig. 5.19). Thus, the transmission in a moderate power regime would profit from a reduced pulse width. The pulse width reduction is even more important in the high nonlinear regime (P_{IN}=10 dBm)(Fig. 5.18c). In this case, the SPM-GVD impact becomes significant causing strong pulse distortions for large duty cycles (Fig. 5.19). In pulses with a reduced width, strong timing jitter disturbances occur according to the shift of the central pulse frequency because of inter-pulse interactions, which becomes enhanced at reduced pulse widths. The SPM-GVD impact is less critical for transmission performance due to faster pulse broadening. These results show a good agreement with recently presented experimental works [173], [172], and indicate performance improvement by the pulse width reduction as a case sensitive approach, showing significant improvement in particular for extremely large signal powers.
A detailed look on the total performance of NRZ- and RZ-based modulation formats (Fig. 5.16 and 5.17) indicates that for investigated transmission lengths, RZ formats show a transmission improvement in terms of nonlinear tolerance compared to conventional NRZ or duobinary modulation, but when comparing them to novel NRZ formats (primarily alPNRZ) the differences vanish. Furthermore, the novel RZ-based modulation formats (e.g. alPRZ) outperform all other formats enabling at costs of an increased complexity of signal generation, an performance improvement in 40 Gb/s single channel transmissions. The conclusion can be drawn that in 40 Gb/s single channel point-to-point transmission lines up to 400 km the NRZ based novel modulation formats represent a good solution from the technical and cost point of view, and that an implementation of RZ-based formats will not enable significant transmission improvements, but rather increase the system complexity.

5.6 40 Gb/s single channel long-haul (> 500 km) transmissions

After investigating transmission performance and determining optimized system settings in ASK-based 40 Gb/s single channel systems over short distances (<400 km), for a further system evolution, it would be important to characterize transmission behavior at increased transmission lengths (>500 km) for the estimation of the maximum system reach and the analysis of length dependent accumulation of transmission disturbances. In order to provide a more practically oriented investigation, it is necessary to consider the conventional transmission technologies already deployed in field, because it can be expected the system upgrade from lower (e.g. 2.5 or 10 Gb/s) to higher channel rates (e.g. 40 Gb/s) will be realized by the implementation of new components (e.g. transmitters and receivers) at the edges of the optical networks without deployment of new fibers or novel dispersion compensating devices. Accordingly, the long-haul investigation presented in this section is made considering SSMF based transmission line, whose dispersion is compensated with conventional DCFs implemented in simple dispersion compensation schemes (e.g. pre-, post- or hybrid compensation). The aim of this investigation was not the optimization of system settings for long-haul transmission, but investigation of transmission performance.
For the performance investigation in the long-haul case, two power ranges have to be considered, in order to enable a better insight into different system limitations. Focusing on dominant transmission line limitations, low DCF input powers (P_{DCF}=-4 dBm) were used for all investigated modulation formats, enabling a linear operation of DCFs. The ASE-noise impacts are considered and characterized by noise figures of implemented EDFAs, which equal 4 dB. The evaluation of results is made using receiver sensitivity penalty (RSP) criterion defined in Chapter 4:

$$\mathrm{RSP\,[dB]} = P_{Rx,trans}@(BER = 10^{-9}) - P_{Rx,BTB}@(BER = 10^{-9}) \tag{5.2}$$

considering the maximum allowable penalty value of 10 dB [236], [218].

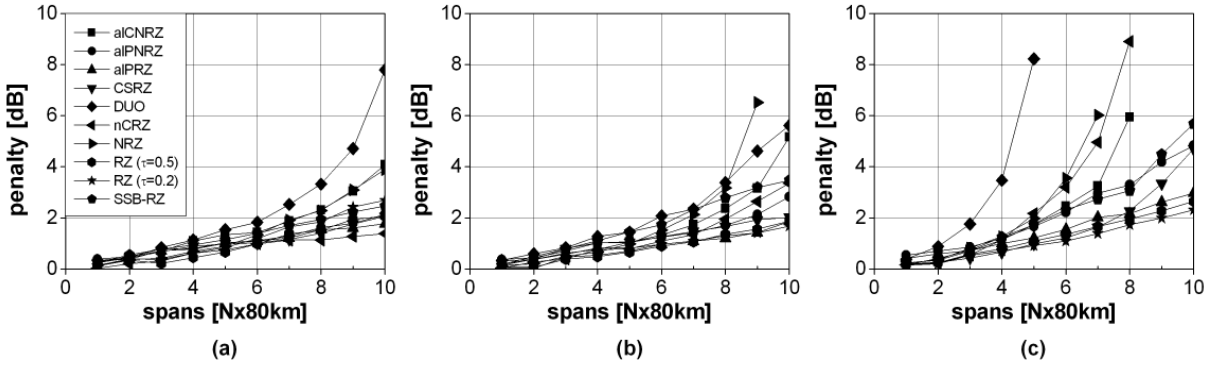

Figure 5.20: Long-haul 40 Gb/s transmission performance over cascaded SSMF spans (80 km) considering various dispersion compensation scheme (P_{IN}=0 dBm, with ASE-noise, P_{DCF}=-4 dBm): a) post- b) hybrid- c) pre-compensation

Figure 5.20 shows investigation results considering 40 Gb/s signal channel propagation in the low power regime (P_{IN}=0 dBm) with different dispersion compensation schemes. This power region is characterized by the impact of linear (e.g. ASE-noise, GVD) and nonlinear (e.g. SMP, IXPM) propagation limitations, whose interaction governs the achievable transmission distance.
If the accumulated dispersion is compensated with a DCF after the SSMF (post-compensation)(Fig. 5.20a) the differences between modulation formats can be neglected up to six spans (∼500 km) owing to the low signal power. With a further transmission distance enhancement, differences between NRZ- and RZ-based modulation formats become evident (Fig. 5.20a), but all considered modulation formats reach transmission distance of 10x80 km with a penalty less than 8 dB. This length dependent performance reduction can be explained by the accumulation of small single-channel disturbances (e.g. SPM, intra-channel effects) with

the transmission length [224], [237]. According to a full dispersion compensation in each span and identical span configurations, the nonlinear disturbances, which are rather small in a single span, accumulate with the distance and become superposed after each span.
Considering transmission behavior of NRZ-based modulation formats, it can be observed that duobinary modulation confirms its reduced transmission performance compared to conventional NRZ, which shows identical penalty values as alCNRZ with a modulation index of 1 rad. The performance of alCNRZ could be further improved, if a larger amount of phase modulation is implemented [199]. alPNRZ shows the best performance among all investigated NRZ-based formats and it even outperforms most RZ-based formats, hence justifying once more its significant transmission characteristics.
All RZ-based formats show relatively similar behavior in the post-compensated case (Fig. 5.20a), which is much better than in the NRZ-based transmissions. No difference can be observed between conventional and novel RZ formats.
The hybrid-compensation based transmission (Fig. 5.20b) shows no significant changes in the transmission behaviour compared to the post-compensation scheme, but a slight penalty increase can be observed, which is caused by larger pulse distortions due to a pulse compression before the transmission line.
The impact of the dispersion compensation scheme becomes evident first after a consideration of the pure pre-compensated transmission case (Fig. 5.20c), which, as expected from previous investigations, represents the worst case scenario especially for NRZ-based formats. Certain amount of pre-compensation can be beneficial for 40 Gb/s transmission up to some degree, but a large amount of pre-compensation limits the maximum transmission distance because of enhanced interactions between optical pulses, resulting in maximum transmission reach of 5-7 spans in case of conventional NRZ-based formats (Fig. 5.20c). The maximum transmission reach is defined as the maximum transmission length for a penalty value smaller than 10 dB. The novel NRZ-based formats (e.g. alCNRZ, alPNRZ) are less impacted by the accumulation of transmission disturbances because of special phase and polarization relations between consecutive pulses, enabling a slight performance improvement compared to conventional ones.
Again, the RZ-based formats remain less affected by the dispersion scheme changes, but certain penalty increase occurs using SSB-RZ and CSRZ pulses. nCRZ pulses indicate a sensitivity to an increase of dispersion pre-compensation, because of their internal chirp originating from nCRZ signal generation, resulting in a significant penalty enhancement after 6 spans. RZ pulses with a reduced duty cycle outperforms other formats showing almost identical performance as alPRZ (τ=0.5) pulses (Fig. 5.20c).

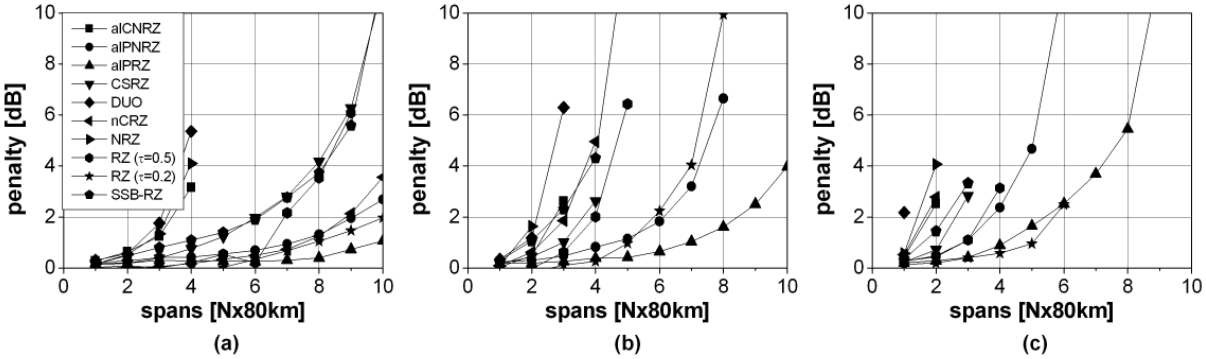

Figure 5.21: Long-haul 40 Gb/s transmission performance over cascaded SSMF spans (80 km) considering various dispersion compensation scheme (P_{IN}=6 dBm, with ASE-noise, P_{DCF}=-4 dBm): a) post- b) hybrid- c) pre-compensation

The classification between the investigated ASK-based modulation formats becomes more clear for a 40 Gb/s single channel propagation in a high power region (P_{IN}=6 dBm, Fig. 5.21) where the nonlinear disturbances prevail. According to achievable transmission performance in the post-compensation case (Fig. 5.21a), a clear separation can be made between three groups of formats: NRZ-based (NRZ, DUO, alCNRZ), RZ-based (RZ, CSRZ, SSB-RZ) and novel modulation formats (alPNRZ, alPRZ, nCRZ, RZ with reduced pulse width).

In all investigated dispersion schemes, the maximum transmission length of NRZ-based formats do not exceed 4 spans (Fig. 5.21). CSRZ and SSB-RZ show a better transmission performance than conventional RZ for the investigated fiber infrastructure over short distances, but for increased transmission distances the differences among these three formats vanish, thus showing a very good agreement with 40 Gb/s long-haul experimental works [238]. This effect can be explained by the accumulation of nonlinear disturbances and spectral changes during long-haul transmission, thus minimizing the differences between these three modulation techniques. In other dispersion schemes, these formats (RZ, CSRZ, SSB-RZ) reach similar maximum transmission distances (Fig. 5.21b,c), which do not exceed 5x10 km.
Despite of the fact that the aim of the development of novel modulation formats was an enhanced nonlinear robustness and increased transmission distance, not all newly proposed formats indicate a superior transmission behavior in comparison with conventional ones. Only modulation formats employing alternate polarization between adjacent pulse can enable a performance improvement independent of the dispersion compensation scheme in used. The RZ modulation with a reduced pulse width can to some extent compete with novel modulation formats.
An increase of dispersion pre-compensation in high power region makes the differences between NRZ- and RZ-based formats vanishing and results in a strong penalty enlargement for all investigated formats. The origin of this behavior can be found in increased pulse distortions caused by a large amount of dispersion pre-compensation and their interaction with large nonlinear impairments during the propagation in transmission fibers. The exception from this behavior can be observed for modulation formats with a significant nonlinear tolerances (e.g. alPNRZ, alPRZ, RZ with reduced pulse width).

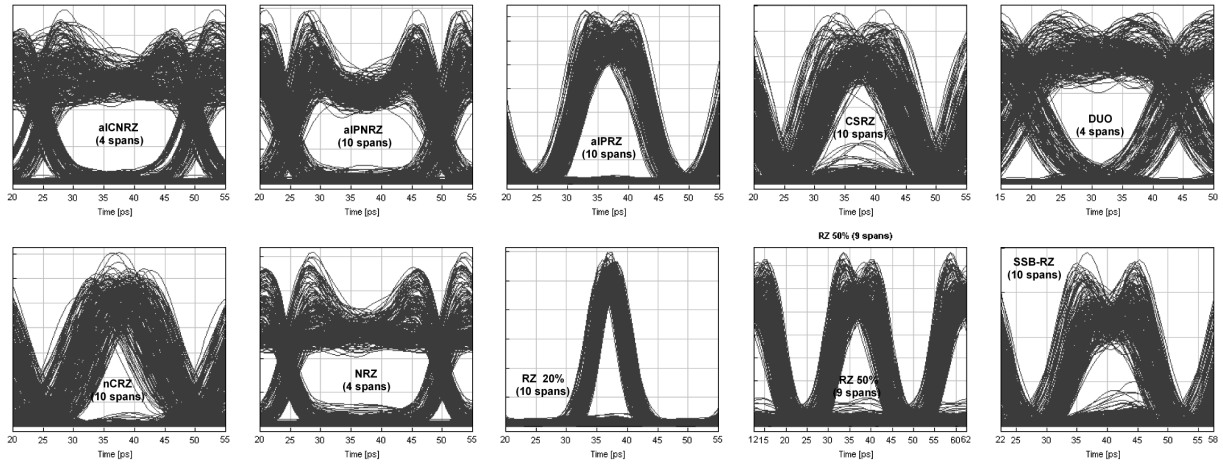

Figure 5.22: Detected 40 Gb/s optical signal eyes at maximal transmission reach (P_{IN}=6 dBm, with ASE-noise, P_{DCF}=-4 dBm, dispersion post-compensation)

In order to give a deeper insight into the limiting effects of long-haul nonlinear transmission, only the post-compensation scheme is considered due to its good transmission characteristics, investigating the typical signal degradations which occur in this case. Figure 5.22 depicts received 40 Gb/s optical signal eye diagrams for all ASK-based formats at the maximum penalty (maximum transmission distance) for different modulation formats, respectively.
Analyzing the presented signal eyes, it can be seen that in NRZ-based transmission over large distance strong timing jitter accompanied by an even stronger SPM-GVD effect is evident in form of significant signal level fluctuations at the signal edges (Fig. 5.22). In RZ-based cases, eye distortions can be characterized by a large amount of timing jitter, small amplitude jitter, and slight ghost pulse generation.
It can be concluded that the transmission behaviour is limited by three types of single channel limitations: SPM, IXPM and IFWM, whose impacts can be observed in the distortions of optical eyes. Depending on the

modulation format, strong amplitude fluctuations at pulse edges indicate SPM limitations and the generation of "ghost pulses" in spaces is caused majorly by IFWM impact [69], but the strongest eye impairments originate from timing jitter, which is a consequence of strong IXPM effects between the pulses (Fig. 5.22) for all investigated modulation formats , showing a good agreement with recently presented works [239], [72], [240]. These IXPM effects are caused by the periodical recovery of pulse shape from span to span because of the implemented span-by-span full dispersion compensation, resulting in a length dependent accumulation of IXPM. On the other hand, because of the periodical pulse regeneration, the nonlinear interactions are limited on neighboring pulses, resulting in a rather reduced IFWM impact (Fig. 5.22). If the accumulated dispersion in each span is not fully compensated (e.g. dispersion under-compensation), it can be expected that the IXPM impact would be less critical [72], [240].
For the characterization of the IXPM impact and a determination of methods for its suppression, the distribution of timing jitter is investigated over transmission distance (Fig. 5.23). Therein, the timing jitter is calculated as the standard deviation of pulse maximum from the middle of the time slot in all "010" bit triplets:

$$\sigma_{TJ} = \mathrm{std}\left(max(P_{peak})\right) \tag{5.3}$$

where P_{peak} represents the maximum pulse level of an isolated 1. Figure 5.23a depicts the timing jitter accumulation in a dispersion post-compensated 40 Gb/s transmission line. Considering the amount of timing jitter accumulated over distance, a clear separation can be made between NRZ- and RZ-based modulation formats, indicating better jitter tolerance of RZ-based formats, which can be interpreted by the faster broadening of RZ-based pulses, reducing the IXPM induced interaction between consecutive pulses. In NRZ case, the timing jitter is accompanied by strong SPM-GVD effects, which results in strong signal level fluctuations at pulse edges. It can be observed (Fig. 5.23a) that the timing jitter accumulation become critical only after certain transmission distance (>400 km). According to these results, the suppression of timing jitter could enable an improvement of transmission performance and reach for both NRZ- and RZ-based modulation formats.
An effective jitter suppression can be achieved by the implementation of a certain amount of pre-compensation at the transmitter side [74], [241]. This pre-compensation results in a pulse compression within the effective length L_{eff} of each span, hence reducing the pulse width in the nonlinear regime on the beginning of each span and enlarging the distance between the pulses in a pulse train, a consequence of which is a reduced interplay of adjacent pulses as well as a reduction of SPM-GVD interplay due to a faster pulse broadening. On the other hand, by the dispersion pre-compensation a sign change of the accumulated dispersion in the effective length L_{eff} occurs, which enables the intra-channel effects to partly reverse each other in both segments (with positive and negative accumulated dispersion) of L_{eff} [125].

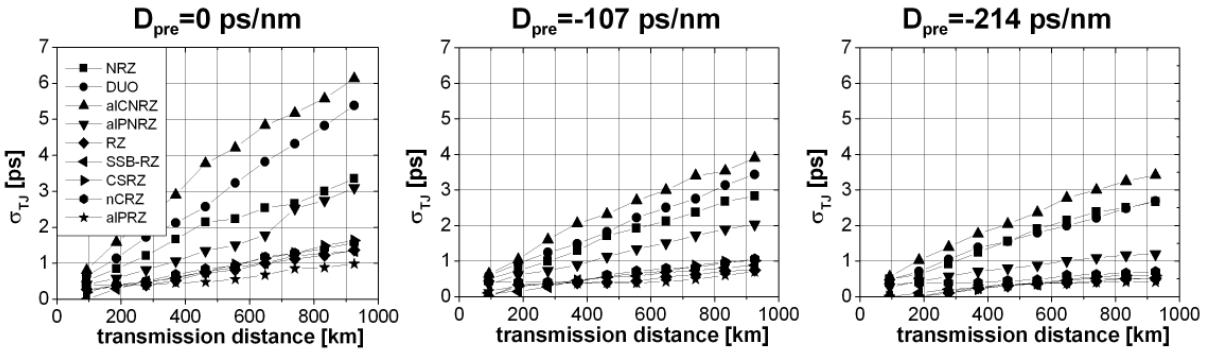

Figure 5.23: Timing jitter suppression in transmission line over Nx80 km SSMF by dispersion pre-compensation at the transmitter side (P_{IN}=6 dBm, P_{DCF}=-4 dBm, with ASE-noise, full dispersion post-compensation per span, residual dispersion compensation at the receiver)

According to the results presented in [74], the optimum amount of dispersion pre-compensation D_{pre} for an

efficient timing-jitter suppression can be calculated as:

$$\mathrm{D_{pre}} = \frac{-D_{SMF}}{\alpha} \ln\left(\frac{2}{1+e^{-\alpha L}}\right) \tag{5.4}$$

where D_{SMF} represents the dispersion and α the attenuation of the transmission fiber. This rule was derived for RZ modulated pulses and is valid for a full dispersion compensation per span. Typically, the optimum amount of pre-compensation depends on the modulation format [241] and it has to be carefully chosen, because its overestimation can be counterproductive to system performance [74], [242]. According to the rule presented in Eq. 7.1, the optimum $\mathrm{D_{pre}}$ value for investigated transmission line equals ≈-219 ps/nm.
In order to look over this, two different amounts of pre-compensation ($\mathrm{D_{pre}}$= -107, -214 ps/nm) were implemented by a piece of DCF fiber at the transmitter side in the investigated transmission line, enabling timing jitter suppression and hence performance improvement both for NRZ- and RZ-based modulation formats (Fig. 5.23b,c). The pre-compensation at the transmitter side provides a suppression of IXPM by governing the overlap between consecutive pulses [69]. The optimum dispersion pre-compensation enables pulses to barely overlap thus reducing IXPM-generation. A better transmission characteristic is observed using larger amount of $\mathrm{D_{pre}}$ (-214 ps/nm) showing a good agreement with Eq. 5.4, but further investigations showed that further increase of $\mathrm{D_{pre}}$ would not be beneficial for the transmission performance because of an IFWM enhancement [74] due to the over-compression of optical pulses and strong interactions between distant pulses.

5.7 Conclusion and outlook

The investigations of ASK-based modulation formats showed that the optimum format for 40 Gb/s transmission has to be robust to linear as well as to nonlinear transmission limitations. The investigations of different modulation formats considering various transmission aspects (e.g. dispersion tolerance evaluation, $\mathrm{P_{max}}$-rule, optimized power settings) indicated that regarding dispersion tolerance and complexity of signal generation, NRZ-based modulation formats basically are superior to RZ-based formats. NRZ formats suffer from a reduced power tolerance especially due to strong SPM-GVD interplay in short distance transmissions, which can be seen as the only weakness of this modulation method. A better transmission robustness in a high power region makes RZ-based formats becoming a better candidate for 40 Gb/s based long-haul transmission at the cost of complex signal generation and a reduced dispersion tolerance, which represents a critical issue in 40 Gb/s transmission with RZ shaped pulses. The performed optimum transmission fiber investigations showed that fibers with a reduced dispersion (e.g. NZDSFs) provide a better transmission performance in 40 Gb/s single channel transmission. This behavior is strongly dependent on the dispersion map implemented within the transmission spans. Considering practically relevant power ranges of -5..5 dBm (due to the EDFA characteristics e.g. ASE-noise and EDFA gain), fiber dispersion represents the most important fiber parameter governing the fast broadening of 40 Gb/s optical pulses and enabling a suppression of nonlinear impairments.
With dispersion compensation scheme investigations, the relation between propagation limitations and different fiber infrastructures was shown. Independently of the modulation format and fiber type, the optimum dispersion compensation can be achieved by a combination of a certain amount of dispersion pre-compensation, which can be realized by an in-line pre-compensation or pre-chirp by dispersion pre-compensation at the transmitter side. The implementation of an optimum amount of dispersion pre-compensation provides a suppression of SPM-GVD impact and timing jitter, which represents dominant system limitation in long-haul transmissions. This effect is evident both in NRZ- and RZ-based transmissions, which suffer from strong intra-channel limitations (e.g. IXPM) accompanied by SPM-GVD interplay especially in NRZ-based transmissions. The accumulated dispersion at the end of the transmission line has to be fully compensated independently on the modulation format due to reduced dispersion tolerance values at 40 Gb/s data rate, making a precise dispersion compensation and an active dispersion compensation at the receiver side necessary.
Comparing transmission performances of conventional and novel modulation formats, it has been shown that novel modulation formats enable a significant system improvement dependent on the specific transmission

infrastructure. The best transmission results in all investigated short and long-haul transmission cases are achieved with modulation formats employing polarization switching between adjacent bits (alPNRZ, alPRZ), due to their excellent nonlinear tolerance. Novel NRZ-based formats indicated a potential for closing the power tolerance gap between conventional NRZ and RZ modulation formats, providing significant enhancement of system performance achieved with relatively simple signal generation methods.
Summarizing the investigation results and lessons learned in this chapter, it can be said that optimized settings for 40 Gb/s single channel transmission can only be derived for a specific fiber infrastructure and specific maximum transmission distance. The comparison between different transmission infrastructures is rather complex and delivers not always a clear insight into important advantages and drawbacks, if multiple system parameters are considered.
In future works dealing with 40 Gb/s single channel transmission, the PMD impact on the transmission performance as well as its interplay with fiber nonlinearities has to be investigated, due to the fact that large PMD values in already deployed fibers can significantly reduce system performance especially in long haul transmissions.

6 40 Gb/s WDM and DWDM investigations

6.1 Overview

After investigation of 40 Gb/s single channel transmission characteristics and highlighting dominant system limitations, the next step into the direction of future transmission systems is made considering multi-channel 40 Gb/s systems employing the wavelength division multiplexing (WDM) technique. The numerical investigations taking into account various transmission aspects were performed in order to determine and describe the capacity upgrade mechanisms which could enable a better utilization of the available system bandwidth. It is distinguished between WDM systems with a spectral efficiency smaller or equal than 0.4 bit/s/Hz, and dense WDM (DWDM) systems employing spectral efficiency larger than 0.4 bit/s/Hz. Since at the start of the works presented here, the realization of 40 Gb/s DWDM systems was not sufficiently investigated by means of theoretical or experimental investigations, the design rules for spectrally efficient 40 Gb/s DWDM systems are developed and presented in this work.
As representatives for WDM and DWDM systems, transmission systems with channel spacings of 100 and 50 GHz have been investigated, corresponding to a spectral efficiency of 0.4 and 0.8 bit/s/Hz, respectively in the 40 Gb/s case. The investigations presented in this chapter are made considering parameters of already available system components for intensity modulated direct detection systems. In order to concentrate on transmission effects and characterize system behavior, the investigated transmission lines do not contain any sophisticated technologies, e.g. super FEC codes or orthogonal polarization between adjacent channels. The investigations were started with an optimization of filter settings of optical filters deployed in multiplexers and demultiplexers, which turn out to be an important issue for the DWDM system realization. After determination of optimum span lengths (amplifier spacings) for 4x40 Gb/s based WDM/DWDM systems, power investigations were performed, which enable identification of optimum power settings in transmission and dispersion compensating fibers. Using optimized parameters, the interaction between implemented dispersion maps per span and transmission effects is analyzed, drawing conclusions for optimum dispersion compensation schemes both at 100 and 50 GHz channel spacing. The attained insights are used for the investigation of system total performance in WDM and DWDM cases over short distances (up to 4x80 km). All works presented are conducted considering different ASK-based modulation formats, for enabling a fair comparison between them and identify advantages and drawbacks for each format. Contrary to the previous chapter, investigated modulation formats are divided into three groups: NRZ-based, RZ-based and novel modulation formats in order to stress their different linear and nonlinear propagation characteristics. The 40 Gb/s multi-channel works are completed by long-haul investigations with transmission distances up to 10x80 km, whose target was the determination of length dependent performance changes and accumulation of transmission disturbances in multi-span systems.

6.2 Investigated system setups

According to the aim of this work to investigate transmission performance of 40 Gb/s based transmission lines and the system upgrade from single channel to WDM and DWDM transmission systems, the system infrastructure used for investigations presented in this chapter is similar to the setups used for single channel investigations (Chapter 5). For both WDM and DWDM investigations, an identical transmission line infrastructure is used (Fig. 6.1). The differences occur at the system edges i.e. the transmitter and receiver side, where multiple channels are multiplexed and demultiplexed. A typical system setup is depicted in Fig. 6.1. The WDM channels are symmetrically arranged around a central wavelength of 1550 nm, and are modeled using different bit sequences with a length of 2^9 bits (see Appendix C). At the transmitter side, all channels are multiplexed by a MUX filter. The optimization of MUX filter bandwidths was performed in order to determine optimum filter settings for different channel spacings. The filtering losses of the MUX are compen-

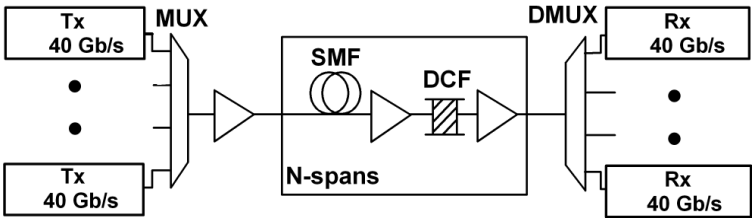

Figure 6.1: 4x40 Gb/s system setup used for the system optimization

sated using an EDFA-based optical booster before the transmission line. The investigated transmission line consists of identical spans employing transmission single-mode fibers and DCFs. The linear and nonlinear parameters in the transmission fibers were varied in order to identify optimum parameter combinations.
As in the single channel case, the accumulated dispersion is fully compensated on a span-by-span basis. Besides pure post-compensation (Fig. 6.1), further dispersion compensation schemes are considered. The investigations are made over different transmission distances, e.g. 2, 4 and 10 spans. After transmission, WDM channels are demultiplexed and detected with a conventional 40 Gb/s NRZ-based receiver. For the investigations presented in this chapter, 40 Gb/s WDM/DWDM systems are considered. This number of channels enables an investigation of the most important inter-channel effects, e.g. XPM and FWM. The SRS effect is considered in the transmission line, but due to the reduced number of channels and the small system total bandwidth, it can be neglected. The performance evaluation is done considering one of the middle channels as a worst-case channel, which is affected by strong multi-channel nonlinear limitations (e.g. XPM, FWM). Different evaluation criteria were used, e.g. Q-factor, EOP, and dynamic range, in order to give an insight into transmission limitations and enable a comparison between various evaluation criteria. For the investigations presented here, it was assumed that all channels are copolarized.

6.3 Optimized optical filtering in WDM and DWDM systems

The right choice of the optical filter type used for multiplexing and demultiplexing in 40 Gb/s based WDM transmission systems is crucial, especially in systems with an increased spectral efficiency [179], [176]. Narrow band filtering has to be employed both at the transmitter and receiver side for a reduced channel spacing (<100 GHz). As stated in Chapter 2, narrow-band filters with sharp filter edges and a flat pass-band characteristics represent the optimum solution for enabling DWDM transmission systems. Such filters are already commercially available for channel spacings of 100 and 50 GHz [243], [244], [245]. For the numerical investigations presented here, the characteristics of flat-top filters are emulated using Gaussian filters of higher filter order ($n \geq 2$) known as super Gaussian filters. The frequency response of super Gaussian filters is defined as:

$$T(f) = \exp\left(-\ln\sqrt{2}\left(\frac{2(f-f_c)}{\Delta f_{3dB}}\right)^{2n}\right) \tag{6.1}$$

where f_c is the filter central frequency, n defines the order of the filter, and Δf_{3dB} represents the 3-dB optical bandwidth of the filter. The filter responses of super Gaussian filters are presented in Fig. 6.2a. It depicts the filter characteristics for different filter orders (n=2,3,4), showing that an increased filter order results in an increased steepness of filter edges. The realization of optical filters with steeper edges could represent a difficult issue, due to the more complex definition of filter parameters and filter phase delay characteristics [246], [21].
For the investigations presented here, 2nd order super Gaussian filters (n=2 in Eq. 6.1) were used without consideration of their phase characteristics (e.g. filter dispersion, phase delay). These filters very well match the filter characteristics of conventional "flat-top" array wave-guide grating (AWG) based filters, which can be practically used as MUX and DMUX (Fig. 6.2a). For numerical realization, MUX and DMUX consist of several super Gaussian filters.

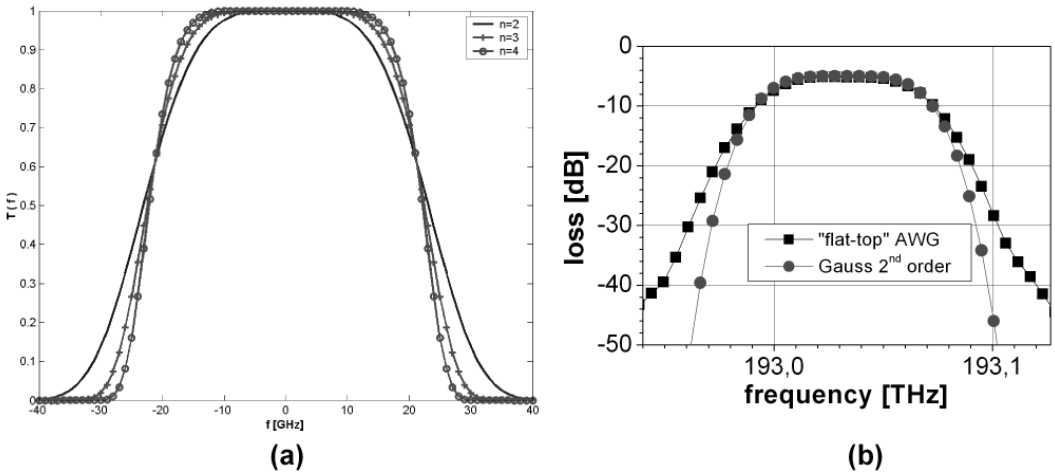

Figure 6.2: Filter characteristics of super Gaussian filters: a) effects of increased filter order b) comparison with commercially available filter (source: Infineon Technologies AG)

After choosing a right filter type, it is necessary, especially for DWDM transmissions, to optimize the filter optical bandwidth (f_{3dB}). The MUX and DMUX bandwidths per channel have to be adjusted and optimum bandwidth ranges have to be determined for the realization of DWDM systems with a spectral efficiency higher than 0.4 bit/s/Hz. The filter bandwidth optimization is done considering back-to-back transmission and different modulation formats for channel spacings (grids) of 100 and 50 GHz, respectively, because these values are already standardized representing the following steps in WDM system evolution. In both cases, a symmetrical optical filtering is employed, meaning that the central filter frequency match the carrier frequency of the channel. It must be stated that the implementation of a MUX at the transmitter side for 100 GHz channel spacing is not essentially needed independent of the modulation format, because the channels can be multiplexed with conventional couplers without filtering capability, but in order to enable a better comparison between WDM and DWDM systems, and to highlight some system upgrade aspects, e.g. use of already deployed infrastructure, the WDM systems are considered with a MUX at the transmitter side. Furthermore, it must be stated that the electrical filtering in receivers becomes important at a reduced channel spacing [179], but due to the fact that implemented electrical filter bandwidth is quite large (28 GHz) it causes no additional penalty.

6.3.1 NRZ-based modulation formats

NRZ-based modulation formats - NRZ and duobinary modulation - are characterized by narrow signal spectra, resulting in better narrow-band filtering characteristics. The filter bandwidth optimization for 100 and 50 GHz channel spacing considering a 40 Gb/s back-to-back system are presented in Fig. 6.3. For a large channel spacing, the MUX and DMUX filter settings indicate similar optimum bandwidths (Table 6.4). In this case, the filtering losses in the MUX and DMUX occur for filter bandwidths smaller than 60 GHz due to the fact that narrower filters suppress spectral components of the optical spectrum. According to the good Q values for the 100 GHz grid, it can be concluded that there is no need for MUXs filter at the transmitter side.
Reducing channel spacing to 50 GHz, it can be observed that large filtering losses occur and optimum settings differ for MUXs and DMUXs (Fig. 6.3b). The MUX has to be used in 50 GHz based systems at the transmitter side in order to improve spectral separation between adjacent channels. This happens at the costs of filter induced losses. Both conventional NRZ-based modulation formats indicate better filter detuning tolerance in the MUX than in the DMUX due to a broader optimum filtering ranges for MUXs. As the optical spectrum of the duobinary signal is narrower (spectral width ≈30 GHz) than in the NRZ case, the obtained maximum

Q values are better in the duobinary case. For both modulation formats, optimum DMUX bandwidths are in a region between 40..50 GHz (Table 6.5). As a consequence of narrow-band filtering at 50 GHz, strong inter-symbol interferences occur between adjacent bits. The 40 Gb/s optical duobinary and NRZ signal eyes at 50 GHz channel spacing presented in Fig. 6.3c confirm this. Strong pulse distortions can be observed for both modulation formats, resulting in increased amplitude fluctuations in the marks. Due to a reduced spectral width, the disturbances are less critical in duobinary case.

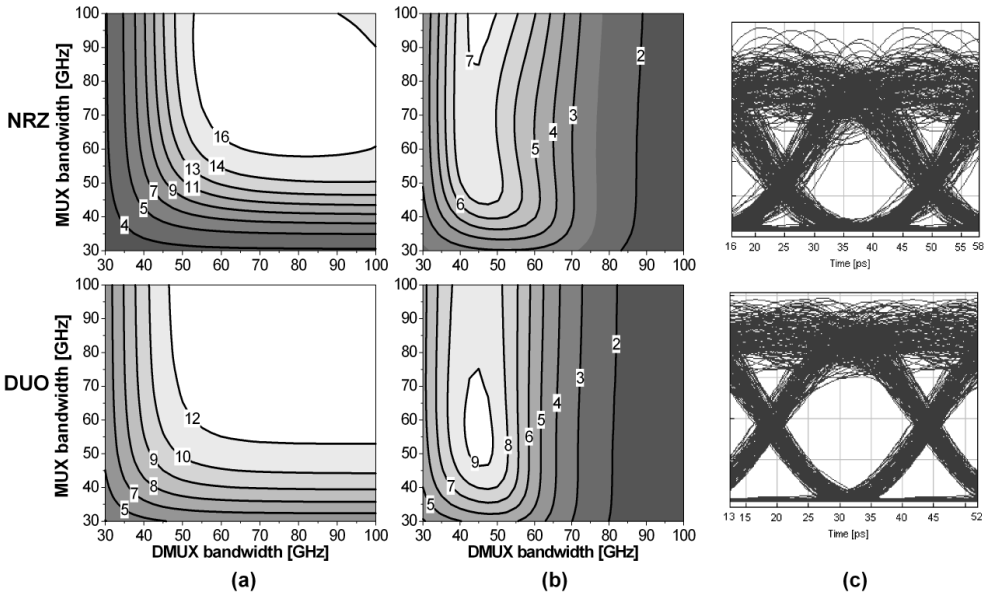

Figure 6.3: NRZ-based modulation formats 4x40 Gb/s - optimized MUX and DMUX filter settings in back-to-back case (linear Q_{ISI} evaluation, P_{IN}=0 dBm/ch): a) 100 GHz channel spacing b) 50 GHz channel spacing c) optical signal eyes at 50 GHz grid with optimum filter settings

Further investigations were performed for 50 GHz channel spacing in order to investigate possible changes of optimum filter settings when transmission line effects (e.g. GVD, Kerr effects) are considered [176]. It was shown that optimum filter settings in the MUX and DMUX are independent of the transmission effects and are maintained even for an increased transmission length.

Modulation format	MUX [GHz]	DMUX [GHz]	Q_{ISI}
alCNRZ	100	70	17
alPNRZ	87.5	55	18.4
alPRZ	80	70	19.4
CSRZ	100	87.5	16.9
DUO	100	75	12.9
nCRZ	85	80	17.7
NRZ	82.5	65	17.2
RZ	100	77.5	16.1
SSB-RZ	80	77.5	14.4

Figure 6.4: Optimum filter settings (super Gauss filter 2nd order) 4x40 Gb/s, channel spacing 100 GHz, back-to-back case, P_{IN}=0 dBm/ch

Modulation format	MUX [GHz]	DMUX [GHz]	Q_{ISI}
alCNRZ	50	45	6.2
alPNRZ	92.5	40	13.3
alPRZ	40	37.5	10.9
CSRZ	47.5	37.5	5.5
DUO	55	45	9.3
nCRZ	42.5	35	9.3
NRZ	100	45	7.5
RZ	42.5	42.5	8.3
SSB-RZ	42.5	42.5	7.1

Figure 6.5: Optimum filter settings (super Gauss filter 2nd order) 4x40 Gb/s, channel spacing 50 GHz, back-to-back case, P_{IN}=0 dBm/ch

6.3.2 RZ-based modulation formats

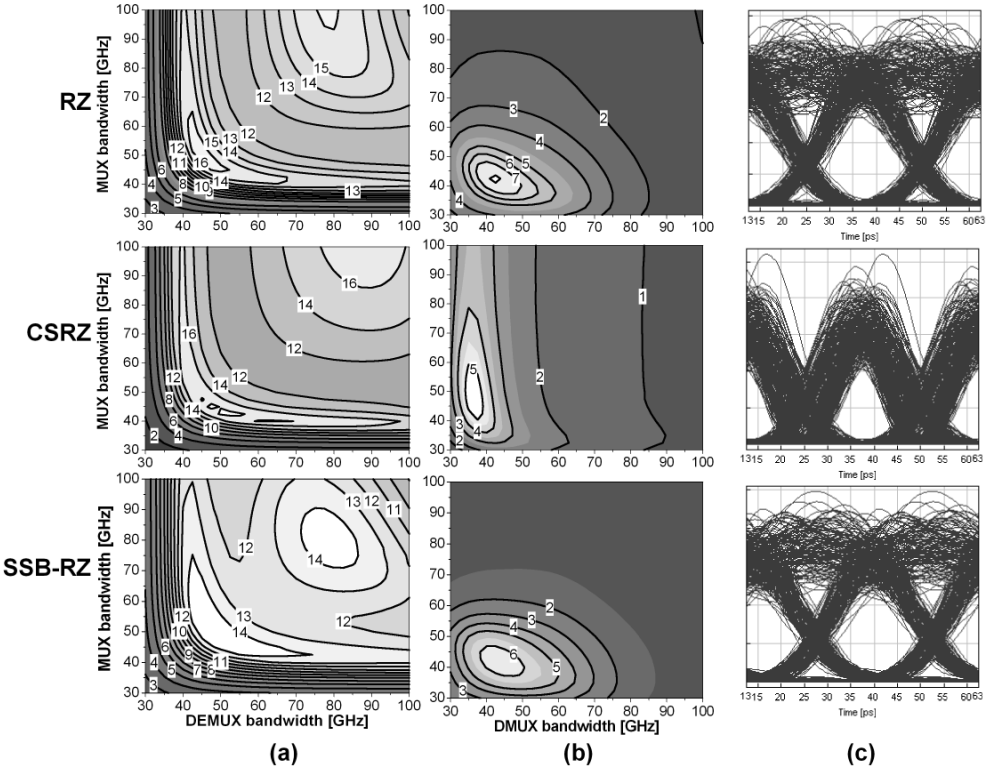

Figure 6.6: RZ-based formats 4x40 Gb/s - optimized MUX and DMUX filter settings in back-to-back case (linear Q_{ISI} evaluation, P_{IN}=0 dBm/ch): a) 100 GHz channel spacing b) 50 GHz channel spacing c) optical eyes at 50 GHz grid with optimum filter settings

Optical filtering in RZ-based modulation formats represents a more critical issue than in the NRZ case due to the broader signal spectra, making an employment of RZ-based formats in 40 Gb/s based DWDM systems difficult. For this investigation, RZ pulses with a duty ratio of τ=0.5 were considered, representing a good compromise between the pulse shape and spectral width. Considering 100 GHz channel spacing, optimum filter settings differ slightly from NRZ-based modulation formats (Fig. 6.6a). In all investigated cases, two optimum filtering regions can be observed. For a larger filter bandwidth in the MUX the RZ pulse shape is maintained and for the narrower filter bandwidth the RZ pulse shape is distorted, so that in this region the pulses have a NRZ shape. As the optimum filter settings at 100 GHz channel spacing the larger bandwidths (Fig. 6.6) are used (Table 6.4). Comparing filtering characteristics of RZ, CSRZ and SSB-RZ, it can be observed that a key for better performance in all cases is signal bandwidth. Hence, RZ shows slightly worse Q values than CSRZ, and SSB-RZ represents the worst case among the three. This SSB-RZ behavior can be clarified by the fact that the optical filtering is done using the carrier frequency as the filter center frequency f_c, which is critical because one side band of SSB-RZ spectrum is already suppressed during the signal generation. Further investigations indicated that by setting the filter central frequency between the carrier and the remaining side band in the SSB-RZ spectrum, improved filtering characteristics can be enabled especially for a reduced channel spacing. All three modulation formats show similar optimum filter settings at 100 GHz grid (Table 6.4).
In the case of a reduced channel spacing (50 GHz), the filtering drawbacks of RZ-based formats become visible. Compared to 100 GHz spaced channels, the bandwidth ranges for optimum filter settings significantly shrink, indicating a reduced detuning tolerance of RZ-based formats (Fig. 6.6b) and strong filtering

losses due to narrow-band filtering. The increased importance of MUX functionality is evident according to the larger RZ spectral width. RZ and SSB-RZ formats have identical optimum filter settings (Table 6.5), whereas CSRZ shows strong deviations compared to them. The consequence of narrow-filtering in RZ pulses is a broadening of the pulse width. Hence, due to an extreme narrow optical filtering, the differences between NRZ- and RZ-based formats vanish. Optical eyes of RZ-based modulation formats considering optimum filter settings for 50 GHz grid indicate, as long as RZ and SSB-RZ pulses are considered (Fig. 6.6c), less difference to NRZ-based eyes (Fig. 6.3c). On the other hand, CSRZ modulated pulses retain their RZ shape, but suffer from large pulse interferences at the pulse edges. In the CSRZ case, the RZ pulse shape is maintained, because of phase relations between adjacent bits, which counteracts the narrow-band filtering impacts. The effect of narrow-band filtering in the MUX on CSRZ pulses is illustrated in Fig. 6.7. Comparing it with ideal CSRZ pulses (Fig. 3.9), it can be observed that the phase relations between adjacent bits are distorted and strong amplitude variations occur.
Although the CSRZ pulses (Fig. 6.6c) show strong disturbances after the DMUX, the clear decision can be made between marks and spaces. At this point, it must be stated that CSRZ signals used for this investigation are generated using an ideal second MZM modulator, known as a carver. Comparing filtering characteristics of CSRZ presented here with experimental data in [183], [18], deviations between the results can be observed. Even more, experimental works indicate CSRZ modulation as the RZ-based format with best filtering characteristics.
Although the exact comparison between experimental and numerical results could not be made, because of use of different signal generation methods, e.g. OTDM, infrastructural differences or orthogonal polarized channels, the deviations between theory and experiments for a carver based CSRZ generation can be explained by the fact that in an experimental setup the ideal generation of CSRZ pulses is a difficult issue due to synchronization problems (e.g. drive amplitude imbalance, drive phase error) between the modulator (MZM) drivers in both modulation stages and component imperfections (e.g. internal chirp, extinction ratio) of the MZM. These effects result in an additional phase modulation of CSRZ pulses in experiments, making them more robust to narrow band filtering [182], and improving their performance characteristics by a pre-chirp at the transmitter side. The impact of carver imperfections also represents a problem during the generation of PSK-based modulation formats as well, e.g. DPSK. Reference [247] gives a good overview of these effects. On the other hand, if 40 Gb/s RZ-based modulation formats are generated and detected using OTDM technique, it is shown [248] that all investigated modulation formats show almost identical filtering characteristics. This can be explained by the fact that an OTDM receiver possesses inherently pulse-reshaping capabilities during the demultiplexing process. Furthermore, employing some unconventional filtering techniques e.g. asymmetrical filtering [181], [183] or vestigial filtering [9], the filtering characteristics of CSRZ and SSB-RZ formats can be improved.

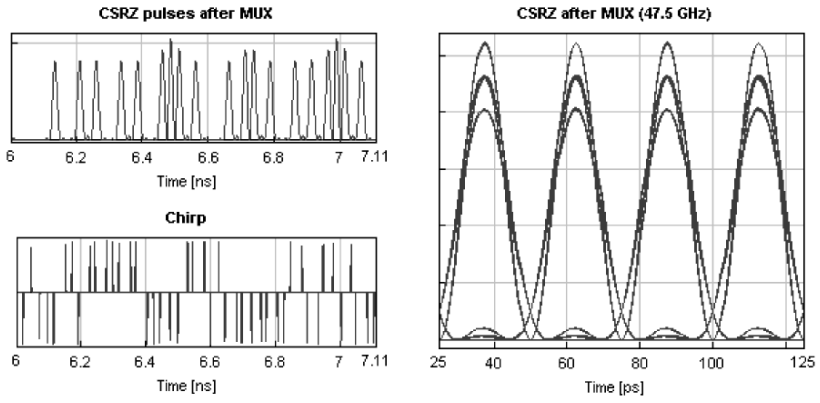

Figure 6.7: CSRZ pulse distortions after narrow-band filtering in MUX (B_{3dB}=47.5 GHz)

The presented optimization of filter bandwidths of RZ-based modulation formats in 40 Gb/s WDM and DWDM systems indicates the weak points of these formats for the realization of DWDMs and it is to show

in this thesis if these weaknesses can be compensated by a good nonlinear tolerance of RZ-based formats, because according to the presented results, it could be expected that as long as the DWDM systems with 50 GHz channel spacing are considered, propagation differences between NRZ- and RZ-based modulation formats vanish.

6.3.3 Novel modulation formats

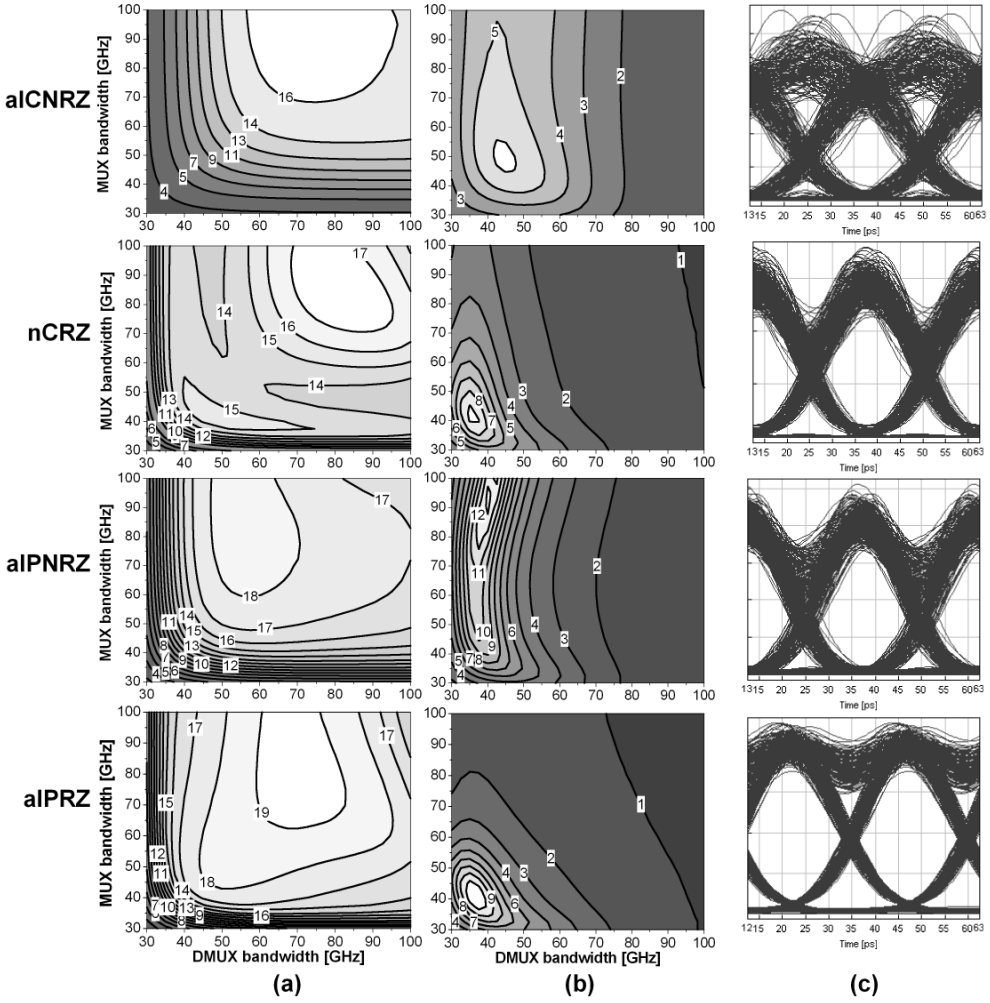

Figure 6.8: Novel modulation formats 4x40 Gb/s - optimized MUX and DMUX filter settings in back-to-back case (linear Q_{ISI} evaluation, P_{IN}= 0 dBm/ch): a) 100 GHz channel spacing b) 50 GHz channel spacing c) optical eyes at 50 GHz grid with optimum filter setting

Recapitulating the signal generation of novel modulation formats presented in Chapter 3, the improvement of transmission characteristics of conventional NRZ- and RZ-based modulation formats can be achieved by employing phase modulation (e.g. in alCNRZ modulation index m=2 rad, in nCRZ m=1.15 rad) or polarization switching between consecutive pulses (e.g. in alPNRZ, alPRZ). Accordingly, different amounts of phase modulation implemented in each of these formats result in varying characteristics and robustness to narrow-band filtering. Contrary to single channel investigations, where transmission performance profits from a larger amount of phase modulation, the right amount of phase modulation in WDM and DWDM

systems represents the trade-off between filtering and transmission characteristics. Hence, due to additional modulation the spectra of novel modulation formats possess spectral widths in the range between NRZ- and RZ-based formats.
Determining optimum filter settings of novel modulation formats for 100 GHz channel spacings (Fig. 6.8), it can be observed that all novel modulation formats show similar optimum settings. The differences between novel and conventional modulation formats become clearly visible at a reduced channel spacing (50 GHz). As expected, novel modulation formats (alPRZ, nCRZ) derived from RZ-based formats indicate reduced tolerance to filter detuning and increased filtering losses. Due to narrow-band filtering, the RZ pulse shape gets lost in the alPRZ case (Fig. 6.8c), but this reshaping effect is significantly less in nCRZ modulated pulses, because of the spectral compactness of this modulation format (Fig. 3.19). The reasons for this are compact spectral form and small amount of alternating phase modulation (m=1.15 rad) implemented between adjacent bits in nCRZ pulse stream. alPNRZ shows a larger tolerance to filter detuning due to a reduced spectral width and the filter bandwidth in MUXs is less critical for the back-to-back performance, whereby alCNRZ indicates the worst filtering tolerance due to large amount of phase modulation (m=2 rad) implemented on NRZ pulses. The interesting point in this investigation is the pulse shape in alPNRZ case (Fig. 6.8c), which is a combination of RZ and NRZ pulse shape. This effect can be explained by the fact that alPNRZ spectrum is actually superposition of two different spectra - NRZ and CSRZ - in two polarizations, which react differently to narrow-band filtering. The CSRZ part of alPNRZ signal counteracts the narrow-band filtering effects resulting in an RZ similar pulse shape after narrow-band filtering. According to their presented filtering characteristics, novel modulation formats could be a good alternative to conventional modulation formats for a realization of spectrally efficient DWDM systems.

6.4 Optimized amplifier spacing

Another important question, which has to be addressed before starting with the design of a transmission system, is the length of the transmission spans characterized by the amplifier spacing in the line. The right decision on the span length represents a compromise between propagation limitations of the transmission line and component costs. The crucial components for the right choice of span length are optical amplifiers. Conventional optical amplification is realized using EDFAs, which enable a lumped amplification with a large impact of ASE-noise, but recently intensively investigated Raman amplifiers [249], [250], [79] represent a good opportunity for the realization of distributed amplification and enables a relaxation of ASE-noise limitations. Considering EDFA-based amplification as the state-of-the-art technology, an increased span length results in enhanced attenuation losses of optical signal within each transmission span.
The strongly attenuated signals are more sensitive to ASE-noise because large EDFA gains needed for their amplification cause an enhanced ASE-noise generation, thus resulting in reduced achievable OSNR values and reduced maximum transmission lengths. On the other hand, shorter span length reduces ASE-noise impacts in the transmission line, but a larger number of amplifiers is needed in the line, hence increasing the total system costs.
The right choice of the span length is dependent on the total transmission distance of the system as well as on the desired reliability and system life time. For example, in under-sea transmission systems, which are characterized by a high operation reliability (e.g. long life time) and difficult deployment conditions, the system performance is more important than system costs resulting in a reduced span length of 25..50 km [3], [51]. On the other hand, in metro area optical networks, where system costs are important design criteria, the desired transmission line is quite simple, consisting of a single span transmission line with a length of 30..150 km with a reduced span complexity and transmission costs, where small number of amplifiers is desirable. In already deployed terrestrial systems, the spans have a varying length in a range of 50..100 km.
In order to determine the optimum span length for 4x40 Gb/s WDM and DWDM systems, the transmission line consists of multiple cascaded spans and a total distance of 1200 km is considered. A simplification of the investigation is made by replacing the transmission and DCF fibers with appropriate attenuators, in order to concentrate on ASE-noise impacts in the transmission line, considering a DCF input power of -6 dBm/ch. Assuming equal noise figures of F=4 dB in all EDFAs, the span length is varied in a range of 40..120 km, resulting in different total number of spans and different ASE-noise impact in the transmission

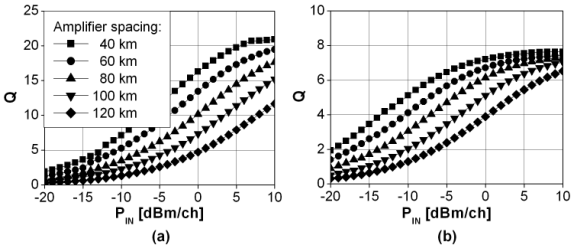

Figure 6.9: NRZ 4x40 Gb/s optimum amplifier spacing investigations (linear Q_{ISI} evaluation, F_{EDFA}=4 dB, total length 1200 km): a) 100 GHz grid b) 50 GHz grid

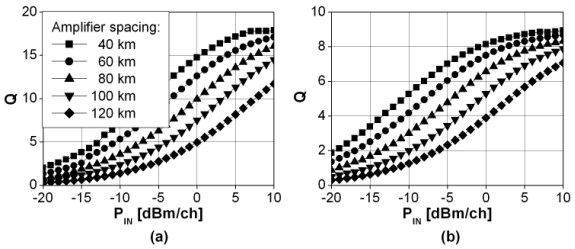

Figure 6.10: RZ 4x40 Gb/s optimum span length investigations (linear Q_{ISI} evaluation, F_{EDFA}=4 dB, total length 1200 km): a) 100 GHz grid b) 50 GHz grid

line. Representative for NRZ- and RZ-based modulation formats, investigations results are presented in Fig. 6.9 and 6.10 only for RZ and NRZ modulations at 100 and 50 GHz channel spacings employing optimum filter settings in MUXs and DMUXs. Both figures illustrate that a reduced span length is beneficial for a total system performance independently on the channel spacing and modulation format in use. The transmission differences for different span lengths are visible in the lower power region, where ASE-noise impacts represent dominant system limitations. The differences vanish for extreme large power values (>10 dBm), which are from the practical point of view less relevant for future system design. Identical transmission behavior was observed for all other modulation formats. These investigations indicate that a span length of 80 km represents a good compromise between ASE-noise limitations and system costs in point-to-point transmission networks. This span length is used for further investigation in this chapter.

6.5 Optimized power settings

After determination of the optimum MUX and DMUX settings and optimum span lengths for WDM (100 GHz grid) and DWDM (50 GHz grid) systems, the next step in the investigation of transmission performances is made by the optimization of optical input power into transmission and DCF fibers. Identical transmission line infrastructures are used as in the single channel case (Fig. 5.1). This investigation provides a good comparison with the single channel power optimization, thus giving an insight into system linear and nonlinear characteristics, which depend on the number of channels, channel spacing and power settings in the transmission line. Furthermore, the differences between different modulation formats can be illustrated. The scope of this numerical work was the upgrade capability from single to multiple channel 40 Gb/s transmission considering already deployed network infrastructures. Accordingly, considering SSMF fibers as widely buried transmission fiber type, the investigated system setups for power optimization consist of SSMF fibers, whose dispersion is compensated in a span-by-span disperison post-compensation scheme. This scheme is chosen, because it already showed good characteristics in the single channel investigations, and its performance is afterwards compared to other dispersion schemes (Chapter 6.6). Due to increased time and resource consumption needed for multi-channel numerical simulations due to the reduced step-width used for split-step Fourier method, the transmission line in this investigation consists of just two identical transmission spans. This number of spans represents the minimum span number allowable for the characterization of multi-channel nonlinear effects like XPM or FWM, because it enables the investigation of length dependent accumulation of multi-channel effects. The power setting optimization is done considering optimum filter settings for channel spacings of 100 and 50 GHz, respectively. The filtering losses caused by the narrow-band filtering were compensated before transmission by an EDFA-based booster.

6.5.1 NRZ-based modulation formats

The calculated optimum power settings for NRZ and duobinary modulation are presented in Fig. 6.11. If these results are compared to the single channel investigations (Chapter 5.5.1), it can be observed that in the 100 GHz case, achievable Q values are larger than in the single channel case, which can be explained by the reduction of transmission distance in WDM investigations. Furthermore, 100 GHz based WDM and single channel transmission indicate identical optimum power regions both for SSMF and DCF fibers independently of the modulation format in use. This behavior can be explained by the fact that in a 100 GHz based WDM transmission, single-channel nonlinearities represent the dominant system limitation [165]. The XPM and FWM effects are less relevant in this case, due to relatively large channel spacing, large fiber dispersion and a small pulse width. The large channel spacing is crucial for the transmission behavior, which results in a reduced walk-off length between adjacent channels enabling a suppression of multi-channel effects. These observations are in good agreement with experimentally presented works [232], [3], [251]. The consequence of single-channel effect dominance at the 100 GHz grid is that, as in single channel case, NRZ outperforms duobinary modulation. At the same time, both modulation formats possess similar optimum power ranges (P_{SSMF}=-2..2 dBm, P_{DCF}=-6..-4 dBm). Making a comparison between optimum power settings in transmission and DCF fiber, it can be observed that a difference of approximately 6 dB occurs. This can be explained by large nonlinear distortions in DCFs, whose efficient suppression can only be achieved by small DCF input power.

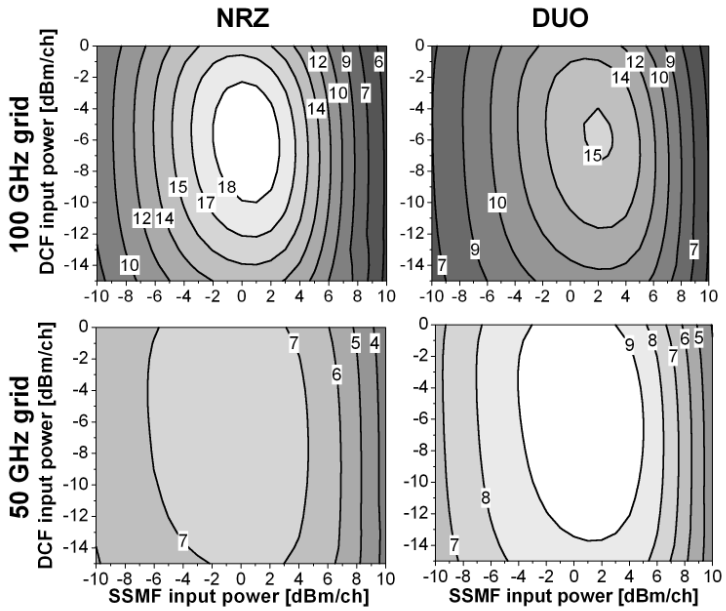

Figure 6.11: NRZ-based modulation formats 4x40 Gb/s - power investigations (P_{SSMF} and P_{DCF}) over 2x80 km SSMF (linear Q_{ISI} evaluation, filter settings from Tables 6.4 and 6.5, full dispersion post-compensation per span): a) 100 GHz channel spacing b) 50 GHz channel spacing

Considering DWDM transmission at 50 GHz channel spacing, transmission performance becomes reduced (Fig. 6.11) compared to the WDM case. Besides filtering-caused pulse distortions, the multi-channel effects become evident, hence masking single channel limitations. The XPM impact is larger than the FWM impact, because of a large local dispersion causing a phase-mismatch between the DWDM channels, thus reducing the FWM efficiency. Accordingly, it can be expected that the implementation of NZDSF fibers in DWDM transmission would cause increased multi-channel limitations, because of the low local dispersion and large nonlinear coefficient. Comparison between NRZ and duobinary modulation in DWDM systems, show small benefits of duobinary modulations due to its slightly better narrow-band filtering robustness. Maximum Q

Format	P_{SMF} [dBm/ch]	P_{DCF} [dBm/ch]
alCNRZ	1	-6
alPNRZ	5	-2
alPRZ	5	-2
CSRZ	4	-3
DUO	2	-6
nCRZ	4	-2
NRZ	0	-6
RZ	2	-5
SSBRZ	1	-5

Table 6.1: Optimized fiber power settings for 4x40 Gb/s WDM with 100 GHz channel spacing over 2x80 km SSMF employing full dispersion post-compensation per span

Format	P_{SMF} [dBm/ch]	P_{DCF} [dBm/ch]
alCNRZ	0	-5
alPNRZ	2	-3
alPRZ	2	-3
CSRZ	3	-6
DUO	1	-5
nCRZ	1	-4
NRZ	0	-5
RZ	0	-4
SSBRZ	0	-5

Table 6.2: Optimized fiber power settings for 4x40 Gb/s WDM with 50 GHz channel spacing over 2x80 km SSMF employing full dispersion post-compensation per span

values of 7 and 9 for NRZ and duobinary case, indicate a reduced system power budget and significantly reduced maximum transmission distance compared to the 100 GHz channel spacing results.
According to presented results (Fig. 6.11), the system upgrade from 40 Gb/s single channel to WDM systems can be easily performed without performance losses. A further upgrade to DWDM system would represent a critical issue, because of additional multi-channel impacts. Hence, it can be expected that optimum system settings in DWDM systems would differ from optimum settings for WDM and single channel transmission, increasing the complexity and deployment costs of spectrally efficient DWDM systems.

6.5.2 RZ-based modulation formats

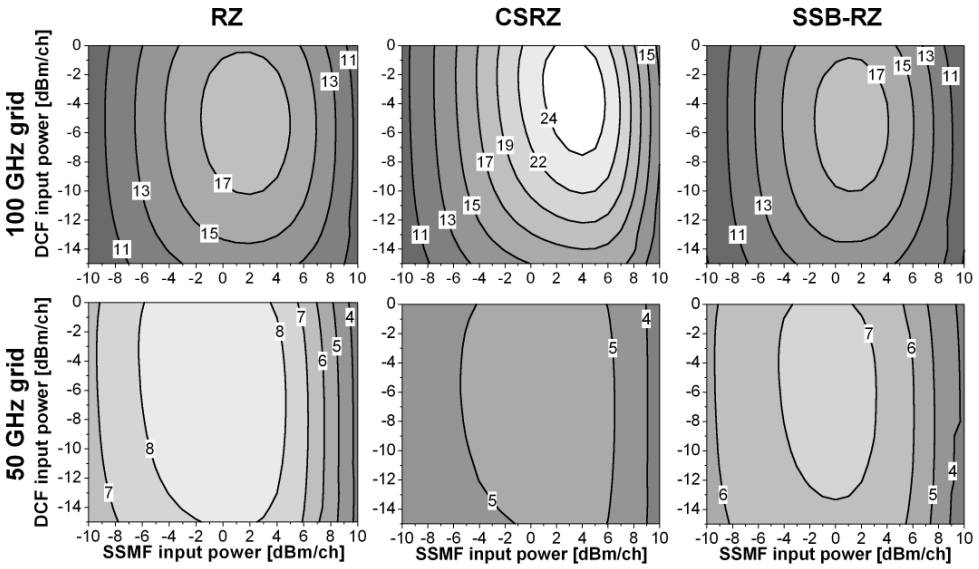

Figure 6.12: RZ-based modulation formats 4x40 Gb/s - power investigations (P_{SSMF} and P_{DCF}) over 2x80 km SSMF (linear Q_{ISI} evaluation, filter settings in Tables 6.4 and 6.5, full dispersion post-compensation per span): a) 100 GHz channel spacing b) 50 GHz channel spacing

Investigations of optimum power settings for RZ-based modulation formats indicate similar effects of reduced channel spacing as for NRZ-based modulation formats (Fig. 6.12). As in NRZ cases, the width of the

optimum power ranges depends on the nature of the limiting transmission effects. Transmission at a larger channel spacing is limited by single channel effects, e.g. SPM-GVD interaction and intra-channel effects (IXPM,IFWM). Considering the optimum power region for DCF fibers, larger DCF powers are acceptable due to better nonlinear tolerance of RZ-based formats. The optimum power settings in transmission fibers are about 2 dB larger than in NRZ cases. While on one hand, RZ-based WDM transmission in the 100 GHz grid shows an improved performance compared to the NRZ-based case and less differences compared to single channel transmission, the RZ-based modulation formats on the other hand suffer more from the narrow-band filtering in DWDM systems with a 50 GHz grid. This effect is especially significant for CSRZ modulation, which shows the best performance at larger channel spacings and the worst performance at reduced channel spacings, due to its reduced filtering tolerance. In DWDM systems, all RZ-based formats perform near the quality limit of Q=6 despite a short transmission distance (2x80 km). Due to a short transmission length and smaller optimum power values, it can be expected that transmission performance of RZ-based DWDM systems is limited by narrow-band filtering effects. Furthermore, because of RZ pulse shape distortions by narrow-band filtering the good nonlinear characteristics vanish at 50 GHz channel spacing, due to RZ to NRZ pulse shape transformation.

6.5.3 Novel modulation formats

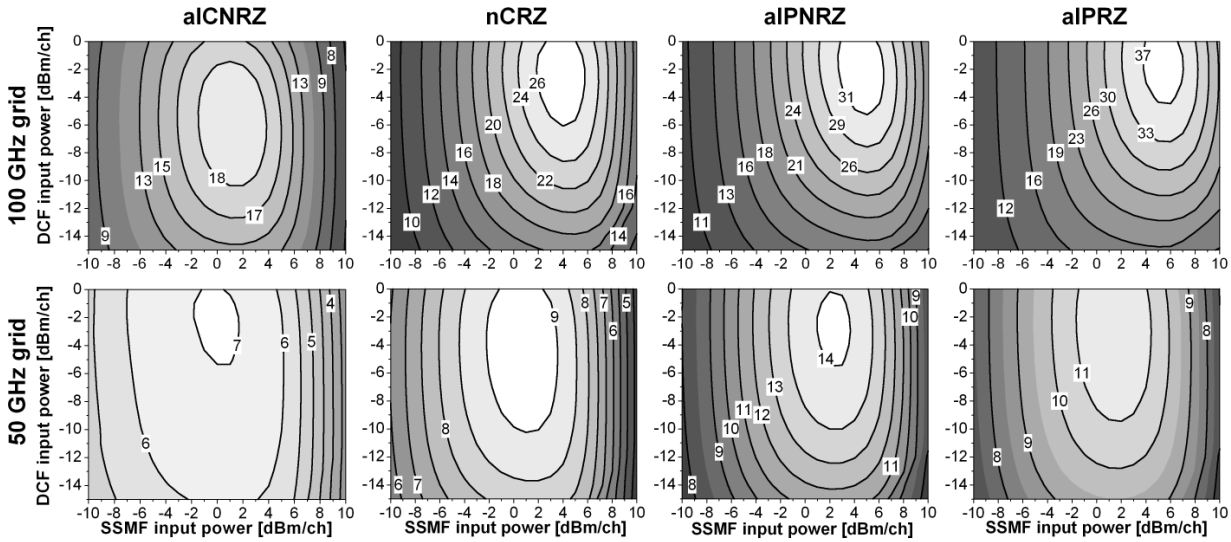

Figure 6.13: Novel modulation formats 4x40 Gb/s - power investigations (P_{SSMF} and P_{DCF}) over 2x80 km SSMF (linear Q_{ISI} evaluation, filter settings in Tables 6.4 and 6.5, full dispersion post-compensation per span): a) 100 GHz channel spacing b) 50 GHz channel spacing

The implementation of novel modulation formats in 40 Gb/s WDM and DWDM systems enables an enhancement of optimum power regions both for transmission and DCF fibers (Fig. 6.13). The novel modulation formats can outperform conventional RZ- and NRZ-based formats in terms of better Q-values and larger optimum power settings as in the single channel investigations. Considering results for 50 GHz channel spacing, a performance reduction can be observed versus the 100 GHz case, but comparing these results to the NRZ- and RZ-based cases, a better transmission performance is evident. This can be explained by a better spectral compactness of novel modulation techniques (e.g. alPNRZ), making these formats more robust to narrow-band filtering. At the same time, the implemented phase and polarization modulations partly suppress multi-channel impairments. The optimum power regions for transmission fibers compared to conventional NRZ- and RZ-based formats are shifted towards larger powers. Maximum optimum power shifts amount up to 4 dB compared to conventional RZ formats and up to 6 dB compared to NRZ-based

formats. NRZ and RZ pulses employing alternate polarizations between consecutive bits (alPNRZ, alPRZ) show best transmission performance due to their better nonlinear characteristics and an improved robustness to narrow-band filtering.

6.6 Optimized dispersion compensating schemes

After investigating optimum filter settings and power tolerances of different modulation formats in 40 Gb/s WDM and DWDM systems, further system optimization concentrated on the effects of different dispersion maps on the total system performance and determination of optimum dispersion compensating schemes. The transmission line consists of multiple spans with identical span infrastructure and dispersion compensation is done on a span-by-span basis. As the periodical span-by-span dispersion compensation is not beneficial for suppression of inter-channel effects, e.g. XPM [252], [253] it can be considered as the worst-case scenario for the characterization of system settings. Full compensation of accumulated SSMF dispersion is performed in each span, as a combination of in-line pre- and post-compensation. The transmission line is made up of SSMF fibers, due to the fact that these fibers are the most widely deployed in today's optical networks. Contrary to single channel investigations, where the power settings in the transmission and DCF fibers were optimized for each amount of dispersion pre-compensation, three different power regions (P_{IN}= -5, 0 and 5 dBm/ch) are considered in order to investigate the interaction between the nonlinearities and dispersion map. This method enables a better characterization of transmission behavior and enables identification of dominant system limitations. The DCF input power used in these investigations is 6 dB lower (according to optimum power investigations) than the SSMF power (P_{DCF}=-11, -6 and 1 dBm/ch) in order to enable similar ASE-noise effects in all investigated cases, and to suppress the nonlinearities in DCFs. The performance is estimated using the Q_{ISI} criterion described in Chapter 4.

6.6.1 NRZ-based modulation formats

The results of dispersion map investigations at channel spacings of 100 and 50 GHz are illustrated in Fig. 6.14. Comparing the results at different channel spacings, the differences occur at an increased power per channel when the propagation nonlinearities become dominant. The behavior in the 100 GHz based cases indicates that the dispersion map plays a less important role as long as the linear effects, e.g. ASE-noise and GVD, represent the dominant limitations for -5 dBm/ch input power. An increase of the input power to 0 dBm/ch indicates slight changes of the transmission behavior, depending on the amount of pre-compensation. In the duobinary case, even at 0 dBm/ch the variations become visible due to a reduced power tolerance. For larger power values (e.g. 5 dBm/ch) the transmission behavior is strongly dominated by nonlinear effects in the transmission line.

Since the single-channel limitations dominate the transmission behavior at larger channel spacing, the optimum dispersion map is characterized by a certain amount of pre-compensation (≈20 %), implying large similarity to optimum dispersion compensation observed in the 40 Gb/s single channel investigations. On the other hand, the pure post-compensation performs better than pure pre-compensation. This can be explained by the fact that the 40 Gb/s based WDM transmission systems over SSMF at 100 GHz channel spacing are impacted mainly by single channel impairments (in this case SPM-GVD interplay), as due to large channel spacing and a large local dispersion, inter-channel effects (XPM, FWM) can be efficiently mitigated. These results are in a good agreement with recently presented works [254], [255], indicating that the future system upgrade of 40 Gb/s systems from single channel to WDM can be done without deployment of new fiber infrastructures (sophisticated dispersion schemes) up to a spectral efficiency of 0.4 bit/s/Hz. Hence, the upgrade can be easy enabled by implementation of additional transmitters cards. The use of duobinary modulation in 40 Gb/s WDM system would enable slight performance improvement compared to NRZ only in a linear transmission regime ($P_{IN} \leq$ 0 dBm/ch), due to its better linear characteristics.A reduction of channel spacing below 100 GHz causes changes of the transmission behavior. Our initial investigations [165] indicated that up to a channel spacing of 80 GHz in 40 Gb/s based WDM systems no significant performance changes can be observed, compared to single channel transmission.

In order to investigate the impact of inter-channel effects, the channel spacing is reduced to 50 GHz. The system with a 50 GHz grid is at the same time strongly impacted by the narrow-band filtering (filter settings presented in Table 6.5), which has an effect not only on the filtering losses and linear crosstalk, but also on nonlinear system behavior because of induced pulse broadening. It can be observed (Fig. 6.14b) that the realization of the implemented dispersion map is again less critical in a linear propagation regime (P_{IN} =-

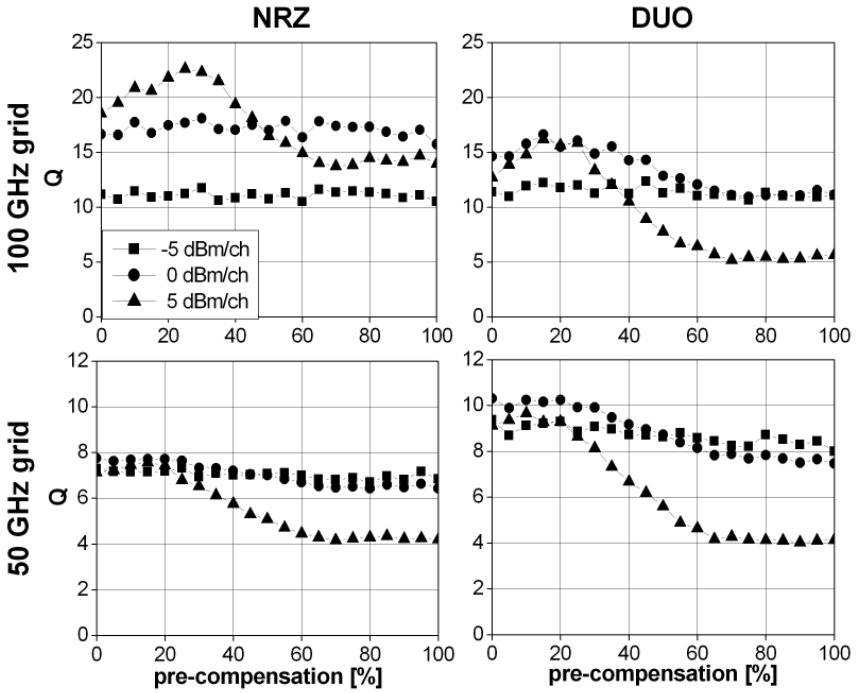

Figure 6.14: NRZ-based modulation formats 4x40 Gb/s 2x80 km SSMF - dispersion scheme investigations (linear Q_{ISI} evaluation, with ASE-noise, F_{EDFA}=4 dB, P_{DCF}=P_{IN}-6 dBm/ch, full compensation per span)

5 dBm/ch), but according to an increased impact of inter-channel nonlinearities at reduced channel spacing, the dispersion map dependent performance limitations can be observed already at 0 dBm/ch, and become even more important at increased channel powers. The impacts of single channel limitations become masked by the inter-channel effects. Analyzing the nature of inter-channel limitation, it can be distinguished between the XPM and FWM effect. Although the equal channel spacing used here is rather a disadvantage from FWM point of view, it can be expected that a large local dispersion in the transmission fibers (D=16 ps/nm·km) induces a phase mismatch between the channels, resulting in a reduced FWM efficiency even at 50 GHz channel spacing.
The XPM disturbances are caused by the interaction of optical pulses propagating in neighboring channels. These interactions cause frequency shifts of opposite signs at the trailing and rising pulse edges. For symmetric interactions between the pulses, characterized by equal amounts of phase modulation on the trailing and rising edges, the resulting frequency shifts cancel each other without affecting the transmission performance. But the interactions are symmetric, only if pulse power (energy) is maintained during propagation. Due to fiber losses and lumped optical amplification scheme employed in transmission line, the interactions observed here are not symmetric, hence different frequency shifts occur at the pulse edges. The XPM impact in ASK-based systems becomes evident only after interaction with GVD in the fibers, which induces PM-IM conversion, resulting in different pulse arrival times at the receiver side, giving rise to timing and amplitude jitter occurrence. The efficiency of XPM is dependent on the duration of the pulse interactions, which are proportional to the walk-off length $L_{walk-off}$ given as:

$$L_{walk-off} = \frac{\Delta\tau}{|D|\Delta\lambda} \tag{6.2}$$

where $\Delta\tau$ is the transition/rise time of rising and falling pulse edges, D is the fiber dispersion, and $\Delta\lambda$ is the channel spacing. Accordingly, a reduced walk-off length e.g. due to a reduced pulse width or large local dispersion causes a suppression of XPM effects in the line. The target for XPM suppression is enabling of

a walk-off length much smaller than the fiber effective length L_{eff} [64]. Without dispersion compensation, the XPM effect would occur at the beginning of the transmission line and the nonlinear effects between the bits in neighboring channels would be averaged out because of decorrelation between the channels during propagation in multiple spans. In the line infrastructure considered here, it can be expected that owing to the periodical full dispersion compensation, the XPM effects accumulate resonantly, because identical bit interactions take place at the beginning of each span.
The WDM propagation at the 50 GHz grid (Fig. 6.14) with large channel power (5 dBm/ch) indicates, both for NRZ and duobinary modulation, an advantage of post- over pure pre-compensation. This can be explained by the fact that if the pulses in neighboring channels are fed undisturbed (without pre-compensation) into a transmission fiber with a large local dispersion, the timing jitter due to the XPM can be efficiently suppressed [94], enabling a better transmission performance. Combining post-compensation with a small amount of pre-compensation (<10 %), a slight improvement can be achieved due to the decorrelation between the channels and limited pattern dependent distortions as a consequence of small pre-compensation. In a pure dispersion pre-compensation scheme, the interactions between strongly distorted optical pulses due to large pre-compensation and nonlinear impairments in the effective length L_{eff} of each span can not be compensated in DCF, thus causing worse transmission characteristics. Comparing duobinary and NRZ-based DWDM transmission, it can be observed that duobinary transmission profits from the better narrow-band filtering robustness resulting in better Q values. In order to analyze the dependence of the transmission

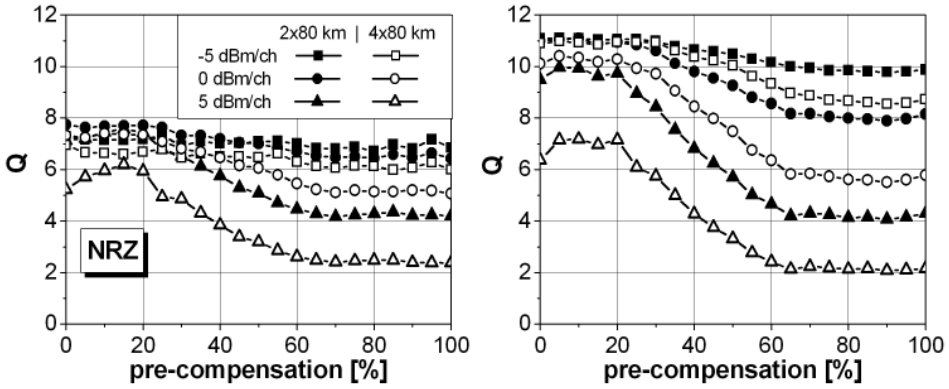

Figure 6.15: 4x40 Gb/s optimum dispersion compensation scheme investigations at 50 GHz grid over 2/4x80 km SSMF (linear Q_{ISI} evaluation, without ASE-noise, P_{DCF}=P_{IN}-6 dBm/ch)

behavior on the dispersion map in 40 Gb/s based DWDM systems (50 GHz grid) with an increased number of cascaded spans, the transmission line was extended to 4x80 km. ASE-noise is not considered in the transmission line in order to focus on length dependence of fiber nonlinearities. The results are presented in Fig. 6.15 both for NRZ and duobinary modulations. The increased transmission length causes performance changes at all investigated power settings. The length-dependent deviations are less critical at lower input powers (e.g. -5 dBm/ch) implying a system performance independence on the dispersion map. Consideration of ASE-noise impariments would cause changes of this behavior at lower powers due to the length dependent noise accumulation. At an increased signal power, the length impact becomes more evident. Although the total dependence of transmission performance on dispersion map is maintained, like in the two spans transmission, the achievable Q values shrink.
The more the XPM impact dominates transmission performance, the Q dependence on length becomes more visible. For a 5 dBm/ch based transmission, the induced Q reduction is almost independent of the dispersion map and amounts to 2, implying that penalty Q $\propto 1/N$, where N is the number of spans in XPM limited transmission line. This can be explained by the fact that due to cascading of identical spans with full dispersion compensation per span, equal XPM-induced distortions are generated in each span, and su-

perpose from span to span. This behavior is in a good agreement with recently presented works [256], [257], which showed that the XPM-induced standard deviation is proportional to number of transmitted spans N, $\sigma_{XPM} \propto$ N. These results can be used as design rules for the characterization of the achievable system margin and transmission performance in the future 40 Gb/s DWDM transmission systems.

6.6.2 RZ-based modulation formats

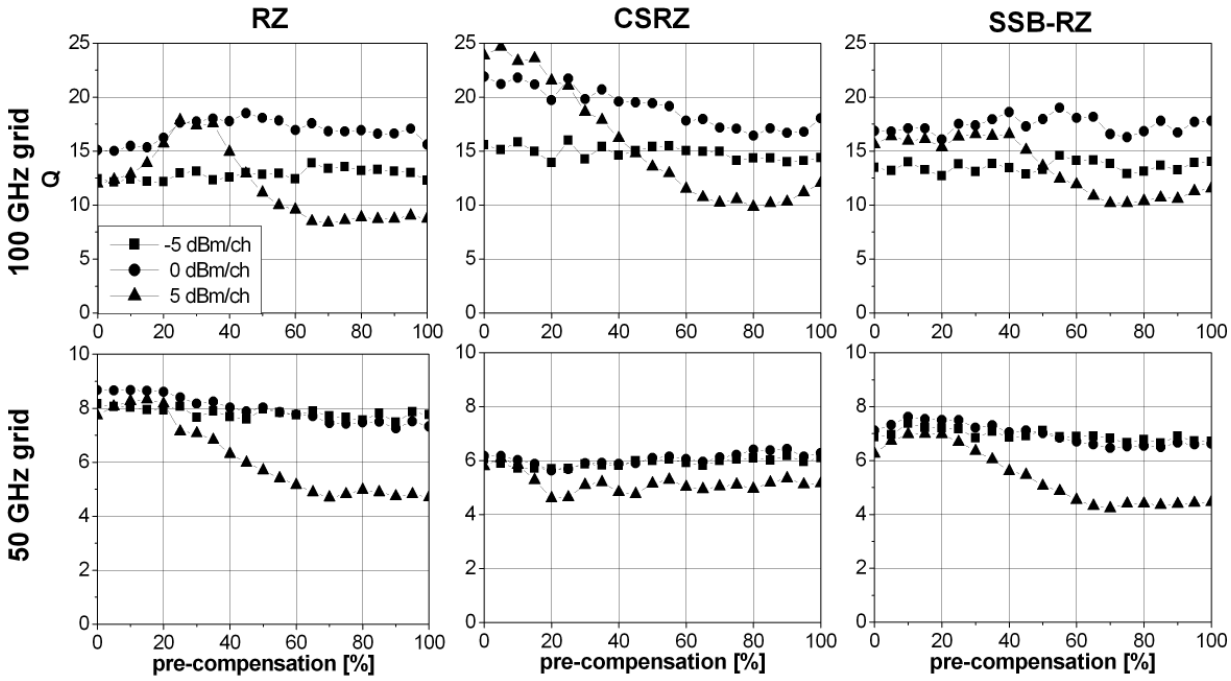

Figure 6.16: RZ-based formats 4x40 Gb/s 2x80 km - dispersion compensation investigations (liner Q_{ISI} evaluation, with ASE-noise, F_{EDFA}=4 dB, P_{DCF}=P_{IN}-6 dBm/ch, full compensation per span)

Figure 6.16 depicts results for optimal dispersion schemes for RZ-based modulation formats considering channel spacings of 100 and 50 GHz in 40 Gb/s based transmission lines. Generally speaking, similar differences are visible between different channel spacings like in the NRZ-based investigations. In 100 GHz based transmission at low channel power, the dispersion map shows no effect on the transmission performance for all investigated formats. The dispersion map impact on total performance becomes first visible at an increased power per channel (e.g. 5 dBm/ch), indicating that the system performance in this case is governed by the interaction between nonlinear effects in the transmission fiber and span infrastructure. Investigated systems at 100 GHz grid indicate a behavior similar to single channel investigations, thus the transmission limitations arise from single channel limitations, e.g. intra-channel effects (IXPM, IFWM). Their transmission behavior is characterized (as in the single channel case) by an optimum dispersion scheme with a small amount of pre-compensation.
These results imply that in RZ-based systems, a system upgrade by implementation of additional channels can be done using identical infrastructure as in the single channel case. According to the transmission limitations caused by intra-channel effects, the use of transmission fibers with reduced local dispersion (e.g. NZDSFs) would improve transmission characteristics in this case [232]. Comparing performances of different modulation formats at 100 GHz channel spacing, it can be observed that CSRZ modulated pulses show the best transmission performance, due to their better tolerance to intra-channel effects, governed by the phase relations between consecutive pulses, which are shown to be beneficial for intra-channel suppression (Chapter 5).

The implementation of narrow-band optical filters, needed for enabling 50 GHz grid based 40 Gb/s DWDM systems, causes significant changes in transmission behavior of all RZ-based formats, because the RZ signal shape becomes distorted. The signal shape distortions are much larger in RZ and SSB-RZ pulses according to their broader signal spectra, and in these case a transmission behavior similar to NRZ can be expected. In CSRZ case, despite of the fact that the RZ pulse shape is maintained, the transmission performance is

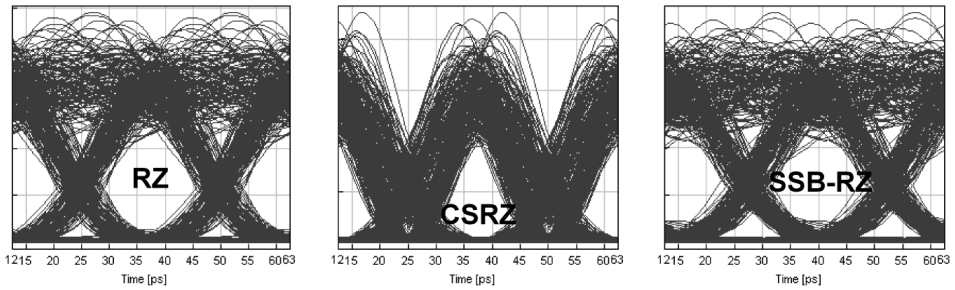

Figure 6.17: Detected signal eyes in 4x40 Gb/s with 50 GHz grid over 2x80 km post compensated SSMF (P_{IN}=5 dBm/ch, P_{DCF}=-1 dBm/ch)

worse. This can be explained by the fact that the CSRZ signals due to the narrow-band filtering loose their CSRZ characteristics, because the phase inversions between adjacent pulses are destroyed due to the induced pulse broadening, hence causing reduced nonlinear tolerance. The transmitted pulses can be described as a mixture of CSRZ and duobinary features [179]. A stronger narrow-band filtering in the DMUX will cause a complete disappearance of CSRZ characteristics and in this case, the pulses show duobinary characteristics at the transmitter side. In the case of RZ-based DWDM transmissions, XPM represents the dominant limitation inducing large amounts of timing and amplitude jitter in detected signal eyes (Fig. 6.17). Another interesting point is the dependence of transmission performance (Q value) on the dispersion map. As in the NRZ-based case, transmission performance profits from a small amount of dispersion pre-compensation, and in 40 Gb/s DWDM systems with an increased spectral efficiency (>0.4 bit/s/Hz, typically) unique optimum dispersion map (e.g. post-compensation) can be used independently on the modulation format in use.

As in NRZ-based investigations, the number of spans was increased to 4 in order to observe if significant

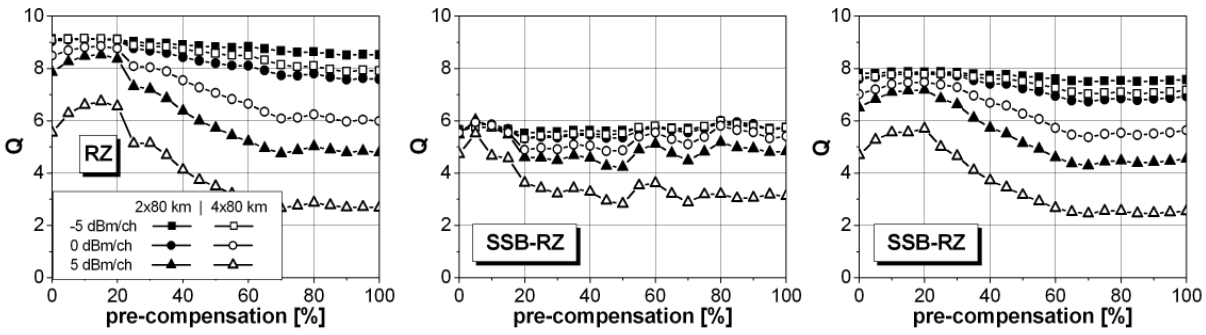

Figure 6.18: 4x40 Gb/s optimum dispersion compensation scheme investigations at 50 GHz grid over 2/4x80 km SSMF (linear Q_{ISI} evaluation, without ASE-noise, P_{DCF}=P_{IN}-6 dBm/ch)

changes in the dispersion map dependence occur. The results presented in Fig. 6.18 show almost identical characteristics for RZ and SSB-RZ-based cases as in the NRZ case, due to similar pulse shapes. Thereby, the Q penalty caused by the increased transmission length is again proportional to N (N number of spans). The length dependence of CSRZ transmission is not so straightforward. It deviates from the above rule, because

XPM effects interact with strong CSRZ pulse distortions.

6.6.3 Novel modulation formats

The results of optimum dispersion compensation scheme investigations done considering novel modulation formats - alCNRZ, nCRZ, alPNRZ and alPRZ - in transmission lines with 100 and 50 GHz channel spacing are illustrated in Fig. 6.19. Transmission at 100 GHz channel spacing is, like in previous cases, characterized by a good transmission performance and a dominance of single channel limitations, which are better suppressed due to the use of phase and polarization modulation for the signal generation. Again, the importance of the dispersion map in the transmission line becomes evident only for large channel power (5 dBm/ch), and as in the single channel case, the transmission performance profits from a certain amount of dispersion pre-compensation, which was already observed in NRZ- as well as in RZ-based WDM transmission systems. Novel modulation formats outperform all other formats in 100 GHz channel spacing transmissions, and depending on the pulse shape of the novel formats, the optimum amounts of dispersion pre-compensation comply with results of NRZ- and RZ-based cases.

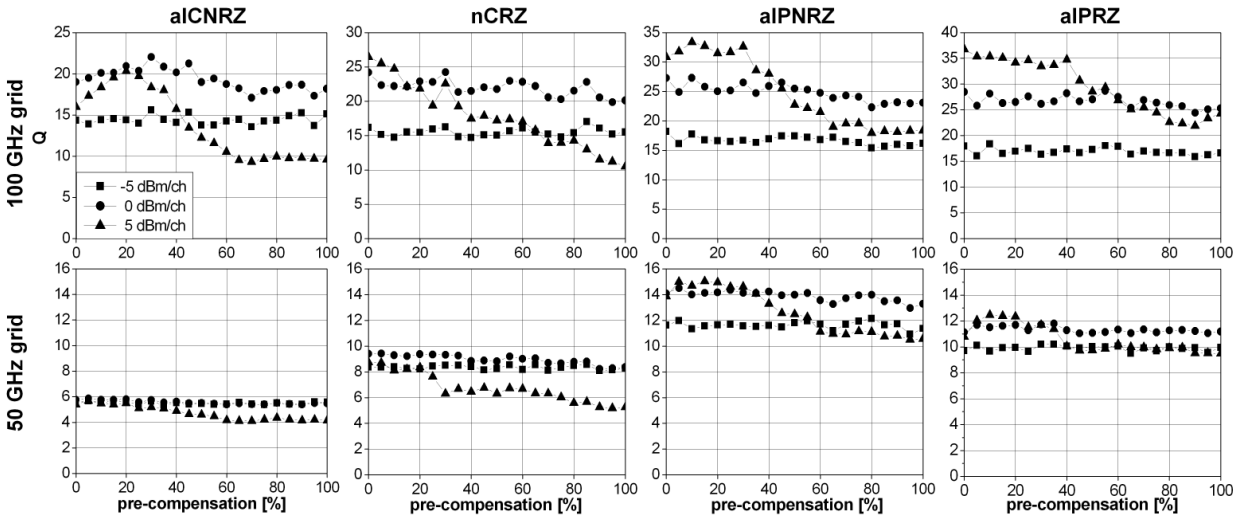

Figure 6.19: Novel modulation formats 4x40 Gb/s 2x80 km - dispersion compensation scheme investigations (linear Q_{ISI} evaluation, without ASE-noise, P_{DCF}=P_{IN}-6 dBm/ch)

The reduction of channel spacing to 50 GHz results in a clearer differentiation between different novel modulation formats (Fig. 6.19 bottom line). The use of narrow-band filtering induces strong pulse distortions, but depending on the original pulse shape and method of generation, novel modulation formats show different behavior. As in other 50 GHz investigations, the XPM effect can be identified as the dominant limitation, hence resulting in a large amount of timing jitter at the receiver side (Fig. 6.20). The dependence of the transmission performance on the dispersion map is similar to the NRZ- and RZ-based modulation formats, indicating dispersion post-compensation as the optimum dispersion scheme, due to a better suppression of XPM effect in the transmission line. Accordingly, it can be concluded that all ASK-based modulation formats - novel and conventional ones - show identical dispersion map dependencies in 40 Gb/s DWDM-based systems. Making a comparison between the investigated novel modulation formats, it can be seen that polarization switched modulation formats enable less penalty in 50 GHz grid based 40 Gb/s systems (Fig. 6.19). In order to illustrate the differences between the formats, the received signal eyes are shown in Fig. 6.20. alCNRZ eyes indicate typical NRZ distortions and the phase modulation implemented between adjacent bits can just partly reduce the introduced ISI-effects between them.
According to a larger amount of the implemented phase modulation (m=1.15 rad), RZ pulse shape and a compactness of the signal spectrum, nCRZ modulation counterparts the narrow-band filtering, thus main-

taining the RZ pulse shape, which enables a performance improvement compared to the alCNRZ case, and a strong timing jitter observed in detected signal eyes indicates typical XPM limitations. The consideration of alPNRZ and alPRZ eyes illustrates an unconventional behavior of polarization switched modulation formats, because alPNRZ and alPRZ signal spectra represent the combination of NRZ and CSRZ, and RZ and CSRZ spectra in single polarizations, respectively. In the alPNRZ case, according to good filtering robustness of NRZ and a polarization (phase) inversion between adjacent bits due to phase modulation in y-polarization (see alPNRZ signal generation in Chapter 3), the pulse distortions can be efficiently suppressed, causing slight changes of signal shape and resulting in a RZ-NRZ characteristic of alPNRZ pulses (Fig. 6.20c) after transmission. In the alPRZ case, the RZ signal shape suffers strong distortions as a consequence of narrow-band filtering resulting in large interference between consecutive bits.

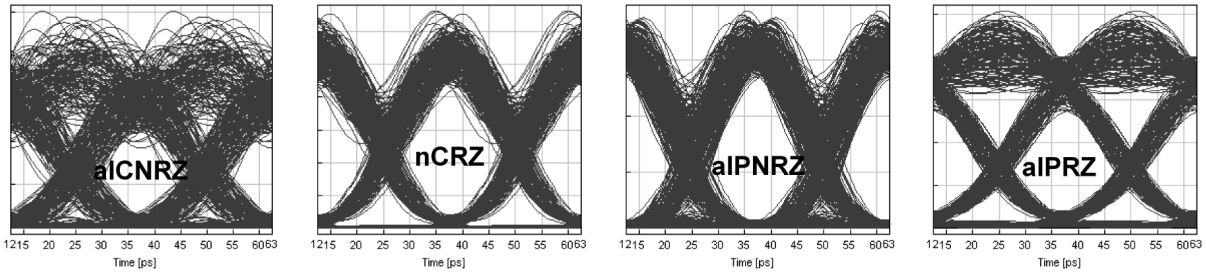

Figure 6.20: Detected signal eyes in 4x40 Gb/s with 50 GHz grid over 2x80 km post compensated SSMF (P_{IN}=5 dBm/ch, P_{DCF}=-1 dBm/ch)

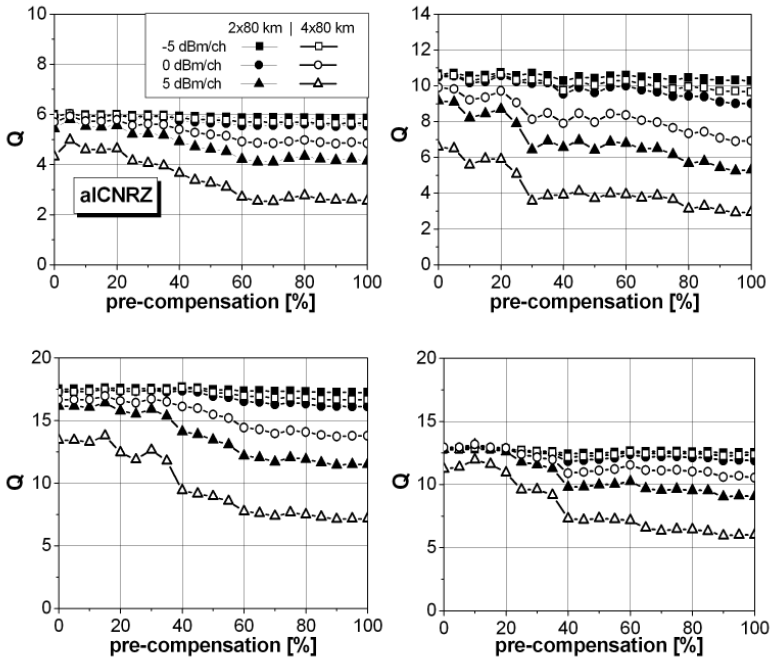

Figure 6.21: 4x40 Gb/s optimum dispersion compensation scheme at 50 GHz grid over 2/4x80 km SSMF (linear Q_{ISI} evaluation, without ASE-noise, P_{DCF}=P_{IN}-6 dBm/ch)

As for NRZ- and RZ-based modulation formats, the total length of the transmission line was increased in

order to identify possible length dependence of the optimum dispersion map. The results of these investigations presented in Fig. 6.21 show that the optimum dispersion map is maintained even for an increased transmission reach. The length induced transmission penalties become evident only for larger channel powers (5 dBm/ch) and are proportional to the total number of spans N. Small deviations from this rule observed in alPRZ case are caused rather by numerical inaccuracy (quality evaluation criteria) than by the transmission effects. These results show that different modulation formats possess identical optimum dispersion maps caused characteristics independently on the total system reach. Furthermore, similar investigations performed considering 40 Gb/s based WDM systems with 100 GHz channel spacing indicated that the dispersion map dependence observed at 2x80 km is maintained for an increased number of spans, but the penalty reduction at 100 GHz channel spacing deviates from N-proportionality, because of different nature of system limitations (intra-channel effects domination).

6.7 Optimum transmission fiber investigations

As shown in Chapter 5, the right choice of transmission fiber can improve the transmission performance of the system, thus enabling a better utilization of total system capacity. The description of fiber's transmission characteristics can be simplified using two dominant fiber parameters - effective area (A_{eff}) and fiber dispersion (D) - which govern linear and nonlinear effects in the transmission fiber. The fiber parameters become more important for an increased number of propagation effects, which is exactly the case in WDM transmission systems with a reduced channel spacing and a large number of channels. Accordingly, the optimization and a detailed investigation of transmission fibers is required for a successful system design. The investigations presented in this chapter are done considering various values of the fiber's A_{eff} in a range of 50..90 μm^2 and D between 0..20 ps/nm·km with a constant attenuation of 0.22 dB/km in all investigated cases. The investigated setup consists of two identical transmission spans with a full dispersion post-compensation, because this scheme indicated good transmission performance both for 100 and 50 GHz channel spacing based 40 Gb/s WDM systems. Identical DCF (Table 5.1) is used for dispersion compensation in all investigated cases. The power settings in transmission fibers were extracted from optimum power investigations presented in previous chapters.

6.7.1 NRZ-based modulation formats

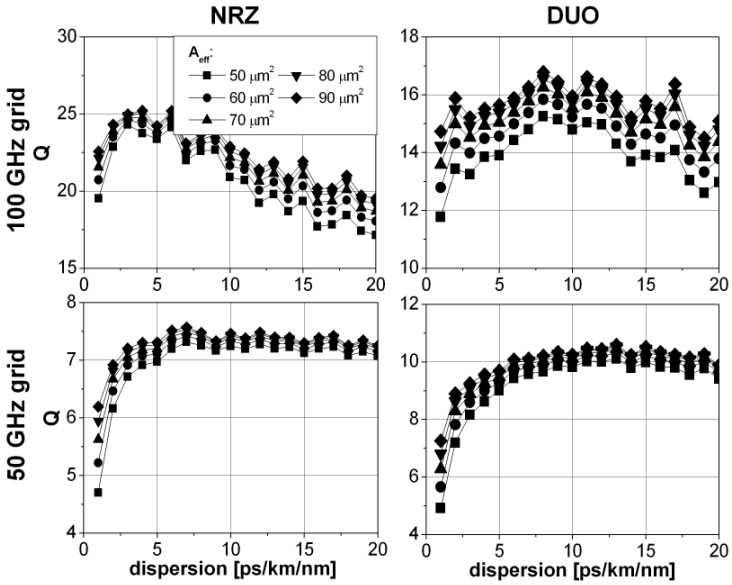

Figure 6.22: NRZ-based modulation formats in 4x40 Gb/s WDM and DWDM systems - optimized fiber settings (A_{eff}, D) investigations over 2x80 km transmission line with a pure dispersion post-compensation (linear Q_{ISI} evaluation, with ASE-noise, P_{SMF} and P_{DCF} settings from Tables 6.1 and 6.2)

Figure 6.22 depicts the results of fiber parameter investigations for NRZ and duobinary based WDM and DWDM transmissions. According to the different nature of dominant propagation limitations, different optimum fiber parameters can be observed in 100 and 50 GHz channel spacing transmission. As already shown, the 100 GHz case suffers from strong single channel limitations, which in NRZ-based formats appear in form of a strong SPM-GVD interplay. The consequence is that both modulation formats favor transmission fibers with a lower dispersion of 4..6 ps/nm·km. Comparing these results with single channel investigations, a good agreement can be observed (Chapter 5). It must be noticed, that in NRZ modulation the fiber dispersion represents the dominant fiber parameter, whereas the core area A_{eff} indicates reduced importance for transmission performance. This can be explained by relatively low power settings used in these investigations

(Tables 6.1 and 6.2). Here, the transmission performance benefits from the reduced SPM-GVD effect and a reduced PM-IM conversion caused by a reduced fiber dispersion. In the duobinary case, the dependence on fiber core area becomes more evident, due to a reduced nonlinear tolerance of duobinary modulation to single channel limitations. These results are in a good agreement with recently presented numerical and experimental works [232], [94].
By reducing the channel spacing to 50 GHz, the multi-channel effects (e.g. XPM, FWM) prevail and partly mask the single channel limitations. Contrary to the 100 GHz case, the increase of fiber dispersion in DWDM systems (Fig. 6.22) enables an efficient suppression of multi-channel effects, hence fibers with possibly large dispersion represent the best choice, which can be confirmed by experimental results [258]. It can be observed that above a certain dispersion value (e.g. D=5 ps/nm·km), only slight changes in total performance occur. For lower dispersion values, FWM and XPM dominate the transmission performance according to dense channel spacing. The phase-mismatch caused by an increased local dispersion efficiently reduces FWM and to some extent XPM effects as well, but a dispersion map dependent part of XPM remains. According to a reduced impact of A_{eff}, it can be expected that as long as the fiber dispersion is larger than 5 ps/nm·km different fibers types will perform similar. On the other hand, the choice of the optimum transmission fibers will be dispersion map sensitive, due to different interactions of propagation disturbances with the deployed dispersion compensation scheme.
In order to verify this, additional investigations were performed, considering three typical fiber types (as in the single channel case, Table 6.3) - SSMF, NZDSF1 and NZDSF2 - in conventional dispersion compensation schemes, e.g. pre-, hybrid-, and post-compensation. For each fiber type and each dispersion compensation scheme, an investigation identical to Fig. 6.22 is made. For a better understanding, the results are presented in a different manner (Fig. 6.23), attempting to show the dependence of the optimum fiber type on dispersion maps used in transmission line.

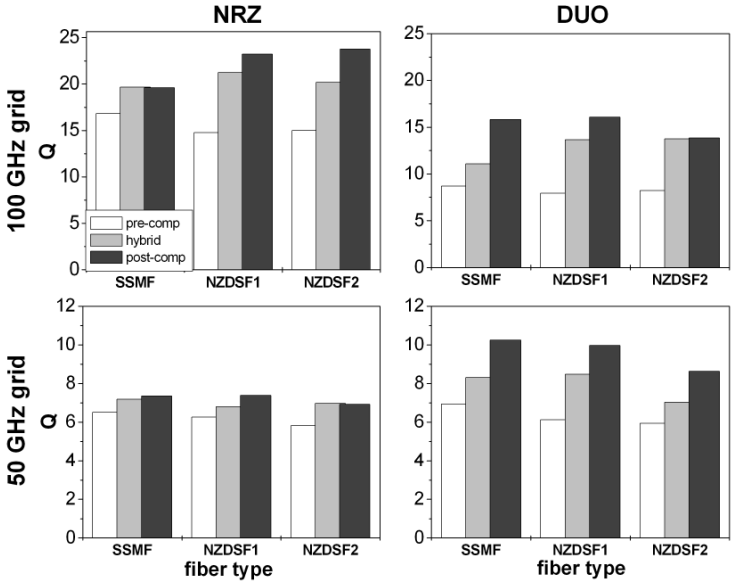

Figure 6.23: NRZ-based formats 4x40 Gb/s 2x80 km - optimum dispersion compensation for different transmission fiber types (linear Q_{ISI} evaluation, with ASE-noise, P_{SMF} and P_{DCF} settings from Tables 6.1 and 6.2, fiber parameters from Table 6.3)

The results for both modulation formats and both channel spacings indicate the dispersion post-compensation scheme as the optimum among the three independent from the transmission fiber and channel spacing. At 100 GHz channel spacing, the effect of the dispersion map on the optimum transmission fiber can be clearly seen, especially in NRZ case. It can be observed that in post-compensation a reduced fiber dispersion is beneficial for total performance, owing to strong SPM impact. On the other hand, in the case of pure dispersion

	Fiber parameters						
fiber type	α [dB/km]	β_2 [ps^2/km]	β_3 [ps^3/km]	D [ps/nm · km]	S [ps/nm^2 · km]	γ [1/Wkm]	A_{eff} [μm^2]
SSMF	0.22	-20.41	0.164	16	0.08	1.32	80
NZDSF1	0.21	-10.2	0.082	8	0.04	1.68	62.7
NZDSF2	0.25	-5.36	0.043	4.2	0.021	2.05	51.3
DCF	0.5	114.79	-0.925	-90	-0.45	3.51	30

Table 6.3: Fiber parameters

pre-compensation scheme, where the interaction of pre-compensation caused pulse disturbances and non-linearities takes place, SSMF indicates better performance due better nonlinear characteristics. Duobinary based transmission at 100 GHz benefits from larger fiber effective area, thus explaining better transmission characteristics in SSMF and NZDSF1 in comparison with NZDSF2.
The differences of optimum fiber type for NRZ modulation vanish at a reduced channel spacing (50 GHz, Fig. 6.23), which implies increased impact of multi-channel nonlinearities and narrow-band filtering. Duobinary based 40 Gb/s DWDM systems favor transmission fibers with a larger dispersion (Fig. 6.23) and better non-linear characteristics. For all investigated transmission fibers, the performance differences between dispersion maps are unique, indicating dispersion post-compensation as the optimum scheme in all cases.
According to its better tolerance to XPM effects [259], SSMF fibers represent the best choice fiber at 50 GHz channel spacing. It can be observed that performance differences between SSMF and NZDSF1 are rather small, which can be explained by the fact that in the 40 Gb/s based DWDM case, as long the fiber dispersion is larger than a certain value (e.g. 5 ps/nm·km), the differences between fiber types for investigated power settings are less critical for a total transmission performance.

6.7.2 RZ-based modulation formats

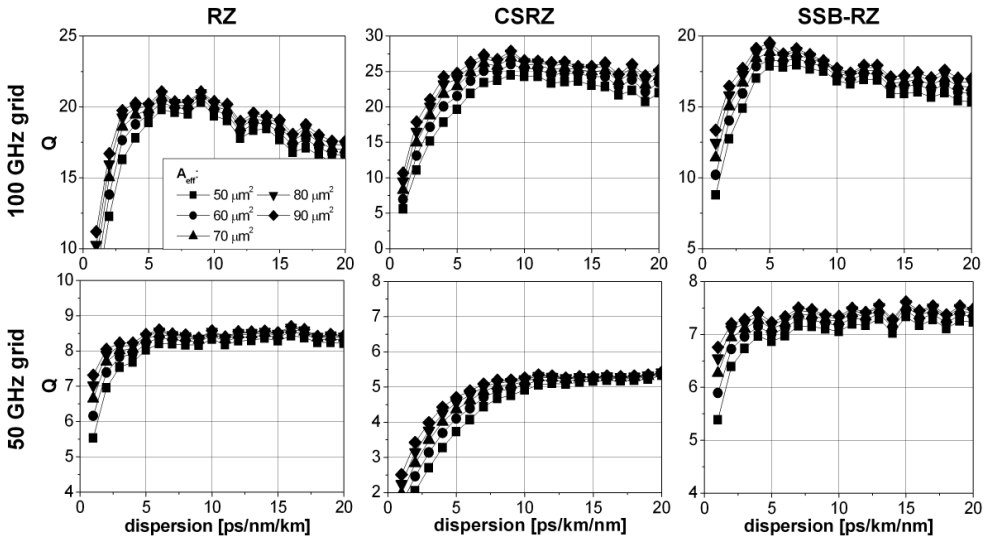

Figure 6.24: RZ-based modulation formats in 4x40 Gb/s WDM and DWDM systems - optimized fiber settings (A_{eff}, D) investigations over 2x80 km transmission line with a pure dispersion post-compensation (linear Q_{ISI} evaluation, with ASE-noise, P_{SMF} and P_{DCF} settings from Tables 6.1 and 6.2)

Due to the faster pulse broadening as a characteristic of RZ-based modulation formats, it can be expected

that as long as single channel limitations represent the dominant propagation limitation, the optimum fiber has to be robust to intra-channel effects (IXPM, IFWM). Having in mind, that 40 Gb/s WDM systems with a 100 GHz channel spacing are dominated by single channel effects, justifying similarities to results of single channel investigations, the system performance would be improved by the use of fibers with a moderate dispersion. This expectation was confirmed by numerical simulations (Fig. 6.24). It can be observed that all RZ-based formats favorite lower dispersions (4..8 ps/nm·km), but for extremely low dispersion values (<4 ps/nm·km) the multi-channel effects become evident (especially FWM). Lower dispersion values enable reduction of intra-channel caused interactions between consecutive pulses, resulting in a suppression of timing jitter as a consequence of IXPM. The impacts of IFWM are, as in the single channel case, less critical due to the periodical dispersion compensation on a span-by-span basis [230] implemented in the investigated system setup. CSRZ modulated pulses at 100 GHz channel spacing show optimum performance in a larger dispersion region compared to RZ and SSB-RZ pulses, which can be explained by better tolerance of CSRZ to intra-channel effects due to the phase inversion between adjacent pulses. As in NRZ-based investigations, the transmission characteristics of the system are governed by fiber dispersion, where the effect of fiber core area can be almost neglected.
At 50 GHz channel spacing, all investigated RZ formats show explicitly that transmission fibers have to possess larger dispersion (>8 ps/nm·km) for an efficient suppression of XPM effects between densely spaced channels. The RZ pulse shape distortion caused by narrow-band filtering explains the similarity of optimum dispersion region to NRZ-based cases (Fig. 6.22). CSRZ modulation indicates a similar optimum dispersion region, although the RZ pulse shape is retained (Fig. 6.17). This can be explained by the fact that narrow-band filtering distorts the phase-relations between the pulses, resulting in vanishing of the large nonlinear tolerance of CSRZ pulses. In all investigated RZ cases, the transmission performance is widely independent of the fiber's core area for investigated power settings.

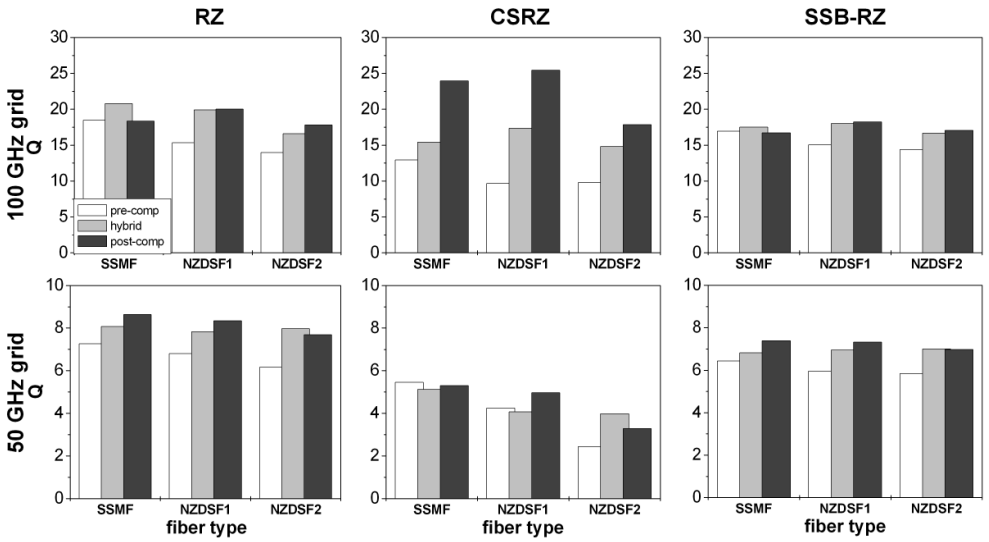

Figure 6.25: RZ-based formats 4x40 Gb/s 2x80 km - optimum dispersion compensation for different transmission fiber types (linear Q_{ISI} evaluation, with ASE-noise, P_{SMF} and P_{DCF} settings from Tables 6.1 and 6.2, fiber parameters from Table 6.3)

Further investigations (Fig. 6.25) of different dispersion compensation schemes in transmission spans are done in order to check the validity of the results presented above for different transmission fibers. For a channel spacing of 100 GHz, it can be generally observed (Fig. 6.25) that fibers with medium dispersion values perform better. A slight deviation from this behavior is evident in a dispersion pre-compensation scheme, where reduced nonlinearities in SSMF fibers and large fiber dispersion can be beneficial. The results

indicate that dispersion-post compensation is the best dispersion map among all investigated, but it can be expected that an even better performance can be achieved considering the optimum dispersion scheme, which in 100 GHz spaced systems is characterized by a small amount of pre-compensation (Fig. 6.16). The rather small differences between investigated dispersion schemes at 100 GHz can be explained by the short transmission distances considered here. Further investigations showed that with an increased transmission length, relation between different dispersion compensation schemes is maintained.
In the investigated RZ-based 40 Gb/s DWDM systems with 50 GHz channel spacing, SSMF fibers could be identified as the best choice, but other considered fibers show, according to the short distance and a fiber dispersion larger than 4 ps/nm·km similar characteristics. Although the dispersion in NZDSFs is lower by a factor of two and four, respectively, than SSMF dispersion, the expected increase of FWM efficiency was rather small in all investigated cases.
Comparing optimum fiber results for NRZ- and RZ-based modulation formats at different channel spacings, it can be observed that the performance differences are rather small at 100 GHz spacing, because both group of formats favor fibers with moderate dispersion. Differences between the formats disappear in DWDM systems, where the same disturbance mechanism (e.g. XPM) dominates both groups of modulation formats. Analyzing the presented results from the system upgrade (channel spacing 100 → 50 GHz) point of view, it can be concluded that transmission fibers with a dispersion of >8 ps/nm·km and a possibly large core area would be a good solution for WDM systems with a spectral efficiency larger than 0.4 bit/s/Hz. This confirms conventional SSMFs as a good candidate for the next generation WDM and DWDM systems. Thereby, a further improvement of transmission performance can be expected, if sophisticated in-line dispersion compensation schemes, e.g. all-at-the-end dispersion compensation [72] or different dispersion schemes per span [260], in combination with distributed [261] or symmetrical optical amplification [126] are implemented in the transmission line.

6.7.3 Novel modulation formats

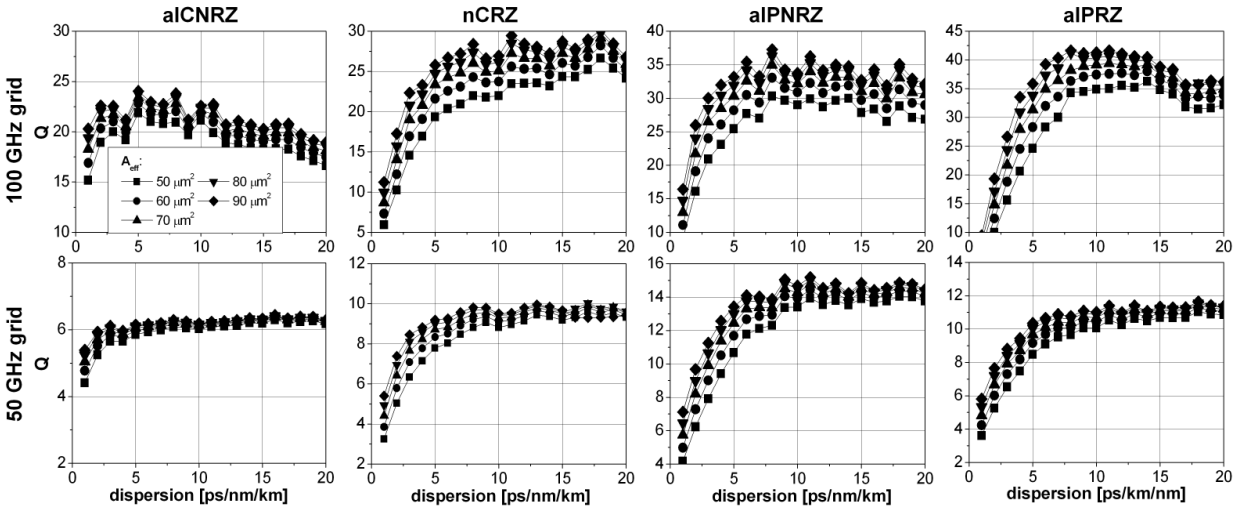

Figure 6.26: Novel modulation formats in 4x40 Gb/s WDM and DWDM systems - optimized fiber settings (A_{eff}, D) investigations over 2x80 km with a pure dispersion post-compensation (linear Q_{ISI} evaluation, with ASE-noise, P_{SMF} and P_{DCF} settings from Tables 6.1 and 6.2)

Figure 6.26 illustrates the results of optimum fiber investigations for novel modulation formats based 40 Gb/s WDM and DWDM systems. It can be observed that the implementation of phase or polarization modulation in conventional NRZ and RZ formats can improve their tolerance to large fiber dispersion in transmission lines with 100 GHz channel spacing. This can be explained by the fact that phase and polarization modulation

between adjacent bits enables a suppression of both intra-pulse distortions (SPM) as well as intra-channel distortions, which are characteristic for fast dispersing 40 Gb/s pulses. The consequence of this behavior is that dispersion limitations observed in conventional NRZ- and RZ-based 100 GHz spaced transmissions become slightly relaxed, thus enabling an improved transmission performance even over conventionally deployed SSMFs, which basically do not represent the best choice fiber for this channel spacing. Furthermore, by using novel modulation formats, the already deployed fiber infrastructure can be used for next generation systems. At this point, it must be stated that further investigations have to be made considering PMD effects in the transmission fiber, in order to prove the general validity of this statement. The novel modulation formats investigations considering a reduced channel spacing show no significant changes in transmission behavior compared to NRZ- and RZ-based investigations. Again, transmission performance profits from large fiber dispersion values due to the XPM limitations in line, indicating conventional SSMF fibers as best choice solutions. It can be observed that implementation of polarization switching enables much better transmission performance compared to conventional formats at 50 GHz channel spacing. This is due to the fact that the nonlinearities (e.g. XPM) become partly averaged using orthogonal polarizations [68]. Novel format investigations at 50 GHz channel spacing indicate once more that as long as propagation disturbances arise from the same transmission effect, the identical transmission fiber represent the optimum choice for different modulation formats, and the fiber dispersion represents the dominant fiber parameter.

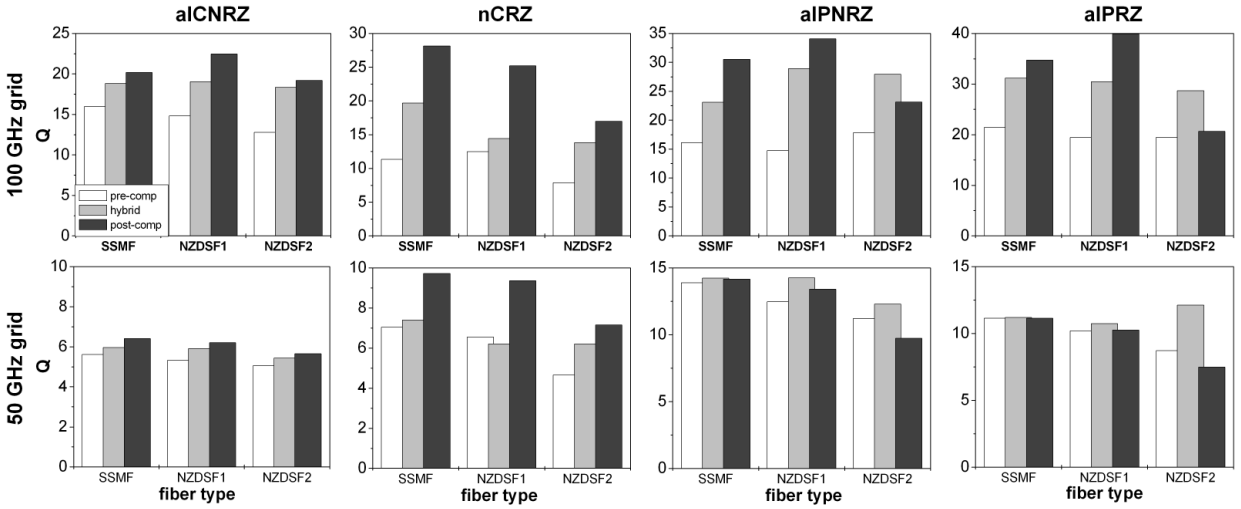

Figure 6.27: Novel modulation formats 4x40 Gb/s 2x80 km - optimum dispersion compensation for different transmission fiber types (linear Q_{ISI} evaluation, with ASE-noise, P_{SMF} and P_{DCF} settings from Tables 6.1 and 6.2, fiber parameter from Table 6.3)

Further investigations were performed in order to analyze the optimum fiber dependence on the dispersion map at 100 and 50 GHz channel spacing. The presented results (Fig. 6.27) for three conventional dispersion maps indicate that the right transmission fiber choice is dependent on the dispersion map in use. This is especially the case in WDM systems with 100 GHz channel spacing, due to the fact that all investigated fiber type, show dispersion map dependent propagation limitations (Fig. 6.27). This makes the determination of the optimum fiber type for 100 GHz channel spacing case-sensitive and difficult. Considering, transmission performance differences between different maps, in can be seen that dispersion post-compensation brings benefits in comparison with other schemes. Exception from this behavior can be observed in case of NZDFS2 fibers in alPNRZ and alPRZ cases, where transmission performance in hybrid compensation is better than in pure post-compensation. For these two formats, it was observed that the optimum amount of dispersion pre-compensation is relatively large (approximately, 30 %) and that pure post-compensation does not represents the optimum solution. Similar behavior was observed at a reduced channel spacing as well (Fig. 6.27). This effect can be explained by low local dispersion and poor nonlinear characteristics of NZFDS2 fibers.

Considering DWDM propagation at 50 GHz channel spacing, SSMF in a pure dispersion post-compensation represents the best choice solutions independently of the modulation format in use, due to the strong suppression of XPM caused disturbance.

6.8 Transmission performance investigations

In previous sections of this chapter, the optimization of various system parameters (e.g. filter settings, dispersion map, transmission fiber) are done considering different modulation formats and channel spacings of 100 and 50 GHz. Using insights from these investigations, 4x40 Gb/s WDM systems are designed considering various optimum system settings for all modulation formats, in order to investigate their total system performances at 100 and 50 GHz channel spacing. The 100 GHz channel spacing investigations are characterized by dispersion maps with a certain amount of pre-compensation (Table 6.4) realized with transmission fibers with various local dispersion (D=4..16 ps/nm·km) in transmission fiber, depending on the modulation format. The P_{DCF} used in this investigation are slightly different from the values in Table 6.1, where the optimum DCF powers for pure dispersion post-compensation are presented.
Common to all investigations at 50 GHz channel spacing is the use of SSMF fibers in the transmission line, whose local dispersion is compensated in a span-by-span full post-compensation scheme. The P_{DCF} values used to 50 GHz investigations are presented in Table 6.2. In all investigation the fiber core area is set to 80 μm^2. The target of this investigation is a possibly fair comparison between different modulation formats in multi-span 40 Gb/s based WDM and DWDM transmission lines. The results are presented separately for NRZ-based, RZ-based and novel modulation formats.

Modulation format	pre-comp. [%]	P_{DCF}@100GHz [dBm/ch]	P_{DCF}@50GHz [dBm/ch]	D@100GHz [ps/nm·km]
alCNRZ	30	-6	-5	10
alPNRZ	15	-2	-3	11
alPRZ	10	-2	-3	11
CSRZ	5	-3	-6	8
DUO	20	-6	-5	13
nCRZ	15	-2	-4	12
NRZ	30	-6	-5	8
RZ	40	-5	-4	16
SSB-RZ	40	-5	-5	16

Table 6.4: 4x40 Gb/s Optimum dispersion pre-compensation and power settings of dispersion compensating fibers (D@50GHz=16 ps/nm·km, 2x80 km transmission fiber)

6.8.1 NRZ-based modulation formats

The total transmission performances of NRZ-based modulation formats in 4x40 Gb/s based WDM and DWDM systems over 4x80 km transmission fiber are illustrated in Fig. 6.28. Considering transmission at 100 GHz channel spacing, both modulation formats show good transmission performance characterized by larger power tolerance at Q=6 (large dynamic range values) and large achievable Q-values. Comparing these results to transmission performance investigations in 40 Gb/s single channel transmission (Fig. 5.16), a similar transmission behaviour can be observed, hence justifying the domination of single channel limitations at 100 GHz channel spacing. Both formats have similar dynamic range values (Table 6.5), thus implying a similar maximum transmission distance of approximately ≈2500 km according to the dynamic range (DR)-rule (Chapter 4) defined as:

$$\mathrm{DR\,[dB]} = P_{max}@(\mathrm{Q}=6) - P_{min}@(\mathrm{Q}=6) \tag{6.3}$$

Optimum channel power, defined as power at the maximum Q-value, equals 2 dBm/ch for both modulation formats. The transmission investigations at 50 GHz channel spacing indicate large transmission penalty compared to the 100 GHz case and reduction of total dynamic range values. The duobinary modulation shows slightly better transmission characteristics than NRZ, due to better tolerance to the narrow-band filtering, which results in less distortions of signal shape and less ISI-effects between consecutive pulses.
An increased spectral efficiency causes a reduction of the maximum transmission distance to 1800 km according to the DR-rule. The increased XPM-impact in 50 GHz based systems results in a shift of the optimum power per channel to lower power regions (0 dBm/ch). Trying to identify the consequences of increased spectral efficiency on the system design, it can be said that the increased spectral efficiency can be achieved at the cost of maximum transmission distance.

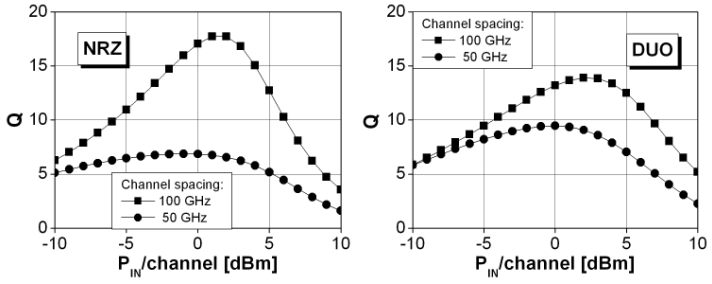

Figure 6.28: Transmission performance of NRZ-based modulation formats 100/50 GHz grids 4x40 Gb/s over 4x80 km with optimized system settings (linear Q_{ISI} evaluation, fiber dispersion and DCF power settings from Table 6.4, with ASE-noise)

	Dynamic range [dB]	
Format	100 GHz grid	50 GHz grid
alCNRZ	≈ 18.9	–
alPNRZ	≈ 26.5	≈18.6
alPRZ	≈ 28.4	16.8
CSRZ	≈ 21.9	–
DUO	≈ 19.2	15.8
nCRZ	≈ 20.6	13.6
NRZ	≈ 18.5	10.5
RZ (τ=0.5)	≈ 19.5	12.6
SSB-RZ	≈ 17.8	9.4

Table 6.5: Dynamic ranges for 4x40 Gb/s WDM over 4x80 km with 100 and 50 GHz channel spacing

6.8.2 RZ-based modulation formats

Figure 6.29 depicts the results of total performance investigations considering RZ-based modulation formats. Comparing these results to previous NRZ-based WDM transmission, a large performance improvement can be observed especially for CSRZ signal modulation, which in terms of optimum channel power (≈5 dBm/ch) and dynamic range (≈22 dB) significantly outperforms the other two formats (RZ and SSB-RZ). The transmission performance is very similar to the single channel case investigation. This performance relation among all investigated RZ-based formats gets lost with a reduction of the channel spacing to 50 GHz. While RZ and SSB-RZ in DWDM transmission show similar behavior due to similar narrow-band filtering caused pulse shape distortions, the performance of CSRZ becomes reduced compared to the 100 GHz case despite of

maintained RZ pulse shape, resulting in vanishing of the dynamic range (Q<6) in the CSRZ transmission case. It is obvious that the advantages of RZ-based modulation formats observed in single channel and 100 GHz WDM transmission vanish at reduced channel spacing, and the total transmission performance becomes even worse that in NRZ-based systems, thus making the use of RZ-based formats rather questionable for spectrally efficient 40 Gb/s DWDM systems.

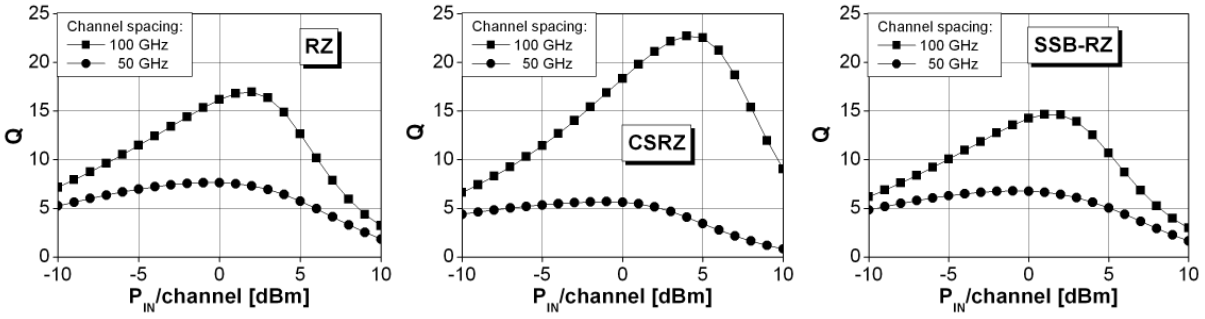

Figure 6.29: Transmission performance of RZ-based modulation formats 4x40 Gb/s 100/50 GHz grids over 4x80 km with optimized system settings (linear Q_{ISI} evaluation, fiber dispersion and DCF power settings from Table 6.4, with ASE-noise)

For the WDM and DWDM investigations presented here, a duty cycle of τ=0.5 was considered for all RZ-based formats. In single channel investigations, the reduction of the pulse duty cycle enables a performance improvement due to the suppression of single-channel limitations, but it is questionable if this behavior remains maintained in WDM systems.

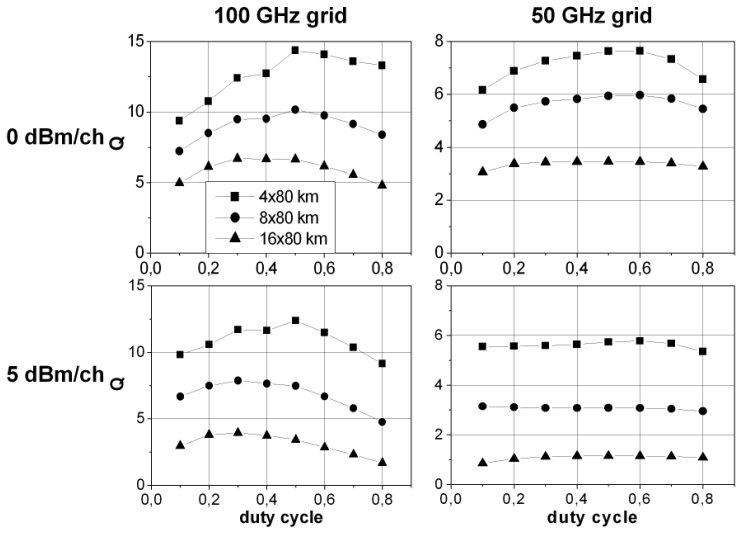

Figure 6.30: Impact of duty cycle in RZ pulses on the transmission performance (Q_{ISI} evaluation, with ASE-noise, 80 km SSMF based spans, full dispersion post-compensation scheme, P_{DCF}=-6 dBm)

In order to investigate the effects of duty cycle on transmission performance in RZ-based WDM systems, the optimization of filter settings is done for different duty cycles. Using optimized filter settings for each duty cycle value in a post-dispersion compensated transmission over 4x80 km SSMF fiber, the transmission behaviour of pulses with different duty cycles is investigated considering two power values - 0 and 5 dBm/ch

- in order to focus on two different propagation regimes - linearly and nonlinearly dominated. The results of this investigation considering an increased transmission length (from 4..16x80 km) are presented in Fig. 6.30. It can be observed that for a channel power of 0 dBm/ch both 100 and 50 GHz spaced transmission benefit from increased duty cycles. This can be explained by the fact that in this transmission regime the linear effects (e.g. ASE-noise) dominate the pulse propagation and nonlinear impacts can be neglected, thus, according to better linear characteristics (e.g. narrower signal spectrum) of pulses with larger duty cycles, they represent the better solution in this case.
The increase of the channel power (5 dBm/ch, Fig. 6.30 bottom line) manifests differently in 100 and 50 GHz based systems. The transmission performance in the 100 GHz case (Fig. 6.30) benefits from a reduction of the duty cycle due to suppression of single channel effects (e.g. SPM-GVD). In 50 GHz based DWDM systems, the narrow-band filtering caused distortions are significant distorting the RZ pulse shape for all investigated duty cycles, thus resulting in an equal system performance independent of the duty cycle in use (Fig. 6.30). Accordingly, it can be concluded that pulse width reduction as a method for a performance improvement in 40 Gb/s based transmissions, can be used only in systems without narrow-band filtering affected by strong nonlinear impacts. A similar behavior can be expected in SSB-RZ and CSRZ based WDM systems with a reduced duty cycles.

6.8.3 Novel modulation formats

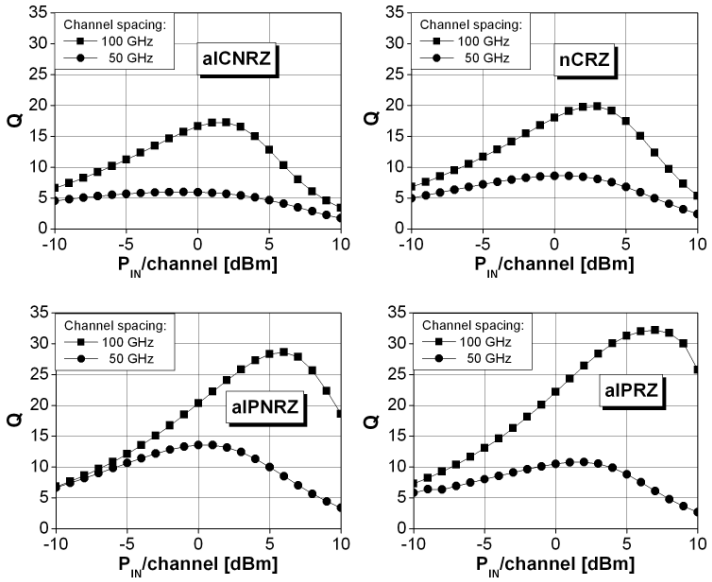

Figure 6.31: Transmission performance of novel modulation formats 4x40 Gb/s 100/50 GHz grids 4x80 km with optimized system settings (linear Q_{ISI} evaluation, fiber dispersion and DCF power settings from Table 6.4, with ASE-noise)

The implementation of novel modulation formats in 40 Gb/s WDM and DWDM transmission lines enables an improvement of total transmission characteristics as well as an enhancement of maximum transmission distance. The results for WDM transmission with 100 GHz channel spacing (Fig. 6.31) indicate no difference to single channel investigations presented previously (Chapter 5). Accordingly, novel modulation formats show for 100 GHz channel spacings excellent transmission characteristics due to the better tolerance to single channel impacts. In terms of optimum power per channel, which, depending on modulation format, equals 3..7 dBm/ch and dynamic range values larger than 18 dB in all investigated cases (Table 6.5), novel modulation formats from case to case significantly outperfrom conventional modulation formats in 100 GHz based

WDM systems. This can be explained by the implementation of polarization switching and phase modulation at the transmitter side, which can efficiently improve the nonlinear tolerance of transmitted pulses affected by single channel limitations e.g. SPM and intra-channel effects. This improvement becomes especially visible in cases of alPNRZ and alPRZ formats which by far showed the best transmission characteristics among all investigated formats.
In DWDM systems with 50 GHz channel spacing, the total performance degrades especially for alCNRZ modulation, which suffer from narrow-band filtering implemented in MUX, but other novel modulation formats indicate large dynamic ranges and improved optimum power values in a region between 0..4 dBm/ch. Comparing the total performance of each novel format, it can be observed that alternatively polarized formats enable a better trade-off between the tolerance to narrow-band filtering and power robustness, indicating first of all alPNRZ as a possible candidate for next generation 40 Gb/s DWDM systems. According to its better filtering tolerance and a pulse shape, which is a mix between RZ and NRZ pulse shape, the alPNRZ show at 50 GHz channel spacing even better characteristics than alPRZ modulation, which becomes highly affected by narrow-band filtering destroying its good transmission characteristics observed in previous investigations at larger channel spacings. The presented results stress that specific novel modulation formats show much better performance compared to conventional formats independently of the number of channels (single channel or WDM) and of the spectral efficiency in 40 Gb/s based transmission lines.

6.9 Investigation of 40 Gb/s based WDM and DWDM long-haul (> 500 km) transmissions

The previous investigations in this chapter, whose target was the optimization of important system settings, considered rather a short total transmission distance (up to 4x80 km). Nevertheless, even these investigations indicated a different transmission behavior of different modulation formats in 40 Gb/s based WDM and DWDM transmission lines.
In order to further highlight the advantages and drawbacks of conventional and novel modulation formats, their transmission characteristics are investigated considering an increased transmission length of up to 10x80 km SSMF, thus enabling an investigation of transmission behavior in the long-haul case. The decision for using SSMF based lines is met according to good transmission characteristics of this fiber type observed previously in WDM and DWDM system. According to investigations of length dependence of optimum dispersion compensation scheme (e.g. Fig. 6.21) it can be expected that optimum dispersion schemes maintain their transmission characteristics even with an increased transmission distance. For long-haul investigations three basic dispersion schemes are considered: post-, hybrid-, and pre-compensation. These compensating schemes are investigated for two different transmission regimes - linear and nonlinear - taking channel powers of 0 and 6 dBm/ch into account, and DCF input powers were set to -6 and 0 dBm/ch, respectively. The performance evaluation is done using receiver sensitivity penalty (RSP), because this evaluation criterion indicates the differences between different transmission behaviors and enables a comparison with presented experimental works dealing with the similar topic.

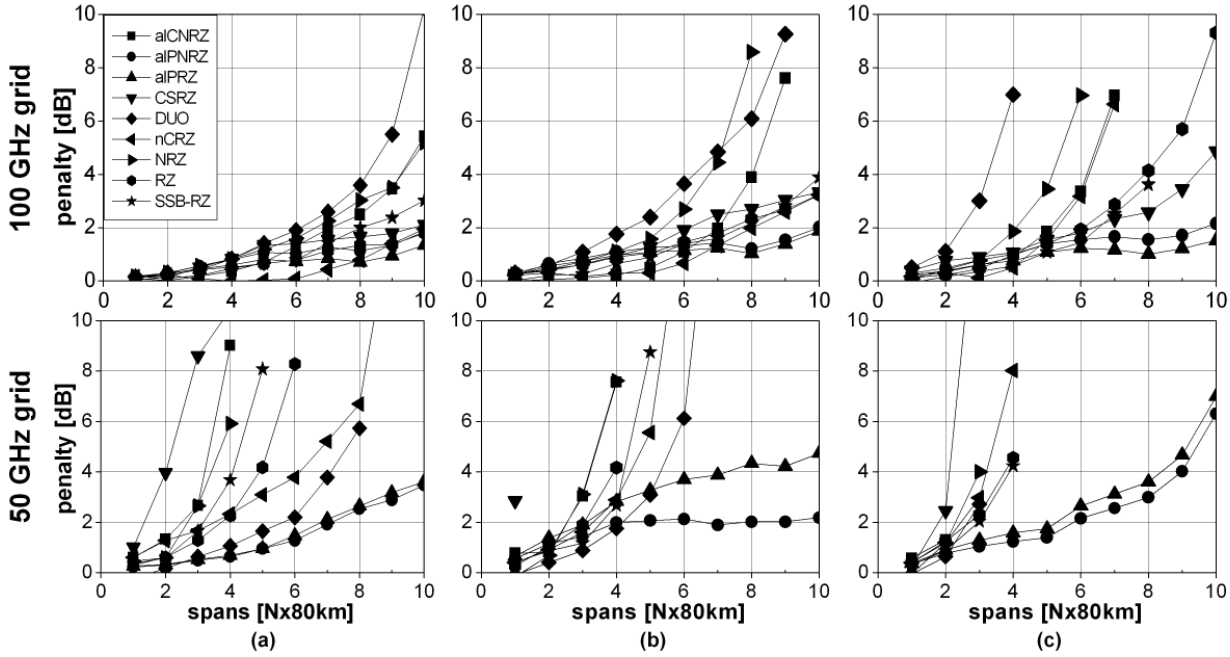

Figure 6.32: Long-haul 4x40 Gb/s transmission performance over multiple cascaded SSMF spans considering various dispersion compensation scheme (P_{IN}=0 dBm/ch, P_{DCF}=-6 dBm/ch, with ASE-noise): a) post- b) hybrid- c) pre-compensation

The results of WDM and DWDM investigations with channel spacings of 100 and 50 GHz for 0 dBm/ch are presented in Fig. 6.32. At 100 GHz channel spacing, all investigated modulation formats reach 10x80 km distance with more or less penalty. The RZ-based and novel modulation formats indicated better transmission characteristics than the NRZ-based formats, due to the better tolerance to single-channel limitations, which represent the dominant disturbance in this case. As in the single channel investigations, the pure post-

compensation shows the best transmission characteristics among all investigated compensation schemes. The transmission behaviour of WDM systems is similar to single channel transmission described in previous chapter. The transmission performance is manly limited by strong impact of IXPM, which accumulates with increasing transmission distance.

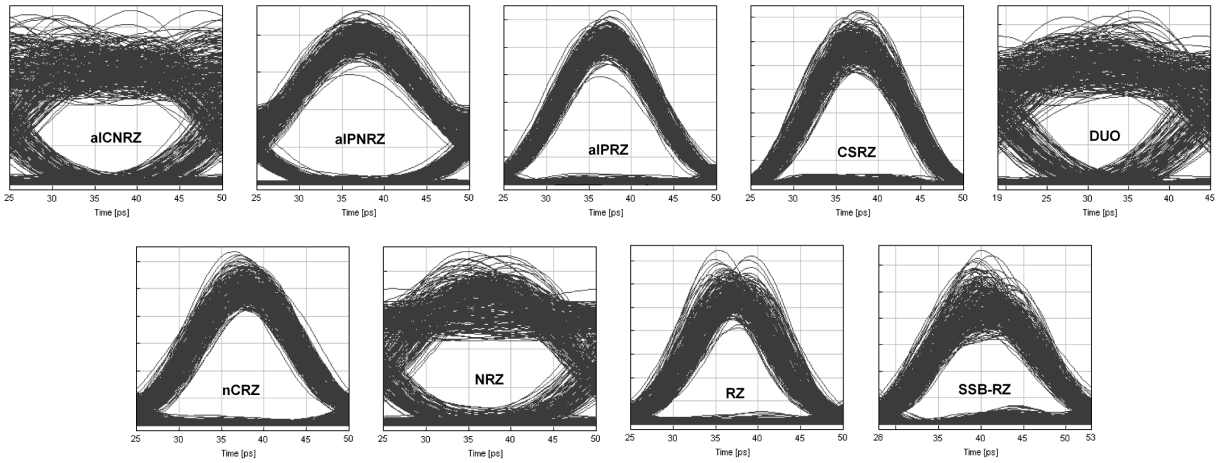

Figure 6.33: Detected optical signal eyes in 4x40 Gb/s transmission (100 GHz grid) after transmission over 10x80 km SSMF in the post-compensation scheme (P_{IN}=0 dBm/ch, P_{DCF}=-6 dBm/ch, with ASE-noise)

The differences between the modulation formats are especially visible for the worst case compensation scheme - pure dispersion pre-compensation, where a large amount of pre-compensation distorts optical pulses before they are fed in the transmission line. The interesting point in this investigation is that novel modulation formats are more tolerant to these disturbances than conventional, basically because the interactions between the pre-compensation caused distortions and fiber nonlinearities is reduced, thus making the compensation of disturbances possible in the following DCF at the end of each span.

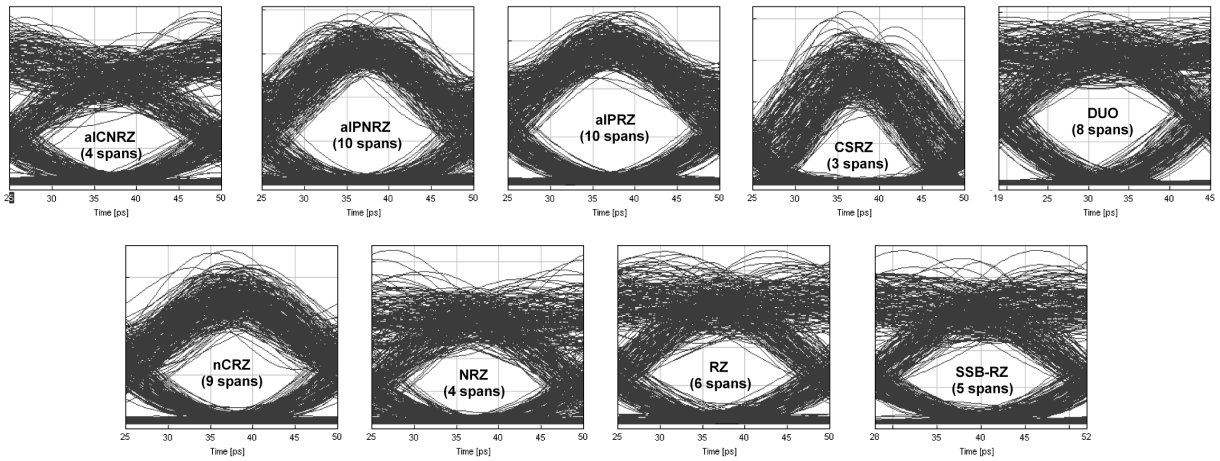

Figure 6.34: Detected optical signal eyes in 4x40 Gb/s transmission (50 GHz grid) at maximum transmission distance over SSMF in the post-compensation scheme (P_{IN}=0 dBm/ch, P_{DCF}=-6 dBm/ch, with ASE-noise)

The investigation of 50 GHz channel spacing (Fig. 6.32) shows quite different behavior compared to the 100 GHz case because of strong filtering effects and increased multi-channel nonlinearities (XPM). Thus, the formats with good filtering tolerance (e.g. duobinary) or an increased power tolerance (e.g. alPRNZ, alPRZ) showed better transmission characteristics in 50 GHz based systems, independently on the dispersion map. Once more, the pure post-compensation shows advantages to other dispersion maps, due to smaller pulse pre-distortions, which in combination with a large local dispersion enables an efficient XPM suppression.
In order to visualize the characteristic pulse distortions generated at 100 and 50 GHz channel spacing, the optical signal eyes are illustrated at the receiver side after 10x80km SSMF transmission in Fig. 6.33 and Fig. 6.34 for all investigated modulation formats. The 100 GHz eyes are characterized by strong timing jitter in all investigated cases. The origin of this jitter can be found in the effects of intra-channel limitations (e.g. IXMP), which accumulate from span to span. Considering 50 GHz eyes, the conventional RZ-based formats (except CSRZ) lose their RZ pulse shape as a consequence of narrow-band filtering, and strong ISI effects can be observed in all other eyes. Duobinary and novel modulation formats indicate wide open eyes even after 10x80 km. It can be observed, that additional multi-channel effects become dominant, resulting in an increased timing jitter compared to the presented 100 GHz eyes.

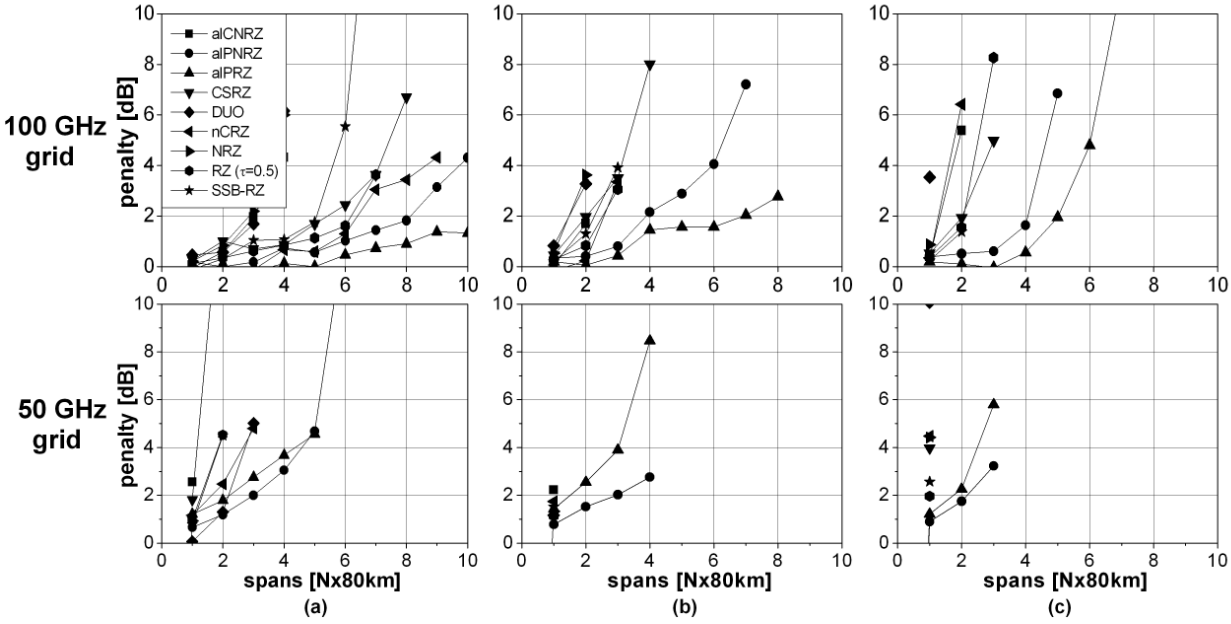

Figure 6.35: Long-haul 4x40 Gb/s transmission performance over cascaded SSMF spans (80 km) considering various dispersion compensation scheme (P_{IN}=6 dBm/ch, P_{DCF}=0 dBm/ch, with ASE-noise): a) post- b) hybrid- c) pre-compensation

The results of long-haul investigations employing 6 dBm/ch channel power are presented in Fig. 6.35. This input power is chosen in order to enable better representation of nonlinear effects within the transmission line and study their dependence from transmission distance. The increase of the channel power induces additional nonlinear effects like strong SPM-GVD interplay at 100 GHz channel spacing and enhances the already observed domination of XPM in transmission with 50 GHz channel spacing. The SPM-GVD impact becomes a dominant limitation in NRZ-based modulation formats at 100 GHz channel spacing, resulting in a significant penalty increase compared to other formats. This can be observed when analyzing the detected optical signal eyes at 100 GHz channel spacing presented in Fig. 6.36. In the case of NRZ, duobinary and alCNRZ, strong signal amplitude fluctuations can be seen at the signal edges as a consequence of the strong SPM-impact. The RZ-based formats deal better with SPM-GVD interplay due to a faster pulse broadening

than in NRZ-based formats, but a larger signal power enhances the intra-channel nonlinearities inducing larger timing jitter in RZ shaped pulses. Novel modulation formats (e.g. alPNRZ, alPRZ) show less penalty increase, because of their better tolerance to single channel (IXPM) as well as to multi-channel limitations (IXPM). Considering dispersion map interaction with fiber nonlinearities, it can be observed that post-compensation represents the best scheme (Fig. 6.35).
The large channel power is more dramatic in DWDM systems, resulting that no modulation format seems to be capable to reach a transmission distance of 10x80 km (Fig. 6.35). The maximum distance reached in this case is 6x80 km achievable by alPRZ and alPNRZ modulation using a dispersion post-compensation scheme. Conventional NRZ- and RZ-based modulation formats suffer even more from nonlinear impacts, resulting in a maximum transmission distance of less than 3x80 km.

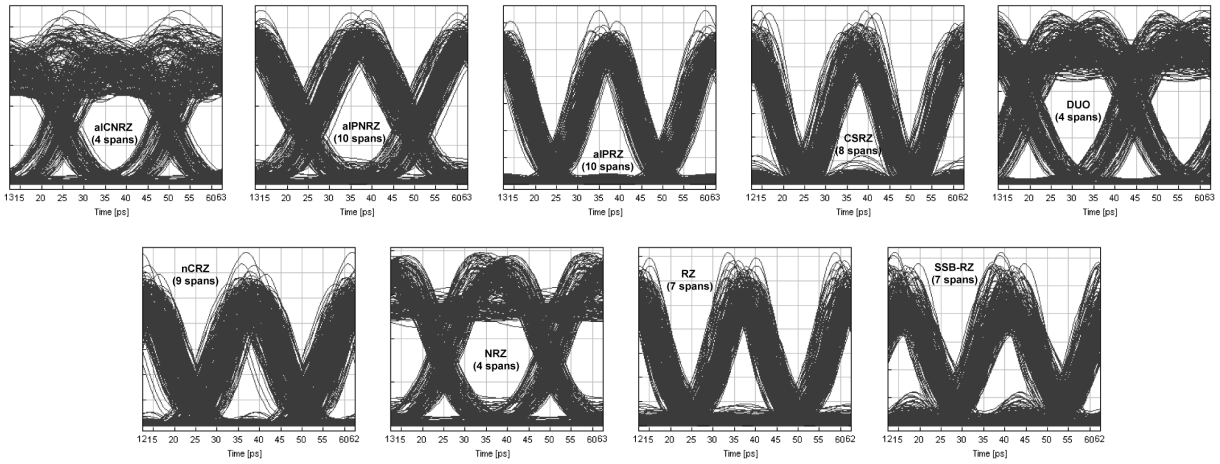

Figure 6.36: Detected optical signal eyes in 4x40 Gb/s transmission (100 GHz grid) at maximum penalty in the post-compensation scheme (P_{IN}=6 dBm/ch, P_{DCF}=0 dBm/ch, with ASE-noise)

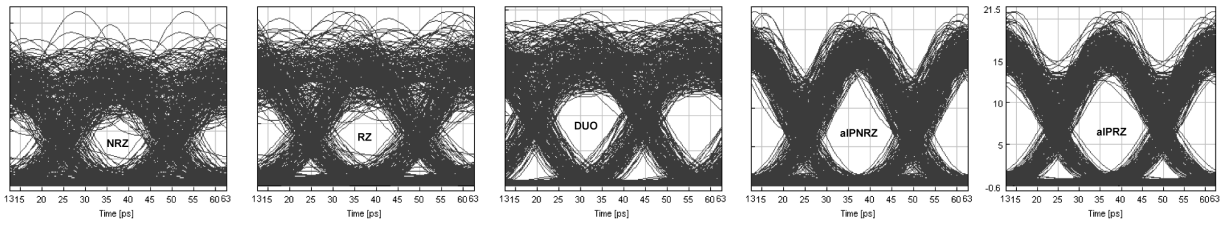

Figure 6.37: Detected optical signal eyes in 4x40 Gb/s transmission (50 GHz grid) after transmission in 10x80 km SSMF in the post-compensation scheme (P_{IN}=6 dBm/ch, P_{DCF}=0 dBm/ch, with ASE-noise)

In order to analyze the dominant distortion in 50 GHz spaced DWDM systems, the optical signal eyes are investigated for selected modulation formats at maximum penalty (Fig. 6.37). It can be observed that, due to a large local dispersion, the amplitude jitter, which represents one of the typical XPM consequences [94], is efficiently suppressed in all shown eyes. While conventional RZ and NRZ signals show significant distortions, duobinary and especially alternate polarized formats (alPNRZ, alPRZ) indicate relatively wide open eyes despite extremely large penalties exceeding 10 dB. Accordingly, due to relatively wide opened eyes it can be concluded that in experimental investigations even better Q-values (BER-values) could be achieved due to the use of specific performance evaluation technique (e.g. BER determination by error counting), and 40 Gb/s DWDM systems over large transmission distances would be feasible.

Indicating timing jitter caused by the inter- and intra-channel interactions as the dominant transmission limitation both in WDM and DWDM 40 Gb/s systems, its generation is investigated over transmission distance (Fig. 6.38). The timing-jitter is calculated as the standard deviation of pulse peaks (Chapter 5, Eq. 5.3). It can be observed that the timing jitter generation in the 50 GHz case is larger than that in 100 GHz. This difference can be explained by strong ISI-effects in the 50 GHz case, which partly enhance timing jitter at pulse edges accompanied by XPM caused jitter accumulation from span to span. As in the single channel investigation, in order to reduce the timing jitter, a certain amount of pre-compensation (Eq. 5.4) is employed at the transmitter side, enabling an under-compensation in each span. The under-compensation or certain amount of pre-compensation enables a decorrelation between the channels at the beginning of each span, resulting in a reduced walk-off length between the channels and hence reduced XPM impact. The residual dispersion is compensated at the receiver side. The investigation shows that this method is efficient for suppression of timing jitter caused by intra-channel effects like IXPM or IFWM, because on one hand the distances between the pulses in the pulse stream become larger, thus reducing the pulse interactions, and on the other hand the accumulation from intra-channel effects in multi-cascaded systems can be efficiently suppressed. Thus, the transmitter sided pre-compensation could be used in 40 Gb/s single channel and WDM transmissions with a reduced spectral efficiency ($\leq$0.4 bit/s/Hz). This observation is in a good agreement with recently presented works [262], [72]. In systems with an increased spectral efficiency (>0.4 bit/s/Hz), the timing jitter is induced by strong XPM-impacts, which can just partly be suppressed by employing pre-compensation at the transmitter side, because of strong ISI-effects and pulse distortions caused by narrow-band filtering. In this case, sophisticated solutions for XPM suppression could be used, e.g. by introducing time delays between the adjacent channels after each span in a fully dispersion compensated line [263], [264] or by a channel-by-channel dispersion compensation enabling constant time delay for each channel in the system [265]. It can be expected that the timing jitter suppression will work better when the signal shape is less distorted by narrow-band filtering. The implementation of transmission fibers with a smaller local dispersion (e.g. NZDSF, DSF) would cause even larger timing-jitter impacts due to increased walk-off lengths between adjacent channels.

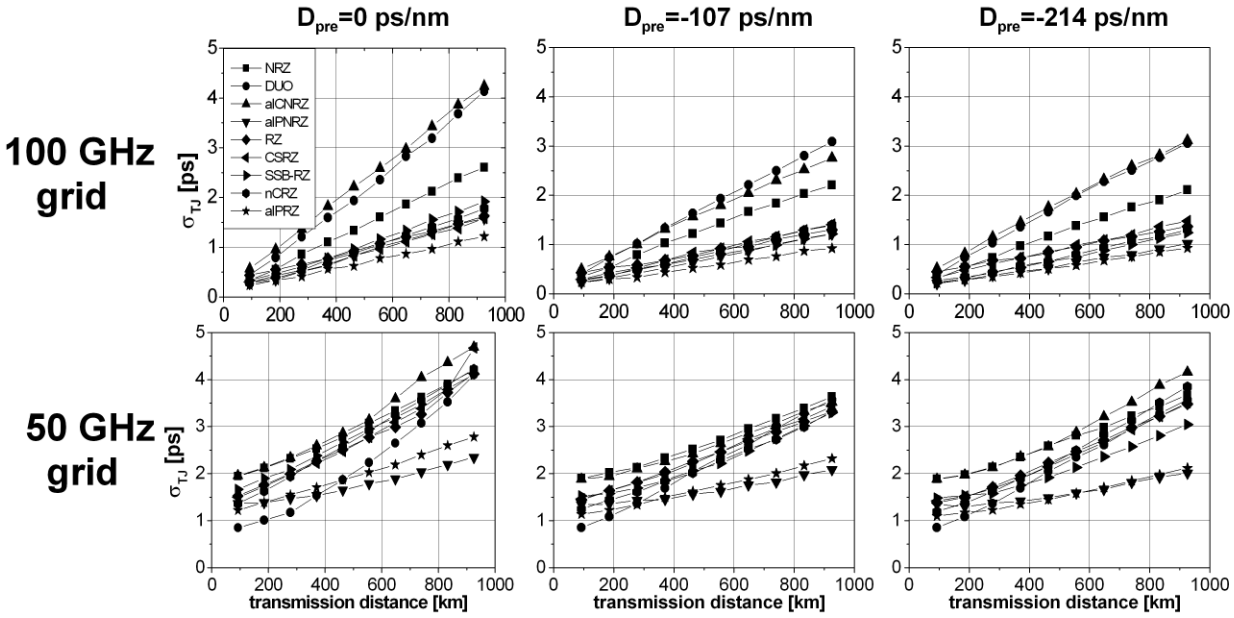

Figure 6.38: Timing jitter suppression in transmission line over Nx80 km SSMF by dispersion pre-compensation at the transmitter side in 40 Gb/s WDM systems with 100/50 channel spacing (P_{IN}=6 dBm/ch, P_{DCF}=0 dBm/ch, with ASE-noise, full dispersion post-compensation per span, rest dispersion compensation at the receiver)

6.10 Conclusions and outlook

The works presented in this chapter, indicated the complexity of a multi-dimensional system design. It is shown that optical narrow-band filtering represents one of the key enabling technologies for 40 Gb/s WDM transmission with an increased spectral efficiency. The narrow-band filtering has to be implemented both at the transmitter as well as at the receiver side. According to narrower and compact signal spectra, NRZ-based modulation formats and derived novel modulation formats show better filtering tolerance than conventional RZ formats. Implementing narrow-band filtering in RZ-based formats makes the differences between NRZ- and RZ-shaped optical pulses disappear, with the consequence that the total transmission characteristics in both cases become similar.
Contrary to single channel investigations, RZ pulses with smaller duty cycle suffer stronger pulse distortions in DWDM systems. Narrow-band filtering can be seen as well as a dominant limitation in case of CSRZ modulated pulses, because the phase relations between adjacent pulses, which make CSRZ modulation more tolerant to nonlinear distortions, are distorted, resulting in the fact that at 50 GHz channel spacing, the signals maintain a CSRZ spectral form and RZ pulse shape, but the transmission characteristics are even worse than in the conventional RZ case.
It was observed that WDM systems employing 100 GHz channel spacing show similar transmission behavior as single channel transmission, which is explained by the domination of single channel limitations, e.g. SPM-GVD interplay and intra-channel limitations. Accordingly, the results of optimum power settings, optimum transmission fiber and optimum dispersion compensation scheme investigations for 100 GHz channel spacing are in a good agreement with presented single channel investigations, hence making a system upgrade from single to multi-channel transmission straightforward for lower spectral efficiency values (<0.5 bit/s/Hz).
The total performance investigation with optimized system settings enabling a fair comparison between different modulation formats, showed that RZ-based and novel modulation formats outperform conventional NRZ formats, independently of the fiber type and dispersion map in use (Fig. 6.39). This transmission behaviour was observed both in short- and long-haul transmission lines. In long-haul transmission, the differences between RZ-based formats vanish, and the advantages of novel modulation formats (especially with alternate polarization) become evident. It was shown that the implementation of some sophisticated dispersion maps, e.g. pre-compensation at the transmitter side combined with in-line dispersion compensation, can enable even further improvement of transmission performance.

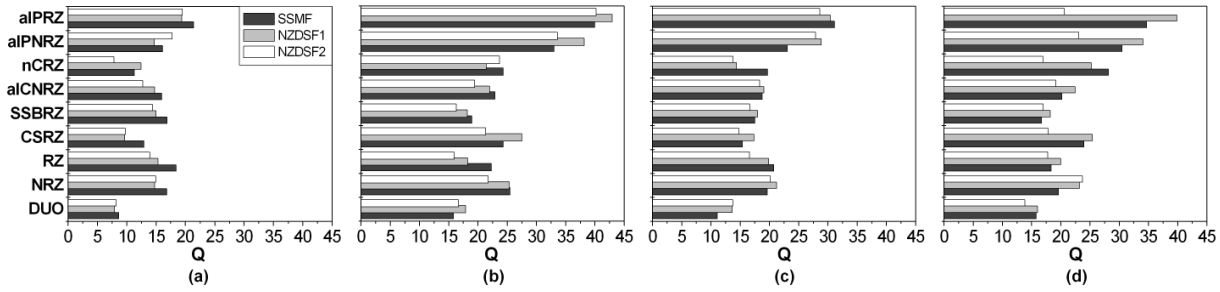

Figure 6.39: All modulation formats 4x40 Gb/s at 100 GHz channel spacing in 2x80 km transmission line (linear Q_{ISI} evaluation, with ASE-noise, P_{SMF} and P_{DCF} settings from Table 6.1, fiber parameter from Table 6.3): a) pre-compensation b) optimum c) hybrid compensation d) post-compensation

Considering transmission at 50 GHz channel spacing, the transmission performance indicates a strong dependence on the transmission fiber and the implemented dispersion map. For a fiber dispersion smaller than 4 ps/nm · km, a strong FWM impact was observed, dominating the propagation characteristics of DWDM systems with XPM. In fibers with dispersion values larger than 4 ps/nm·km, the XPM becomes the dominant limitation, whose impact masks single-channel limitations. The dispersion maps with almost pure-post compensation indicated best transmission characteristics independently of the fiber type and modulation

format. Furthermore, all modulation formats indicated a similar performance dependence on the dispersion map, which is, according to identical span infrastructure used in presented investigations, proportional to the transmission length (number of spans N). The fiber type investigation showed, contrary to 100 GHz investigations, that the optimum fiber type for 40 Gb/s DWDM transmission should possess large dispersion, and fiber dispersion can be identified as the most important fiber parameter. NRZ-based and novel modulation formats show better transmission characteristics than conventional RZ formats (Fig. 6.40) at reduced channel spacing, which can be explained by distortions of RZ pulse shapes and their phase relations. Considering both transmission cases (100 and 50 GHz channel spacing), it becomes evident that novel modulation formats employing phase and polarization modulation can be used as a method for improving of NRZ-based modulation formats, whose good filtering and linear tolerance make them a candidate for realization of 40 Gb/s DWDM systems over already existing fiber infrastructure.

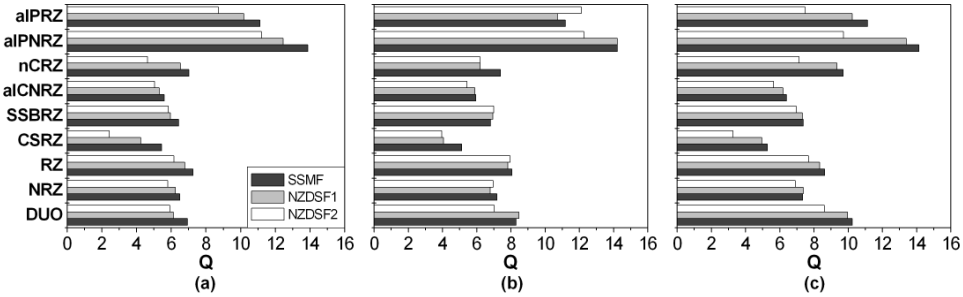

Figure 6.40: All modulation formats 4x40 Gb/s at 50 GHz channel spacing in 2x80 km transmission line (linear Q_{ISI} evaluation, with ASE-noise, P_{SMF} and P_{DCF} settings from Table 6.2, fiber parameter from Table 6.3): a) pre-compensation b) hybrid compensation c) post-compensation

For a more detailed characterization of 40 Gb/s based DWDM systems, further work is needed. As in the single channel case, first of all the PMD effects and their interaction with fiber nonlinearities have to be investigated, because of reduced tolerance of short optical pulses to PMD distortions in the line. The implementation of tunable PMD in-line compensators will depend on the PMD robustness of modulation formats used in 40 Gb/s systems, which would cause increased system complexity and costs. Furthermore, due to the importance of narrow-band filtering for the realization of DWDM systems, the phase characteristics of the filter and their interactions with phase relations between the pulses has to be considered.

7 Enabling technologies for future transmission systems

7.1 Overview

The drawbacks of 40 Gb/s based transmission in terms of a reduced total transmission distance and a reduced robustness to linear disturbances compared to 10 Gb/s based transmissions can be balanced by the use of more sophisticated transmission technologies. After the transmission performance investigations at 40 Gb/s data rate were performed in single channel, WDM and DWDM cases, it can be concluded that a spectral efficiency larger than 0.8 bit/s/Hz represents is a difficult issue in ASK-based transmission systems. The investigations presented in this chapter were performed considering sophisticated technologies and methods, which could enable an enhancement of spectral efficiency beyond 0.8 bit/s/Hz accompanied by an increase in the total system reach. The aim of these works was the identification of promising technologies for next generation optical networks. The requirements for new technologies are a reduced complexity of implementation, low costs, and a compatibility with existing system components. Recently presented works introduce novel enabling technologies: orthogonal polarization between adjacent WDM channels [266], [68]and PSK-based modulation formats (DPSK, DQPSK) [144], [267], which show a potential for an improvement of transmission performance in terms of increasing the maximum transmission distance and enabling better utilization of the system bandwidth. The numerical investigations indicated the advantages and drawbacks of these DWDM enabling technologies. On the beginning, the narrow-band filtering in ASK-based transmission is further investigated in order to find its upper limit considering spectrally efficient ASK modulation formats (e.g. duobinary, alPNRZ, NRZ).

7.2 Narrow-band filtered ASK-based modulation formats

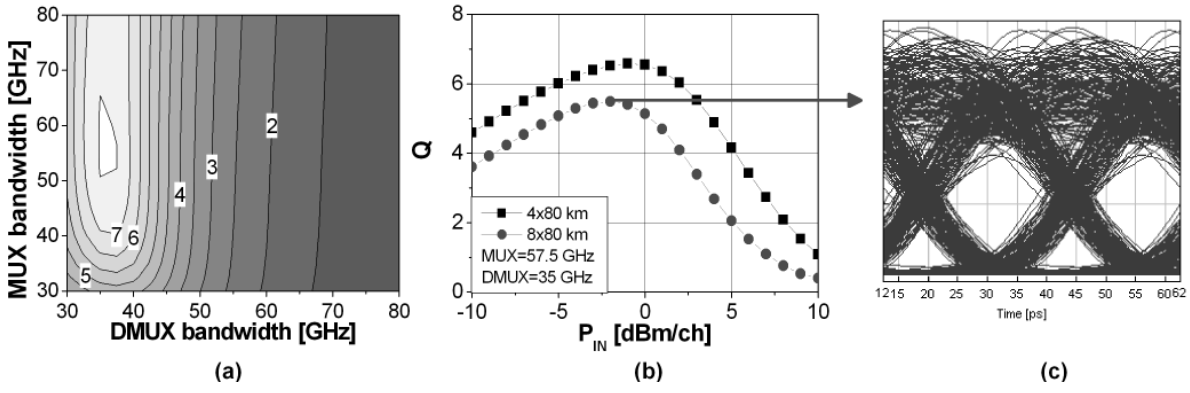

Figure 7.1: 4x40 Gb/s duobinary transmission at 40 GHz channel spacing over SSMF: a) MUX/DMUX optimization b) transmission performance c) detected signal eye after 8x80 km SSMF (P_{IN}=-2 dBm/ch, P_{DCF}=-6 dBm/ch)

The investigations of 40 Gb/s based DWDM systems identified narrow-band filtering both at the transmitter and the receiver side as a key DWDM enabling technology. The narrower-band filtering of ASK-based modulation formats with a small and compact spectral width - NRZ, duobinary, alPNRZ - is performed at a channel spacing of 40 GHz corresponding to a spectral efficiency of 1 bit/s/Hz. Due to its reduced

spectral width, duobinary modulation showed the best filtering tolerance even at this dense channel spacing. The optimized MUX and DMUX filter settings for duobinary modulation presented in Fig. 7.1 indicate the importance of DMUX filtering. Using the optimum filter setting for MUX (MUX_{3dB}=57.5 GHz) and DMUX ($DMUX_{3dB}$=35 GHz) the transmission performance of a 4x40 Gb/s duobinary system at 40 GHz channel spacing is investigated over 4 and 8x80 km SSMF with a span-by-span dispersion post-compensation (Fig. 7.1). In four span transmission, Q values larger than 6 are observed, indicating a dynamic range of ≈6 dB. Enhancing transmission distance to 8x80 km, the Q of 6 is slightly missed, but the detected optical eye at input power of -2 dBm/ch (Fig. 7.1) indicates relatively large eye opening and decision between marks and zeros can be clearly made. The transmission performance of the duobinary based DWDM system with a spectral efficiency of 1 bit/s/Hz can even be improved by the implementation of sophisticated techniques presented in following chapters. Further investigations are made considering alPNRZ and NRZ formats. After optimizing the filter settings for transmission at 40 GHz channel spacing, large signal distortions were observed even in the back-to-back case, identifying that the use of these formats is not recommended in DWDM systems with spectral efficiencies larger than 0.8 bit/s/Hz.

7.3 Orthogonally polarized channels

The investigations of 40 Gb/s based DWDM transmission systems indicated that the dominant transmission limitations are caused by nonlinear interaction between neighboring channels, identifying XPM and FWM (in fibers with a small dispersion) as dominant system limitations and as the barriers for the increased spectral efficiency and transmission reach. Numerous applications e.g. novel fiber types, sophisticated dispersion compensating schemes, or novel modulation formats can be used to suppress inter-channel interactions. A relatively simple and efficient method for suppression of fiber nonlinearities is the orthogonal launch of adjacent channels in a DWDM systems. The orthogonality between relative states of polarization (SOP) in adjacent channel is a proven method for suppression of XPM and FWM effects [68], [268], [266]. This method is widely used in recently presented "hero" transmission experiments for a simple doubling of the spectral efficiency [7], [8], [11], [175]. The orthogonality is realized by coupling even and odd channels using a polarization beam combiner (PBC) at the transmitter side. Contrary to polarization multiplex based transmission requiring special transmitter and receiver configurations, the conventional direct detection receiver can be used at the receiver side in this case. The implementation of polarization orthogonality between neighboring channels enables nearly total FWM suppression and a XPM suppression with a factor of 1/3. In particular, the terms describing XPM for the parallel polarized ($A_{1y} = A_{2y} = 0$) and orthogonally polarized ($A_{1y} = A_{2x} = 0$) channels are given by:

- $A_{1y} = A_{2y} = 0$ (parallel) : $2i\gamma_1 \left|A_{2x}\right|^2 A_{1x}$ and $2i\gamma_2 \left|A_{1x}\right|^2 A_{2x}$
- $A_{1y} = A_{2x} = 0$ (orthogonal) : $\frac{2}{3}i\gamma_1 \left|A_{2y}\right|^2 A_{1x}$ and $\frac{2}{3}i\gamma_2 \left|A_{1x}\right|^2 A_{2y}$

Comparing these terms leads to the conclusion that XPM between two co-propagating waves is reduced by a factor of 1/3 if both waves are orthogonally polarized.
The nonlinear light amplitude E^{NL} can be used for description of the generated FWM light at frequency ω_4, which relates to the originating wave frequencies as $\omega_4 = \omega_1 + \omega_2 - \omega_3$. The total nonlinear amplitude vector is found to be [269]:

$$\mathbf{E}^{NL} = \eta \left|E_1(0)\right| \left|E_2(0)\right| \left|E_3(0)\right| \cdot \left\{\left[\mathbf{e}_2 \cdot \mathbf{e}_3^*\right] \mathbf{e}_1 + \left[\mathbf{e}_1 \cdot \mathbf{e}_3^*\right] \mathbf{e}_2\right\} \tag{7.1}$$

For the case that all waves are identically polarized ($\mathbf{e}_1 = \mathbf{e}_2 = \mathbf{e}_3$), equation (7.1) can be rewritten as:

$$\mathbf{E}^{NL} = 2\eta \left|E_1(0)\right| \left|E_2(0)\right| \left|E_3(0)\right| \cdot \mathbf{e}_1 \tag{7.2}$$

and

$$\left|\mathbf{E}^{NL}\right|^2 = 4\left|\eta\right|^2 \left|E_1(0)\right|^2 \left|E_2(0)\right|^2 \left|E_3(0)\right|^2. \tag{7.3}$$

Similarly, one can obtain the result for the case of two waves being co-polarized and the third being orthogonally polarized from equation (7.1). For $\mathbf{e}_1 \perp \mathbf{e}_2 = \mathbf{e}_3$, it becomes:

$$\left|\mathbf{E}^{NL}\right|^2 = |\eta|^2 \left|E_1(0)\right|^2 \left|E_2(0)\right|^2 \left|E_3(0)\right|^2 \tag{7.4}$$

as $[\mathbf{e}_1 \cdot \mathbf{e}_3] = 0$ and $[\mathbf{e}_2 \cdot \mathbf{e}_3] = 1$ and FWM efficiency drops to 1/4 compared to the case of all waves having identical polarization. For $\mathbf{e}_1 = \mathbf{e}_2 \perp \mathbf{e}_3$, both $[\mathbf{e}_1 \cdot \mathbf{e}_3] = 0$ and $[\mathbf{e}_2 \cdot \mathbf{e}_3] = 0$, and FWM efficiency becomes zero. In the case of $\mathbf{e}_1 = \mathbf{e}_3 \perp \mathbf{e}_2$, FWM efficiency will also become 1/4, but the output polarization of the generated wave will be $\mathbf{e}_2$ instead of $\mathbf{e}_1$.
The drawback of this method is the fact that because of the impact of PMD in the transmission line, the orthogonal channels loss their relative SOPs, caused by PMD-dependent orthogonality distortions even after a short transmission distance [12] because of the frequency (wavelength) dependence of PMD, causing different PMD effects in different channels. This process is governed by the PMD values of transmission fibers, which vary from $0.05\,\mathrm{ps}/\sqrt{\mathrm{km}}$ in new transmission fibers up to $5\,\mathrm{ps}/\sqrt{\mathrm{km}}$ in already deployed ones. At the same time, the polarization orthogonality is dependent on the channel separation, indicating that the polarization orthogonality is maintained over longer distances at a smaller channel spacings [266]. Considering the principal state propagation approximation derived in [266], the channel spacing at which PMD and transmission length start to affect the orthogonality between the channel is given by:

$$\Delta f \approx \frac{1}{4\langle \Delta t \rangle} = \left(4 D_{PMD} \sqrt{L}\right)^{-1} \tag{7.5}$$

where $\langle \Delta t \rangle$ represents the mean DGD and L is the total transmission length. This equation implies that the loss of the orthogonality is independent on the channel data rate. In order to give an insight into length, PMD-, and channel spacing dependent changes of polarization orthogonality in a DWDM transmission, the distribution of SOPs of the two orthogonal channels is investigated.
It must be stated that the numerical investigation of PMD affected transmission represents a difficult issue, because the stochastic nature of PMD has to be numerically modeled. The most widely used method for PMD modeling based on concatenation of PMD characteristics in multiple fiber segments (see chapter 2.3.1) is known as ***coarse-step*** method. This method is realized by concatenation of short pieces of polarization maintaining fiber (PMF), which are connected by polarizations scramblers. Initially, all sections had equal length and birefringence. However, it was shown [270] that this approach leads to a periodic DGD spectrum, thus resulting in a limited practical validity of this approach. This behavior was also observed with the PMD emulator used in this work and is shown in Figure 7.2. With a constant per-section DGD of 1 ps, the DGD spectrum will be periodic in 1 THz intervals. The proposed remedy was to use random section lengths, preferably Gaussian distributed with at least 20 % standard deviation. The effectiveness of this approach is illustrated by the dotted line in Figure 7.2, which no longer shows any periodicities even over a larger spectral range. As the deviation of the Gaussian length distribution is increased, these peaks degrade into a smoother, continuous curve. At 20 % deviation there are no longer peaks discernible.
Figure 7.3 depicts the distribution of SOPs of the two channels versus fiber length. The fiber PMD coefficient was set to $1.0\,\mathrm{ps}/\sqrt{km}$ and the channel spacing was 25 GHz, but the results are scalable for larger PMD values too. The results were plotted using a logarithmic scale. The angle is measured in Stokes coordinates, an angle of 180 degrees corresponding to polarization orthogonality. It can be observed that the polarization orthogonality is lost as early as after only few kilometers into the fiber and the channel polarization separation angle becomes distributed between a decreasing lower bound and orthogonality. The distribution of the polarization separation angles between both channels after propagating 100 km of fiber extends from 0 to 180 degrees. This means that there is a greater-than-zero probability of the benefits of orthogonally polarized channels concerning the reduction of nonlinear interactions to completely vanish at that point. Figure 7.4 illustrates "slices" of Fig. 7.3 taken after fiber lengths of 20, 40, 60, 80 and 100 km. It shows that the probability for the channel polarization to be perfectly orthogonal is only small despite relatively small channel spacing (25 GHz). The mean angle in the curves decreases with distance while its variance increases. Figure 7.5 shows the same slices for a channel separation of 12.5 GHz. Clearly, the distribution's mean increases and its variance decreases as the channel spacing is reduced. Accordingly, a much greater benefit of using orthogonal channels can be expected than with a larger channel spacing. This behavior

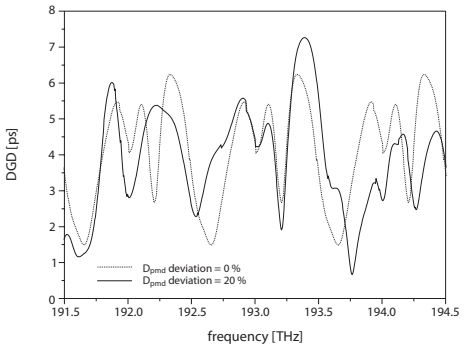

Figure 7.2: DGD vs. freqeuncy for constant (solid line) and Gaussian distributed (dotted line) of PMD coefficients in coarse-step model

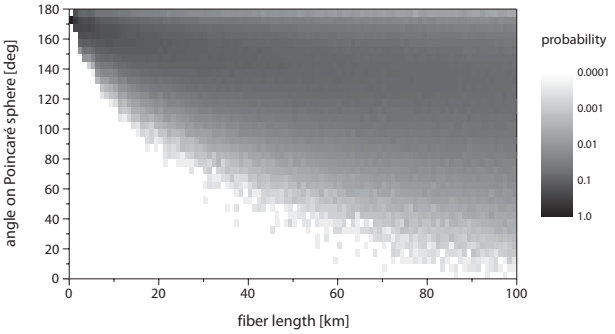

Figure 7.3: polarization angle between channels 25 GHz apart, fiber PMD coefficient 1.0 ps/$\sqrt{\text{km}}$, logarithmic scale

was anticipated, since in the DGD (first-order PMD) simulations, channels separated by smaller channel spacings generally tended to have more similar DGDs. This is due to the fact that the DGD versus carrier frequency plot (Fig. 7.2) is a continuous curve. Fibers with smaller PMD coefficients should also be less affected by PMD orders (both first and higher order). Reduced second-order PMD will still yield different PMD vectors at different wavelengths, but the difference between them is much smaller. The SOP separation between the channels remains large and has a smaller variance than with a PMD coefficient of 1.0 ps/$\sqrt{km}$. Newer fibers exhibit PMD coefficients well below 1.0 ps/$\sqrt{km}$. Therefore, simulations with a PMD coefficient of 0.1 ps/$\sqrt{km}$ were performed [205], showing that with modern fibers, channel spacings of up to 25 GHz are feasible when requiring the benefits of using orthogonally polarized neighboring channels. Accordingly, DWDM systems with smaller channel data rates (e.g. 10 Gb/s) would more profit from the implementation of orthogonal polarization over a large range of distances. But, considering propagation at 40 Gb/s or 160 Gb/s per channel with an increased spectral efficiency (>0.4 bit/s/Hz), it can be expected that the polarization orthogonality, even if new fibers with reduced PMD values are implemented in the transmission line, will be distorted after 100-200 km [271] (even earlier in the 160 Gb/s/ch case), hence indicating the length limitation of polarization orthogonality method as a critical drawback for the implementation in 40 Gb/s and 160 Gb/s based DWDM transmissions.

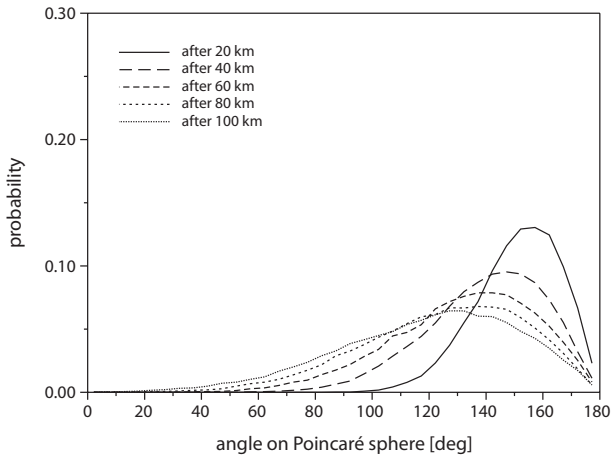

Figure 7.4: polarization angle between channels 25 GHz apart, fiber PMD coefficient 1.0 ps/$\sqrt{\text{km}}$, at 20 km fiber length steps

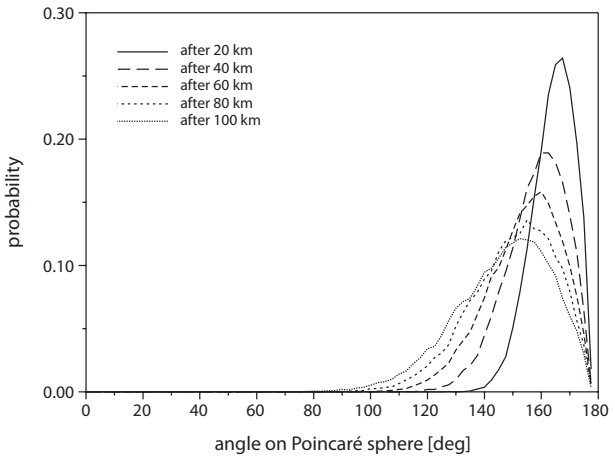

Figure 7.5: polarization angle between channels 12.5 GHz apart, fiber PMD coefficient 1.0 ps/$\sqrt{\text{km}}$, at 20 km fiber length steps

7.4 PSK-based modulation formats

The ever rising demand for transmission bandwidth requires more spectrally efficient and more robust modulation formats for the next generation of high speed optical transmission networks. Recently presented experimental and numerical works [146], [272], [273], [274] showed that phase shift keying (PSK) based modulation formats, e.g. differential PSK (DPSK) or differential quadrature PSK (DQPSK), could represent an alternative to ASK-based modulation techniques for the implementation in DWDM systems with a spectral efficiency larger 0.4 bit/s/Hz. For an improvement of nonlinear characteristics of DPSK and DQPSK modulations, RZ shaping can be used, enabling the generation of RZ-DPSK and RZ-DQPSK modulated signals by an additional amplitude modulation at the transmitter side. Accordingly, the RZ-DPSK pulses show RZ spectral characteristics with a phase shift between consecutive pulses, hence enabling a better suppression of SPM and intra-channel effects. In this case, the power level is not constant like in conventional DPSK case, and the RZ-DPSK pulse stream can be described as a sequence of RZ marks. PSK-based modulation formats enable a better receiver sensitivity due to lower quantum limit values for this kind of signals. The DPSK quantum limit amounts to 20 photons/bit, compared to 38 photons/bit needed for ASK-based signals [144]. Accordingly, the DPSK signals enable approximately 3 dB reduction of the OSNR compared to ASK, resulting in an increase of the system margin. Even further reduction of the DPSK quantum limit is possible in combination with sophisticated FECs [275]. The DQPSK modulation is characterized by half the symbol rate (20 Gb/s for 40 Gb/s signal), resulting in better narrow-band filtering characteristics and an improved dispersion and PMD tolerance [276]. At the same time, the orthogonality between channels can be implemented more efficiently in DQPSK based systems than in ASK or DPSK systems, because of the reduced symbol rate and the increased filtering tolerance, thus enabling improvement of the spectral efficiency and system reach. The generation and signal detection of DPSK and DQPSK signal is made by use of conventional ASK compatible equipment. The major drawback of these modulation formats is the increased complexity at the receiver side, where an interferometric detection is required. Furthermore, the amplitude-to-phase noise conversation (know as Gordon-Mollenauer effect) [277] represents an issue in PSK-based systems, which can become an important transmission limitation in systems with an increased transmission distance and a large number of channels.

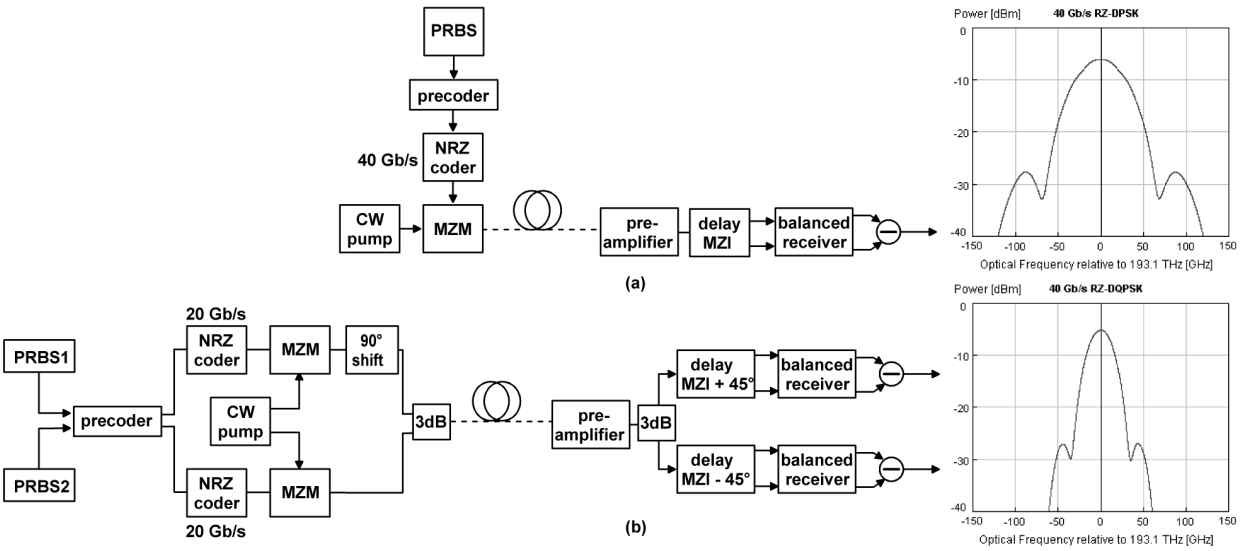

Figure 7.6: Transmitter and receiver setup for (a) DPSK and (b) DQPSK signal generation and detection

The potential of PSK-based modulation formats for enabling spectral efficincies ≥0.8 bit/s/Hz in DWDM systems is recently experimentally shown. Considering DWDM transmission at a channel data rate of 25 Gb/s and 25 GHz channel spacing, RZ-DQPSK experiments [267] demonstrated the maximum transmission dis-

tance of 1200 km at BER=10^{-12} (after employing FEC). Combining DPSK with CSRZ modulation [146], the transmission distance reached 1200 km in a system with 25x40 Gb/s copolarized channels without use of FEC codes. Good transmission characteristics of PSK based formats are maintained even at increased channel rate (e.g. 86 Gb/s or 160 Gb/s) [276], showing an improved chromatic dispersion and nonlinear tolerance of 86 Gb/s RZ-DQPSK compared to both 43 Gb/s NRZ-ASK and 86 Gb/s NRZ-DQPSK systems, and the PMD tolerance was shown to be equal in 43 Gb/s NRZ-ASK and 86 Gb/s RZ-DQPSK systems, as well as significant advantage of RZ-DPSK compared to ASK in 160 Gb/s transmission in terms of the reduced receiver sensitivity [278].
The optical generation of DPSK and DQPSK signals is illustrated in Fig. 7.6. In PSK modulation employing differential encoding, the information is encoded in the difference of phase angles between two successive symbols. The original data stream modified using a differential encoder is used to modulate the phase of a CW-laser source employing NRZ coding. Mach-Zehnder-Modulators (MZM) in push-pull mode act as a phase modulator when the applied voltage for a resulting phase change of π is set to 2Vpp. In case of DQPSK signaling, two pre-coded data streams are individually phase modulated and then combined with a relative phase shift of $\pi/2$ resulting in a four-phase signal with in-phase and quadrature components representing the two bit streams (Fig. 7.6b). The symbol rate in DQPSK systems is therefore only half of the nominal bit rate. At the receiver side, the decoded bits arrive, due to the use of a balanced receiver [141], [140], as bipolar data where the "high" and "low" levels are mapped to "1" and "0" logical data, respectively. Considering linear approximation of phase error, the quality of the received signal depends on the bit-to-bit phase fluctuations ($\delta\phi$) and the received intensity (P_S) according to the receiver equations for the respective transmission scheme:

$$\begin{aligned} P_{DPSK} &= P_S \cdot \cos(\delta\phi) \\ P_{DQPSK} &= P_S \cdot [\cos(\delta\phi) \pm \sin(\delta\phi)] \\ &\approx P_S \cdot \left(1 \pm \frac{4\delta\phi}{\pi}\right) \end{aligned}$$

The numerical performance evaluation of PSK-based transmissions is more difficult to calculate than in ASK-based systems, due to interaction of ASE-noise and nonlinearities, hence modifying the nature of the probability density function (*pdf*) used for BER calculation. It has been shown [279], [280] that nonlinear phase noise in PSK systems induced by amplified spontaneous emission (ASE) does not have characteristics of a gaussian *pdf*. The new *pdf* can be accurately described by a summation of independently distributed noncentral χ-square random variables with two degrees of freedom. The nonlinear phase noise can be modeled as a summation of two random variables [279]. The influence of the first EDFA in the chain of a periodically amplified system makes up for a largest contribution of the overall phase noise and can be modeled as a noncentral χ-squared distribution, whereas the rest of the amplifier chain can be summarized using Gaussian characteristics. In any case, the resulting *pdf* cannot be approximated by a gaussian distribution, thus Q-factor or BER calculation based on purely χ-squared or Gaussian distributions cannot be used to evaluate the system performance. Since no numerical recipes exist at present to overcome this dilemma, the investigations presented here were evaluated using the eye-opening-penalty (EOP).

In order to compare the transmission characteristics of ASK- and PSK-based modulation formats in a 40 Gb/s DWDM transmission with 50 GHz channel spacing over up to 10x80 km SSMF fiber, the optimization of MUX and DMUX filter settings is made first and an optimum SSMF power is numerically determined for each number of spans, respectively. Full dispersion post-compensation was employed in each span for all investigated modulation formats. The results of this investigation are illustrated in Fig. 7.7. It can be observed that ASK transmission formats and DPSKs suffer great penalties due to narrow-band optical filtering. In comparison, the penalty of DQPSK based signals is just slightly changed, mainly due to a large tolerance to narrow-band filtering and improved nonlinear tolerance. The measure of the plotted EOP can be more easily understood when looking at the eye diagrams taken after 1, 4, 7 and 10 spans. The differences can be observed between ASK and PSK eyes (bipolar), due to the use of balanced receivers in investigated PSK cases. The most significant feature is that (RZ-)DPSK signals are hardly affected during transmission. They suffer high filtering penalties, but the EOPs hardly change, even after 10 spans. It should be noted that the high level, or logical '1', is severely affected by filtering and is just above the threshold of '0'. The probability of error

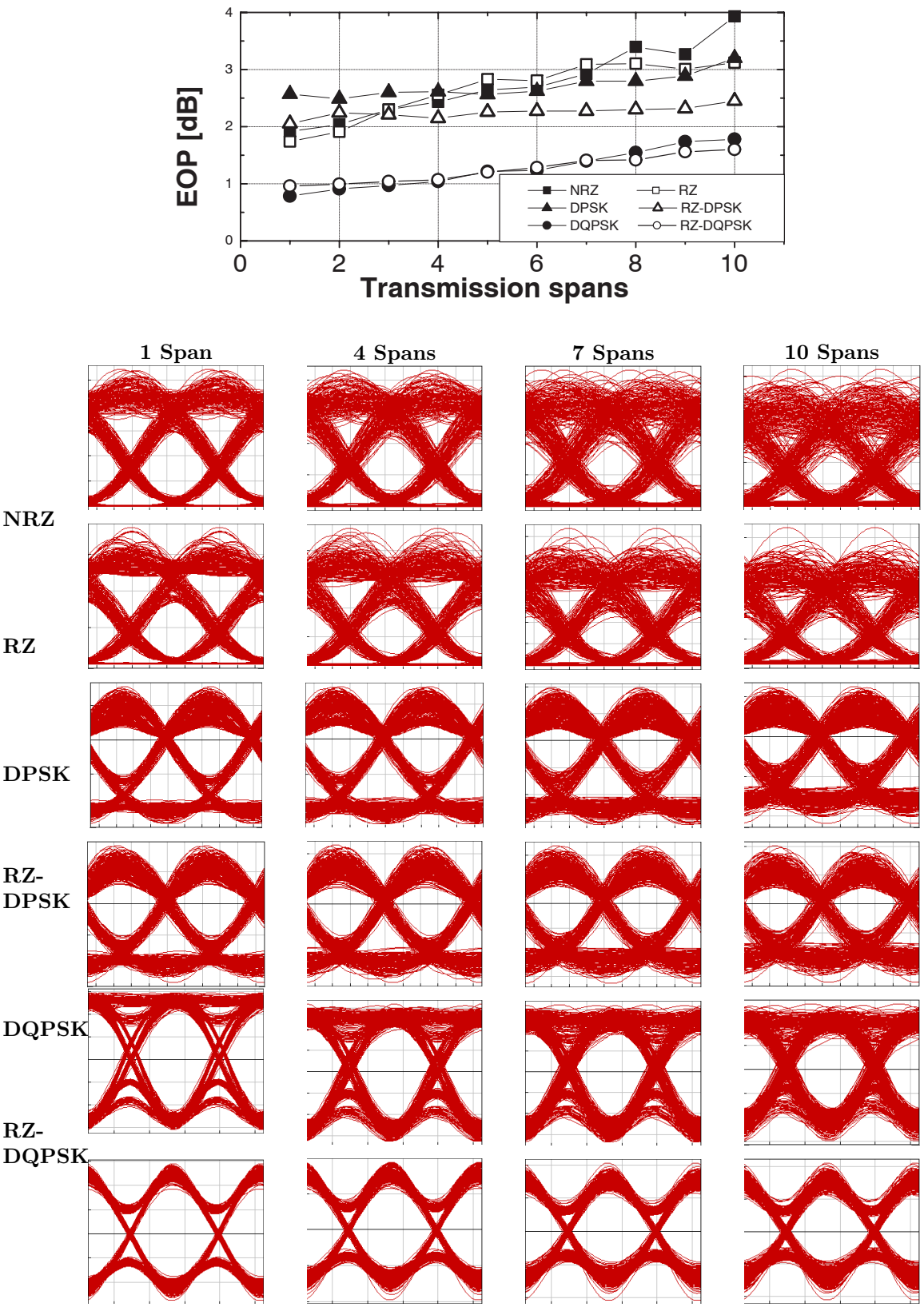

Figure 7.7: 40 Gb/s/ch DWDM transmission at 0.8 bit/s/Hz with the measured eye patterns after 1, 4, 7 and 10 SSMF based spans

should be increased for this state due to its vicinity to the threshold value, which cannot be calculated using EOP measurement, because only the eye opening is considered, and not the relative position of the received signal in relation to the threshold value. Even more the comparison between ASK- and PSK-based formats using EOP evolution does not consider the receiver sensitivity improvement (3 dB), which is achievable with PSK formats. The transmission characteristics of RZ-DPSK based DWDM systems are similar to RZ and NRZ systems, due to strong narrow-band filtering, thus distorting phase relations between the adjacent bits. These results do not recommend implementation of RZ-DPSK in 0.8 bit/s/Hz based 40 Gb/s DWDM systems, but it can be expected that the transmission systems with a reduced spectral efficiency (≤ 0.4 bit/s/Hz) would profit from RZ-DPSK implementation because of suppression of intra-channel limitations. Figure 7.7 shows that (RZ-)DQPSK offers the best transmission results up to 1000 km. This is certainly due to its low symbol rate, which suppresses the effects of fiber dispersion and subsequent nonlinear effects on the signal as well as good narrow-band filtering characteristics. In comparison to (RZ-)DPSK though, the signal quality steadily decreases at faster speed. This can be attributed to the effects of ASE induced phase noise, which accumulate as the transmission distance increases, resulting in larger phase fluctuations and possible errors in detection process. (RZ-)DPSK can cope better with these effects and is less severely affected, because of the a better error tolerance at the receiver side compared to DQPSK. Further investigation [281] showed that implementation of sophisticated dispersion compensating schemes realized as a combination of the dispersion under-compensation per span and the post-compensation at the receiver side enable a performance improvement both in RZ-DPSK and RZ-DQPSK 40 Gb/s based DWDM systems.

The results presented in this chapter, showed that the sophisticated transmission technologies can enable a further increase of the transmission performance and spectral efficiency in DWDM systems. Contrary to other ASK based modulation formats, duobinary modulation becomes a promising technology in spectrally efficient DWDM transmissions, possessing the potential of enabling a spectral efficiency even larger 0.8 bit/s/Hz over shorter transmission distances. Employing this format in combination with some sophisticated techniques e.g. super FEC codes or Raman amplification can further improve transmission performance in ASK-based DWDM systems with 40 Gb/s channel data rates. Considering orthogonal polarization between the channels, it is shown that this method can be beneficial in systems with a dense channel spacing (<25 GHz). For a larger channel spacing, the improvement achieved by this method is limited to short-distance transmissions. The excellent DWDM transmission characteristics of PSK-based optical signals were shown, making them a good alternative to ASK, but a more complex generation and detection of PSK based formats can be seen as the main cause for a delayed system implementation. Comparing DPSK and DQPSK modulation, it can be said that DQPSK due to a reduced symbol rate indicates better transmission characteristics for the implementation in the next generation of optical DWDM systems. Furthermore, for a better characterization of PSK-based transmissions, improved evaluation criteria are required due to the fact that Gaussian probability density function can not be used for BER calculation in this case.

8 Summary

The investigations presented in this work focusing on 40 Gb/s based optical transmission systems with a varying number of channels and various spectral efficiencies showed the potential of 40 Gb/s technologies for the implementation in the next generation optical transmission networks. The system design guidelines are delivered, which enable a better understanding of propagation limitations in high bit rate transmission systems and give useful system insights needed for the upgrade of existing transmission lines. Considering different conventional ASK-based and by the author proposed novel modulation formats, the optimization of the system settings is performed in 40 Gb/s single channel, WDM and DWDM transmission lines, enabling a comparison between different modulation formats in terms of the total transmission distance and the maximum achievable spectral efficiency.
At the beginning of the work, a substantial overview of different transmission components and dominant propagation effects is given considering state-of-the-art technologies used in field and experiments. The basic physical component (e.g. fiber, EDFA, receiver) models are introduced and their validity region is described due to the numerical nature of this work. Furthermore, various evaluation criteria used for the performance estimation in numerical and experimental works are described in detail in order to point out their advantages and drawbacks, and describe the relations between them.
According to the fact that the scope of this work lies particularly on the modulation format enabled performance improvement in 40 Gb/s based transmission lines, the signal generation and dominant transmission characteristics of various conventional - NRZ, RZ, duobinary, SSB-RZ, CSRZ - and novel modulation formats - alCNRZ, nCRZ, alPNRZ, alPRZ - are introduced, and fundamental signal characteristics are explained. The idea behind the development of novel modulation formats was the performance improvement of the existing transmission lines with possibly low signal generation complexity, employing conventional ASK-based receiver configuration for the signal detection.
The 40 Gb/s transmission investigations are started with the single channel case, representing the first step of the network evolution towards high bit rate based transmission systems. Considering two groups of modulation formats - NRZ- and RZ-based - differentiated by the pulse form, their tolerances to linear (e.g. GVD) and nonlinear (e.g. Kerr-effect) disturbances are investigated, indicating that an implementation of NRZ-based modulation formats provides a better dispersion tolerance, but suffers from strong nonlinear limitations. The use of novel NRZ-based formats enables a significant improvement of nonlinear transmission characteristics at the cost of a slightly increased transmitter complexity used for the implementation of phase (e.g. alCNRZ) or polarization modulation (e.g. alPNRZ) on conventional NRZ pulses. RZ-based formats are characterized by an increased sensitivity to residual dispersion and a significant nonlinear tolerance. Additional phase or polarization modulation of RZ pulses enables more compact signal spectra and a further improvement of already good nonlinear robustness, resulting in an increased maximum transmission distance. Strong intra-channel limitations (e.g. IXPM) are indicated as the dominant transmission limitation especially in RZ-based formats characterized by strong interactions of consecutive pulses within the bit stream, due to the fast broadening of short optical pulses at 40 Gb/s. This effect is accompanied by a SPM-GVD interplay, which becomes evident in both format groups at larger channel powers. The nature of the dominant single channel limitation affects the choice of the transmission fiber for 40 Gb/s transmissions. The intra-channel effects dominance requires the implementation of transmission fibers with lower dispersion values (4-8 ps/nm·km), whereby a larger fiber dispersion can be beneficial for the suppression of SPM-GVD interplay. After optimization of fiber power settings and dispersion compensation schemes for transmission lines with commercially available fiber types (e.g. SSMF, NZDSFs), the relation between the optimum dispersion compensation scheme and dominant propagation disturbance is investigated. It was shown, that as long as intra-channel effects dominate transmission performance, the best dispersion compensation scheme, is characterized by a small amount of dispersion pre-compensation, which, due to pulse compression before transmission line reduces the interactions between adjacent pulses. The amount of dis-

persion pre-compensation is dependent on the modulation format in use, because of the interplay between the pulse internal chirp, e.g. caused by phase modulation at the transmitter side, and the local dispersion in DCF fibers used for pre-compensation. The importance of pre-compensation even increases in long-haul transmission lines employing dispersion compensation on a span-by-span basis, because of constructive superposition of IXPM contributions after each span. The investigations of the total transmission performance of different modulation formats with optimized system settings showed that conventional RZ-based formats (e.g. CSRZ, RZ) basically enable better performance compared to conventional NRZ-based formats (e.g. NRZ, duobinary), but the implementation of novel NRZ-based modulation formats (e.g. alPNRZ) makes this difference vanish. The modulation formats employing polarization switching between consecutive pulses are identified as best solution for the performance enhancement in 40 Gb/s single channel based transmission lines.

The followed 40 Gb/s investigations were performed considering WDM and DWDM transmission systems with spectral efficiencies of 0.4 and 0.8 bit/s/Hz. Narrow-band filtering is shown to be essential both at the transmitter and the receiver side for the achievement of an increased spectral efficiency at 40 Gb/s channel data rate. The WDM investigations for different modulation formats indicated almost identical transmission behaviour to single channel transmission, which can be explained by the dominance of single-channel effects in 40 Gb/s systems with a channel spacing of 100 GHz, thus resulting in similar optimum transmission settings, e.g. optimum fiber type and dispersion compensating scheme in single channel and WDM transmission lines. As in the single channel case, RZ-based formats indicated a significant robustness to nonlinear propagation effects, which can be outperformed only by the use of novel modulation formats with NRZ or RZ pulses. Comparing single channel and WDM results under consideration of the total transmission performance in terms of maximum dynamic range, identical behavior is observed in both cases. This leads to the conclusion that a system upgrade from single channel to WDM at 40 Gb/s channel data rate can be made without modification of transmission infrastructure. Considering optimum transmission fiber choice, it can be concluded that transmission fibers with moderate dispersion (D=4..8 ps/nm·km) provide due to suppression of intra-channel effects the best transmission performance in both cases. The channel spacing reduction to 50 GHz in DWDM case results RZ-based modulation formats to show strong pulse distortions, because of the reduced tolerance to implemented narrow-band filtering. Hence the differences between RZ and NRZ pulses vanish in DWDM transmissions. The transmission performance in this case is governed by strong interactions between adjacent channels in form of XPM, affecting the choice of the optimum transmission fiber and optimum dispersion scheme. It was shown that transmission fibers with a large chromatic dispersion (D >8 ps/nm·km) represent the better solution in DWDM transmission systems, because of the suppression of dominant multi-channel effects independently of the modulation format in use. Accordingly, already deployed fibers (e.g. G.652) can be further used in next generation of DWDM transmission systems. The optimum dispersion compensation scheme in combination with a large local fiber dispersion enables suppression of XPM-effects through implementation of a small amount of dispersion pre-compensation which enables the decorrelation between the adjacent channels and reduces the walk-off length between the channels in nonlinear region on the beginning of each span. Furthermore, considering concatenation of identical spans in a DWDM transmission line, it was observed that XPM-induced impacts superpose constructively from span to span independently of the implemented dispersion compensation scheme, resulting in an transmission penalty, which is in high power regime proportional to number of concatenated spans N. This behavior enables together with P_{max}-rule an efficient estimation of the maximum transmission performance and distance in 40 Gb/s DWDM systems.

RZ-based modulation formats outperform the NRZ-based ones in 40 Gb/s single channel and WDM transmissions, where the advantages of RZs become more evident with an increased transmission distance. In DWDM transmissions, the differences between these two groups of formats vanish, because of the distortion of RZ pulse shape due to implemented narrow-band filtering. The additional investigations over long-haul distances (up to 10x80 km) justified this behavior. The novel modulation formats based on polarization switching (alPNRZ, alPRZ) indicated the best transmission performances in terms of largest dynamic ranges and an enhanced power tolerance. Their excellent transmission characteristics become especially evident in 40 Gb/s DWDM transmissions, enabling significant transmission performance due to the reduced impact of multi-channel nonlinearities.

Summarizing the dominant characteristics of different modulation formats in Table 8.1 according to per-

Modulation format	**Advantages**	**Disadvantages**	**Implementation areas**
NRZ	simple signal generation state-of-the art format dispersion tolerant spectrally efficient	low nonlinear tolerance reduced transmission reach	metro + regional WDM, DWDM
Duobinary	dispersion tolerance spectrally efficient	low nonlinear tolerance drive signal electrical pre-coding	metro + regional DWDM
alCNRZ	improved nonlinear tolerance simple signal generation	reduced dispersion tolerance	regional WDM
alPNRZ	significant nonlinear tolerance narrow-band filtering tolerant conventional receiver	additional polarization modulation	metro + long-haul WDM, DWDM
RZ	nonlinear tolerant	complex generation reduced dispersion tolerance narrow-band filtering sensitive	long-haul WDM
SSB-RZ	nonlinear tolerance dispersion tolerance	complex signal generation narrow-band filtering sensitive	long-haul WDM
CSRZ	nonlinear tolerance dispersion tolerance spectrally efficient	complex signal generation narrow-band filtering sensitive	long-haul WDM
alPRZ	significant nonlinear tolerance conventional receiver	additional polarization modulation	long-haul WDM, DWDM
nCRZ	compact signal spectrum good nonlinear tolerance	additional phase modulation dispersion tolerance narrow-band filtering sensitive	long-haul WDM, DWDM

Table 8.1: Comparison of ASK-based modulation formats in 40 Gb/s systems

formed 40 Gb/s investigations, it can be concluded that conventional NRZ-based formats are suited for the implementation in short reach networks based on WDM and DWDM technology, while the RZ-based formats better meet requirements of long-haul WDM systems with a reduced spectral efficiency ($\leq$0.4 bit/s/Hz). Novel modulation techniques can be seen as methods for enabling the realization of long-haul WDM and DWDM systems, because of their excellent nonlinear tolerances. Novel modulation formats (e.g. alPNRZ) with NRZ pulse shape indicated a potential to fill the nonlinear tolerance gap between conventional NRZ- and RZ-based formats.
This work is completed by transmission characteristics investigation of promising enabling technologies, e.g. polarization orthogonality between the channels and PSK-based modulation formats, for an increased spectral efficiency (beyond 0.8 bit/s/Hz) and an enhanced maximum transmission distance. These technologies are chosen because of their reduced implementation complexity and maturity shown in recent experimental works. Before these investigations, the barriers of narrow-band filtering are determined, indicating that the maximum achievable spectral efficiency of an ASK format amounts to 1 bit/s/Hz using duobinary modulated signals over a transmission distance of up to 8x80 km. Considering orthogonal polarization as a method for doubling the spectral efficiency and the efficient suppression of multi-channel effects (e.g. FWM, XPM), its PMD-caused length dependence was shown, especially in systems with larger channel spacings (>25 GHz), to limit the 40 Gb/s implementation of this method on short reach systems, because of a fast disappearance of polarization orthogonality. The investigations of PSK-based modulation formats, which are characterized by the increased complexity of signal generation and detection, showed that not all recently proposed PSK-

based system can compete against ASK-based formats for implementation in DWDM systems. The DPSK and RZ-DPSK based 40 Gb/s systems would enable a performance improvement compared to conventional ASK (e.g. NRZ or RZ) formats in WDM systems with a reduced spectral efficiency, because of their better nonlinear tolerance, but according to similar narrow-band filtering characteristics, they would provide no additional benefits in DWDM systems. DQPSK based modulation formats were identified as a potential candidate for the implementation in future spectrally efficient DWDM systems, because of their good transmission characteristics originating form the reduced symbol data rate (half the bit rate).
From the 40 Gb/s system design point of view, future works have to be performed addressing the PMD impacts and the need for its compensation as well as the sophisticated dispersion compensation schemes combined with sophisticated optical amplification methods (e.g. EDFA + Raman optical amplification). The rising importance of numerical tools for the system design requires improved evaluation criteria, which should enable a better comparison between numerical and experimental works.

Bibliography

[1] Insight Research. *Traffic growth trends*, Juni 1998.

[2] Nortel Networks Inc. *Fiber infrastructure*, 1999.

[3] E. Desurvire, D. Bayart, B. Desthieux, and S. Bigo. *Erbium-doped Fiber Amplifiers - Device and System Developments*. Number ISBN 0-471-41903-6. A John Wiley and Sons, Inc., Publication, 2002.

[4] A. Paoletti, A. Schiffini, A. Pagano, and M. Schiano. 40 Gbit/s WDM transmission for long haul applications: network functionalities and transmission technologies unlocking ultrafast all-optical networks. *Europian Conference on Optical Communication (ECOC)*, 5(We1.1.1):74–75, September 2003.

[5] J. P. Elbers, C. Scheerer, A. Färbert, C. Glingener, A. Schöpflin, E. Gottwald, and G. Fischer. 3.2 Tbit/s (80x40 Gbit/s) bidirectinal DWDM/ETDM transmission. *European Conference on Optical Communication (ECOC)*, Postdeadline Papers(PD2), September 1999.

[6] Y. Miyamoto, K. yonenaga, S. Kuwahara, M. Tomizawa, A. Hirano andH. Toba, K. Murata, Y. Tada, Y. Umeda, and H. Miyazawa. 1.2-Tbit/s(30x42.7-Gbit/s ETDM optical channel) WDM transmission over 376 km with 125-km spacing using forward error correction and carrier-suppressed RZ format. *Optical Fiber Communication Conference (OFC)*, 4(PD26):245–247, March 2000.

[7] A. Färbert, G. Mohs, S. Spälter, J. P. Elbers, C. Fürst, A. Schöpflin, E. Gottwald, C. Scheerer, and C. Glingener. 7 Tb/s (176x40 Gb/s) bidirectional interleaved transmission with 50 GHz channel spacing. *European Conference on Optical Communication (ECOC)*, Postdeadline Pepers(PD1.3), September 2000.

[8] Y. Zhu, W. S. Lee, C. Scahill, C. Fludger, D. Witley, M. Jones, J. Homan, B. Shaw, and A. Hadjifotiou. 1.28 Tbit/s (32x40 Gbit/s) transmission over 1000 km with only 6 spans. *European Conference on Optical Communication (ECOC)*, Postdeadline Papers(PD1.4), September 2000.

[9] W. Idler, S. Bigo, Y. Frignac, B. Franz, and G. Veith. Vestigial side band demultiplexing for ultra high capacity (0.64 bit/s/Hz) transmission of 128x40 Gb/s channels. *Optical Fiber Communication Conference (OFC)*, 1(MM3), March 2001.

[10] T. Ito, K. Fukuchi, K. Sekiya, D. Ogasahara, R. Ohhira, and T. Ono. 6.4 Tb/s (160x40 Gb/s) WDM transmission experiment with 0.8 bit/s/Hz spectral efficiency. *European Conference on Optical Communication (ECOC)*, Postdeadline Papers(PD1.1), September 2000.

[11] S. Bigo, Y. Frignac, G. Charlet, W. Idler, S. Borne, H. Gross, R. Dischler, W. Poehlmann, P. Tran, C. Simonneau, D. Bayart, G. Veith, A. Jourdan, and J. P. Hamaide. 10.2 Tbit/s (256x42.7 Gbit/s PDM/WDM) transmission over 100 km TeraLight fiber with 1.28 bit/s/Hz spectral efficiency. *Optical Fiber Communication Conference (OFC)*, Postdeadline Papers(PD25), March 2001.

[12] Y. Zhu, W. S. Lee, P. Lobb, C. Schahill, D. Witley, S. Savory, C. Fludger, B. Shaw, and A. Hadjifotiou. Polarization-channel-inetrleaved carrier-suppressed RZ ETDM/DWDM transmission at 40 Gbit/s with 0.8 bit/s/Hz spectral efficiency. *European Conference on Optical Communication (ECOC)*, 1:54–55, September 2001.

[13] Y. Frignac, G. Charlet, W. Idler, R. Dischler, P. Tran, S. Lanne, S. Borne, C. Martinelli, G. Veith, A. Jourdan, J. P. Hamaide, and S. Bigo. Transmission of 256 wavelength-division and polarization-division-multiplexed channels at 42.7 Gb/s (10.2 Tb/s capacity) over 3x100 km of TeraLight fiber. *Optical Fiber Communication Conference (OFC)*, Postdeadline Paper(FC5), March 2001.

[14] W. Idler, G. Charlet, R. Dischler, Y. Frignac, and S. Bigo. 0.8 bit/s/Hz of information spectral density by vestigal sideband filtering of 42.66 Gb/s NRZ. *European Conference on Optical Communication (ECOC)*, 3(8.1.5), September 2002.

[15] T. Tsuritani, A. Agata, I. Morita, N. Yoshukane, K. Imai, and N. Edagawa. 40 GHz-pased 21.4 Gb/s x 82 WDM VSB-RZ transmission over 8260 km using Raman/EDFA hybrid repeaters and symmetrically dispersion-managed fiber. *European Conference on Optical Communication (ECOC)*, 4(9.1.4), September 2002.

[16] J. X. Cai, M. Nissov, C. R. Davidson, Y. Cai, A. N. Pilipetski, H. Li, M. A. Mills, R. M. Mu, U. Feiste, L. Xu, A. J. Lucero, D. G. Fuorsa, and N. S. Bergano. Transmission of thirty-eight 40 Gb/s channels (>1.5 Tb/s) over transoceanic distances. *Optical Fiber Communication Conference (OFC)*, Postdeadline Paper(FC4), March 2002.

[17] C. Rasmussen, S. Dey, F. Liu, J. Bennike, B. Mikkelsen, P. Mamyshev, M. Kimmitt, K. Springer, D. Gapontsev, and V. Ivshin. Transmission of 40x42.7 Gb/s over 5200 km UltraWave fiber with terrestrial 100 km spans using turn-key ETDM transmitter and receiver. *European Conference on Optical Communication (ECOC)*, 4(PD4.4), September 2002.

[18] A. Agarwal, S. Banerjee, D. F. Grosz, A. P. Küng, D. N. Maywar, A. Gurevich, and T. H. Wood. Ultra-high-capacity long-haul 40-Gb/s WDM transmission with 0.8-bit/s/Hz spctral efficiency by means of strong optical filtering. *IEEE Photonics Technology Letters*, 15(3):470–472, March 2003.

[19] I. Morita and N. Edagawa. 50 GHz - spaced 64x42.7 Gbit/s transmission over 8200 km using pre-filtered CS-RZ DPSK signal and EDFA repeaters. *European Conference on Optical Communication (ECOC)*, 6:60–61, September 2003.

[20] G. Charlet, J. Lazaro, E. Corbel, P. Tran, A. Klekamp, T. Lopez, H. Mardoyan, W. Idler, A. Koncykowska, J. P. Thiery, R. Dischler, and S. Bigo. One-hundert WDM-channel transatlantic transmission experiment at 43 Gbit/s using Raman repeaters with large 65km spacing. *European Conference on Optical Communication (ECOC)*, Postdeadline Papers:64–65, September 2003.

[21] K. Petermann. *Laser Diode Modulation and Noise*. Kluwer Academics Publishers, 1988.

[22] E. Voges and K. Peteramann. *Optische Kommunikationstechnik - Handbuch für Wissenschaft un Industrie*. Springer-Verlag Berlin Heidelberg, 1 edition, 2002.

[23] G. P. Agrawal. *Nonlinear Fiber Optics*. Number ISBN 0-12-045143-3. Academic Press, 3 edition, 2001.

[24] S. Reddy, L. Taira, and M. Resso. Signal Intergrity Concerns when Modulating Laser Transmitters at Gigabit Rates. *DesignCon 2002*, 1, 2002.

[25] J. Kreissl, U. Troppenz, W. Rehbein, B. Hüttl, E. Lenz, and H. Venghaus. High single-mode-yield multiple-wavelength DFB-laser arrays in the 1.55 μm range. *European Conference on Optical Communication (ECOC)*, 2(Tu.B.1):118–119, September 2001.

[26] NEC Inc. *NEC Laser Diode NX8562: 1550 nm InGaAsP MQW-DFB laser diode module CW light source for DWDM applications - Data Sheet*, 2002.

[27] K. Takaki, T. Kise, K. Maruyama, K. Hiraiwa, N. Yamanaka, M. Funabashi, and A. Kasukawa. High-power CW-DFB LDs for optical communications. *Furakawa Review*, (23):1–5, January 2003.

[28] M. Funabashi, K. Hiraiwa, S. Koizumi, N. Yamanaka, and A. Kusukawa. Low operating current 40 mW PM fiber coupled DFB laser modules for exterbally modulated 1550 nm WDM sources. *European Conference on Optical Communication (ECOC)*, 2(Tu.B.1.3):122–123, September 2001.

[29] L. Bjerkan, A. Royset, L. Hafskjear, and D. Myhre. Measurement of laser paramterers for simulation of high-speed fiberoptic parameters. *Journal of Lightwave Technology*, 14(5):839–850, May 1996.

[30] I. Tomkos, D. Chowdhury, J. Conradi, D. Culverhouse, K. Ennser, C. Giroux, B. Hallock, T. Kennedy, A. Kruse, S. Kumar, N. Lascar, I. Ruodas, M. Sharma, R. S. Vodhanel, and C. C. Wang. Demonstration of negative dispersion fibers for DWDM metropolian are networks. *IEEE Journal on Selected Topics in Quantum Electronics*, 7(3):439–460, May/June 2001.

[31] C. Kurtzke. *Kapazitätsgrenzen digitaler optische Übertragungssysteme*. PhD thesis, Technische Universität Berlin, 1995.

[32] VPI Systems Inc. *VPI Transmission Maker: Photonics Modules Reference Manual*.

[33] G. Wenke and M. Klimmek. Consideration on the alpha-Factor of Nonideal, external optical Mach-Zehnder Modulators. *Journal of Optical Communications*, 17(2):42–48, February 1996.

[34] J. Kondo, A. Kondo, K. Aoki, S. Takatsuji, O. Mitomi, M. Imaeda, Y. Kozuka, and M. Minakata. Lowe-drive-voltage 40 Gb/s modulator on X-cut $LiNbO_3$ wafer. *European Conference on Optical Communication (ECOC)*, 3(We.F.3.3):334–335, October 2001.

[35] F. Koyama and K. Iga. Frequency Chirping in External Modulators. *Journal of Lightwave Technology*, 6(1):87–92, January 1988.

[36] A. Djupsjobacka. Residual chirp in integrated-optic modulators. *IEEE Photonics Technology Letters*, 4(1):41–43, January 1992.

[37] A. H. Gnauck, S. K. Korotky, J. J. Veselka, J. Nagel, C. T. Kemmerer, W. J. Minford, and D. T. Moser. Dispersion penalty reduction using an optical modulator with adjustable chirp. *IEEE Photonics Technology Letters*, 3(10):916–918, October 1991.

[38] Agere Systems Inc. *Agere 40 Gbit/s Lithium Niobate Electro-Optic Modulator - data sheet information*, 2002.

[39] JDS Uniphase Inc. *JDS OC-768 - 40 Gbit/s Amplitude Modulator - product bulletin*, 2002.

[40] Corning Inc. *Corning SD-40 integrated optic intensity modulator - data sheet information*, 2003.

[41] T. Yamanaka. Ultrafast electroabsorption modulators with traveling-wave electrodes. *European Conference on Optical Communication (ECOC)*, 3(We.F.3.1):328–331, October 2001.

[42] H. Kawanishi, Y. Yamauchi, N. Mineo, Y. Shibuya, H. Murai, K. Yamada, and H. Wada. Over 40 GHz modulation bandwidth of EAM-integrated DFB Laser Modules. *Optical Fiber Communication Conference (OFC)*, 1:MJ3, March 2001.

[43] D. G. Moodie, A. D. Ellis, P. J. Cionnard, C. W. Ford, H. Barrell, R. T. Moore, S. D. Perrin, R. I. McLaughlin, and F. Garcia. 40 Gbit/s modulator with low drive lotage and high optical output power. *European Conference on Optical Communication (ECOC)*, 3(We.F.3.2), October 2001.

[44] D. Moodie, A. Ellis, X. Chen, F. Garcia, D. Rogers, S. Perrin, C. Cannard, R. McLaughlin, M. Roberts, S. Amos, S. Cole, C. Ford, and I. Reid. Application of electroabsorption modulators in high bit-rate extended reach transmission systems. *Optical Fiber Communication Conference (OFC)*, 2(TuP1), March 2003.

[45] K. Prosyk, R. Moore, I. Betty, R. Foster, J. Greeenspan, P. Singh, S. O.'Keefe, J. Oosterom, and P. Langlois. Low loss, low chirp. low voltage, polarization independent 40 Gb/s bulk electro-absorption modulator module. *Optical Fiber Communication Conference (OFC)*, 2(TuP3), March 2003.

[46] K. Takagi, H. Tada, E. Ishimura, T. Aoyagi, T. Nishimura, and E. Omura. Highly reliable 40 Gb/s electroabsorption modulator grown on InP:Fe substrat. *Optical Fiber Communication Conference (OFC)*, 1(MJ2), March 2001.

[47] S. Irmscher, R. Lewen, U. Eriksson, U. Westergren, and L. Thylen. High-speed semiconductor electroabsorption modulators. *European Conference on Optical Communication (ECOC)*, 4(10.5.5.), September 2002.

[48] Y. Kim, S. K. Kim, J. Lee, Y. Kim, J. Kang, W. Choi, and J. Jeong. Characteristics of 10 Gb/s electroabsorbtion modulator integrated distributed feedback lasers for long-haul optical transmission systems. *Optical Fiber Technology*, 7(1):84–100, January 2001.

[49] M. Matsuda, K. Morito, K. Yamaji, T. Fujii, and Y. Kotaki. A novel method for designing chrip characteristics in electroabsorption MQW optical modulators. *IEEE Photonics Technology Letters*, 10(3):364–366, March 1998.

[50] H. Kawanishi, Y. Yamaguchi, N. Mineo, Y. Shibuya, H. Murai, K. Yamada, and H. Wada. EAM-integrated DFB laser modules with more than 40-GHz bandwidth. *IEEE Photonics Technology Letters*, 13(9):954–956, September 2001.

[51] G. P. Agrawal. *Fiber-Optic Communication Systems*. Number ISBN 0-471-17540-4 in Wiley Series in Microwave and Optical Engineering. John Wiley and Sons, Inc., 3 edition, 2002.

[52] K. Petermann. Vorlesungsskript - Einführung in die optische Nachrichtentechnik, 2003.

[53] S. R. Nagel, J. B. MacChesney, and K. L. Walker. An overview of the modified chemical vapor deposition (MCVD) process and performance. *IEEE Journal of Quantum Electronics*, QE-18(4):459–476, April 1982.

[54] Lucent Technologies Bell Labs Innovations. *Lucent Technologies TrueWave RS Nonzero-Dispersion Optical Fiber: Product manual*, May 2001.

[55] J. P. Gordon and H. Kogelnik. PMD fundamentals: Polarization mode dispersion in optical fibers. *PNAS*, 97(9):4541–4550, April 2000.

[56] J. M. Fini and H. A. Haus. Accumulation of polarization-mode dispersion in cascades of compensated optical fibers. *IEEE Photonics Technology Letters*, 13(2):124–126, February 2001.

[57] R. Khosravani and A. E. Willner. System Performance Evaluation in Terrestrial Systems with High Polarization Mode Dispersion and the Effect of Chirping. *IEEE Photonics Technlogy Letters*, 13(4):296–298, April 2001.

[58] Corning Inc. *Corning LEAF Optical Fiber: Product manual*, January 2001.

[59] G. J. Foschini and C.D. Poole. Statistical theory of polarization dispersion in single mode fibers. *Journal of Lightwave Technology*, 9(11):1439–1456, November 1991.

[60] M. Karlsson. Probability density functions of the differential group delay in optical fiber communication systems. *Journal of Lightwave Technology*, 19(3):324–331, March 2001.

[61] International Telecommunication Union. ITU-T Recommendation G.691 Series G: Transmission systems and media, digital systems and networks - Optical interfaces for single channel STM-64, STM-256 and other SDH systems with optical amplifiers, October 2000.

[62] H. Sunnerud, C. Xie, M. Karlsson, and P. A. Andrekson. Outage probability in PMD compensated transmission systems. *European Conference on Optical Communication (ECOC)*, 2:204–205, 2001.

[63] L. S. Yan, Q. Yu, T. Lou, A. E. Willner, and X. S. Yao. Compensation of higher order polarization-mode dispersion using phase modulation and polarization control in the transmitter. *IEEE Photonics Technology Letters*, 14(6):858–860, June 2002.

[64] I. Kaminow and T. Li. *Optical Fiber Telecommunications IVB*. Number ISBN 0-12-395173-9. Academic Press, 2002.

[65] K. O. Hill, D. C. Johnson, B. S. Kawasaki, and R. I. MacDonald. CW three-wave mixing in single-mode optical fibers. *Journal of Applied Physics*, 49(10):5098–5106, October 1978.

[66] N. Shibata, R. P. Braun, and R. G. Waarts. Phase-mismatch dependance of efficiency of wave generation through four-wave mixing in a single-mode optical fiber. *IEEE Journal of Quantum Electronics*, 23(7):1205–1210, July 1987.

[67] F. Forghieri, R. W. Tkach, and A. R. Chraplyvy. WDM Systems with Unequally Spaced Channels. *Journal of Lightwave Technology*, 13(5):889–897, May 1995.

[68] K. Inoue. Arrangement of orthogonal polarized signals for suppresing fiber four-wave mixing in optical multichannel transmission systems. *IEEE Photonics Technology Letters*, 3(6):560–563, June 1991.

[69] P. V. Mamyshev and N. A. Mamysheva. Pulse-overlapped dispersion-managed data transmission and intrachannel four-wave mixing. *Optics Letters*, 24(21):1454–1456, November 1999.

[70] S. Kumar. Intrachannel four-wave mixing in dispersion managed RZ systems. *IEEE Photonics Technology Letters*, 13(8):800–802, August 2001.

[71] S. Kumar, J. C. Mauro, S. Ranghavan, and D. Q. Chowdhury. Intrachannel nonlinear penalties in dispersion-managed transmission systems. *IEEE Journal of Selected Topics in Quantum Electronics*, 8(3):626–631, May/June 2002.

[72] A. Pizzinat, A. Schiffini, F. Alberti, F. Matera, A. N. Pinto, and P. Almeida. 40-Gb/s systems on G.625 fibers: Comparison between periodic and all-at-the-end dispersion compensation. *Journal of Lightwave Technology*, 20(9):1673–1679, September 2002.

[73] B. Konrad and K. Petermann. Optimum fiber dispersion in high-speed TDM systems. *IEEE Photonics Technology Letters*, 13(4):299–301, April 2001.

[74] R. I. Killey, H. J. Thiele, V. Mikhailov, and P. Beyvel. Reduction of intrachannel nonlinear distortion in 40-Gb/s-based WDM transmission over standard fiber. *IEEE Photonics Technology Letters*, 12(12):1624–1626, December 2000.

[75] R. H. Stolen and E. P. Ippen. Raman gain in glass optical waveguides. *Applied Physics Letters*, 22(6):276–279, March 1973.

[76] A. F. Evans, J. Grochocinski, A. Rahman, C. REynolds, and M. Vasilyev. Distributed amplification: How Raan gain impacts other fiber nonlinearities. *Optical Fiber Communication Conference (OFC)*, 1(MA7), March 2001.

[77] Y. Emori. Ultrabroadband fiber Raman amplifiers. *European Conference on Optical Communication (ECOC)*, 3(3.2), September 2002.

[78] S. G. Farwell and C. R. S. Fludger. Experimental determination of variation of the Raman gain efficiency coefficient with fiber mode field diameter and effect on Raman gain. *European Conference on Optical Communication (ECOC)*, 2(5.2.5), September 2002.

[79] M. W. Chbat and H. A. Fevrier. Low-cost, high-capacity ultra-long-haul WDM systems based on wide-band Raman amplification. *European Conference on Optical Communication (ECOC)*, 3(3.7), September 2002.

[80] R. G. Smith. Optical power handling capacity of low loss optical fibers as determined by stitulated Raman and Brillouin scattering. *Applied Optics*, 11(11):2489–2160, November 1972.

[81] A. R. Chraplyvy. Optical power limits in multi-channel wavelength-division-multiplexed systems due to Stimulated Raman Scattering. *Electronics Letters*, 20(2):58–59, January 1984.

[82] A. Hasegawa and F. Tappert. Transmission of stationary nonlinear optical pulses in dispersive dielectric fibers I. Anomalous dispersion. *Applied Physics Letters*, 23(3):142–143, August 1973.

[83] T. R. Taha and M. J. Ablowitz. Analytical and numerical aspects of certain nonlinear evolution equations II. numerical nonlinear Schrödinger equation. *Journal of Computational Physics*, 55:203–230, 1984.

[84] R. H. Hardin and F. D. Tappert. Applications of the split-step Fourier method to the numerical solution of nonlinear and variable coefficient wave equations. *SIAM Review Chronical*, 15:423, 1973.

[85] D. Marcuse. *Theory of dielectric optical waveguides*. Academics Press Inc., 2 edition, 1989.

[86] F. Matera, A. Mecozzi, M. Romagnoli, and M. Settembre. Sideband instability induced by periodic power variation in long-distance fiber links. *Optics Letters*, 18(18):1499–1501, September 1993.

[87] C. Francia. Constant step-size analysis in numerical simulations for correct four-wave-mixing power evaluation in optical fiber transmission systems. *IEEE Photonics Technology Letters*, 11(1):69–71, January 1999.

[88] G. Bosco, A. Carena, V. Curri, R. Gaudino, P. Poggiolini, and S. Benedetto. Suppression of spurious tones induced by the spli-step method in fibre systems simulations. *IEEE Photonics Technology Letters*, 12(5):489–491, May 2000.

[89] B. Wedding and B. Franz. Unregenerated optical transmission at 10 Gbit/s via 204 km of standard single mode fiber using a directly modulated laser diode. *Electronics Letters*, 29(4):402–403, February 1993.

[90] B. Wedding, B. Franz, and B. Junginger. 10-Gb/s optical transmission up to 253 km via standard single-mode fiber using the method of dispersion-supported transmission. *Journal of Lightwave Technology*, 12(10):1720–1727, October 1994.

[91] N. Henmi, T. Saito, and T. Ishida. Prechirp technique as a linear dispersion compensation for ultrahigh-speed long-span intensity modulation directed detection optical communication systems. *Journal of Lightwave Technology*, 12(10):1706–1719, October 1994.

[92] K. Yonenaga and S. Kuwano. Dispersion-tolerant optical transmission system using duobinary transmitter and binary receiver. *Journal of Lightwave Technology*, 15(8):1530–1537, August 1997.

[93] S. Won, J. Lee, Y. Kim, S. Kim, and J. Jeong. Performance limits of 10-Gb/s optical duobinary transmissions using reduced bandwidth single-arm Mach-Zehnder modulators considering residual chirp and dc-Bias offset. *IEEE Photonics Technology Letters*, 15(3):479–481, March 2003.

[94] A. Sano, Y. Miyamoto, S. Kuwahara, and H. Tobo. A 40 Gb/s/ch WDM Trasmission with SPM/XPM Suppression Through Prechirping and Dispersion Management. *Journal of Lightwave Technology*, 18(11):1519–1527, November 2000.

[95] H. Bulow. Electronic equalization of transmission impairments. *Optical Fiber Communication Conference (OFC)*, 2(TuE4):24–25, March 2002.

[96] S. Kasturia and J. Winters. Techniques for high-speed implementation of nonlinear cancellation. *IEEE Journal of Selected Areas in Communications*, 9(5):711–717, June 1991.

[97] S. Otte and W. Rosenkranz. Performance of electronic compensator for chromatic dispersion and SPM. *European Conference on Optical Communication (ECOC)*, pages 117–118, September 2000.

[98] K. Aikawa, Y. Nagasawa, K. Suzuki, S. Shimizu, T. Suzuki, M. Nakayama, K. Kaneda, and K. Himeno. High-performance Dispersion-slope and Dispersion Compensation Modules. Technical report, Fujikura Technical Report, 2003.

[99] E. Iannone, F. Matera, A. Mecozzi, and M. Settembre. *Nonlinear Optical Communication Networks*. John Wiley and Sons, 1 edition, March 1998.

[100] Fujikura Inc. *Fujikura Technical Review : Dispersion compensating Fiber Module for NZ-DSF with a Large Effective Area for NZ-DSF with a Large Effective Area*, January 2001.

[101] T. Suzuki. Large-effective-area dispersion compensating fibers for dispersion accommodation both in the C and L band. *Digest of fifth Optoelectronics and communications conference (OECC)*, 1(14C4-4):554–555, 2000.

[102] T. N. Nielsen, A. J. Stentz, K. Rottwitt, D.S. Vengsarkar, Z. J. Chen, P. B. Hansen, J. H. Park, K.S. Feder, T. A. Strasser, S. Cabot, S. Stulz, D. W. Peckham, L. Hsu, C. K. Kan, A. F. Judy, J. Sulhoff, S. Y. Park, L. E. Nelson, and L. Grüner-Nielsen. 3.28-Tb/s (82x40 Gb/s) transmission over 3x100 km nonzero-dispersion fiber using dual C- and L-band hybrid Raman/Erbium-doped inline amplifier. *Optical Fiber Communication Conference (OFC)*, 4(PD23):236–238, March 2000.

[103] K. Petermann. Constraints for fundamental-mode spot size for broadband dispersion-compensated single-mode fibers. *Electronics Letters*, 19(18):712–713, September 1983.

[104] M. Wandel, P. Kristensen, T. Veng, Y. Qian, Q. Le, and L. Gruener-Nielsen. Dispersion compensating fibers for non-zero dispersion fibers. *Optical Fiber Communication Conference (OFC)*, March 2001.

[105] F. Ouellette, J. F. Cliche, and S. Gagnon. All-fiber devices for chromatic dispersion compensation based on chirped distributed resonant coupling. *Journal of Lightwave Technology*, 12(10):1728–1738, October 1994.

[106] R. E. Epworth. Chromatic dispersion equalization on optical fiber transmission systems. UK patent GB 2161612B, 1984.

[107] B. J. Eggleton, T. Stephens, P. A. Krug, G. Dhosi, Z. Brodzeli, and F. Ouellette. Dispersion compensation using a fibre grating in transmission. *Electronics Letters*, 32(17):1610–1611, August 1996.

[108] Y. Painchaud, A. Mailloux, H. Chotard, E. Pelletier, and M. Guy. Multi-channel fiber Bragg gratings for dispersion and slope compensation. *Optical Fiber Communication Conference (OFC)*, March 2002.

[109] R. Ramaswami and K. N. Sivarajan. *Optical Networks - A practical perspective*. Morgan Kaufmann Publishers, 2nd edition, 2002.

[110] J. F. Brennan, E. Hernandez, J. A. Valenti, P. G. Sinha, M. R. Matthews, D. E. Elder, G. A. Beauchesne, and C. H. Byrd. Dispersion and dispersion-slope correction with a fiber Bragg grating over the full C-band. *Optical Fiber Communication Conference (OFC)*, 4(PD12), March 2001.

[111] J. Brennan. Dispersion management with long-length fiber Bragg gratings. *Optical Fiber Communication Conference (OFC)*, 5(FC1), March 2003.

[112] R. L. Lachance, S. Levievre, and Y. Painchaud. 50 and 100 GHz multi-channel tunable chromatic dispersion slope compensator. *Optical Fiber Communication Conference (OFC)*, 2(TuD3), March 2003.

[113] C. D. Poole, J. M. Wiesenfeld, D. J. DiGiovanni, and A. M. Vengsarkar. Optical fiber-based dispersion compensation using higher order modes near cutoff. *Journal of Lightwave Technology*, 12(10):1746–1758, October 1994.

[114] A. H. Gnauck, L. D. Garrett, Y. Danziger, U. Levy, and M. Tur. Dispersion and dispersion-slope compensation of NZDSF over entire C band using higher-order-mode fibers. *Electronics Letters*, 36(23):1946–1947, November 2000.

[115] S. Ghalmi, S. Ramachandar, E. Monberg, Z. Wang, M. Yan, F. Dimarcello, W. Reed P. Wisk, and J. Fleming. Low-loss, all-fibre higher-order-mode dispersion compensators for lumped or multi-span compensation. *Electronics Letters*, 38(24):1597–1508, November 2002.

[116] E. L. Goldstein and L. Eskildsen. Scaling limitations in transparent optical networks due to low-level crosstalk. *IEEE Photonics Technology Letters*, 7(1):93–94, January 1995.

[117] S. Ramachandran. Higher-order-mode dispersion compensation for broadband dispersion and nonlinearity management in transmission systems. *Optical Fiber Communication Conference (OFC)*, March 2002.

[118] S. Ramachandran, M. Yan, L. Cowsar, A. Carra, P. Wisk, R. Huff, and D. Packham. Large bandwidth, highly efficient mode coupling using long-period gratings in dispersion tailored fibers. *Optical Fiber Communication Conference (OFC)*, 1(MC2), March 2001.

[119] S. Ramachandran, B. Mikkelsen, L. C. Cowsar, M. F. Yan, G. Raybon, L. Boivin, M. Fishteyn, W. A. Reed, P. Wisk, D. Brownlow, R. G. Huff, and L. Gruner-Nielsen. All-fiber grating-based higher order mode dispersion compensator for broad-band compensation and 1000-km transmission at 40 Gb/s. *IEEE Photonics Technology Letters*, 13(6):632–635, June 2001.

[120] M. C. Tatham, G. Sherlock, and L. D. Westbrook. Compensation of fibre chromatic dispersion by optical phase conjugation in a semiconductor laser amplifier. *Electronics Letters*, 29(21):1851–1852, October 1993.

[121] A. Yariv, D. Fekete, and D. M. Pepper. Compensation of chromatic dispersion by nonlinear optical phase conjugation. *Optics Letters*, 4(1):52–54, January 1979.

[122] A. H. Gnauck, R. M. Jopsen, and R. M. Derosier. 10-Gb/s 360-km transmission over dispersive fiber using midsystem spectral inversion. *IEEE Photonics Technology Letters*, 5(6):663–665, June 1993.

[123] R. M. Jopson, A. H. Gnauck, and R. M. Derosier. Compensation of fibre chromatic dispersion by spectral inversion. *Electronics Letters*, 29(7):576–577, April 1993.

[124] N. S. Bergano, C. R. Davidson, and F. Heismann. Bit-synchronous polarization and phase modulation improves th eperformance of optical amplifier transmission systems. *Optical Fiber Communication Conference (OFC)*, 1:70, March 1996.

[125] A. Mecozzi, C. B. Clausen, and M. Shtaif. System impact of intra-channel nonlinear effects in highly dispersed optical pulse transmission. *IEEE Photonics Technology Letters*, 12(12):1633–1635, December 2000.

[126] A. Mecozzi, C. B. Clausen, M. Shtaif, S. G. Park, and A. H. Gnauck. Cancelation of timing and amplitude jitter in symmetrical links using highly dispersed pulses. *IEEE Photonics Technology Letters*, 13(5):445–447, May 2001.

[127] B. Konrad, A. Hodzic, and K. Petermann. Dispersion compensation schemes for 160 Gb/s TDM - transmission over SSMF and NZDSF. *European Conference on Optical Communication (ECOC)*, 2(Tu.L.2.4):188–189, September 2001.

[128] B. Nyman, M. Farries, and C. Si. Technology trends in dense WDM demultiplexers. *Optical Fiber Technology*, 7:255–274, July 2001.

[129] J. C. Chon, H. Luo, C. H. Huang, R. Hunag, J. Chen, and J. R. Bautista. Expandable 50-GHz and 100-GHz dense wavelength division multiplexers based on unbalanced and cascaded-fiber Mach-Zehnder architectures. *National Fiber Optic Engineers Conference (NFOEC)*, 1999.

[130] G. Lenz, G. Nykolak, and B. J. Eggleton. Dispersion of optical filters in WDM systems: theory and experiment. *European Conference on Optical Communication (ECOC)*, 2:271–272, September 1998.

[131] J. P. Gordon and L. F. Mollenauer. Effects of fiber nonlinearities and amplifier spacing on ultra-long distance transmission. *Journal of Lightwave Technology*, 9(2):170–173, February 1991.

[132] N. Yasuoka, M. Makiuchi, M. Miyata, O. Aoki, and M. Ekawa. High-efficiency PIN photo-diodes with a spot-size converter for 40 Gb/s transmission systems. *European Conference on Optical Communication (ECOC)*, 4(Th.M.2.4):558–559, September 2001.

[133] H. G. Bach, W. Schlaak, G. G. Mekonnen, R. Steingrüber, A. Seeger, W. Passenberg, W. Ebert, G. Jacumeit, T. Eckhard, R. Ziegler, A. Beling, B. Schmauss, A. Munk, T. Engel, and A. Umbach. 50 GHz photoreceiver modules for RZ and NRZ modulation format comprising InP-OEICs. *European Conference on Optical Communication (ECOC)*, 4(Th.M.2.5):560–561, September 2001.

[134] H. G. Bach, A. Beling, G. G. Mekonnen, W. Schlaak, and C. Bornholdt. 60 Gbit/s InP-based monolithical photoreceiver. *European Conference on Optical Communication (ECOC)*, 4(10.5.2), September 2002.

[135] M. Wada, T. Umezawa, T. Kudou, T. Mogi, S. Araki, S. Araki, M. Dobashi, S. Oka, T. Fujita, S. Kobayashi, T. Yakihara, and A. Miura. Full-WDM-band photodiode modules for optical communications at 40 Gb/s ans beyond. *Optical Fiber Communication Conference (OFC)*, 3(WF2), March 2003.

[136] M. Nakaji, E. Ishimura, Y. Hanamaki, T. Aoyagi, and Y. Mitsui. Highly reliable wave-guide photodiode with wide bandwidth of 50 GHz at the low operation voltage of -1.5 V. *Optical Fiber Communication Conference (OFC)*, 4(WF6), March 2003.

[137] R. C. Steele, G. R. Walker, and N. G. Walker. Sensitivity of optically preamplified receivers with optical filtering. *IEEE Photonics Technology Letters*, 3(6):545–547, June 1991.

[138] M. Saruwatari and K. Hagimoto. *Optical Amplifiers and their Applications*. John Wiley and Sons, 1994.

[139] B. Wedding. Analysis of fibre transfer function and determination of receiver frequency response for dispersion supported transmission. *Electronics Letters*, 30(1):58–59, January 1994.

[140] R. Gross. Differential encoder for QPSK systems. *IEE Electronics Letters*, 27(14):1256–1257, July 1991.

[141] M. Rhode, C. Caspar, N. Heimes, M. Konitzer, E. J. Bachus, and N. Hanik. Robustness of DPSK direct detection transmission format in standard fiber WDM systems. *Electronics Letters*, 26(17):1483–1484, August 2000.

[142] C. Wree, J. Leibrich, and W. Rosenkranz. RZ-DQPSK format with high spectral efficiency and high robustness towards fiber nonlinearities. *European Conference on Optical Communication (ECOC)*, 4(9.6.6), September 2002.

[143] R. Griffin, R. Johnstone, R. Walker, S. Wadsworth, and A. Carter. Integrated DQPSK transmitter for dispersion-tolerant and dispersion-managed DWDM transmission. *Optical Fiber Communication Conference (OFC)*, 2(FP6):770–771, March 2003.

[144] A. H. Gnauck, G. Raybon, S. Chandrasekhar, J. Leuthold, C. Doerr, L. Stulz, A. Agarwal, S. Banerjee, D. Grosz, S. Hunsche, A. Kung, A. Marhelyuk, D. Maywar, M. Movassaghi, X. Liu, C. Xu, X. Wei, and D. M. Gill. 2.5 Tb/s (64x42.7 Gb/s) transmission over 40x100 km NZDSF using RZ-DPSK format and all-Raman-amplified spans. *Optical Fiber Communication Conference (OFC)*, Postdeadline Paper(FC2), March 2002.

[145] V. S. Grigoryan, P. S. Cho, and I. Shpanter. Nonlinear penalty reduction of RZ-DBPSK versus RZ-OOK modulation format in fiber communications. *European Conference on Optical Communication (ECOC)*, 3(P3.29), September 2002.

[146] A. H. Gnauck, G. Raybon, S. Chandrasekhar, J. Leuthold, C.Doerr, L. Stulz, and E. Burrows. 25x40-Gb/s copolarized DPSK transmission over 12x100-km NZDF with 50-GHz channel spacing. *IEEE Photonics Technology Letters*, 15(3):467–469, March 2003.

[147] S. Benedetto and P. Poggiolini. Theory of polarization shift keying modulation. *IEEE Transaction on Communication*, 40(4):708–721, April 1992.

[148] A. Carena, V. Curri, R. Gaudino, N. Greco, P. Poggiolini, and S. Benedetto. Polarization modulation in ultra-long haul transmission systems: A promising alternative to intensity modulation. *European Conference on Optical Communication (ECOC)*, 1:429–430, September 1998.

[149] S. Benedetto, R. Gaudino, and P. Poggiolini. Direct detection of optical digital transmission based on polarization shift keying. *IEEE Journal of Selected Areas in Communications*, 3(3):531–542, April 1995.

[150] G. Mohs, C. Fürst, H. Geiger, and G. Fischer. Advantages of nonlinear RZ and NRZ on 10 Gb/s single-span links. *Optical Fiber Communication Conference (OFC)*, 4(FC2):35–37, March 2000.

[151] A. Lender. Correlative level coding for binary-data transmission. *IEEE Spectrum*, 3:104–115, February 1966.

[152] A. J. Price and N. Le Mercier. Reduced bandwidth optical digital intensity modulation with improved chromatic dispersion tolerance. *Electronics Letters*, 31(1):58–59, January 1995.

[153] K. Yonenaga, S. Kuwano, S. Norimatsu, and N. Shibata. Optical duobinary transmission system with no receiver sensitivity degradation. *Electronics Letters*, 31(4):302–304, February 1995.

[154] W. Keiser, M. Wichers, T. Wuth, W. Rosenkranz, C. Scheerer, C. Glingener, A. Färbert, J. P. Elbers, and G. Fischer. SPM limit of duobinary transmission. *European Conference on Optical Communication (ECOC)*, (7.2.2), September 2000.

[155] T. Ito, T. Ono, Y. Yano, K. Fukuchi, H. Yamazaki, M. Yamaguchi, and K. Emura. Feasibility study on over 1 bit/s/Hz high spectral efficiency WDM with optical duobinary coding and polarization interleave multiplexing. *Optical Fiber Communication Conference (OFC)*, 2(TuJ1):43–44, March 1997.

[156] T. Ono, Y. Yano, K. Fukichi, T. Ito, H. Yamazaki, M. Yamaguchi, and K. Emura. Characteristics of optical duobinary signals in Terabit/s capacity, high-spectral efficiency WDM systems. *Journal of Lightwave Technology*, 16(5):788–797, May 1998.

[157] C. Wree, M. Bohn, and W. Rosenkranz. Upgrading of Nx40 Gbit/s WDM system from 100 GHz to 50 GHz channel spacing by duobinary interleaving concept with optical tranversal filters. *European Conference on Optical Communication (ECOC)*, 4(Th.B.1.5), October 2001.

[158] M. Wichers and W. Rosenkranz. Chirped duobinary transmission (CDBT) for mitigating the self-phase modulation limiting effect. *Optical Fiber Communication Conference (OFC)*, 3(WD43), March 2001.

[159] A. Djopsjöbacka. Prechirped duobinary modulation. *IEEE Photonocs Technology Letters*, 10(8):1159–1161, August 1998.

[160] S. K. Kim, J. Lee, and J. Joeng. Transmission performance of 10-Gb/s optical duobinary transmission systems considering adjustable chirp of nonideal LiNbO3 Mach-Zehnder modulators due to applied voltage ratio and filter bandwidth. *Journal of Lightwave Technology*, 19(4):465–470, April 2001.

[161] Y. Miyamoto, K. Yonenaga, A. Hirano, H. Toba, K. Murata, and H. Miyazawa. Duobinary carrier-suppressed return-to-zero format and its application to 100 GHz-spaced 8x43-Gbit/s DWDM unrepeated transmission over 163 km. *Optical Fiber Communication Conference (OFC)*, 2(TuU4), March 2001.

[162] A. Uemura, K. Shimomura, K. Sawada, S. Kozaki, K. Shimizu, and H. Ichibangase. Novel method of duobinary signal generation with half-bitrate signal sources. *European Conference on Optical Communication (ECOC)*, 4(Th.B.1.3), September 2001.

[163] C. X. Yu, S. Chandrasekhar, L. Buhl, A. Gnauck, S. Radic, X. Wei, and X. Liu. 10.7 Gbit/s transmission over >200 km of standard singlemode fiber using forward error correction and duobinary modulation. *Electronics Letters*, 39(1):76–77, January 2003.

[164] R. A. Griffin, R. G. Walker, R. I. Johnstone, R. Harris, N. M. B. Perney, N. D. Whibread, T. Widdowson, and P. Harper. Integrated 10 Gb/s chirped return-to-zero transmitter using GaAs/AlGaAs modulators. *Optical Fiber Communication Conference (OFC)*, Postdeadline paper(PD15), March 2001.

[165] A. Hodzic, B. Konrad, and K. Petermann. Alternative modulation formats in Nx40 Gb/s WDM standard fiber RZ-transmission systems. *Journal of Lightwave Technology*, 20(4):598–607, April 2002.

[166] P. J. Winzer and J. Leuthold. Return-to-zero modulator using a single NRZ drive signal and an optical delay interferometer. *IEEE Photonics Technology Letters*, 13(12):1298–1300, December 2001.

[167] P. J. Winzer and A. Kalmar. Sensitivity enhancement of optical receivers by impulsive coding. *Journal of Lightwave Technology*, 17(2):171–177, February 1999.

[168] P. J. Winzer, A. H. Gnauck, G. Raybon, S. Chandrasekhar, Y. Su, and J. Leuthold. 40-Gb/s return-to-zero alternate-mark-inversion (RZ-AMI) transmission over 2000 km. *IEEE Photonics Technology Letters*, 15(5):766–768, May 2003.

[169] D. Breuer and K. Petermann. Comparison of NRZ and RZ modulation format for 40-Gb/s TDM standard-fiber systems. *IEEE Photonics Technology Letters*, 9(3):398–400, March 1997.

[170] H. Sunnerud, M. Karlsson, and P. A. Andrekson. A comparison between NRZ and RZ data formats with respect to PMD-induced system degradations. *IEEE Photonics Technology Letters*, 13(5):448–450, May 2001.

[171] L. Boivin, M. C. Nuss, J. Shah, D. A. B. Miller, and H. A. Haus. Receiver sensitivity improvement by impulsive coding. *IEEE Photonics Technology Letters*, 9(5):684–686, May 1997.

[172] S. G. Park, A. H. Gnauck, J. M. Wiesenfeld, and L. D. Garrett. 40-Gb/s transmission over multiple 120-km spans of conventional single-mode fiber using highly dispersed pulses. *IEEE Photonics Technology Letters*, 12(8):1085–1087, August 2000.

[173] A. H. Gnauck, S. G. Park, J. M. Wiesenfeld, and L. D. Garrett. Highly dispersed pulses for 2x40 Gbit/s transmission over 800 km of conventional singlemode fiber. *Electronics Letters*, 35(25):2218–2219, December 1999.

[174] G. C. Gupta, R. E. Tench, O. Mizuhara, L. L. Wang, N. N. Dang, N. Chand, B. Mason, A. Ougazzaden, and C. W. Lentz. 3.2 Tbit/s (40x80 Gb/s) transmission over 1000 km with 100 km span (25 dB loss) and 0.8 bit/s/Hz of spectral efficiency. *Optical Fiber Communication Conference (OFC)*, 2(TuA5), March 2003.

[175] K. Tanaka, I. Morita, and N. Edagawa. 50 GHz spaced 40 Gbit/s x 25 WDM transmission over 480 km using bandlimited RZ signals. *Electronics Letters*, 37(12):775–776, June 2001.

[176] A. Hodzic, B. Konrad, S. Randel, and K. Petermann. Optimized filtering for 40-Gb/s/channel-based DWDM transmission systems over standard single mode fiber. *IEEE Photonics Technology Letters*, July 2003.

[177] Y. Miyamoto, A. Hirano, K. Yonenaga, A. Sano, H. Toba, K. Murata, and O. Mitomi. 320 Gbit/s (8x40 Gbit/s) WDM transmission over 367 km with 120 km repeater spacing using carrier-suppressed return-to-zero format. *Electronics Letters*, 35(23):2041–2042, November 1999.

[178] Y. Miyamoto. 40-Gbit/s transport system: Its WDM upgrade. *Optical Fiber Communication Conference (OFC)*, 3(ThW4):323–325, March 2000.

[179] G. Bosco, A. Carena, V. Curri, R. Gaudino, and P. Poggiolini. On the use of NRZ, RZ and CSRZ modulation formats for ultra-dense WDM at 40 Gb/s. *European Conference on Optical Communication (ECOC)*, 3(P3.7), September 2002.

[180] G. Castanon and T. Hoshida. Impact of dispersion slope in NRZ, CSRZ, IMDPSK and RZ formats on ultra high bit-rate systems. *European Conference on Optical Communication (ECOC)*, 4(9.6.1), September 2002.

[181] A. Agata, I. Morita, T. Tsuritani, and N. Edagawa. Characteristics of asymmetrically filtered 40 Gbit/s CS-RZ signals. *Optical Fiber Communication Conference (OFC)*, 1(MF78):97–98, March 2003.

[182] A. Sano and Y. Miyamoto. Performance Evaluation of Prechirped RZ and CS-RZ Formats in High-Speed Transmission Systems With Dispersion Management. *Journal of Lightwave Technology*, 19(12):1864–1871, December 2001.

[183] T. Tsuritani, I. Morita, A. Agata, and N. Edagawa. Study on optimum optical pre-filtering condition for highly spectral-efficient ultralong-haul trasnsmission using 40 Gb/s CS-RZ signal and all-Raman repeaters. *Optical Fiber Communication Conference (OFC)*, 2(FE4):660–661, March 2003.

[184] M. Sieben, J. Conradi, D. Dodds, B. Davies, and S. Walkin. 10 Gbit/s optical single sideband system. *Electronics Letters*, 33(11):971–972, May 1997.

[185] K. Yonenaga and N. Takachio. A fiber chromatic dispersion compensation technique with an optical SSB transmission in optical homodyne detection systems. *IEEE Photonics Technology Letters*, 5(8):949–951, August 1993.

[186] R. Olshansky. Single sideband optical modulator for lightwave systems. *US Patent No. 5,301,058*, 1994.

[187] J. Conradi, B. Davies, M. Sieben, D. Dodds, and S. Walklin. Optical single sideband (OSSB) transmission for dispersion avoidance and electrical diseprsion compensation in microwave subcarrier and baseband digital systems. *Optical Fiber Communication Conference (OFC)*, Postdeadline Paper(PD29), February 1997.

[188] S. Bigo and Y. Frignac. Multi-terabit/s WDM transmission at 40 Gbit/s channel rate. *Advanced Semiconductor Lasers and Applications/Ultraviolet and Blue Lasers and Their Applications/Ultralong Haul DWDM Transmission and Networking/WDM Components - LEOS Summer Meeting*, 2:35–36, 2001.

[189] T. Tsuritani, A. Agata, I. Morita, K. Tanaka, and N. Edagawa. Performance comparison between DSB and VSB signals in 20 Gbit/s-based ultra-long-haul WDM systems. *Optical Fiber Communication Conference (OFC)*, 1(MM5), March 2001.

[190] S. Bigo. Improving spectral efficiency by ultra-narrow optical filtering to achieve multiterabit/s capacities. *Optical Fiber Communication Conference (OFC)*, 3:362–364, March 2001.

[191] N. S. Bergano, C. R. Davidson, M. A. Mills, P. C. Corbett, S. G. Evangelides, B. Pederson, R. Menges, J. L. Zyskind, J. W. Sulhoff, A. K. Srivastava, C. Wolf, and J. Judkins. Long-haul WDM transmission using optimum channel modulation: A 160 Gb/s (32x5 Gb/s) 9,300 km demonstration. *Optical Fiber Communication Conference (OFC)*, Postdeadline Papers(PD16), March 1997.

[192] N. S. Bergano, C. R. Davidson, C. J. Chen, B. Pedersen, M. A. Mills, N. Ramanujam, H. D. Kidorf, A. B. Puc, M. D. Levonas, and H. Abdelkader. 640 Gb/s transmission of sixty-four 10 Gb/s WDM channels over 7200 km with 0.33 (bit/s)/Hz spectral efficiency. *Optical Fiber Communication Conference (OFC)*, Postdeadline Papers(PD2), March 1999.

[193] T. Tsuritani, Y. Yamada, A. Agata, N. Takada, N. Edagawa, and M. Suzuki. 1 Tbit/s (100x10.7 Gbit/s) transpacific transmission using single-stage 980 nm-pumped C.band optical repeaters without forward error correction. *Electronics Letters*, 36(18):1566–1568, August 2000.

[194] D. Le Guen, F. Favre, M. L. Moulinard, M. Henry, G. Michard, L. Mace, F. Devaux, B. Charbonnier, and T. Georges. 200 Gbit/s 100km-span soliton WDM transmission over 1000 km of standard fiber with dispersion compensation and pre-chirping. *Optical Fiber Communication Conference (OFC)*, Postdeadline Papers(PD17), March 1998.

[195] F. Liu, X. zheng, C. Peucheret, S. N. Knudsen, R. J. S. Pedersen, and P. Jeppsen. Chirped return-to-zero source used in 8x10 Gbit/s transmission over 2000 km of standard singlemode fiber. *Electronics Letters*, 36(16):1399–1400, August 2000.

[196] A. Sano, Y. Miyamoto, K. Yonenaga, and H. Toba. 20 Gbit/s chirped return-to-zero transmitter with simplified configuration using electro-absorption modulator. *Electronics Letters*, 36(22):1858–1859, October 2000.

[197] E. A. Golovchenko, A. N. Pilipetskii, N. S. Bergano, C. R. Davidson, F. I. Khatri, R. M. Kimball, and V. J. Marurczyk. Modeling of Transoceanic Fiber-Optic WDM Communication Systems. *IEEE Journal of Selected Topics in Quantum Electronics*, 6(2):337–347, March/April 2000.

[198] B. Bakhshi, M. Vaa, E. A. Glovchenko, W. W. Petterson, R. L. Maybach, and N. S. Bergano. Comparison of CRZ, RZ and NRZ modulation formats in a 64x12.3 Gb/s WDM transmission experiment over 9000km. *Optical Fiber Communication Conference (OFC)*, 3(WF4), March 2001.

[199] A. Hodzic, B. Konrad, and K. Petermann. Improvement of NRZ based 40 Gbit/s single channel and WDM transmission. *LEOS Annual Meeting*, 2(TuK3), November 2001.

[200] A. Hodzic, B. Konrad, and K. Peteramann. Novel modulation format for Nx40 Gbit/s WDM transmission with 50 GHz channel spacing. *European Conference on Optical Communications (ECOC)*, 1:90–91, September 2001.

[201] A. Hodzic, B. Konrad, and K. Petermann. Improvement of system performance in Nx40-Gb/s WDM transmission using alternate polarization. *IEEE Photonics Technology Letters*, 15(1):153–155, January 2003.

[202] A. Hodzic, N. Hecker-Denschlag, M. Winter, S. Jansen, K. Saucke, and K. Petermann. 10 Gbit/s based NRZ DWDM systems using polarisation switching in single wavelength channel. *Electronics Letters*, 39(18):1329–1330, September 2003.

[203] R. Ohhira, D. Ogasahara, and T. Ono. Novel RZ signal format with alternate-chirp for suppression of nonlinear degradation in 40 Gb/s based WDM. *Optical Fiber Communication Conference (OFC)*, 3(WM2), March 2001.

[204] K.S. Cheng and J. Conradi. Reduction of pulse-to-pulse interaction using alternative RZ formats in 40-Gb/s systems. *IEEE Photonics Technology Letters*, 14(1):98–100, January 2002.

[205] M. Winter. Untersuchung von Polarisations Moden Dispersion (PMD) in N x 40 Gbit/s optischen Übertragungssystemen. Master's thesis, Diplomarbeit, Technische Universität Berlin, 2004.

[206] F. Matera, M. Settembre, M. Tamburrini, F. Favre, D. Le Guen, T. Georges, M. Henry, G. Michaud, P. Franco, A. Schiffini, M. Romagnoli, M. Guglielmucci, and S. Cascelli. Field demonstration of 40 Gbit/s soliton transmission with alternate polarizations polarizations. *Journal of Lightwave Technology*, 17(11):2225–2234, November 1999.

[207] B. Mikkelsen, G. Raybon, and R. J. Essiambre. 160 Gb/s TDM transmission systems. *European Conference on Optical Communication (ECOC)*, 2:125–128, September 2000.

[208] V. Mikhailov, R. I. Killey, S. Appathurai, and P. Bayvel. Investigation of intra-channel nonlinear distrortion in 40 Gb/s transmission over non-zero dispersion shifted fiber. *European Conference on Optical Communication (ECOC)*, 3(8.1.6), September 2001.

[209] A. E. Elrefaie, J. K. Townsend, M. B. Romeiser, and K. S. Shanmugan. Computer simulation of digital lightwave links. *IEEE Journal of Selected Areas in Communications*, 6(1):94–105, January 1988.

[210] J. K. Townsend and K. S. Shanmugan. On improving the computational efficiency of digital lightwave link simulations. *IEEE Transactions on Communications*, 38(11):2040–2048, November 1990.

[211] R. Freund. *On Computer Aided Modeling of Photonics Systems and Networks*. PhD thesis, Technische Universität Ilmenau, April 2002.

[212] D. Marcuse. Derivation of analytical expressions for the bit-error probability in lightwave systems with optical amplifiers. *Journal of Lightwave Technology*, 8(12):1816–1823, December 1990.

[213] F. Abramovich and P. Bayvel. Some statistical remarks on the derivation of BER in amplified optical communication systems. *IEEE Transactions on Communications*, 45(9):1032–1034, September 1997.

[214] P. A. Humblet and M. Azizoglu. On the bit error rate of lightwave systems with optical amplifiers. *Journal of Lightwave Technology*, 9(11):1576–1583, November 1991.

[215] D. Marcuse. Calculation of bit-error probability for lightwave systems with optical amplifiers and post-detection Gaussian noise. *Journal of Lightwave Technology*, 9(4):505–513, April 1991.

[216] N. S. Bergano, F. W. Kerfoot, and C. R. Davidson. Margin measurements in optical amplifier systems. *IEEE Photonics Technology Letters*, 5(3):304–306, March 1993.

[217] W. H. Press, B. P. Flannery, S. A. Teukolsky, and W. T. Vetterling. *Numerical Recipes*. Cambridge University Press, 1989.

[218] C. Caspar, K. Habel, N. Heimes, M. Konitzer, M. Malach, M. Özdem, M. Rohde, F. Schmidt, E. J. Bachus, and N. Hanik. Penalties through XPM crosstalk in a switched long haul standard fiber WDM system based on normalized transmission sections. *Optical Fiber Communication Conference (OFC)*, 3(WI5), March 2001.

[219] S. D. Personic. Receiver design for digital fiber optic communications systems. *Bell System Technology Journal*, 52(6), July 1973.

[220] C. J. Anderson and J. A. Lyle. Technique for evaluating system performance using Q in numerical simulations exibiting intersymbol interference. *Electronics Letters*, 30(1):71–72, January 1994.

[221] R. Bach, W. Moench, and G. Strohmaier. In-service optical performance monitoring of high-speed transparent networks based on Q measurements . *3rd International Conference on Transparent Optical Networks (ICTON)*, 1(We.B.4):210–217, June 2001.

[222] A. Richter, W. Fischler, H. Bock, R. Bach, and W. Grupp. Optical performance monitoring in transparent and configurable DWDM networks . *IEE Proceedings - Optoelectronics*, 149(1):1–5, February 2002.

[223] A. R. Chraplyvy and R. W. Tkach. What is the actual capacity of single-mode fibers in amplified Lightwave Systems? *IEEE Photonics Technology Letters*, 5(6):666–668, June 1993.

[224] J. P. Elbers, A. Färbert, C. Scheerer, C. Glingener, and G. Fischer. Reduced model to describe SPM-limited fiber transmission in dispersion-managed lightwave systems. *IEEE Journal of Selected Topics in Quantum Electronics*, 6(2):276–281, March/April 2000.

[225] ITU-T Telecommunication standardization sector of ITU. *ITU-T G.692: Optical interfaces for multi-channel systems with optical amplifiers*, October 1998.

[226] R. Rasztovits-Wiech, M. Danner, and W. R. Leeb. Optical signal-to-noise ratio measurement in WDM networks using polarization extinction. *European Conference on Optical Communication (ECOC)*, 1:549–550, September 1998.

[227] ITU Telecommunication Standardization Sector. *ITU-T G.693: Transmitter eye mask and reference receiver proposal for serial 40G*, January 2002.

[228] E. Voges and K. Petermann. *Optische Kommunikationstechnik - Handbuch für Wissenschaft und Industrie*. Springer, 2002.

[229] D. Breuer. *Untersuchungen zu optischen Übertragungssystemen bei 10 Gbit/s und 40 Gbit/s im verlegten Glasfasernetz*. PhD thesis, Technische Universität Berlin, 1999.

[230] A. Pizzinat, A. Schiffini, F. Alberti, A. Paoletti, D. Caccioli, . Griggio, P. Minzioni, and F. Matera. Numerical and experimental comparison of dispersion compensation techniques on different fibers. *IEEE Photonics Technology Letters*, 14(10):1415–1417, October 2002.

[231] J. X. Cai, M. Nissov, C. R. Davidson, A. N. Pilipetskii, G. Mohs, H. Li, Y. Cai, E. A. Golovchenko, A. J. Lucero, D. G. Fuorsa, and N. S. Bergano. Long-haul 40 Gb/s DWDM transmission with aggregate capacities exceeding 1 Tb/s. *IEEE Journal of Lightwave Technology*, 20(12):2247–2258, December 2002.

[232] A. F. Judy. Optimum fiber dispersion for multiwavelength 40 Gbit/s NRZ and RZ transmission. *European Conference on Optical Communication (ECOC)*, 2:280–281, September 1999.

[233] R. I. Killey, V. Mikhailov, S. Appathurai, and P. Bayvel. Investigation of nonlinear distortion in 40 -Gb/s transmission with higher order mode fiber dispersion compensators. *Journal of Lightwave Technology*, 20(12):2282–2289, December 2002.

[234] P. Johannisson, D. Anderson, M. Marklund, A. Berntson, M. Forzati, and J. Martensson. Suppresion of nonlinear effects by phase alternation in strongly dispersion-managed optical transmission. *Optics Letters*, 27(12):1073–1075, June 2002.

[235] X. Liu, X. Wei, A. H. Gnauck, C. Xu, and L. K. Wickham. Suppression of intrachannel four-wave-mixing-induced ghost pulses in high-speed transmissions by phase inversion between adjacent marker blocks. *Optics Letters*, 27(13):1177–1179, July 2002.

[236] C. Caspar, H. M. Foisel, A. Gladisch, N. Hanik, F. Küppers, R. Ludwig, A. Mattheus, W. Pieper, B. Strebel, and H. G. Weber. RZ versus NRZ modulation format for dispersion compensated SMF-based 10 Gb/s transmission with more than 100-km amplifier spacing. *IEEE Photonics Technology Letters*, 11(4):481–483, April 1999.

[237] A. R. Chraplyvy. Limitations on lightwave communications imposed by optical-fiber nonlinearities. *Journal of Lightwave Technology*, 8(10):1548–1557, October 1990.

[238] E. Golovchenko. Challenges of designing long-haul WDM systems. *Optical Fiber Communication Conference (OFC)*, Tutorials(TuL):1–52, March 2002.

[239] R. J. Essiambre, B. Mikkelson, and G. Raybon. Intra-channel cross-phase modulation and four-wave mixing in high speed TDM systems. *Electronics Letters*, 35(18):1576–1578, September 1999.

[240] M. Zitelli, F. Matera, and M. Settembre. Single-channel transmission in dispersion managed links in conditions of very strong pulse broadening: Application to 40 Gb/s signals on step-index fibers. *Journal of Lightwave Technology*, 17(12):2498–2504, December 1999.

[241] S. Appathurai, V. Mikhailov, R. I. Killey, and P. Bayvel. Suppression of intra-channel nonlinear distortion in 40 Gbit/s transmission over standard single mode fibre using alternate-phase RZ and optimised pre-compensation. *European Conference on Optical Communication (ECOC)*, 2(Tu3.6.5):270–271, September 2003.

[242] Y. Frignac, J.-C. Antona, S. Bigo, and J.-P. Hamaida. Numerical optimization of pre- and in-line dispersion compensation in dispersion-managed systems at 40 Gb/s. *Optical Fiber Communication Conference (OFC)*, 4(ThFF5):612–613, March 2002. ThFF5.

[243] JDS Uniphase. *Product Bulletin: 50 GHz Arrayed Waveguide Grating (AWG)*, March 2003.

[244] TeraXion Inc. *TF-WDM: FBG Dense Wavelength Division Multiplexing Filters*, December 2002.

[245] NEL NTT Electronics. *NEL: AWG Multi/Demultiplexer*, August 2001.

[246] G. Lenz, B. J. Eggleton, C. K. Madson, C. R. Giles, and G. Nykolak. Optimal dispersion of optical filters for WDM systems. *IEEE Photonics Technology Letters*, 10(4):567–569, April 1998.

[247] P. J. Winzer, D. Stahl, and H. Kim. Impact of carver chirp on RZ-DPSK receiver perfromance. *European Conference on Optical Communication (ECOC)*, 3(We3.5.6):530–531, September 2003.

[248] I. Morita, T. Tsuritani, and N. Edagawa. Experimental study on optically band-limited 40-Gb/s RZ signals with optically time-division demultiplexing receiver. *Journal of Lightwave Technology*, 20(12):2182–2188, December 2002.

[249] A. Carena, V. Curri, and P. Poggiolini. Comparison between different configurations of hybrid Raman/erbium-doped fiber amplifiers. *Optical Fiber Communication Conference (OFC)*, 2(TuA3), March 2001.

[250] J. C. Bouteiller, K. Brar, and C. Headley. Quasi-constant signal power transmission. *European Conference on Optical Communication (ECOC)*, 3(3.4), September 2002.

[251] S. Bigo, G. Bellotti, and M. W. Chbat. Investigation of cross-phase modulation limitations on 10 Gbit/s transmission over various types of fiber infrastructure. *Optical Fiber Communication Conference (OFC)*, 2(ThC3):40–42, February 1999.

[252] R. Hui, K. R. Demarest, and C. T. Allen. Cross-phase modulation in multispan WDM optical fiber systems. *Journal of Lightwave Technology*, 17(6):1018–1026, June 1999.

[253] C. Fürst, C. Scheerer, G. Mohs, J. P. Elbers, and C. Glingener. Influence of the dispersion map on limitations due to cross-phase modulation in WDM multispan transmission systems. *Optical Fiber Communication Conference (OFC)*, 1(MF4), March 2001.

[254] C. M. Weinert, R. Ludwig, W. Piepert, H. G. Weber, D. Breuer, K. Petermann, and F. Küppers. 40 Gb/s and 4x40 Gb/s TDM/WDM standard fiber transmission. *Journal of Lightwave Technology*, 17(11):2276–2284, November 1999.

[255] B. Dany, O. Leclerc, F. Neddam, and P. Le Lourec. Optimization of 40 Gbit/s dispersion maps for long-haul WDM transmissions with up to 0.4 bit/s/Hz spectral efficiency. *Optical Fiber Communication Conference (OFC)*, 2(TuN5), March 2001.

[256] A. V. T. Cartaxo. Cross-phase modulation in intensity modulation direct detection WDM systems with multiple optical amplifiers and dispersion compensators. *Journal of Lightwave Technology*, 17(2):178–190, February 1999.

[257] Z. Jiang and C. Fan. A comprehensive study on XPM- and SRS-induced noise in cascaded IM-DD optical fiber transmission systems. *Journal of Lightwave Technology*, 21(4):953–960, April 2003.

[258] T. Okuno, T. Ooishi, T. Kato, Y. Yokoyama, M. Yoshida, Y. Takahashi, Y. Makio, and M. Nishimura. Optimum dispersion of non-zero dispersion shifted fiber for high bit rate DWDM systems. *Optical Fiber Communication Conference (OFC)*, 2(TuH4), March 2001.

[259] S. Bigo, G. Bellotti, and M. W. Chbat. Investigation of cross-phase modulation limitation over various types of fiber infrastructure. *IEEE Photonics Technology Letters*, 11(5):605–607, May 1999.

[260] D. Breuer, N. Hanik, C. Casper, F. Raub, G. Bramann, M. Rohde, E.-J. Bachus, S. McLeod, and M. Edwards. WDM-transmission over mixed fiber infrastructure. *European Conference on Optical Communication (ECOC)*, 3(P3.28), September 2002.

[261] R. Hainberger, J. Kumasako, K. Nakamura, T. Terahara, and H. Onaka. Optimum span configuration of Raman-amplified dispersion-managed fibers. *Optical Fiber Conference (OFC)*, Technical Digest(MI5), March 2001.

[262] R. I. Killey, H. J. Thiele, and P. Bayvel. Improving the performance of 40 Gb/s based WDM transmission over standard fiber. *European Conference on Optical Communication (ECOC)*, 3(7.2.1):29–30, September 2000.

[263] G. Bellotti and S. Bigo. Cross-phase modulation suppressor for multispan dispersion-managed WDM transmissions. *IEEE Photonics Technology Letters*, 12(6):726–728, June 2000.

[264] G. Bellotti, S. Bigo, S. Gauchard, P. Y. Cortes, and S. LaRochelle. 10x10 Gb/s cross-phase modulation suppressor using WDM narrowband fiber Bragg gratings. *Optical Fiber Communication Conference (OFC)*, 4(PD32):263–265, March 2000.

[265] M. Eiselt. Does spectrally periodic dispersion compensation reduce non-linear effects? *European Conference on Optical Communication (ECOC)*, 1(3027):3027/1–3027/2, September 1999.

[266] D. I. Kovsh, L. Liu, B. Bakhsi, A. N. Pilipetski, E. A. Golovchenko, and N. S. Bergano. Reducing interchannel crosstalk in long-haul DWDM systems. *IEEE Journal of Selected Topics in Quantum Electronics*, 8(3):597–602, May/Juni 2002.

[267] P. S. Cho, V. S. Grigoryan, Y. A. Godin, A. Salamon, and Y. Achiam. Transmission of 25-Gb/s RZ-DQPSK signals with 25-GHz channel spacing over 1000 km over SMF-28 fiber. *IEEE Photonics Technology Letters*, 15(3):473–475, March 2003.

[268] N. S. Bergano, C. R. Davidson, M. Ma, A. Pilipetskii, S. G. Evangelides, H. D. Kidorf, J. M. Darcie, E. Golovchenko, K. Rottwitt, P. C. Corbett, R. Menges, M. A. Mills, B. Pedersen, D. Packham, A. A. Abramov, and A. M. Vengsarker. 320 Gb/s WDM transmission (64x5 Gb/s) over 7,200 km using large mode fiber spans and chirped return-to-zero signals. *Optical Fiber Communication Conference (OFC)*, Postdeadline Papers(PD12), March 1998.

[269] K. Inoue. Polarization effect on four-wave mixing efficiency in a single-mode fiber. *IEEE Journal of Quantum Electronics*, 28(4):883–894, April 1992.

[270] A. O. Dal Forno, A. Paradisi, R. Passy, and J. P. Von der Weid. Experimental and theoretical modeling of polarization-mode diseprsion in single-mode fibers. *IEEE Photonics Technology Letters*, 12(3):296–298, March 2000.

[271] Y. Zhu, W. S. Lee, P. Lobb, C. Ward, D. Watley, S. Savory, C. R. S. Fludger, B. Shaw, and A. Hadjifotiou. Polarization-channel-interleaved CS-RZ transmission at 40 Gbit/s with 0.8 bit/s/Hz spectral efficiency. *Electronics Letters*, 38(8):381–382, April 2002.

[272] V. Grigoryan, P. Cho, and Y. Godin. Novel modulation techniques. *Optical Fiber Communication Conference (OFC)*, 2(FD1):646–647, March 2003.

[273] C. Wree, J. Leibrich, J. Eick, W. Rosenkranz, and D. Mohr. Experimental investigation of receiver sensitivity of RZ-DQPSK modulation format using balanced detection. *Optical Fiber Communication Conference (OFC)*, 2(ThE5):456–457, March 2003.

[274] W. Idler, A. Klekamp, R. Dischler, J. Lazaro, and A. Konczykowski. System performance and tolerances of 43 Gb/s ASK and DPSK modulation formats. *European Conference on Optical Communication (ECOC)*, 4(Th2.6.3):1006–1007, September 2003.

[275] T. Kobayashi, K. Shimizu, K. Ouchi, K. Ishida, Y. Miyata, T. Tokura, J. Abe, T. Mizuochi, and K. Motoshima. 10 Gbit/s RZ-DPSK receiver with a sensitivity of -50.5 dBm (7 photons per information bit) using Block Turbo Code FEC. *European Conference on Optical Communication (ECOC)*, 2(Tu1.6.6):204–205, September 2003.

[276] O. Vassilieva, T. Hoshida, S. Choudhary, and H. Kuwahara. Non-linear tolerant and spectrally efficient 86 Gb/s RZ-DQPDK format for a system upgrade. *Optical Fiber Communication Conference (OFC)*, 2(ThE7):458–459, March 2003.

[277] J. P. Gordon and L. F. Mollenauer. Phase noise in photonic communication systems using linear amplifiers. *Optics Letters*, 15(23):1351–1353, x 1990.

[278] S. Ferber, R. Ludwig, C. Boerner, A. Wietfeld, B. Schmauss, J. Berger, C. Schubert, G. Unterboersch, and H. G. Weber. Comparison of DPSK and OOK modulation formats in a 160 Gb/s transmission system. *European Conference on Optical Communication (ECOC)*, 4(Th2.6.2):1004–1005, September 2003.

[279] K. P. Ho. Asymptotic probabilty density of nonlinear phase noise. *Optics Letters*, 28(15):1350–1352, August 2003.

[280] H. Kim and A. H. Gnauck. Experimental investigation of the performance limitation of DPSK systems due to nonlinear phase noise. *IEEE Photonics Technology Letters*, 15(2):320–322, February 2003.

[281] T. Kroener. Vergleich von ASK und PSK (DPSK, QPSK) Modulationsformaten in 40 Gb/s WDM optischen Übertragungssystemen. Master's thesis, Technische Universität Berlin, 2003.

A List of symbols

A_{eff}	fiber effective core area
$A(z,t)$	complex field envelope
B_o	optical bandwidth
B_e	electrical bandwidth
C	Rayleigh constant
c	speed of light in vacuum (c=2.99792458 $\times$ 10^8 [m/s])
D	dispersion coefficient
$\mathbf{D}$	degeneracy factor
D_M	material dispersion
D_{PMD}	polarization mode dispersion
D_W	waveguide dispersion
d	walk-off length
$\mathbf{E}$	electric field vector
$\mathbf{E}(\omega)$	pulse energy
F	noise figure
$F(x,y)$	transversal field distribution
G	amplifier gain
g_B	Brillouin gain factor
g_R	Raman gain factor
I_D	decision threshold
h	Planck's constant (h=6.62607 $\times 10^{-34}$ [Ws^2]
L	fiber length
L_D	linear length
L_{eff}	effective fiber length
L_{NL}	nonlinear length
N	electron pupulation
$n(\omega)$	refractive index
n_0	linear refractive index
n_2	nonlinear refractive index
n_{sp}	spontaneous emission factor
m	modulation index
$\mathbf{P}$	electric polarization vector
P_{ASE}	ASE-noise power
R	responsitivity
q	electron charge (q=1.60218 $\times$ 10^{-19} [C])
S	slope of dispersion coefficient D
t, T	time, normalized time
T_{bit}	time slot duration
T_{FWHM}	pulse width at half maximum
v_g	group velocity
α_L	laser line-width enhancement factor (Henry factor)
α_R	Rayleight scattering loss
$\beta(\omega)$	mode propagation constant
β_1	inverse of group velocity v_g
β_2	group velocity dispersion (GVD), chromatic dispersion
β_3	group velocity dispersion slope

κ_L	laser adiabatic chirp coefficient
γ	nonlinear coefficient
η	FWM efficiency
λ	wavelength
$\sigma_{1,0}$	standard deviation of marks and spaces
$\mu_{1,0}$	mean value of marks and spaces
ρ_{ASE}	ASE-noise spectral density
$\Delta\beta$	phase mismatch
Δf_{sig}	signal bandwidth
$\Delta\phi$	phase change
$\Delta\Phi$	phase difference
Δn	effective index change
ω	angular frequency
$\Delta\omega_L$	laser chirp
ΔT	pulse broadening
$\Delta\tau$	differential group delay
Δz	step size in split-step Fourier method
χ_{1111}	third order nonlinear susceptibility
τ	duty cycle

B Acronyms

al-RZ	Alternate Chirped Return-to-Zero
ASE	Amplified Spontaneous Emission
AWG	Arrayed Waveguide Grating
al-CNRZ	Alternate Chirped Non-Return-to-Zero
al-PNRZ	Alternate Polarized Non Return-to-Zero
al-PRZ	Alternate Polarized Return-to-Zero
BER	Bit Error Rate
CRZ	Chirped Return-to-Zero
CSRZ	Carrier Suppressed Return-to-Zero
DCF	Dispersion Compensating Fiber
DCS-RZ	Duobinary Carrier Suppressed Return-to-Zero
DD	Direct Detection
DFB	Distributed Feedback
DGD	Differential Group Delay
DQPSK	Differential Quadrature Phase Shift Keying
DPSK	Differential Phase Shift Keying
DR	Dynamic Range
DRZ	Duobinary Return-to-Zero
DMUX	Demultiplexer
DSF	Dispersion Shifted Fiber
DSL	Digital Subscriber Line
DWDM	Dense Wavelength Division Multiplexing
EAM	Electro Absorption Modulator
EDFA	Erbium Doped Fiber Amplifier
EOP	Eye Opening Penalty
ER	Extinction Ratio
ETDM	Electrical Time Division Multiplexing
FBG	Fiber Bragg Grating
FEC	Forward Error Correction
FFT	Fast Fourier Transformation
FKE	Franz Kaldysh Effect
FM	Frequency Modulation
FOM	Figure of Merit
FP	Fabry Perot
FSK	Frequency Shift Keying
FWHM	Full Width at Half Maximum
FWM	Four Wave Mixing
GD	Group Delay
GVD	Group Velocity Dispersion
HOM	Higher Order Mode
IFWM	Intrachannel Four Wave Mixing
IL	Insertion Loss
IP	Internet Protokol
IM	Intensity Modulation
IM-DD	Intensity Modulation Direct Detection
ISI	Inter Symbol Interference

ITU	International Telecommunication Union
IXPM	Intrachannel Cross Phase Modulation
LPF	Low Pass Filter
MAN	Metro Area Netweorks
MC	Monte Carlo
MSK	Minimum Shift Keying
MSSI	Mid-span Spectral Inversion
MPI	Multi Path Interference
MQW	Multi Quantum Well
MUX	Multiplexer
MZI	Mach Zehnder Interferometer
MZM	Mach Zehnder Modulator
nCRZ	Novel Chirped Return-to-Zero
NF	Noise Figure
NLSE	Nonlinear Schrödinger Equation
NRZ	Non Return-to-Zero
NZDSF	Non Zero Dispersion Shifted Fiber
OSNR	Optical Signal-to-Noise Ratio
OADF	Optical Add Drop Filters
OSI	Open System Interconnection
OXC	Optical Cross Connect
QCSE	Quantum-Confined Stokes Effect
QoS	Quality of Service
QW	Quantum Well
PBC	Polarization Beam Combiner
PBS	Polarization Beam Splitter
PDF	Probability Density Function
PDL	Polarization Dependent Loss
PLL	Phase Locked Loop
PolM	Polarization Modulator
PolSK	Polarization Shift Keying
PRBS	Pseudo Random Bit Sequence
PM	Phase Modulator
PMD	Polarization Mode Dispersion
PMF	Polarization Maintaining Fiber
PSD	Power Spectral Density
PSK	Phase Shift Keying
RSP	Receiver Sensitivity Penalty
RZ	Return-to-Zero
SBS	Stimulated Brillouin Scattering
SOA	Semiconductor Optical Amplifier
SOP	State Of Polarization
SPM	Self Phase Modulation
SRS	Stimulated Raman Scattering
SSB-RZ	Single Side Band Return-to-Zero
SSFM	Split Step Fourier Method
SSMF	Standard Single Mode Fiber
TFF	Thin Film Filters
VSB	Vestigial Side Band
WDM	Wavelength Division Multiplexing
XPM	Cross Phase Modulation

C Sufficient amount of bits for 40 Gb/s numerical investigation

Before the transmission systems are investigated it was necessary to determine the sufficient lengths of pseudo-random bit sequences (PRBS) for use in numerical simulations in order to enable a precise and a computing time effective analysis of transmission systems. The optimum number of bits for the numerical simulation is determined considering the two most important evaluation criteria - EOP and BER. The investigation is made considering a system setup for 40 Gbit/s RZ single channel transmission over 4x80 km at a constant input power (P_{IN} = 3dBm). The Q-factor versus number of bits is illustrated in Fig.C.1a. The random bit words with lengths from 2^6 to 2^{15} bits are considered. Each bit word consists of equal number of marks and spaces. For calculation of each point in Fig.C.1a twenty different noise distributions are considered, so that each point represents the mean value of different noise distributions. It can be seen that a random word length of 2^9 bits is sufficient for a correct numerical simulation of 40 Gbit/s transmission system. There are almost no differences between Q-factor values at 2^9 and 2^{15} bits. In order to check if this behaviour is maintained for larger input power EOP is investigated considering PRBS words with different lengths for a power range between 0..10 dBm (Fig.C.1). It can be seen that starting from 2^9 bits the transmission behavior remains independent on the number of bits.

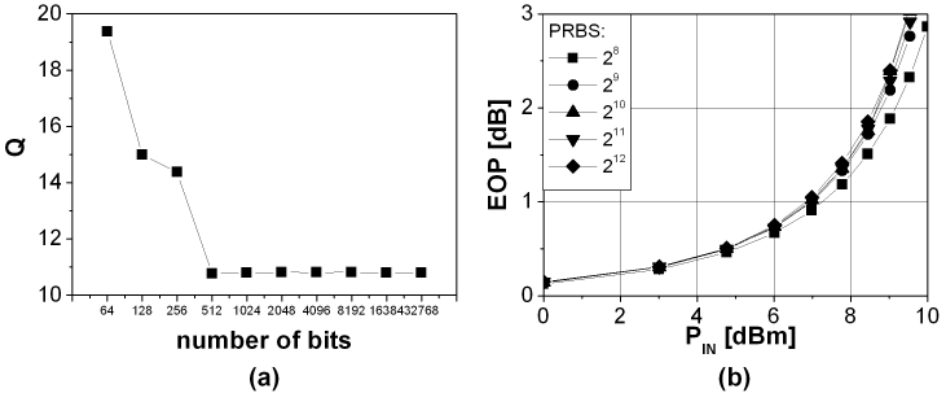

Figure C.1: Optimum length of PRBS length for numerical investigation of 40 Gb/s transmissions: a) Q versus number of bits (P_{IN}=3 dBm) (b) EOP versus input power

D Optimized power settings for 40 Gb/s single channel transmission

Table D.1: Optimum powers for different amounts of dispersion pre-compensation

	NRZ						**Duobinary**					
	SSMF		NZDSF1		NZDSF2		SSMF		NZDSF1		NZDSF2	
pre-comp. [%]	P_{SMF} [dBm]	P_{DCF} [dBm]	P_{SMF} [dBm]	P_{DCF} [dBm]	P_{SMF} [dBm]	P_{DCF} [dBm]	P_{SMF} [dBm]	P_{DCF} [dBm]	P_{SMF} [dBm]	P_{DCF} [dBm]	P_{SMF} [dBm]	P_{DCF} [dBm]
0	1	-7	1	-5	0	-4	1	-6	1	-4	0	-4
5	1	-6	2	-5	1	-4	1	-6	1	-4	0	-5
10	1	-6	2	-5	2	-4	2	-6	2	-5	1	-5
15	1	-6	2	-6	3	-3	2	-6	3	-6	3	-5
20	2	-6	2	-7	3	-3	2	-6	3	-5	4	-4
25	2	-5	2	-6	2	-3	3	-5	3	-5	4	-3
30	2	-4	3	-5	1	-3	2	-4	3	-5	3	-3
35	2	-3	1	-2	1	-3	1	-2	4	-4	3	-3
40	1	-2	0	1	2	-3	1	0	5	-2	3	-2
45	1	0	0	2	2	-3	1	2	4	3	3	-2
50	0	1	-1	1	2	-2	2	4	2	5	3	-1
55	-1	1	-1	-1	1	-2	0	4	1	5	3	-1
60	-1	-1	-1	-3	0	-3	-2	2	0	5	2	-1
65	-2	-2	-2	-4	-1	-3	-2	-3	-1	-3	1	-2
70	-2	-4	-2	-6	-1	-4	-2	-4	-2	-6	0	-3
75	-2	-4	-2	-7	-2	-3	-3	-5	-2	-6	0	-4
80	-2	-5	-2	-7	-2	-4	-3	-5	-2	-7	-1	-3
85	-2	-5	-2	-8	-2	-5	-3	-6	-3	-6	-1	-4
90	-2	-6	-3	-7	-2	-5	-3	-6	-3	-6	-2	-4
95	-2	-7	-3	-7	-2	-5	-3	-6	-3	-7	-2	-6
100	-2	-6	-3	-8	-2	-5	-3	-5	-3	-7	-2	-6
	alCNRZ						**alPNRZ**					
0	1	-5	1	-5	0	-5	5	-3	4	-1	3	-2
5	1	-6	2	-5	1	-6	5	-3	5	-1	4	-3
10	2	-5	2	-6	2	-5	5	-2	5	-1	5	-2
15	2	-5	2	-6	2	-4	5	-2	5	-2	5	-2
20	2	-4	2	-6	1	-4	5	-2	5	-1	5	-1
25	2	-4	2	-6	1	-4	5	-2	5	-1	5	0
30	2	-3	2	-4	1	-4	5	-1	5	0	5	0
35	2	-2	2	-3	1	-5	5	0	5	0	5	1
40	1	-1	1	-2	1	-5	4	3	4	1	4	3
45	1	0	0	-2	1	-4	4	4	4	3	4	4
50	1	1	-1	-3	1	-4	3	5	4	4	4	5
55	0	1	-1	-5	1	-3	3	5	4	1	4	4
60	-1	-1	-1	-5	0	-3	2	3	3	0	4	3
65	-1	-3	-1	-6	0	-3	2	1	3	-2	3	2
70	-1	-3	-1	-5	-1	-3	2	-1	2	-2	3	1
75	-2	-4	-1	-4	-1	-4	2	-1	2	-3	2	1
80	-1	-4	-1	-5	-2	-5	1	-1	1	-2	2	0
85	-1	-4	-2	-5	-2	-5	1	-1	1	-3	2	-1
90	-1	-4	-2	-6	-2	-5	1	-1	1	-3	2	-2
95	-1	-5	-2	-6	-2	-6	1	-1	0	-3	2	-2
100	-1	-5	-2	-7	-2	-6	1	-2	0	-3	2	-2

Table D.1: Optimum powers for different amounts of dispersion pre-compensation

	RZ						**SSB-RZ**					
	SSMF		NZDSF1		NZDSF2		SSMF		NZDSF1		NZDSF2	
pre-comp. [%]	P_{SMF} [dBm]	P_{DCF} [dBm]	P_{SMF} [dBm]	P_{DCF} [dBm]	P_{SMF} [dBm]	P_{DCF} [dBm]	P_{SMF} [dBm]	P_{DCF} [dBm]	P_{SMF} [dBm]	P_{DCF} [dBm]	P_{SMF} [dBm]	P_{DCF} [dBm]
0	3	-5	4	-3	2	-4	3	-4	4	-3	2	-4
5	3	-4	4	-2	3	-4	3	-4	4	-2	3	-4
10	2	-5	5	-2	4	-4	3	-5	5	-2	4	-4
15	3	-5	4	-4	4	-3	3	-4	5	-4	4	-3
20	3	-5	2	-4	3	-1	2	-4	3	-4	4	-2
25	2	-5	3	-4	3	1	2	-5	2	-4	2	0
30	2	-4	3	-3	2	3	2	-4	3	-4	2	-5
35	2	-2	2	-2	1	0	2	-2	2	-3	1	-1
40	2	0	2	1	1	-1	2	0	1	-1	1	-2
45	2	1	2	4	1	0	2	1	2	3	1	-1
50	2	3	1	5	2	5	1	3	1	4	1	0
55	1	3	0	1	2	-2	0	3	0	-2	2	-1
60	0	0	0	-3	1	-3	0	1	0	-3	1	-2
65	0	-2	-1	-3	-1	5	-1	-1	-1	-3	0	-2
70	-1	-3	-1	-4	-1	5	-1	-4	-1	-4	-1	-2
75	-1	-3	-1	-4	-1	-1	-1	-4	-1	-4	-1	-2
80	-1	-4	-1	-4	-1	-2	-1	-4	-1	-6	-1	-2
85	-1	-3	-1	-4	-1	-4	-1	-4	-1	-5	-1	-3
90	-1	-4	-1	-5	-1	-5	-1	-4	-1	-6	-1	-4
95	0	-5	-1	-5	-1	-5	0	-4	-2	-5	- 1	-4
100	0	-4	-2	-6	-1	-5	-1	-4	-2	-6	-1	-5
	CSRZ						**nCRZ**					
0	3	-5	5	-2	3	-4	4	-3	2	-3	2	-5
5	3	-5	3	-4	3	-5	4	-4	3	-3	2	-5
10	3	-5	4	-4	3	-5	2	-4	2	-3	2	-4
15	3	-4	4	-4	4	-5	3	-2	0	-3	1	-2
20	2	-4	3	-5	4	-3	1	-2	1	-4	0	0
25	2	-5	2	-4	3	1	1	-2	2	-4	-2	0
30	2	-3	3	-3	2	2	2	-1	0	-4	-2	0
35	2	-2	2	-3	1	1	2	-1	-1	-5	-2	0
40	2	0	1	-2	0	1	1	0	-1	-6	0	-1
45	2	1	1	2	0	4	1	0	-1	-7	0	-1
50	1	3	1	4	1	5	1	0	-1	-6	-1	-1
55	0	2	0	1	1	5	1	0	0	-5	-2	0
60	0	0	0	-3	-1	5	1	-2	0	-5	-3	2
65	-1	-3	-1	-4	-1	5	0	-2	0	-5	-3	2
70	-1	-3	-1	-3	-1	5	0	-3	0	-4	-3	3
75	-1	-3	-1	-4	-2	4	0	-3	-1	-4	-3	3
80	-1	-4	-1	-4	-1	-5	0	-2	-1	-3	-3	-6
85	-1	-4	-1	-4	-1	-6	0	-2	-1	-3	-2	-6
90	-1	-4	-2	-5	-1	-6	-1	-2	-1	-4	-2	-7
95	-1	-4	-2	-5	-1	-6	-1	-3	-1	-5	-2	-6
100	-1	-4	-2	-4	-1	-5	-1	-3	-1	-6	-1	-6

Table D.1: Optimum powers for different amounts of dispersion pre-compensation

	alPRZ								
	SSMF		NZDSF1		NZDSF2				
pre-comp. [%]	P_{SMF} [dBm]	P_{DCF} [dBm]	P_{SMF} [dBm]	P_{DCF} [dBm]	P_{SMF} [dBm]	P_{DCF} [dBm]			
0	5	-2	5	0	5	-1			
5	5	-2	5	0	5	-2			
10	5	-1	5	0	5	-2			
15	5	-2	5	-1	5	-1			
20	4	-2	5	0	5	-1			
25	4	-2	5	1	5	1			
30	5	-1	5	2	5	5			
35	5	-1	4	2	5	3			
40	4	3	3	3	4	2			
45	4	5	3	5	3	4			
50	4	5	4	5	4	5			
55	3	5	4	5	4	3			
60	2	2	3	3	2	1			
65	2	2	3	0	2	0			
70	2	-1	2	2	1	1			
75	2	-1	2	-1	1	0			
80	2	-1	1	0	1	-2			
85	1	0	1	-1	1	-3			
90	2	0	1	-1	1	-3			
95	2	0	1	-3	2	-3			
100	2	-1	1	-3	2	-3			

Publications

Conferences and Workshops

1. A. Hodžić, T. Kröner, K. Petermann, "Analytical model for the design of PSK based single channel and DWDM transmission systems", Optical Fiber Communication Conference (OFC) 2004, vol. 2, paper TuN2, Los Angeles, USA, February 2004.

2. A. Hodžić, N. Hecker-Denschlag, M. Winter, S. Jansen, K. Saucke, K. Petermann, "Performance Improvement of 10 Gb/s based NRZ DWDM Systems Using Orthogonal Polarizations of Adjacent Bits in a Single Wavelength Channel", IEEE LEOS 2003 Annual Meeting, vol. 1, Tucson, Arizona, October 2003.

3. H. Louchet, A. Hodžić, K. Petermann, "Analytical Model for Nonlinear DWDM Transmissions", In Proc. of European Conference on Optical Communications (ECOC) 2003, vol. 3, paper We4.P.116, Rimini, Italy, September 2003.

4. B. Konrad, S. Randel, A. Hodžić, K. Petermann, "Optimum Fiber Chromatic Dispersion for Nx40 Gbit/s and Nx40 Gbit/s DWDM Systems", European Conference on Optical Communications (ECOC) 2003, vol. 3, paper We4.P.120, Rimini, Italy, September 2003.

5. S. Randel, B. Konrad, A. Hodžić, K. Petermann, "Comparison of Modulation Formats for DWDM Transmission of 160 Gbit/s OTDM Channels with Spectral Efficiency of 0.8 bit/s/Hz", European Conference on Optical Communications (ECOC) 2003, vol. 1, paper Mo4.2.6, Rimini, Italy, September 2003.

6. A. Hodžić, M. Winter, B. Konrad, S. Randel, K. Petermann, "Optimum Channel Data Rate for DWDM Transmission Systems with the Spectral Efficiency of 0.8 bit/s/Hz", European Conference on Optical Communications (ECOC) 2003, vol. 3, paper We4.P.104, Rimini, Italy, September 2003.

7. A. Hodžić, K. Petermann, "Comparison of 10/40/160 Gb/s based DWDM Transmission Systems with an Equal System Capacity and an Equal Spectral Efficiency (0.8 bit/s/Hz)", ITcom, Orlando, Florida, vol. 1, pp. 1002-1004, September 2003.

8. B. Konrad, A. Hodžić, S. Randel, K. Petermann, "Optimale Faserdispersion in Optischen Nx160 Gb/s WDM-Übertragungssystemen", 4.ITG-Fachtagung "Photonische Netze", Leipzig, Germany, pp. 131-136, May 2003.

9. A. Hodžić, M. Winter, B. Konrad, S. Randel, K. Petermann, "Comparison of 10/40/160 Gb/s/ch based DWDM Transmission Systems with Constant System Capacity", 4.ITG-Fachtagung "Photonische Netze", pp. 119-124, Leipzig, Germany, May 2003.

10. A. Hodžić, K. Petermann, "Implementation of novel FEC-Codes in 10/40 Gb/s RZ and NRZ based WDM networks", ITG Workshop Modellierung photonischer Komponenten und Systeme, Berlin, Germany, January 2003.

11. A. Hodžić, B. Konrad, S. Randel, K. Petermann, "Improved Nx40 Gb/s NRZ based WDM Transmission Performance with Polarization Switching", IEEE LEOS 2002 Annual Meeting, vol. 1, paper MN3, Glasgow,

UK, November 2002.

12. A. Hodžić, B. Konrad, S. Randel, K. Petermann, "Performance Comparison of 4Nx40 Gb/s and Nx160 Gb/s Transmission Systems", European Conference on Optical Communications (ECOC) 2002, vol. 3, paper P3.24, Copenhagen, Denmark, September 2002.

13. S. Randel, B. Konrad, A. Hodžić, K. Petermann, "Influence of Bitwise Phase Changes on the Performance of 160 Gb/s Transmission Systems", European Conference on Optical Communications (ECOC) 2002, vol. 3, paper P3.31, Copenhagen, Denmark, September 2002.

14. A. Hodžić, B. Konrad, K. Petermann, "Alternative Modulationformats for 40 Gb/s WDM Transmission Systems", 3.ITG-Fachtagung "Photonische Netze", pp. 95-104, Leipzig, Germany, April 2002.

15. A. Hodžić, K. Petermann, "Optimized dispersion compensation schemes in Nx10 Gb/s NRZ and RZ based transmission systems with 25 GHz channel spacing", ITG Workshop Modellierung photonischer Komponenten und Systeme, Nürnberg, Germany, June 2002.

16. A. Hodžić, B. Konrad, K. Petermann, "Improvement of NRZ based 40 Gbit/s Single Channel and WDM Transmission", LEOS 2001 Annual Meeting, vol. 2, paper TuK3, San Diego, USA, November 2001.

17. A. Hodžić, K. Petermann, "Impact of bit-synchronous polarization in WDM systems", ITG Workshop Modellierung photonischer Komponenten und Systeme, Stuttgart, Germany, November 2001.

18. B. Konrad, A. Hodžić, K. Petermann, "Dispersion Compensation Schemes for 160 Gbit/s TDM-transmission over SSMF and NZDSF", In Proc. of European Conference on Optical Communications (ECOC) 2001, vol. 2, pp. 188-189, Amsterdam, The Netherlands, September 2001.

19. A. Hodžić, B. Konrad, K. Petermann, "Novel Modulation Format for Nx40 Gbit/s WDM Transmission with 50 GHz Channel Spacing", European Conference on Optical Communications (ECOC) 2001, vol. 1, pp. 90-91, Amsterdam, The Netherlands, September 2001.

20. A. Hodžić, B. Konrad, K. Petermann, "Vergleich von RZ- und CS-RZ-Modulationsformaten in optischer Nx40 Gbit/s WDM-Übertragung über Standardfaser", 2.ITG-Fachtagung "Photonische Netze", pp. 151-156, Dresden, Germany, February 2001.

21. A. Hodžić, K. Petermann, "Alternative Modulationsformaten für Nx40 Gbit/s Übertragungssystems ", ITG Workshop Modellierung photonischer Komponenten und Systeme, Stuttgart, Germany, January 2001.

22. A. Hodžić, K. Petermann, "Vergleich der 40 Gbit/s Übertragungssysteme mit "return-to-zero"(RZ)- und "carrier-suppressed return-to-zero"(CS-RZ)-Modulationsformaten", ITG Workshop Modellierung photonischer Komponenten und Systeme, Berlin, Germany, June 2000.

Invited talks

1. A. Hodžić, B. Konrad, H. Louchet, K. Petermann, S. Randel, "Spectrally Efficient Optical Fiber Communication Systems with Intensity Modulation", Asia-Pacific Optical and Wireless Communications (APOC), Wuhan, China, November 2003.

2. A. Hodžić, K. Petermann, "10 Gb/s based NRZ DWDM systems using polarization switching in a single

wavelength channel", Avanex Inc., Milan, Italy, September 2003.

3. A. Hodžić, B. Konrad, S. Randel, K. Petermann, H. Louchet, "Strategies for Spectrally Efficient Optical Fiber Communication Systems with Direct Detection", International Conference on Transparent Optical Networks (ICTON) 2003, pp. 131-136, Warsaw, Poland, June 2003.

4. A. Hodžić, K. Petermann, "Modulation Formats for Robust WDM 40 Gbit/s Transmission Systems", Photonics North, vol. 2, paper Tu-M1-TCT-12, Quebec City, Canada, June 2002.

5. A. Hodžić, K. Petermann, "Impacts of Bit-Synchronous Polarization in 40 Gbit/s/ch WDM Systems", Optical Fiber Communication Conference (OFC) 2001, Anaheim, California, USA, Workshop W203: Modulation Formats and Ultimate Capacity, March 2002.

Journals

1. A. Hodžić, N. Hecker-Denschlag, M. Winter, S. Jansen, K. Saucke, K. Petermann, "10 Gb/s based NRZ DWDM Systems Using Polarization Switching", Electronics Letters, vol. 39, no. 18, pp. 1329-1330, September 2003.

2. H. Louchet, A. Hodžić, K. Petermann, "Analytical Model for the Performance Evaluation of DWDM Transmission Systems", IEEE Photonics Technology Letters, vol. 15, no. 9, pp. 1219-1221, September 2003.

3. A. Hodžić, M. Winter, B. Konrad, S. Randel, K. Petermann, "Optimized Filtering for 40-Gb/s/Ch-based DWDM Transmission Systems Over Standard Single-Mode Fiber", IEEE Photonics Technology Letters, vol. 15, no. 7, pp. 1002-1004, July 2003.

4. A. Hodžić, B. Konrad, K. Petermann, "Improvement of System Performance in Nx40-Gb/s WDM Transmission Using Alternate Polarizations", IEEE Photonics Technology Letters, vol. 15, no. 1, pp. 153-155, January 2003.

5. A. Hodžić, B. Konrad, K. Petermann, "Alternative Modulation Formats in N x 40 Gb/s WDM Standard Fiber RZ-Transmission Systems", Journal of Lightwave Technology, vol. 20, no. 4, April 2002.

6. A. Hodžić, B. Konrad, K. Petermann, "Prechirp in NRZ-Based 40-Gb/s Single-Channel and WDM Transmission Systems", IEEE Photonics Technology Letters, vol. 14, no. 2, pp. 152-154, February 2002.